THERMOCHEMICAL CONVERSION OF BIOMASS:

ACID CATALYSED PATHWAYS AND KINETICS OF CELLULOSE PYROLYSIS

SHAIK MOHAMED SALIM

NATIONAL UNIVERSITY OF SINGAPORE

2012

THERMOCHEMICAL CONVERSION OF BIOMASS:

ACID CATALYSED PATHWAYS AND KINETICS OF CELLULOSE PYROLYSIS

SHAIK MOHAMED SALIM

(B.Eng (Hons.), NUS)

(M.Eng, NUS)

A THESIS SUBMITTED

FOR THE DEGREE OF DOCTOR OF PHILOSOPHY

DEPARTMENT OF CHEMICAL AND BIOMOLECULAR ENGINEERING

NATIONAL UNIVERSITY OF SINGAPORE

2012

DECLARATION

I hereby declare that this thesis is my original work and it has been written by me in its entirety. I have duly acknowledged all the sources of information which have been used in the thesis.

This thesis has also not been submitted for any degree in any university previously.

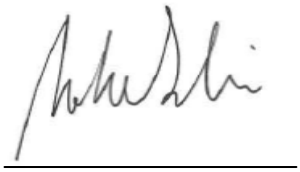

Shaik Mohamed Salim
23rd July 2013

ACKNOWLEDGEMENT

I would like to express my heartfelt appreciation to Prof. Reginald Tan for his guidance and patience over the past few years. I would also like to thank Prof. Paul Sharratt and Dr Keith Carpenter for their advice and support in the Institute of Chemical and Engineering Sciences (ICES). In addition, I would like to acknowledge A*STAR for their support of my studies via their award of the scholarship under the Scientific Staff Development Scheme (SSDS).

To my wife, Rohaila, I would like to say a special thank you for her patience and understanding and my parents for making me the person I am. To my children Syahmi, Rasyiqah, Raushana and Rakinah, their curiosity and energy have inspired me. But most of all I would like to thank God without whom nothing will exist.

I would like to dedicate this thesis to the memory of my late father

Shaik Abdul Mannan bin Shaik Abdul Hamid

(Al-Fatihah - الفاتحـــة).

TABLE OF CONTENTS

SUMMARY

The value of biomass as a renewable resource can be enhanced by subjecting it to a biological or thermochemical conversion to obtain simpler organic molecules that can be used as fuels and chemicals. This work focuses on the thermal/thermochemical conversion of biomass with the aim of enhancing the yields of highly valued anhydrosaccharide intermediates such as levoglucosan and levoglucosenone.

Cellulose thermal degradation proceeds initially via intermolecular transglycosylation reactions within the glucose monomers of cellulose to produce anhydrosaccharides (levoglucosan, levoglucosenone, 1,4:3,6-dianhydro-α-d-glucopyranose, 1,6-anhydro-β-D-glucofuranose). Alternatively, cellulose can also depolymerise via β-elimination to produce furans and other light organic volatiles.

Here, with the use of experiments and modelling, we have studied the qualitative, quantitative and kinetic effects of acids (H_2SO_4, H_3PO_4 and H_3BO_3) and alkalis ($Ba(OH)_2$, $Ca(OH)_2$ and NH_4OH) on the yields of anhydrosaccharides. Based on experiments using a fixed-bed reactor, the levels of anhydrosaccharides were found to have been lowered by the acids and raised by the alkalis. This shows that the β-elimination pathway is catalysed by the presence of acidic species (H^+ ions). The extent of cellulose conversion via the β-elimination pathway is dependent on the type, amount and strength of acid infused within the cellulose matrix. Alternatively, the β-elimination route is suppressed by the introduction of a neutralising species (OH^- ions) from alkalis.

A second method using thermogravimetric experiments and modelling was used to obtain kinetics parameters to bolster the findings above. It was found that the apparent activation energy for the thermal degradation of the acid-infused cellulose increased to ca. 250 kJ/mol and whilst those of the alkali-infused cellulose decreased to ca. 180 kJ/mol. This shift in the apparent activation energy when compared to that of pure cellulose (200 kJ/mol) signifies the predominance of β-elimination and transglycosylation due to the presence of the acidic and alkaline species respectively.

Subsequently, experiments using a stirred batch reactor were conducted to demonstrate the utility of manipulating H^+ ion concentration via alkali addition to enhance anhydrosaccharide yields. In these experiments, it was found that the conversion of cellulose in alkaline sulfolane increased anhydrosaccharide yields by up to 20 % and demonstrated the likelihood of an optimal H^+ ion concentration of between $1x10^{-10}$ mol/dm^3 and $1x10^{-9}$ mol/dm^3. Hence, a new method towards the selective production of chiral intermediates (anhydrosaccharides) via manipulation/decrease of $[H^+]$ has been demonstrated. This new method is in contrast to the state-of-the art method for levoglucosan and levoglucosenone production which mainly relies on acids such as H_3PO_4 to enhance yields.

.

NOMENCLATURE

Nomenclature	Description
A	pre-exponent factor, 1/s
a_{H+}	hydrogen ion activity
B_0	permeability, m^2
c_{pg}	specific heat capacity of volatiles, J/kg K
c_{ps}	specific heat capacity of substrate, J/kg K
D_{eff}	effective mass diffusivity, m^2/s
E	activation energy, kJ/mol
F	Faraday constant
h	convective heat transfer coefficient, W/m K
k	Arrhenius rate constant
K	thermal conductivity of substrate, W/m^2K
M	molar concentration, mol/dm^3
m/z	mass-to-charge ratio
mol%	mole percent
n	sample size
p	pressure, Pa
pKa	acid dissociation constant
r	characteristic length, m
R	gas constant, J/K mol
S^2	variance
T	temperature, K
t	time, s
W_0	sample weight at time = 0, kg

Nomenclature	Description
W_f	sample weight at the end, kg
W_t	sample weight at time = t, kg
wt%	weight percent
x	unreacted fraction
$\bar{y}$	sample mean

Greek Letters	Description
α	conversion
β	heating rate, K/s
ε	measured potential, V
ε^0	standard electrode potential, V
μ	viscosity, Pa.s
ρ_A	density of active cellulose, kg/m^3
ρ_c	density of char, kg/m^3
ρ_G	density of gases, kg/m^3
ρ_g	density of volatiles, kg/m^3
ρ_s	density of solids, kg/m^3
ρ_{SD}	density of dry solid biomass, kg/m^3
ρ_T	density of tars, kg/m^3
ρ_W	density of wood, kg/m^3

ABBREVIATIONS

Abbreviation	Description
AGF	1,6-anhydro-β-D-glucofuranose
BTEM	Band-Target Entropy Minimisation
bbl	oil barrel
ca.	circa
DAE	distributed activation energy
DFT	density functional theory
DGP	1,4:3,6-dianhydro-α-d-glucopyranose
DMF	dimethylformamide
DMSO	dimethyl sulfoxide
DSC	differential scanning calorimetry
EI	electron impact ionisation
FF	furfural
FTIR	Fourier transform infra-red
GC	gas chromatography
GC-MS	gas chromatography – mass spectrometry
GP	glucopyranose
H^+	hydrogen ion
HIV	Human immunodeficiency virus
HMF	5-hydroxymethyl furfural
HPLC	high pressure liquid chromatography
ID	internal diameter
IAC	intermediate active cellulose
ILC	intermediate liquid compound

Abbreviation	Description
LC	liquid chromatography
LG	levoglucosan (1,6-anhydro-β-D-glucopyranose)
LV	levulinic acid
LS	levoglucosenone (1,6-anhydro-3,4-dideoxy-β-D-pyranosen-2-one)
mp	melting point
NIST	National Institute of Standards and Technology
OH^-	hydroxyl ion
PDR	pathway degradation ratio
RID	refractive index detector
S$	Singapore dollars
TG	thermogravimetry
TGA	thermogravimetric analyser
US$	US dollars
UV	ultraviolet

LIST OF FIGURES

Appendix

LIST OF TABLES

Appendix

CHAPTERS

1. Introduction

Renewable energy and chemical feedstock are growing in importance due to environmental and sustainability concerns over fossil fuel usage. Alternatives to fossil fuels have also come into the spotlight due to the dramatic fluctuations (ca. 35 to 147 US$/bbl) in crude oil prices since 2004. In addition, the need for carbon neutral fuels and chemical feedstock to combat climate change has resulted in greater interest in biomass. Wood and other forms of biomass such as agricultural/forestry wastes, municipal solid waste, sewage sludge and microalgae are some of the main renewable resources available.

Biomass-based liquids (e.g. ethanol, bio-diesel) have been studied as a logical alternative to current fossil fuels because they can easily fit into existing liquid fuel logistics and distribution networks. However they face a severe limitation due to the transportation cost of the solid biomass. A maximum distance which was found to be ca. 100 km [1] limits the amount of biomass that can be harvested for conversion. This in turn affects the size of the biomass conversion plant and thus the amount of fuel that can be economically produced. As an illustration, a pyrolysis plant built in Malaysia to process palm oil empty fruit bunches from a crude palm oil extraction mill had a capacity of approximately 30 tons/day. This illustration shows that biomass conversion plants are relatively small (less than 50 tons/day) when compared with a typical oil refinery or a petrochemical plant (100,000 barrels/day ≈ 15,000 tons/day).

Problems related to the harvesting, pre-processing, transport and conversion of biomass have also led to questions being raised with regards to its carbon-footprint and life-cycle energy demands. In some cases, life-cycle assessments have shown that more energy is required to produce a fuel that has lower energy content [2-4].

Although this hampers the potential use of biomass as fuels, smaller-scale biomass conversion plants or bio-refineries [5, 6] can still be used for the production of higher value chemicals and other platform chemicals [7, 8] as these are usually produced in smaller quantities. Valuable chiral molecules such as levoglucosenone have been touted as potential intermediates in the production of fine chemicals and pharmaceuticals [9, 10] such as HIV drugs [11].

One method of using biomass as a renewable resource is by subjecting it to a biological or thermal/thermochemical conversion [12, 13] to obtain simpler organic molecules that can be used as chemical intermediates. Biological transformations (e.g. fermentation, anaerobic digestion) are carried out via the use of enzymes or microorganisms (e.g. bacteria, yeast) [14-16]. Alternatively, as shown in Figure 1.1, biomass can be subjected to thermal/thermochemical conversion. This thermal conversion process produces solids (char), condensable organic liquids/tars (pyrolytic oils) and non-condensable gases (e.g. CO, CO_2, H_2 and CH_4). Thermal conversion is not a new process and was known in ancient Egypt where wood distillation was practised to obtain tars and organic acids for embalming.

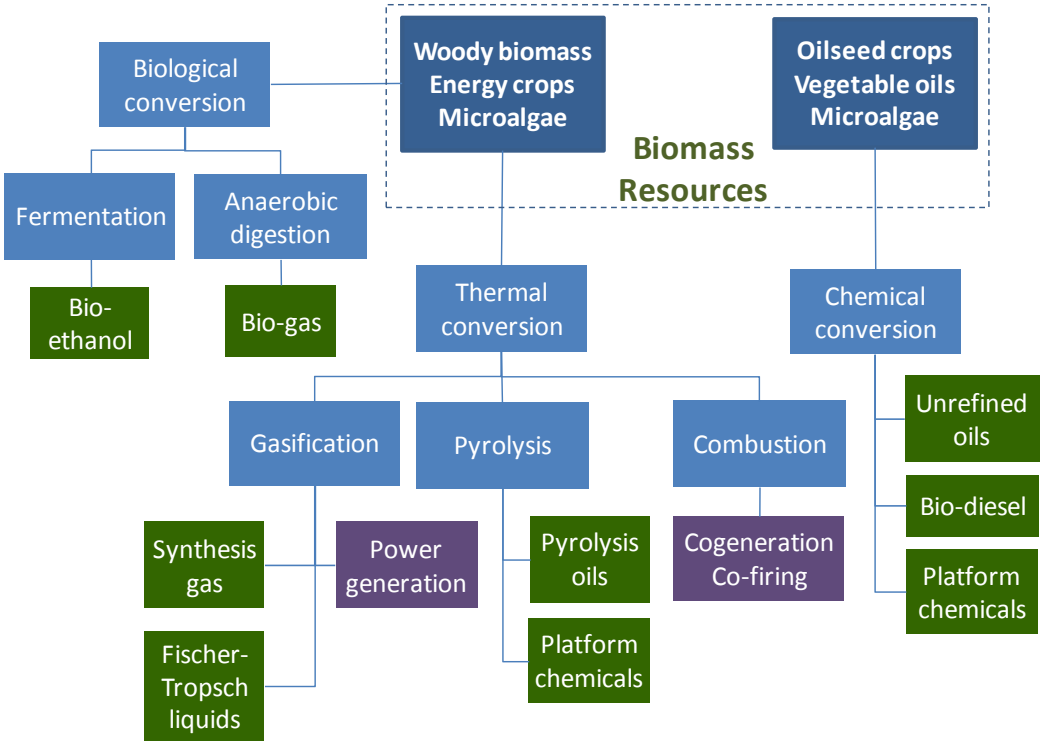

Figure 1.1: Conversion options for the utilisation of biomass for the production of fuels and chemicals [17]

Cellulose pyrolysis has been the subject of many studies due to it being the largest component (ca. 40 – 50 %) of plant biomass sources and its use does not impact on food supplies. It has been suggested that cellulose pyrolysis proceeds (initially) via two competing, parallel reactions (β-elimination and transglycosylation). A phenomenological description of cellulose pyrolysis was hypothesised by Mamleev et al. [18]. The main thermal degradation pathway is via intermolecular transglycosylation reactions within the glucose monomers of cellulose [19, 20]. Anhydrosaccharides (e.g. levoglucosan) are the primary products of this route. Cellulose degradation/depolymerisation can also occur via β-elimination. Under this mechanism, volatile acids (e.g. carboxylic acids) formed from the initial cellulose thermal degradation attack the remaining cellulose as Brønsted acids thus catalysing heterolytic (ring-opening) reactions. Based on the work done by Mamleev et al. [18],

Shafizadeh [20], Li et al. [21] and Shen and Gu [22] a schematic representation of the two main pathways and a few subsequent conversion steps are shown in Figure 1.2.

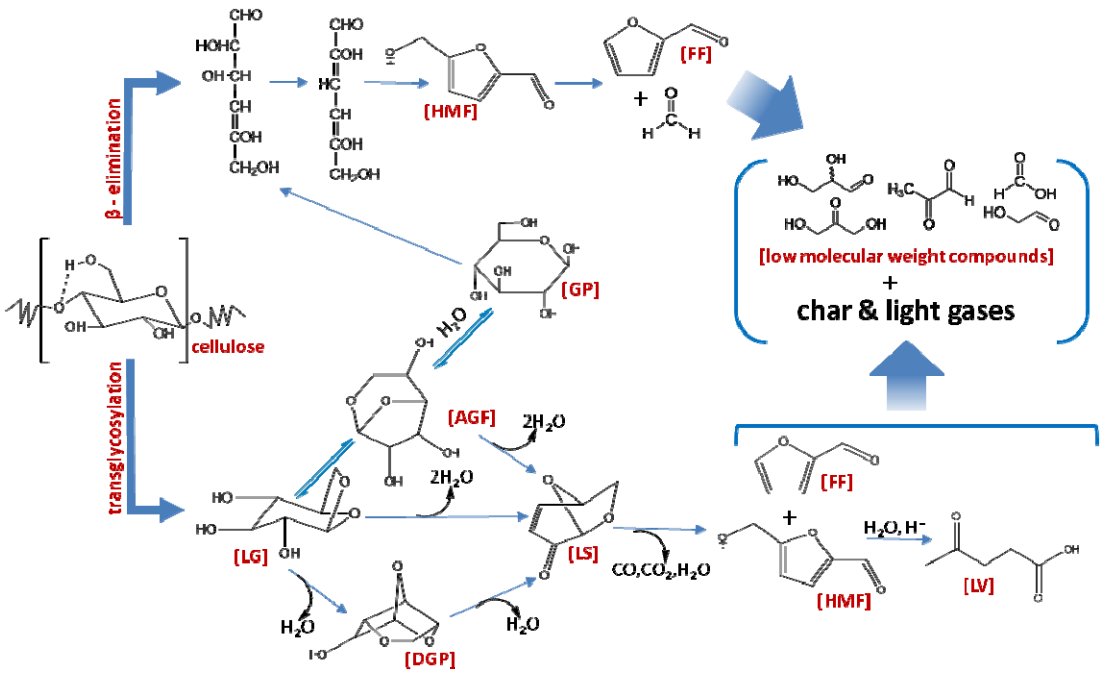

Figure 1.2: Schematic of possible mechanism for the conversion of cellulose to levoglucosan and its derivatives

In addition to this hypothesised role of volatile acids in cellulose pyrolysis chemistry, it has been known that acid or alkalis can significantly impact the yields and product composition. The influence of acids and alkalis on the two cellulose conversion pathways (transglycosylation and β-elimination) has not been demonstrated in literature. Instead, the current literature has shown rather conflicting results with most of the work focussing on the use of acids to enhance the yields of anhydrosaccharides (e.g. levoglucosan, levoglucosenone). These studies showed that the increased anhydrosaccharide yields from acid treatments were due to the removal of inorganic impurities, alteration of crystallinity and degree of polymerisation of cellulose [23-26]. The potential use of alkalis and by extension, controlling the levels of hydrogen ions [H^+] to manipulate cellulose degradation pathways and anhydrosaccharide yields have

not been attempted. Instead, the state-of-the-art methods for levoglucosan and levoglucosenone production found in patents [27-29] also relied on the use of acids, in particular H_3PO_4, to enhance yields.

Previously, the kinetics associated with cellulose pyrolysis has mainly been studied via the use of the lumped parameter method. However, in moving towards the production of high value intermediates, lumped analysis of tars, chars and gases is insufficient. There is a need to study the kinetics of intermediates formation to optimise the yields of anhydrosaccharides. In addition, the kinetics themselves would also be able to shed further light on the dominance of each of the two pathways in the presence of acids and alkalis. Indeed, such views are gaining currency as highlighted in the recent molecular simulation works of Agarwal et al. [30] and Mettler at al. [31].

1.1 Research Objectives

The current high prices and limited supply of bio-based chemicals for example levoglucosan (150 S$/g) and levoglucosenone (450 S$/g) are the main impediments to them being more widely used as intermediates in the production of fine chemicals and pharmaceuticals. Industry's need for renewable feedstock is real and is reflected in industry grants like GlaxoSmithKline's S$ 33 million Green and Sustainable Manufacturing Programme. In order to achieve greater adoption of such renewable chemicals, enhancements in the yields and selectivity of these valuable intermediates would be required.

In addition to being valuable intermediates in themselves, levoglucosan and levoglucosenone are also the primary anhydrosaccharides formed via transglycosylation during thermal/thermochemical conversion of cellulose. Therefore, to achieve the required yield and selectivity improvements, we need to study the chemistry and understand the behaviour of the two pathways (β-elimination and transglycosylation).

We therefore hypothesise that if hydrogen ions [H^+] catalyse the β-elimination pathway, an increase or decrease in [H^+] will either promote or suppress this conversion route respectively. A decrease in [H^+] should in turn allow more cellulose degradation via transglycosylation thus resulting in higher anhydrosaccharide yields.

An important application of this would be in improving the selectivity during thermal/thermochemical conversion to produce higher value compounds that could be used as chemical intermediates or platform chemicals (e.g. levoglucosan, levoglucosenone, 5-hydroxymethyl furfural and furfural) [7, 32]. Another application of this knowledge would be to better control the yields from pyrolysing different types of biomass that have intrinsic amounts of acidic or alkaline content.

A better understanding of the kinetics will offer us additional insights into the predominance (or otherwise) of each of the pathways (transglycosylation and β-elimination) under varying acidic/alkaline conditions as seen via their activation energies. This would also be the first step in developing kinetic models of cellulose pyrolysis that are able to analyse intermediates and not just lumped parameters designated as tars, chars and gases.

1.2 Organization of Thesis and Scope

This thesis is divided into seven main chapters beginning with an Introduction (Chapter 1) that covers research motivation, objectives, thesis overview, and organisation. This is followed by a Literature Review (Chapter 2) on the various aspect of biomass thermal/thermochemical conversion with an emphasis on cellulose. The review starts with the chemistry and mechanisms occurring during cellulose thermal/thermochemical conversion. It also includes relevant areas on cellulose conversion kinetics and the associated thermal analysis methods.

The thesis then moves to the first experimental chapter that looks at the influence of acids and alkalis on cellulose pyrolysis pathways (Chapter 3). This chapter describes and discusses the effects of acids (H_2SO_4, H_3PO_4 and H_3BO_3) and alkalis ($Ca(OH)_2$ and NH_4OH) on the yields of anhydrosaccharides (levoglucosan, levoglucosenone, 1,4:3,6-dianhydro-α-d-glucopyranose, 1,6-anhydro-β-D-glucofuranose). Acid and alkali-infused cellulose were pyrolysed in a fixed-bed reactor system. The condensable pyrolysis products were collected and analysed using a GC-MS to quantify the amount of anhydrosaccharides produced. These anhydrosaccharide yields reflect the relative dominance between the two conversion pathways under the different acid and alkali treatments.

A second method to study the influence of acids and alkalis on cellulose thermal/thermochemical conversion is presented in Chapter 4. Thermogravimetric experiments were conducted to study how cellulose infused with acids (H_3PO_4, H_3BO_3 and H_2SO_4) and alkalis ($Ba(OH)_2$ and $Ca(OH)_2$, NH_4OH) affect the apparent activation

energy of cellulose thermal conversion/degradation. The apparent activation energy was found using the model-free isoconversional method. Subsequently, a model-fitting method based on first-order decomposition kinetics was used to obtain the extent of cellulose conversion via the transglycosylation and β-elimination pathways. The apparent activation energy and the fraction of cellulose conversion via the pathways indicate the relative dominance of the transglycosylation and β-elimination in the presence of acid and alkaline additives.

After having found that using alkalis can enhance the yield of anhydrosaccharides, the study proceeded to demonstrate how selective anhydrosaccharide production from cellulose conversion can be achieved. Chapter 5 covers the thermal/thermochemical conversion of cellulose in neat, acidified (0.13 M H_3PO_4) and alkaline (0.01 M $Ba(OH)_2$) sulfolane (polar, aprotic solvent) at varying temperatures (180 °C, 190 °C, 200 °C, 210 °C and 220 °C) in a batch reactor. Samples from the reactor were measured for pH, anhydrosaccharide and furan levels. Changes in the hydrogen ion [H^+] concentration were studied as a means to manipulate the yields of anhydrosaccharides. A modelling of this conversion process was attempted with a view of analysing its potential utility, limitations and the future work required.

An understanding of the influence of selected acids and alkalis on cellulose thermal/thermochemical conversion was gained from two different methods (anhydrosaccharide quantification and kinetic analysis) used in this study. The insights gained from the study have provided support for our hypothesis that the β-elimination pathway can be suppressed by manipulating [H^+] levels to increase anhydrosaccharide

yields. A novel method for enhancing anhydrosaccharide yields that is based on pathway manipulation is thus proposed in Chapter 6.

Finally in Chapter 7, opportunities to further develop this novel method for anhydrosaccharide production are discussed. Follow up research work is suggested on different ways to achieve optimal [H^+] levels for anhydrosaccharide production. In addition, upstream research work on elucidating the non-trivial and challenging set of intermediates and pathways within cellulosic thermal/thermochemical conversion process was mooted. A potentially interesting method to achieve this is via the use of in situ spectroscopy coupled with spectral deconvolution (e.g. BTEM).

2. Literature Review

Chemical production is currently based mainly on fossil fuels. Although there are currently commercially available chemicals from renewable resources (e.g. butadiene, ethylene glycol, adipic acid and glycerol [33]), they account for less than 1 % of the US$ 4 trillion global chemical market [34, 35]. However, due to the increasing pressures exerted by climate change, fossil fuel depletion and supply volatility, alternative biomass-based feedstocks are currently getting greater attention.

In biomass-to-chemicals conversion, the concept of biorefinery as described by Ragauskas et al. [5] involves the production of a wide variety of fuels, chemicals and materials from lignocellulosic biomass. The use of lignocellulosic biomass as a feedstock in biorefineries is very important especially due to the social, ethical and economic problems [36, 37] in the use of food sources (e.g. sugars and starches) for fuels and chemicals production.

The production of renewable chemicals from lignocellulosic biomass although attractive is not a simple, single-step process. Instead, it requires a series of reactions, as illustrated in Figure 2.1.

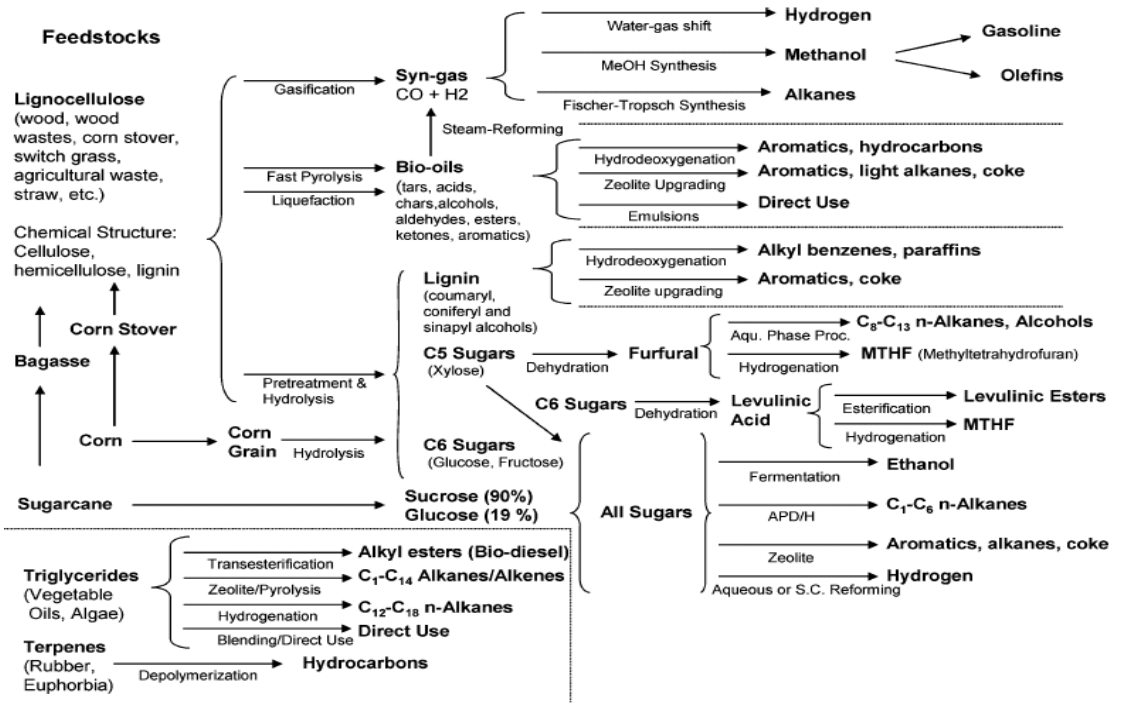

Figure 2.1: Overview of the various routes for the production of fuels and chemicals from lignocellulosic biomass adapted from Huber et al. [38].

At the heart of the thermal conversion of lignocellulosic biomass into chemicals are the three main components namely cellulose, hemicellulose and lignin and this is where the following literature review starts. The thermal conversion of these biomass components produces the three main classes of product that are referred to as chars, tars and gases.

With cellulose being the largest component of biomass and the products of its thermal conversion being of interest, we subsequently delve into the chemistry of cellulose pyrolysis. Cellulose pyrolysis chemistry consists of a complex network of reactions involving numerous intermediates and products. Many different pathways have been proposed but in terms of the initial stage of cellulose pyrolysis there seems to be some consensus that there are at least two main thermal degradation pathways for cellulose. Mirroring these pathways, simplified models and their associated kinetics have been

proposed in the literature. These cellulose thermal conversion models have predominantly been based on a lumped parameter description of chars, tars and gases. The literature review then moves to the main methods for obtaining the kinetic parameters of cellulose thermal conversion from thermogravimetric experiments.

2.1 Thermal Conversion of Biomass

Plant biomass consists of three main components namely, cellulose, hemicelluloses and lignin, The depolymerisation/pyrolysis of the three main biomass components are summarised as follows [19, 39]:

(i) Cellulose (40 – 50 wt%) is a crystalline glucose polymer consisting of linear chains of (1,4)-D-glucopyranose units that are linked 1-4 in the β-configuration. It has an average molecular weight of about 100,000. Cellulose is intermediate in terms of its reactivity and decomposes between 325 °C and 375 °C. The decomposition onset occurs at a higher temperature (and over a narrower range) than hemicellulose and lignin due to its crystalline structure.

(ii) Hemicellulose (20 – 40 wt%) is a mixture of polysaccharides (C5 and C6 sugars). It has a highly branched, amorphous structure with an average molecular weight of less than 30,000. Hemicellulose is also the most reactive component and depolymerises between 225 °C and 325 °C.

(iii) Lignin (10 – 30 wt%) is regarded as a group of amorphous, high-molecular weight biopolymer consisting of 6-carbon ringed, phenyl-propanes as monomers. These 6 carbon rings may have up to 2 methoxy groups attached as side chains. Due to its highly cross-linked structure, lignin is the most thermally stable component and decomposes gradually between 250 °C and 500 °C.

It should be noted that the differences (chemical and physical properties) between these three biomass components along with their varying relative composition in different biomass sources is one of the main reasons behind product variability when they are subjected to thermal conversion.

The main products of biomass pyrolysis can be broadly described as char (solids), condensable organics (liquids), non-condensable organics (gas) and ash (inorganic metals/minerals). The relative fractions of the various solids, liquids and gaseous products are highly dependent on the reactor's operating conditions especially temperature, pressure, heating rates and residence times as shown in Table 2.1 [40].

Table 2.1: Various thermal conversion processes and their typical yields

		Liquid (%)	**Char (%)**	**Gas (%)**
Carbonisation	Low temperature, very long residence time	30	35	35
Pyrolysis	Moderate temperature, short residence time	75	10	15
Gasification	High temperature, long residence times	5	10	85

The gaseous products of biomass depolymerisation would typically consist mainly of carbon monoxide, carbon dioxide, hydrogen, methane and small amounts of other short chain (C2 – C4) hydrocarbons. Meanwhile the solid char produced is not strictly carbon. Instead the various biomass sources have a tendency to produce chars that are primarily polycyclic and aromatic in structure [41]. The chars have a high carbon content (ca. 75 mol%) whilst their hydrogen content (ca. 5 mol%) decreases as the treatment temperature increases. In addition, the oxygen content of the char produced was typically found to be about 20 mol%, which is almost half that of the original biomass.

At heating rates of ca. 50 – 1000 °C/min, the constituents of biomass (cellulose, hemicellulose and lignin) pyrolysis when rapidly cooled or quenched will form a liquid product that is usually termed as pyrolytic liquid or bio-oil. Bio-oil has a water content ranging from 15 – 30 wt%. The water comes from the original moisture within the feedstock and also from dehydration reactions during pyrolysis. The oxygen content of bio-oil (35 – 40 mol%) is similar to that of the original biomass source used in the pyrolysis.

Bio-oil is a multi-component mixture comprising of acids, alcohols, aldehydes, esters, ketones, sugars, phenols, guaiacols, syringols, furans, lignin derived phenols and terpenes with multi-functional groups [38, 42]. A significant proportion (ca. 30 – 40 %) of components identified is phenols with ketones and aldehydes groups attached. The abundance of acids, alcohols, aldehydes, ketones, sugars, phenols, guaiacols, syringols present in bio-oil make it hydrophilic resulting in water removal difficulties.

To carry out the thermal conversion of biomass, a number of pyrolysis technologies ranging from the more established to the novel has been proposed. This spectrum of pyrolysis techniques included fixed/fluidised beds [43, 44], ablative [45], plasma [46], microwave [47], hot-compressed water [48], supercritical water [49] and liquefaction/solvolysis [50-52]. The various thermal conversion technologies [40, 42, 53] are summarised in Appendix B1.

2.2 Cellulose Pyrolysis Chemistry

Due to it being the largest component of plant biomass, cellulose pyrolysis has been the subject of many studies with reviews that looked at its chemistry [54-56], products [14, 57], mechanisms and kinetics [58, 59]. Recently Mamleev et al. [18] proposed a phenomenological description of cellulose pyrolysis. The initial thermal degradation pathway is via intermolecular transglycosylation reactions within the glucose monomers of cellulose [18, 19]. This depolymerisation is illustrated in Figure 2.2.

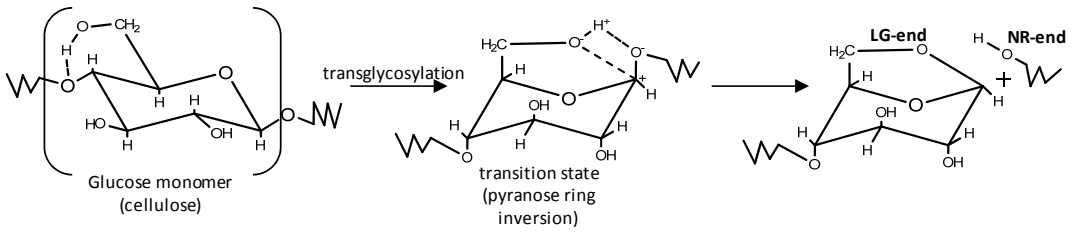

Figure 2.2: Cellulose depolymerisation via transglycosylation within the glucose monomers leading to levoglucosan (LG) ends and non-reducing (NR) ends formation.

During thermal degradation/conversion, temperatures within the cellulose matrix have been found via experimental and numerical simulations to have a practical limitation

of circa 500 °C [60, 61]. At these temperatures, a fusion-like behaviour analogous to melting occurs and produces an intermediate liquid compound (ILC). It is however important to note that the temperature stabilisation seen to correspond with the fusion of cellulose/biomass is a purely thermophysical effect and not a real change of phase of a solid into a liquid. Lédé [62] had used the term intermediate active cellulose (IAC) to describe the phenomenon. He noted that IAC was characterised by a decrease in cellulose's degree of polymerisation and although it was not a true liquid, it can be considered as a high viscosity substance. Lédé indicated that IAC had varying physicochemical properties that depended on experimental conditions (e.g. temperature, heating rate, residence time).

Apart from transglycosylation, formation of liquid tar from cellulose can also occur via β-elimination. Under this mechanism, volatile acids (e.g. carboxylic acids) formed from the initial cellulose decomposition are able to attack the remaining cellulose as Brønsted acids thus catalysing heterolytic (ring-opening) reactions as shown in Figure 2.3.

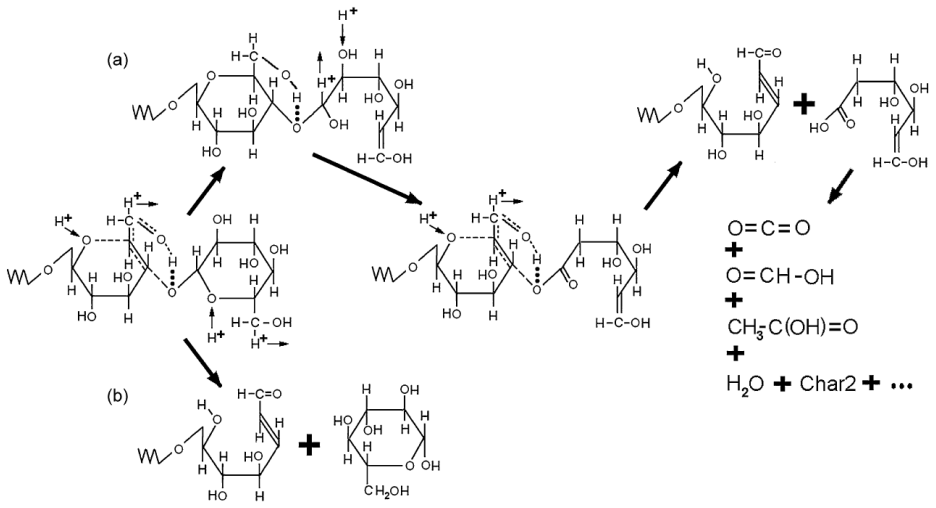

Figure 2.3: Scheme proposed by Mamleev for the formation on carboxyl groups from NR-ends via β-elimination

However, according to the model proposed by Mamleev et al. [18], the acid catalyst exists only within the liquid tar that has been formed and can thus only attack the non-reducing (NR)-ends of cellulose chains that come in contact with this liquid (ILC). Hence, if this liquid tar is removed (along with the volatile acids), this will result in a theoretical yield of 100 % levoglucosan. This aspect of the model helps explain the observation that under vacuum pyrolysis, which encourages the speedy removal of liquid tar formed within the cellulose matrix, the yield of levoglucosan could reach 70 % of the total pyrolysate [63]. Hence, from this observation, we can infer that it might be possible to enhance levoglucosan yields by either removing or neutralising the acids. Alternatively, we should also be able to reduce levoglucosan yields by increasing/adding acids during cellulose thermal degradation.

The production of light gases is the result of fragmenting chain ends of cellulose macromolecules and liquid tar and hence is considered to be a secondary reaction. They are secondary in nature due to them occurring after initial depolymerisation has occurred and requiring the presence of volatile acid catalysts.

Char can be formed via both pathways (i.e. transglycosylation and β-elimination). Experiments have shown that a decrease in initial mass of a cellulosic sample leads to a decrease in char yield. Mamleev et al. [18] indicated that when the initial mass of a sample tends to zero, cellulose should completely decompose towards levoglucosan. It can be inferred that a smaller amount of sample with a corresponding decrease in bed height would decrease the contact time between the volatilising tars and the organic acids from pyrolysis. The reduced residence time within the bed then minimises the organic acids' catalytic effect on subsequent char forming dehydration reactions.

2.2.1 Cellulose Pyrolysis Mechanisms

In their study of cellulose pyrolysis in the presence of flame retardants, Byrne et al. [64] observed that anhydrosaccharides were important intermediates in the degradation process. Following Madorsky et al. [65], Byrne and co-workers proposed that there were two main reaction routes. The first route involved intramolecular rearrangements that yielded anhydrosaccharides whilst the other route involved the formation of carbonium ions that decompose irreversibly (fragmentation).

Based on the observations of two competing pathways for cellulose pyrolysis, Mamleev et al. [18] proposed a cellulose thermal conversion/pyrolysis scheme as shown in Figure 2.4.

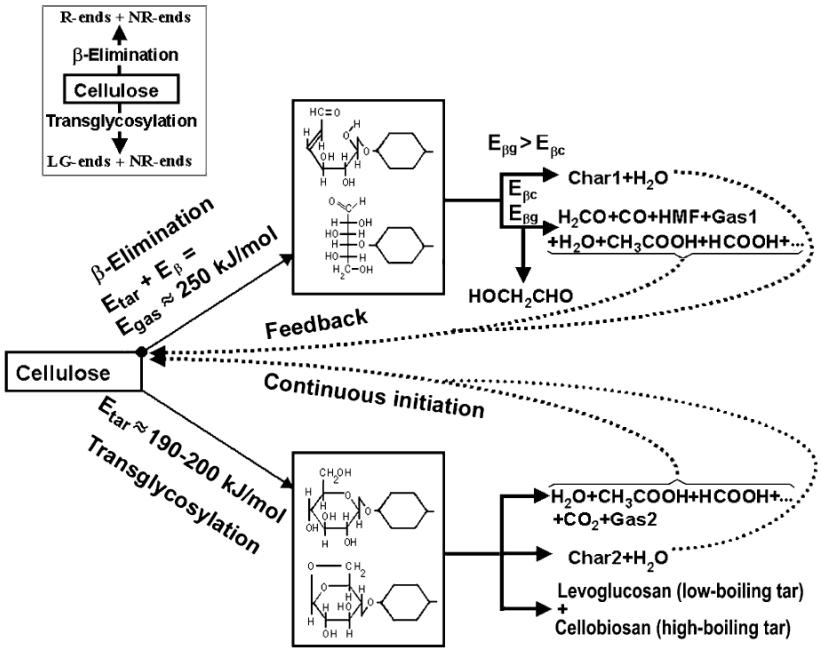

Figure 2.4: Cellulose pyrolysis scheme as proposed by Mamleev et al. [18] which includes an acid-catalysed pathway.

This new cellulose pyrolysis scheme is significantly different from earlier schemes such as the one described by Shafizadeh [20] (see Appendix B2). Shafizadeh's [20] scheme is rather popular and is still currently being used as evidenced by the recent paper by Lin et.al [21]. The major difference between these schemes and the scheme by Mamleev et al. [18] lies mainly in the existence of a second, acid-catalysed pathway (β-elimination).

Apart from the scheme proposed by Mamleev at al. [18], another mechanism for the thermal degradation of cellulose was proposed by Shen and Gu [22]. Here, five chemical pathways for cellulose conversion were suggested out of which two were similar to the transglycosylation and ring-opening routes described earlier. They had also noted that the production of levoglucosan and other anhydrosaccharides were competing against the formation of furans (furfural and 5-hydroxymethyl-furfural). In addition, the chemical reaction pathways that were proposed also showed the possibility of further breakdown of anhydrosaccharides to form furans and other light volatiles (e.g. hydroxyacetone, acetic acid and glyceraldehyde).

Modelling work using density functional theory (DFT) and kinetic calculations were carried out by Zhang et al. [66] to find the Arrhenius parameters for cellulose conversion to levoglucosan and formaldehyde. The results indicated that the activation energy for the levoglucosan formation pathway was 135.9 kJ/mol whilst that for formaldehyde was 203.1 kJ/mol. Qualitatively, this seems to be consistent with the experimental observation of a lower activation energy pathway for transglycosylation and a higher activation energy pathway for β-elimination (ring opening).

2.2.2 Effect of Acidic/Alkaline Additives on Pyrolysis Chemistry

In addition to the hypothesised role of volatile acids in pyrolytic chemistry, it has also been known that acid or alkali content has a significant impact on the yields and product composition during direct liquefaction. Alkalis (e.g. NaOH, KOH, $Ca(OH)_2$) have been routinely used as a catalyst [67-69] in the direct liquefaction of biomass

Budarin and co-workers produced bio-oils via microwave pyrolysis of wheat straw [70]. At the same time, they made use of acidic (HCl and H_2SO_4) and alkaline (NH_3) additives to effect changes in the product distribution and composition of the bio-oils. In this study, the wheat straw pellets were treated with aqueous H_2SO_4 but HCl and NH_3 were introduced as gases. The levoglucosan yields of acid and alkaline treated biomass compared with untreated biomass are shown in Table 2.2 below.

Table 2.2: Comparison of the effects of acids and alkalis on biomass pyrolysis yields.

	Budarin et al.			**Hassan et al.**				
additives	H_2SO_4	HCl	NH_3	H_3PO_4	H_2SO_4	NaOH	$Ca(OH)_2$	NH_4OH
levoglucosan	↓ 26%	↑ 27%	↑ 66%	↓ 54%	↓ 61%	↓ 49%	↑ 72%	↑ 41%

Budarin's results were rather mixed with no clear discernable trends between acidic and alkaline additives. Based on the H_2SO_4 and NH_3 results, we can see that the acid decreased levoglucosan yields whilst the alkali gave the opposite result. A similarly mixed trend was also observed based on the results obtained by Hassan et al. [71] who studied bio-oils from pyrolysed pine wood. We again note that with the exception of NaOH, the other alkalis seem to increase levoglucosan yield. Although some of the results were conflicting, there seems to be some evidence that supports the hypothesis

of acid catalysis activating β-elimination and the suppression of β-elimination and promotion of transglycosylation by alkalis.

In contrast with the results obtained by Budarin et al. [70] with HCl, Muller-Hagedorn et al. [72] studied three different wood species that have been treated with potassium salts (KCl, $KHCO_3$ and K_2SO_4). In this study, it was observed that chlorides have the highest influence in suppressing levoglucosan yield with the order being $Cl^- > SO_4^{2-} > HCO_3^-$.

Similarly, it was also observed that sodium, potassium and calcium ions generally prevents the formation of anhydrosaccharides (e.g. levoglucosan) and increases the relative yields of lower molecular weight compounds (e.g. aldehydes, ketones). As reported by Muller-Hagedorn et al. [72] and Patwardhan et al. [73], the inhibiting influence of the cations are in the order of $K^+ > Na^+ > Ca^{2+}$. Recently, Saddawi et al. [74] have conducted ab initio, DFT modelling of sodium and potassium infused cellulose. The modelling indicated that sodium and potassium could form chelated structures via multiple interactions with the hydroxyl and ether bonds within cellulose. The metals ions chelated at the C6 position in the ring interacts with four oxygen atoms whilst the C2 position allows interaction with two oxygen atoms. The stability of the chelated structures was found to be higher at the C6 position. It was then hypothesised that the changes in geometry due to chelation could favour ring opening thus increasing cellulose degradation by cracking. This would explain the reduction in levoglucosan yields that were observed by other researchers.

In view of our main objective of enhancing the yield and selectivity of valuable anhydrosaccharides, the literature has revealed one major contradiction. It was found that the state-of-the art relied on the use of acids to improve yields. This contradicts the view that acids promote one of the two main cellulose conversion pathways (β-elimination) at the expense of the transglycosylation pathway that generates the anhydrosaccharides.

These apparently conflicting results on the effects of acid and alkalis on cellulose conversion could indicate that the acids might have affected cellulose thermal conversion in other ways not directly related to the two pathways (transglycosylation and β-elimination). Indeed, there is evidence in the literature that show acids having a significant effect on the physical characteristics of cellulose such as ash (inorganic impurity) content, crystallinity and degree of polymerisation. Shafizadeh et al. [23] found that distilled water and dilute acid (H_2SO_4) washes resulted in increased yields of tar and levoglucosan. These experiments raised the possibility that the improved yields of levoglucosan were due to the removal of inorganic impurities or changes in the crystallinity or structure of the cellulose due to the acid pre-treatments.

The presence of H_3PO_4 has been shown by Dobele et al. [24] to alter the relative proportion of levoglucosan (LG) and levoglucosenone (LS) produced from cellulose pyrolysis. As an acid, H_3PO_4 was able to enhance the dehydration of levoglucosan into levoglucosenone. Although H_3PO_4 might appear to raise levoglucosenone levels, the overall anhydrosaccharide (LG+LS) yield showed a downward trend with the anhydrosaccharides decreasing from 23 % to 17 % at higher H_3PO_4 concentrations.

In tandem with this dehydration effect, H_3PO_4 also affected the levoglucosenone yields by changing the degree of polymerisation (DP) and crystalinity of the cellulose sample through a hydrolytic pre-treatment [25]. Dobele et al. [25] concluded that the infusion of cellulose with an acidic catalyst such as H_3PO_4 and subsequent heat treatment resulted in a decrease of DP by hydrolysis in the amorphous regions of cellulose. It is likely that these regions form the basis of nucleation sites as described by Mamleev et al. [18] where cellulose depolymerisation initiates at the interface between the intermediate liquid compound (ILC) and solid cellulose matrix.

In a related work by Dobele et al. [26] that studied the use of biomass (including microcrstalline cellulose) infused with H_3PO_4, they found that elevated production of anhydrosachharides (LG+LS) could be achieved. Dobele et al. [26] found that there was an initial increase in anhydrosaccharide (LG+LS) yield at low infusion level of H_3PO_4 into cellulose from ca. 13 % (untreated) to ca. 63 % (0.5 % H_3PO_4). However, subsequent increase in H_3PO_4 infusion levels resulted in a decrease of anhydrosaccharide yield to ca. 44 % (2.5 % H_3PO_4).

These experiments [24-26] show that H_3PO_4 have two different effects on cellulose pyrolysis namely dehydration and hydrolysis. The acid was able to enhance the yield of levoglucosenone via the dehydration of levoglucosan thus shifting the product composition. In addition, hydrolysis of cellulose by H_3PO_4 and the subsequent decrease in DP resulted in increased anhydrosaccharide yield. However, there seems to be a limit to this increase because higher H_3PO_4 infusion levels showed a decreasing trend in the anhydrosaccharide produced.

Acids were also found to have an effect on the mechanism of cellulose pyrolysis. Cellulose pyrolysis in acidified (H_2SO_4 and H_3PO_4) sulfolane was carried out by Kawamoto et al. [75] with levoglucosenone (LS), furfural (FF), and 5-hydroxymethyl furfural (HMF) being the focus of the study. It was found that the acids promoted the formation of levoglucosenone but at higher acid level (1 wt% H_2SO_4), the level of levoglucosenone decreased significantly whilst the furans (FF+HMF) increased to become the major pyrolysis product. At the same time, water was seen to play an important role in furan formation. Pyrolysis conducted under vacuum (0.1 atm) to remove water formed during dehydration reactions lowered furan yields and increased levoglucosenone levels. In contrast, when pyrolysis experiments were done under steam distillation conditions, higher furan levels and lower levoglucosenone levels were seen.

Another possible interpretation of these results was that the volatile organic acids were removed under vacuum whilst under steam distillation, the organic acids remained behind and acted with the mineral acid to lower the levoglucosenone level. Kawamoto et al. [75] attributed the higher furan formation to the presence of water within the pyrolytic reaction mixture and they proposed a mechanism for the conversion of levoglucosenone into furfural via an oxonium ion intermediate. Although this might be true, alternative mechanisms proposed by Agarwal et al. [30] and Mettler et al. [31] showed the possibility of furan formation directly from cellulose without an anhydrosaccharide intermediate. Therefore, Kawamoto et al. [75] results could be reinterpreted as showing that an acid-catalysed, parallel, competing reaction promoted the formation of furans from cellulose.

The different and conflicting results show that the state-of-the-art method for enhancing anhydrosaccharide yields by the use of acids act through altering the physical state of the cellulose before thermal conversion. The acids achieved this via one or a combination of inorganic impurities removal, changes in the crystallinity and degree of polymerisation. In addition, relatively higher yields of levoglucosenone were achieved via acid dehydration of levoglucosan. However, the literature has shown that levoglucosenone yield enhancements were limited when higher levels of acids were introduced. This supports the view that ultimately, the acids would promote the β-elimination pathway. This shift to the β-elimination pathway is at the expense of transglycosylation which is the route for anhydrosaccharide formation

Hence, experiments that demonstrate the influence of acids and alkalis on the thermal conversion pathways of cellulose and the corresponding anhydrosaccharide yields are needed. This would allow us to demonstrate a new method to enhance anhydrosaccharide yield and selectivity based on pathway manipulation.

2.2.3 Conversion of Cellulose into Anhydrosaccharides

As observed in Section 2.2.1 and Section 2.2.2, cellulose can be converted into a number of anhydrosaccharides. Among them are the high value-added chemicals levoglucosan (LG: 1,6-anhydro-β-D-glucopyranose) and levoglucosenone (LS: 1,6-anhydro-3,4-dideoxy-β-D-pyranosen-2-one). These chemicals are particularly useful for organic synthesis due to their chirality and can serve as important intermediates

[32] for the manufacture of pharmaceuticals, polymers and surfactants. However, they are not widely utilised due to their high cost

Anhydrosaccharides such as LG and LS are usually obtained via a thermal conversion process (pyrolysis) which converts dried cellulosic biomass into a liquid bio-oil (as discussed in Section 2.1) consisting of these valuable chemicals. Cellulose pyrolysis is typically performed under high temperatures (400-600 °C) to maximize bio-oil yield [76]. Under conditions of fast pyrolysis, an LG yield of ca. 30 to 35 wt% (dry feed basis) have been reported whilst vacuum pyrolysis has been reported to achieve yields of ca. 40 to 50 wt% (dry feed basis) [23, 77, 78]. Investigations with superheated steam have also been carried out to maximize oil yield in cellulose pyrolysis but apparently very low amount of LG was detected [79]. The bio-oils obtained from such processes are mixed with other organic products within a viscous, tarry matrix which is difficult to separate. This complex, acidic mixture is unstable as the constituents (including LG and LS) can further react thus lowering the recoverability of these valuable intermediates.

2.2.3.1 Methods for increasing yields from thermal conversion of cellulose

To address the issue of low yield and selectivity of LG and LS from cellulose pyrolysis, several methods have been attempted.

One main method used to boost anhydrosaccharide yield is the pre-treatment of cellulose/biomass with mineral acids such as sulphuric and phosphoric acids [26, 80-82]. It is likely that the pre-treatment of cellulose in hot acids (ca. 100 °C) partially

hydrolyse the raw material and remove alkaline cations that would otherwise promote char and gas production during pyrolysis. This then enhances the yield of anhydrosaccharides, especially LG. This partial breakdown of the crystalline structure of cellulose to form larger/more amorphous regions, allows depolymerisation of cellulose via transglycosylation. In this mechanism, the β(1→4)-D-glycosidic bonds in cellulose cleaves repeatedly and practically unzips the cellulose chain thus producing the anhydrosaccharides.

Another method by Dobele et al. [83] involved Fe^{3+} ions introduced in the form of iron (III) sulphate. The results obtained indicated an anhydrosaccharide (LG+LS) yield of ca. 30 to 45 wt%. An important observation in those experiments was that anhydrosaccharide yields at the higher end of the reported range were obtained when Fe^{3+} ions were introduced via the ion-exchange method. In the ion-exchange method, there was the added benefit of SO_4^{2-} anion removal. It has been observed [70, 71] that the presence of SO_4^{2-} anion seemed to suppress anhydrosaccharide yields.

A third method is based on heterogeneous catalysis. Solid catalysts such as nanopowder metal oxides containing titanium and aluminium [84] were physically mixed with cellulose and the pyrolysis products showed a yield of ca. 15 to 23 wt% of anhydrosaccharides (LS in greater amounts than LG). Another example of this method is the use of sulphated zirconia by Wang et al. [85]. In their experiments, Wang et al. [85] showed that the solid catalyst had a similar performance to the usual phosphoric acid pre-treatment method. The LS yields for sulphated zirconia were ca. 8 wt%.

The fourth method differs from the other methods in that the thermochemical conversion of cellulose takes place within a liquid medium (i.e. wet pyrolysis). Here, instead of acid pre-treatment, the conversion takes place within an acidified, polar, aprotic solvent (e.g. sulfolane) [75, 86-88]. Wet pyrolysis of cellulose in sulfolane with sulfuric acid or phosphoric acid gave levoglucosenone (LS), furfural (FF), and 5-hydroxymethyl furfural (HMF) up to 42.2 %, 26.9 %, and 8.8 %. Water content in the reaction mixture was found to be a crucial factor in determining product selectivity between levoglucosenone and furfural.

In a further variation, solid acid catalysts (i.e. ion-exchange resins, metal oxides, clay and zeolites) were used to convert glucose in polar, aprotic solvents (e.g. dimethylformamide - DMF, dimethyl sulfoxide - DMSO) [89]. Among the solid acid catalysts used, the most successful was Amberlyst-15 (an ion exchange resin) which was able to convert glucose into anhydrosaccharides at yields ranging from 32 to 62 %. Further work involving solid acid and basic catalysts was shown to selectively convert glucose into either anhydrosaccharides or HMF as shown in Figure 2.5 [90]. Here, it is important to note that the formation of anhydrosaccharides and furans is achieved using glucose (monosaccharide) instead of cellulose (polysaccharide). The typical conversion of cellulose to glucose ranges from 20 to 70 % thus the overall yield of anhydrosaccharides (via a 2-stage conversion) would in this case be ca. 40 %.

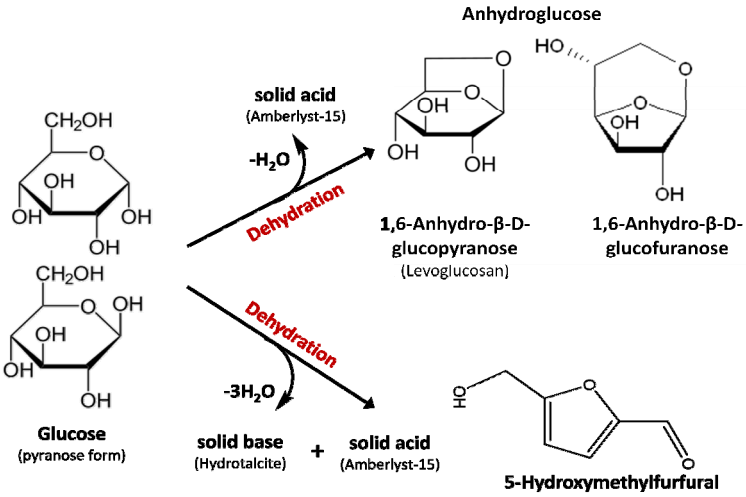

Figure 2.5: Selective dehydration of glucose to anhydroglucose and 5-hydroxymethylfurfural

Ionic liquids have also been used as a solvent in the pyrolysis of lignocellulosic materials to produce anhydrosaccharides and furans [91]. Ionic liquids are able to at least partially dissolve the lignocellulosic particles, thereby enabling a more homogeneous conversion under milder conditions (150 °C to 300 °C). The reported yield of LG was less than 1 % and LS was ca. 3 %.

In the area of levoglucosan and levoglucosenone production, the state-of-the-art methods mainly focussed on the use of acids. This is not surprising especially seen in the light of conflicting results reviewed in Section 2.2.2.

2.3 Biomass Pyrolysis Models and Kinetics

Another important aspect to the thermal conversion of cellulose is the kinetics associated with the reaction pathways. Here, we will cover the various mathematical

models researchers have adopted to determine how fast and how much biomass/cellulose has converted to its products.

2.3.1 Biomass Pyrolysis Modelling

Pyrolysis chemistry alone will not be able to predict the conversion rates of the biomass and its corresponding product distribution. Hence, in order to model pyrolysis processes most researchers have opted to combine reaction kinetics with momentum, heat and mass transport [58, 92-94]. An overview of the physical and chemical process involved in pyrolysis was given by Di Blasi [95] and is shown as a visual summary in Figure 2.6.

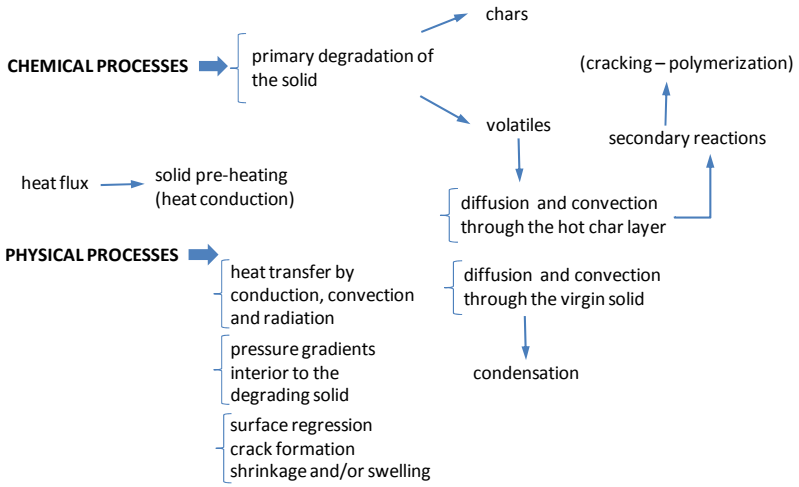

Figure 2.6: Di Blasis's [95] overview of the physical and chemical processes involved in biomass pyrolysis.

Pyrolysis of biomass is conducted on pieces of biomass ranging from wood chips (1×10^{-2} m) to powders (10×10^{-6} m). Apart from the chemical reactions taking place as mentioned in Section 2.2, other factors that would affect the overall pyrolysis

behaviour would include macroscopic effects such as diffusion of gases and vapours, intraparticle fluid flow and convective/conductive heat transfer. Chan et al. [93] had conducted an analysis into these factors based on the permeability, effective diffusivity and effective thermal conductivity for wood. A similar analysis of the time scales of the various transport phenomena in comparison with pyrolysis rates at temperatures and length scales of interest to this study is shown in Table 2.3 whilst the calculation details are shown in Table 2.4. The analysis by Chan et al. [93] assumed that the porous structure remained constant without specific consideration for pore sizes.

Table 2.3: Estimation of time scales for physical and chemical processes during biomass pyrolysis

	Characteristic time (s)					
	(r=10 μm)		(r=100 μm)		(r=1000 μm)	
	500 K	1000 K	500 K	800 K	500 K	800 K
Diffusion mass transfer[a]	10^{-4}	0.3×10^{-4}	10^{-2}	0.3×10^{-2}	10^{0}	0.3×10^{0}
Mass transfer volatile flow[b]	10^{-6}	0.6×10^{-4}	10^{-4}	0.6×10^{-4}	10^{-2}	0.6×10^{-2}
Convective heat transfer[c]	10^{-3}	$>10^{-4}$	10^{-2}	$>10^{-2}$	10^{-1}	$>10^{-1}$
Conductive heat transfer[d]	10^{-4}	$>10^{-4}$	10^{-2}	$>10^{-2}$	10^{0}	$>10^{0}$
Pyrolysis[e]	4×10^{6}	2×10^{-1}	4×10^{6}	1×10^{-1}	4×10^{6}	1×10^{-1}

Table 2.4: Expressions and values for time scale estimation of physical and chemical processes [93].

[a]: r^2/D_{eff}	$D_{eff} \approx 10^{-6}$ m^2s^{-1}.
[b]: $\mu r^2/pB_o$	$\mu \approx 10^{-5}$ Pa.s, $p \approx 10^5$ Pa, $B_o \approx 10^{-14}$ m^2.
[c]: $r(\rho c_p)_g/h$	$(\rho c_p)_g \approx 10^3$ $Jm^{-3}K^{-1}$, $h \approx 10^{-6}$ $Jm^{-2}s^{-1}K^{-1}$.
[d]: $r^2(\rho c_p)_s/k$	$(\rho c_p)_s \approx 10^3$ $Jm^{-3}K^{-1}$, $k \approx 10^{-1}$ $Jm^{-1}s^{-1}K^{-1}$.
[e]: $A\exp(-E/RT)$	$A \approx 10^8$ s^{-1}, $E \approx 140$ $kJmol^{-1}$.

Based on the estimates in Table 2.3, we can see that at temperatures near pyrolysis onset (ca. 500 K), heat and mass transfer processes are several orders of magnitudes faster that the pyrolysis rates. However, as temperature rises to ca. 1000 K, the pyrolysis rates are similar to the heat and mass transfer rates especially when we consider larger biomass particle dimensions (> 100 μm).

Hence, if we carry out experiments using very finely crushed biomass material or powdered cellulose (particle size < 100 μm) and operate at temperatures less than 1000 K, the effects of heat and mass transfer processes can be neglected relative to the reaction rates. In this study, the microcrystalline cellulose powders used had a particle size of ca. 50 μm.

2.3.2 Pyrolysis Kinetics Schemes

A critical component of an integrated pyrolysis model as described by Di Blasi [95] (Figure 2.6) is the reaction kinetics. Much work has been done in the study of

pyrolysis kinetics and several reviews [6, 95-98] have been published on them. Biomass pyrolysis involves numerous reactions interlinked into a complex network with a large number of intermediates and end products. It has been reported that more than 300 compounds [42] have been identified within the condensed organic fraction of pyrolysis along with non-condensable gases (e.g. CO, CO_2, H_2 and CH_4) and solid char.

Hence, formulating an exact reaction mechanism and kinetics to accommodate all the chemical species involved is extremely difficult. Most researchers have simplified the numerous intermediates and end products by considering groups of products in what is commonly referred to as lumped parameter analysis. The end products of pyrolysis have been lumped into three main groups namely tar, char and gases. Several types of reaction mechanisms have been proposed by a number of authors. These mechanisms (or kinetic models) can be broadly classified as:

(i) Single-stage global models

(ii) Single-stage, multi-reaction models

(iii) Multi-stage, semi-global models

2.3.2.1 Single-stage global models

Single-stage global models are the simplest of all the kinetic schemes that have been proposed. It involves a straight forward conversion of the biomass material into volatiles and char in one direct reaction step as shown in (M 1) and (M 2).

$$\mathbf{biomass}_{(s)} \xrightarrow{k} \mathbf{volatiles}_{(g)} + \mathbf{char}_{(s)} \quad \text{(M 1)}$$

$$\mathbf{biomass}_{(s)} \xrightarrow{k} \mathbf{gases}_{(g)} + \mathbf{tar}_{(l)} + \mathbf{char}_{(s)} \quad \text{(M 2)}$$

The reaction rate (k) is expressed in an Arhenius form as expressed in equation (2.1) where A is the pre-exponential factor and E is the activation energy. Some typical kinetic data for single-step global biomass pyrolysis [94, 95, 97] is summarised in Table 2.5

$$\boldsymbol{k = A\exp\left(-E/RT\right)} \quad (2.1)$$

The kinetics are modelled as a unimolecular, first-order reaction rate which can be expressed as:

$$\frac{\partial \rho_S}{\partial t} = -\boldsymbol{k}\left(\rho_S - \rho_C\right) \quad (2.2)$$

where the char density is expressed as a constant fraction of the dry solid biomass density $\rho_C = \boldsymbol{c}\rho_{SD}$

In addition, if this model is used to estimate the distribution of tars and gases, an additional coefficient needs to be introduced as shown in equations (2.3) and (2.4).

$$\frac{\partial \rho_T}{\partial t} = \boldsymbol{ak}\left(\rho_S - \boldsymbol{c}\rho_{SD}\right) \quad (2.3)$$

$$\frac{\partial \rho_G}{\partial t} = \boldsymbol{(1-a)k}\left(\rho_S - \boldsymbol{c}\rho_{SD}\right) \quad (2.4)$$

Table 2.5: Some typical values of kinetic constants for single-stage global models

Feedstock	Temperature (K)	*E* (kJ/mol)	*A* (1/s)
Hardwood	677 - 822	89.52	1.483×10^{6}
Wild cherry	538 - 593	173.7	1.483×10^{11}
Forest waste	498 - 598	124.87	7.68×10^{7}
Cellulose	600 - 850	100.5	1.2×10^{6}
Cellulose	580 - 1070	8.8 – 33.4	0.019 – 0.14
Cellulose	450 - 700	71	6.79×10^{3}
Cellulose	520 - 1270	139.6	6.79×10^{9}
Cellulose	520 - 1270	166.4	3.9×10^{11}
Hemicellulose	520 - 1270	123.7	1.45×10^{9}
Lignin	520 - 1270	141.3	1.2×10^{8}

.

The great variations in the kinetic constants are probably due to different experimental equipment and conditions. The major limitation of single-stage global models is their inability to predict the composition of the volatile fraction and to account for the components that are typically found in biomass. Hence, these models are not suitable for use in comprehensive pyrolysis reaction modelling.

2.3.2.2 Single-stage, multi-reaction models

In order to address single-stage global models' inability to provide a realistic distribution of char, tar and gases, biomass pyrolysis is expressed as a number of parallel reactions as illustrated in model (M 3).

$$\textbf{biomass} - \textbf{component}_{(i)} \xrightarrow{ki} \textbf{volatiles}_{(g)} + \textbf{char}_{(s)} \qquad \text{(M 3)}$$

$$\textbf{cellulose}_{(s)} \xrightarrow{k1} \textbf{volatiles}_{(g)} + \textbf{char}_{(s)}$$

$$\textbf{hemicellul ose}_{(s)} \xrightarrow{k2} \textbf{volatiles}_{(g)} + \textbf{char}_{(s)}$$

$$\textbf{lignin}_{(s)} \xrightarrow{k3} \textbf{volatiles}_{(g)} + \textbf{char}_{(s)}$$

Now, the biomass solid consumption is expressed as the sum of the consumption of the individual components as shown in Equation (2.5).

$$\frac{\partial \rho_s}{\partial t} = -\sum_i k_i \left(\rho_{si} - \rho_{ci}\right) \qquad (2.5)$$

$$\frac{\partial \rho_s}{\partial t} = -k_1\left(\rho_{s1} - \rho_{c1}\right) - k_2\left(\rho_{s2} - \rho_{c2}\right) - k_3\left(\rho_{s3} - \rho_{c3}\right) \qquad (2.6)$$

$$\frac{\partial \rho_s}{\partial t} = -k_1\left(\rho_{s1} - c_1\rho_{sD}\right) - k_2\left(\rho_{s2} - c_2\rho_{sD}\right) - k_3\left(\rho_{s3} - c_3\rho_{sD}\right) \qquad (2.7)$$

Similarly, if we require the distribution of tars and gases to be modelled, we need to introduce another 3 stoichiometric coefficients as shown in Equations (2.8) and (2.9).

$$\frac{\partial \rho_T}{\partial t} = -\alpha_1 k_1 (\rho_{S1} - c_1 \rho_{SD}) - \alpha_2 k_2 (\rho_{S2} - c_2 \rho_{SD}) - \alpha_3 k_3 (\rho_{S3} - c_3 \rho_{SD}) \quad (2.8)$$

$$\frac{\partial \rho_G}{\partial t} = -(1-\alpha_1) k_1 (\rho_{S1} - c_1 \rho_{SD}) - (1-\alpha_2) k_2 (\rho_{S2} - c_2 \rho_{SD}) - (1-\alpha_3) k_3 (\rho_{S3} - c_3 \rho_{SD}) \quad (2.9)$$

Although this model is now able to account for variations in the biomass composition, it is still limited because we would now need to specify a total of 6 coefficients. This method was used by Gronli [99] and the relevant kinetic parameters are shown in Table 2.6.

Table 2.6: Reaction rate constants and stoichiometric coefficients used by Gronli

Reaction i	Component	A_i (1/s)	E_i (kJ/mol)	a_i	c_i
1	Hemicellulose	1.56×10^{8}	119	0.31	0.2
2	Cellulose	2.51×10^{19}	260	0.31	0.2
3	Lignin	5.01×10^{3}	81	0.31	0.5

.

Another form of the single-stage, multiple reaction model was proposed by Shafizadeh and Chin [100] as described in (M 4)

$$biomass_{(s)} \xrightarrow{k} (product)_i \quad (M\ 4)$$

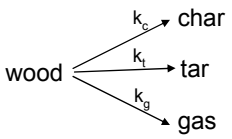

This alternate form of the single-stage, multi reaction model is more robust in its representation of biomass pyrolysis. It does not require the introduction of stoichiometric coefficients in order to obtain the distribution of char, tars and gases. The model is able to achieve this via the relative reaction rates for the production of char, tars and gases.

However, this model seems to allow the formation of char without the corresponding generation of gases if we set $k_g = 0$. Such a situation is not likely given the current understanding of pyrolysis which points to the cracking of tarry intermediates (e.g. levoglucosan and anhydrosacharides) simultaneously producing both char and non-condensible gases.

The conservation equations for the solid fractions can be described as follows:

$$\frac{\partial \rho_S}{\partial t} = -\left(k_c + k_t + k_g\right)\rho_S \tag{2.10}$$

$$\frac{\partial \rho_C}{\partial t} = k_c \rho_S \tag{2.11}$$

Whilst the volatiles are described in the following equations.

$$\frac{\partial \rho_T}{\partial t} = k_t \rho_S \tag{2.12}$$

$$\frac{\partial \rho_G}{\partial t} = k_g \rho_S \tag{2.13}$$

A recent development in one-stage, multi reaction kinetics is the use of distributed activation energy (DAE) method. In the DAE scheme, the pyrolysis reaction is represented by a set of independent and parallel Arrhenius-type reactions. The pre-exponential factors for all the parallel reactions are assumed to be the same. The biomass reactivity is subsequently represented by a continuous distribution of the activation energy (usually a Gaussian distribution).

In spite of all the developments, single-stage multiple reactions' main drawback is that they cannot account for secondary reactions (e.g. the cracking of tars to form chars and gases).

2.3.2.3 Multi-stage, semi-global models

Multi-stage schemes were developed as a response to the need for including secondary reactions into biomass kinetics schemes. This is especially significant at high thermal conversion temperatures and long residence times due to higher extent of tars cracking into light volatiles. Several multi-stage kinetics schemes have been developed over the years and a few of the more popular ones are described here.

Broido [101] had initially proposed a single-stage, multi-reaction type kinetic scheme which had a fixed char fraction of 0.35. Subsequently, Bradbury et al. [102] had modified the scheme to include an intermediate called active cellulose as illustrated in models (M 5) and (M 6)

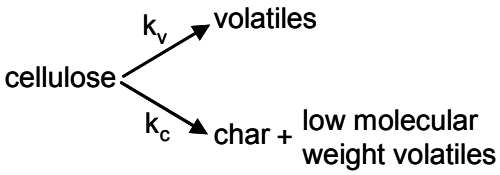

(M 5)

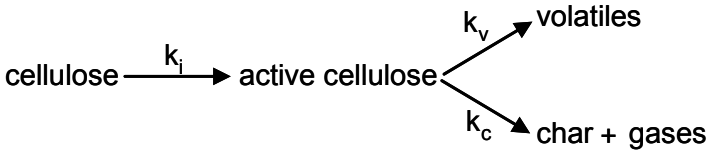

(M 6)

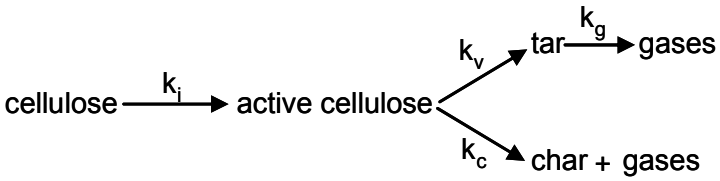

(M 7)

Table 2.7: Kinetic constants for the basic Broido model and its extensions [102, 103].

Reaction i	A_i (s^{-1})	E_i ($kJ.mol^{-1}$)
i	2.83×10^{19}	242.8
v	3.17×10^{14}	198.0
c	1.32×10^{10}	150.7
g	4.28×10^{6}	108.0

The scheme proposed by Bradbury et al. [102] is also sometimes referred to as the Broido-Shafizadeh model and is one of the most widely used multi-stage, semi-global models. It is frequently used to represent biomass pyrolysis kinetics within a comprehensive model that includes heat and mass transport.

Liden et al. [103] extended the basic Broido-Shafizadeh model by including a secondary reaction where the tar reacts further to produce light gases as shown in (M 7). The kinetic constants for the Broido model and its subsequent modifications are listed in Table 2.7.

The Broido-Shafizadeh model is therefore expressed as follows:

$$\frac{\partial \rho_S}{\partial t} = -k_i \rho_S \tag{2.14}$$

$$\frac{\partial \rho_A}{\partial t} = k_i \rho_S - (k_V + k_C)\rho_A \tag{2.15}$$

$$\frac{\partial \rho_C}{\partial t} = \mu k_C \rho_A \tag{2.16}$$

$$\frac{\partial \rho_T}{\partial t} = k_T \rho_A \tag{2.17}$$

$$\frac{\partial \rho_G}{\partial t} = (1-\mu) k_C \rho_A \tag{2.18}$$

Where μ is the stoichiometric coefficient for char formation (usually μ=0.35).

Another commonly used model is based on the Shafizadeh and Chin model that was described earlier in Section 2.3.2.2. The main modifications that have been introduced are again secondary reactions involving the conversion of tars. In the extended Shafizadeh and Chin model (M 9), the tar reacts further to form char and gases [20] whilst Chin et al. (M 10) had proposed that the primary tar formed is converted to secondary gases and tars [93].

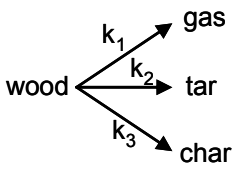

(M 8)

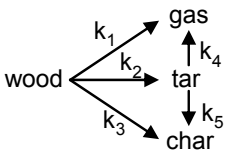

(M 9)

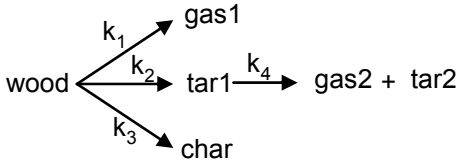

(M 10)

The kinetics constants associated with these models are listed in Table 2.8.

Table 2.8: Kinetic constants for the Shafizadeh-Chin and Chan models

Reaction i	A_i **(s^{-1})**	E_i **(kJ.mol^{-1})**	**Reaction i**	A_i **(s^{-1})**	E_i **(kJ.mol^{-1})**
Shafizadeh-Chin			***Chan***		
1	1.435×10^{4}	88.6	*1*	1.3×10^{8}	140
2	4.125×10^{6}	112.7	*2*	2.0×10^{8}	133
3	7.377×10^{5}	106.5	*3*	1.08×10^{7}	121
4	4.28×10^{6}	108.0	*4*	1.48×10^{6}	144
5	1.00×10^{6}	108.0			

The corresponding conservation equations for the Shafizadeh-Chin model can be written as:

$$\frac{\partial \rho_W}{\partial t} = -(k_1 + k_2 + k_3)\rho_W \tag{2.19}$$

$$\frac{\partial \rho_C}{\partial t} = k_3 \rho_W + k_5 \rho_T \tag{2.20}$$

$$\frac{\partial \rho_T}{\partial t} = k_2 \rho_W - (k_4 + k_5)\rho_T \tag{2.21}$$

$$\frac{\partial \rho_G}{\partial t} = k_1 \rho_W + k_4 \rho_T \tag{2.22}$$

Although extensive work has been done in the area of kinetic modelling, the lumped parameter method is not sufficient to handle specific compounds/intermediates produced during cellulose thermochemical conversion. However, the methods that we have seen for handling parallel-competing reactions, secondary reactions and the use of mass conservation equations (ODE) are relevant and can be applied in our study of the transglycosylation and β-elimination pathways.

2.4 Kinetic Analysis of Isothermal and Non-isothermal Data

In order to find the kinetic parameters associated with the kinetic models that we have seen earlier in Section 2.3, there have been numerous studies on the associated kinetic analysis of cellulose thermal conversion/pyrolysis. The kinetics work found in the literature focussed mainly on obtaining the yields of the three main pyrolysis products namely char, tar and gas. In those studies, to get the kinetic parameters, the char, tar and gas yields needed to be measured instantaneously (differential method) [99, 104, 105] or at the end of each experimental run (integral method) [106-109]. The experimental data was then used to get the best-fitted kinetic parameters via a variety

of non-linear regression methods/algorithms. This experimental method is however unsatisfactory if the compound(s) of interest are intermediates that are extremely difficult to isolate and measure temporally thus making the typical kinetic method unsuitable.

Apart from the lumped parameter method described above, kinetic parameters can also be obtained via isothermal or non-isothermal thermogravimetric analysis. Thermogravimetric analysis is an experimental method that involves the measurement of the time-dependent weight loss experienced by the cellulose sample undergoing thermal conversion. This weight loss data is then subjected to two main types of mathematical methods (model-fitting and model-free) to obtain the relevant Arrhenius kinetic parameters. Several popular model-fitting and model-free methods are described in the subsequent sections.

2.4.1 Model-fitting Method

Thermal analysis of cellulose decomposition are usually carried out using methods that measure a change in an extensive property such as mass (thermogravimetry –TG) or enthalpy (differential scanning calorimetry – DSC) [110]. The kinetics of cellulose decomposition is usually described by a single-step reaction expressed in the form:

$$\frac{d\alpha}{dt} = k(T)f(\alpha) \tag{2.23}$$

Where $f(\alpha)$ is the reaction model, α is the conversion and $k(T)$ is the temperature dependant rate constant usually expressed in the Arrhenius form.

The conversion α is typically defined as:

$$\alpha = \frac{W_0 - W_t}{W_0 - W_f} \tag{2.24}$$

Where W_0, W_t and W_f are the sample weights initially, at time t and at the end of the experiment, respectively.

Under non-isothermal testing conditions, the temperature is varied at a constant heating rate: $\beta = {}^{dT}/_{dt}$ which transforms Equation (**2**.**23**) into:

$$\frac{d\alpha}{dT} = \left(\frac{A}{\beta}\right) e^{\left(\frac{-E_a}{RT}\right)} f(\alpha) \tag{2.25}$$

Where A is the pre-exponential factor, E_a is the activation energy and R is the gas constant and T is the absolute temperature.

Upon separation of variables and integration, Equation (**2**.**25**) yields the expression:

$$g(\alpha) = \int_0^{\alpha} \frac{d\alpha}{f(\alpha)} = \left(\frac{A}{\beta}\right) \int_0^{T} e^{\left(\frac{-E_a}{RT}\right)} dT \tag{2.26}$$

Where $g(\alpha)$ is the integral form of the reaction model. Some examples of reaction models and their corresponding integral forms [111] are listed in Appendix B3.

However, if the reaction model is unknown and by extension $g(\alpha)$ cannot be found directly, an alternative method is needed because the right-hand side of Equation (**2.26**) has no exact integral. This is done by first converting Equation (**2.26**) by defining $x = {E}/{RT}$:

$$\int_0^T e^{\left(\frac{-E_a}{RT}\right)} dT = \frac{E}{R}\int_u^\infty \frac{exp(-x)}{x^2} dx = \frac{E}{R}p(u) \tag{2.27}$$

Several approximations to this temperature integral in the form of the integral $p(u)$ have been suggested in the literature [112] along with the more popular method developed by Coats and Redfern [113] that uses the asymptotic series expansion for approximating the exponential integral as shown in Equation (**2.28**).

$$\int_z^\infty e^{-z}\, z^{-b} dz \approx z^{1-b} e^{-z} \sum_{n=0}^{\infty} \frac{(-1)^n b^n}{z^{n+1}} \tag{2.28}$$

Based on either Equation (**2.26**) or Equation (**2.27**), the kinetic triplet (A, E_a and the reaction model,$f(\alpha)$) for the overall thermal decomposition can then be found via model-fitting from isothermal or non-isothermal experiments. Comparatively, non-isothermal experiments are easier to conduct because there is no need to perform a steep increase in temperature at the start. However, Vyazovkin and Wight [114] have

reported that the use of model-fitting methods to obtain Arrhenius parameters from non-isothermal experiments differed from those obtained from isothermal ones.

One of the main reasons for this is the use of kinetic methods that force-fit non-isothermal data to theoretical reaction models $f(\alpha)$. This method gives ambiguous Arrhenius parameter values due to the ability of different reaction models to fit the thermal decomposition data equally well with significantly different pre-exponential factors and activation energies. The second reason for this difference in isothermal and non-isothermal results is the fact that the two sets of experiments are in effect being conducted at different temperature regions.

As seen in the earlier Section 2.2 and Section 2.3, biomass/cellulose pyrolysis takes place over multiple steps. Therefore, the decomposition rate will naturally vary with both the temperature and extent of reaction. Hence, the activation energy should also vary with the extent of reaction. The typical method of evaluating a single activation energy for the entire process does not reflect the actual progression of a reaction and is actually an average that does not account for changes in the reaction mechanisms.

2.4.2 Model-free Isoconversional Method

These shortcomings can be overcome by using an isoconversional method as suggested by Vyazovkin [114, 115]. This experimental method requires the thermal decomposition to be carried out over a series of different heating rates. One of the biggest advantages of the isoconversional method is that it allows for the determination

of the activation energy without the need for a reaction model to be assumed or defined. It has also been described as a model-free method [114]. In addition, it is able to show the changes in activation energy as the reaction progresses. The basic assumption made within the isoconversional method is that the reaction model as stated in Equation (**2.23**) is independent of temperature or heating rate. Under isothermal conditions, rearranging and integrating Equation (**2.23**) yields:

$$g(\alpha) = k(T)t \tag{2.29}$$

And if the Arrhenius equation is expressed in its logarithmic form, Equation (**2.29**) becomes [114]:

$$-\ln t_{\alpha,i} = \ln\left[\frac{A_\alpha}{g(\alpha)}\right] - \frac{E_\alpha}{RT_i} \tag{2.30}$$

Isothermal experiments conducted at various T_i are then used to find the corresponding time $t_{\alpha,i}$ at which a particular conversion α occurs (e.g. α = 0.3). The plot of $-\ln t_{\alpha,i}$ against $1/T_i$ is then used to find the slope $\left(\frac{E_\alpha}{R}\right)$ and thus the activation energy at the specified value of α.

There have been several other mathematical methods developed for handling both isothermal and non-isothermal experimental data [116-120]. Three of the more commonly used methods, Flynn-Wall-Ozawa, Friedman and Desseyn are described in the following sections

2.4.2.1 Flynn-Wall-Ozawa method

The model-free Flynn-Wall-Ozawa isoconversional method [121, 122] involves non-isothermal experiments conducted at different heating rates β. Equation (**2.25**) is rearranged to give:

$$\ln(\beta_i) = \ln\left[\frac{Af(\alpha)}{d\alpha/_{dT}}\right] - \frac{E_\alpha}{RT_{\alpha,i}} \tag{2.31}$$

In this method, for specific values of α, the corresponding temperatures are found at the different heating rates. Plotting $\ln(\beta_i)$ against the reciprocal of temperature will provide the activation energy at the various specified conversions (α). This method enables us to study the variation (if any) of activation energy as the reaction progresses. Variations in the activation energy should be interpreted as reactions with multi-step mechanisms. This method is also referred to as ASTM E698.

2.4.2.2 Friedman method

In the Friedman model-free isoconversional method [123, 124], Equation (**2.25**) is rearranged to give:

$$\ln\left(\frac{\mathrm{d}\alpha}{\mathrm{d}t}\right)_i = \ln\left[\beta\frac{d\alpha}{dT}\right] = \ln A + \ln[f(\alpha)] - \frac{E_\alpha}{RT_{\alpha,i}} \tag{2.32}$$

Similarly, the activation energy is obtained from the slope of the plot $\ln\left(\frac{\mathrm{d}\alpha}{\mathrm{d}t}\right)_{\mathrm{i}}$ against the reciprocal of temperature at the specific conversion α.

2.4.2.3 Desseyn method

In the general Desseyn method, the basic Equation (**2**.**25**) is re-written as:

$$\ln\left(\frac{\mathrm{d}\alpha}{\mathrm{d}T}\right)_{\mathrm{i}} = \ln\left[\frac{Af(\alpha)}{\beta}\right] - \frac{E_\alpha}{RT_{\alpha,i}} \tag{2.33}$$

Hence, plots of $\ln\left(\frac{\mathrm{d}\alpha}{\mathrm{d}T}\right)_{\mathrm{i}}$ against $\left(\frac{1}{T_{\alpha,i}}\right)$ will give the activation energy at the specified conversions. The Desseyn method can also be converted for use with isothermal data by rewriting the reaction rate equation (**2**.**23**) at a constant temperature *T* as follows:

$$\left(\frac{\mathrm{d}\alpha}{\mathrm{d}t}\right)_{\mathrm{T}} = f(\alpha)Aexp\left(\frac{E_\alpha}{RT_{\alpha,i}}\right) \tag{2.34}$$

However the isothermal method is not model-free because it requires $f(\alpha)$ to be defined as shown below:

$$\ln\left[\frac{(\mathrm{d}\alpha/\mathrm{d}t)_{\mathrm{T}}}{f(\alpha)}\right] = \ln A - \left(\frac{E_\alpha}{RT_{\alpha,i}}\right) \tag{2.35}$$

2.4.3 Evaluation of Model-fitting and Model-free Methods

Model-free, isoconversional methods have the advantage of being able to evaluate activation energy without the need for assuming or defining a specific reaction model. At the same time the isoconversional methods allow us to view the changes in activation energy at different conversions as the reaction progresses. This gives us insight into the multi-step reaction mechanisms that are present in solid state decompositions like cellulose pyrolysis. The plots of conversion against activation energy are also able to identify the kinetic scheme of a complex process. The shapes of the E_α dependency curves have been shown to correlate with:

i. competing reactions [125]:
ii. parallel independent reactions [126]:
iii. series/consecutive reactions [127]:
iv. reversible reactions [128]:
v. reactions with a change in limiting stage [129]

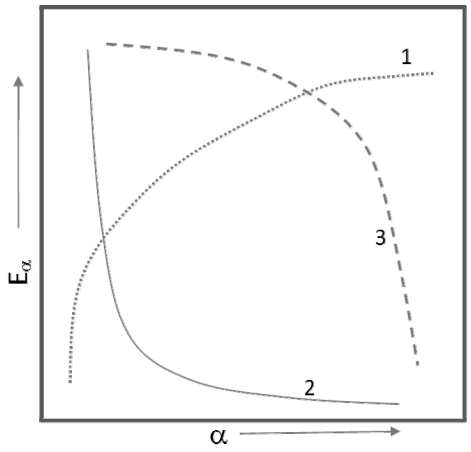

Figure 2.7: Characteristic dependencies of E_α on conversion α of complex processes

This is illustrated in Figure 2.7, where curve 1 corresponds to competitive reactions whilst curve 2 represents reversible reactions and curve 3 relates to reactions with a change in limiting stage (e.g. diffusion). The shape of the dependence for parallel independent reaction is strongly influenced by the ratio of the rates of individual reactions and their partial contribution to the overall reaction. These parallel independent reactions as illustrated in Figure 2.8 can yield curves that are:

i. Increasing (curve 1): temperature at the maximum of the differential thermoanalytical curve for the reaction with the lower activation energy is lower than the temperature for the reaction with the higher activation energy.

ii. Convex decreasing (curve 2): temperature at the maximum of the differential thermoanalytical curve for the reaction with the lower activation energy is higher than the temperature for the reaction with the higher activation energy.

iii. Parabolic (curve 3): temperature at the maximum of the differential thermoanalytical curve for the reaction with the lower activation energy is the same as the temperature for the reaction with the higher activation energy.

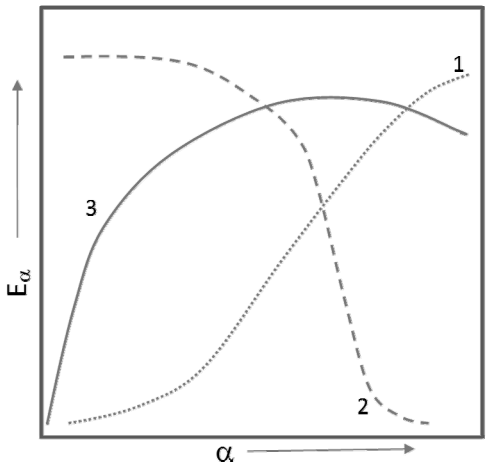

Figure 2.8: Shapes of the E_α dependency curves for parallel independent reactions

For the series/consecutive reactions, the shape of the E_α dependency curves is also highly dependent on relative kinetics of the constituent reactions. It was shown by Vyazovkin [127] that the curves are dependent on both the activation energies and the enthalpies of the consecutive reactions.

On the other hand, model-fitting methods extract a single set of Arrhenius parameters that is actually the average over the entire process. Furthermore, the Arrhenius parameters can vary greatly depending on the reaction model used due to variations being force-fitted or hidden within the reaction model parameters. This ambiguity in the Arrhenius parameters found via model-fitting occurs for both isothermal and non-isothermal data.

In addition, Burnham [119] recommends the use of isoconversional methods because they generate kinetic parameters that conform with those obtained via nonlinear regression of appropriate reaction models. He also strongly discourages the use of single-heating rate methods such as those mentioned in Section 2.4.1. At the same time, Maciejewski [117] indicated that the uses of such single-heating rate methods are

limited in scope and strongly emphasised the utility of multi-heating rate data for kinetic analysis. In a comparative study of isothermal and non-isothermal techniques carried out by Lazaro et al. [130], it was shown that despite its critics, non-isothermal techniques are able to generate kinetic parameters that are comparable to isothermal techniques.

In view of the literature available, it is preferable to use the model-free isoconversional methods to first obtain the activation energy (E_a) of a reaction to ensure that important variations are not inadvertently force-fitted into the parameters of a reaction model. Isoconversional methods would also be useful when looking for the presence or dominance of specific reactions at different stages of a complex, multi-stage reaction network. Once the activation energy has been ascertained, a model-fitting method with suitable reaction models can then be used to obtain the Arrhenius pre-exponent factor (A) and the relevant reaction model parameters.

2.4.4 Recent Application of Isoconversional Methods

In the work carried out by Vlase et al., [131] the Friedman method was recommended due to its utility and model-free characteristics. The authors had also recommended that a minimum of five different heating rates be used to generate the experimental data set for the kinetic analysis. Recently, Sanchez et al. [132] conducted thermal degradation studies on cellulose using the Friedman isoconversional method. The results obtained showed that cellulose degradation had an activation energy of ca. 191 kJ/mol at conversions of between 0.1 and 0.8. However, it was noted that at a

conversion of 0.9, the activation energy dropped significantly to 119 kJ/mol. This seems to be indicative of char forming reactions as shown by Milosavljevic et al. [133]. Extensions to the basic isoconversional methods were also developed recently by Jansen and Machado [134]. They had converted the basic isoconversional equations into a set of ordinary differential equations which were solved by minimising an objective function via a least square error algorithm

2.5 Summary of Literature Review

The literature review has shown that the conversion of lignocellulosic biomass to chemicals is an area of active research driven by environmental and economic demands for alternative feedstocks.

At its core, during thermal conversion, cellulose chemistry proceeds via at least two main competing pathways with one producing anhydrosaccharides via transglycosylation. The alternative β-elimination pathway was found to respond to pH changes, had higher activation energy than transglycosylation and led to the formation of light organic fragments (e.g. glycoaldehyde, formaldehyde).

The literature on the influence of aids and alkalis was found to be rather mixed. The state-of-the-art, based on patent and academic literature, showed the use of acids (e.g. H_3PO_4) for enhancing anhydrosaccharide yields. This seems to contradict with the cellulose chemistry described above. However, this yield enhancement is probably due to physical changes to the ash content, crystallinity and degree of polymerisation

caused by the acids. Consequently, there seemed to be no work done in attempting to enhance anhydrosaccharide yields by manipulating the [H^+] levels during thermal conversion.

The models and the associated kinetics for cellulose pyrolysis have been found to be predominantly based on the lumped parameter description of pyrolysis products namely chars, tars and gases. Considering the interest in high value intermediates (e.g. levoglucosan, levoglucosenone), there is a lack of models that incorporate individual intermediates and end products. This has been recognised in the recent paper by Mettler et al. [31] that future efforts need to focus on the individual compounds of interest. This is a big challenge in terms of identifying and quantifying the time-dependent intermediates produced during cellulose thermal conversion.

Consequently, experimental efforts to link the kinetics of transglycosylation and β-elimination and the influence acids/alkalis exert on the production of anhydrosaccharides can contribute towards the bigger challenge of mapping the reaction network connecting various compounds of interest (e.g. levoglucosan, levoglucosenone, furfural, levulinic acid, glycolaldehyde). In addition, kinetic studies on the effect of acids/alkalis on transglycosylation and β-elimination will support the attempt to enhance the anhydrosaccharide yields via chemical pathway manipulation rather than the current state-of-the-art physical transformation by acid pre-treatment.

Following this literature review, the study will proceed to show the possibility of pathway manipulation to vary anhydrosaccharide yields via the thermal conversion of selected acid and alkali-infused cellulose. This expected shift in pathways will also be

studied in terms the pathways' kinetic response to the selected acids and alkalis. Finally, an experimental demonstration and quantification of yield enhancement that can be achieved via pathway manipulation will be conducted to examine this alternative method's viability.

3. Influence of Acids and Alkalis on Cellulose Pyrolysis Pathways

In this chapter, we will investigate the relationship between acid/alkali content and cellulose thermochemical conversion pathways. Particular emphasis will be placed on the yields of anhydrosaccharides because they are only produced via transglycosylation and could therefore act a pathway marker. The anhydrosaccharides can therefore indicate the dominance (or otherwise) of transglycosylation vis-à-vis β-elimination. Consequently, we will also study how acids, in particular their corresponding $[H^+]$, can affect the β-elimination pathway.

Mamleev's scheme [18] as illustrated in Figure 2.4 is a novel representation of the reactions involved in cellulose pyrolysis. Although it shares some common features with other models like the Broido-Shafizadeh [101, 102] and Shafizadeh-Chin [100] models, Mamleev et al. [18] seems to be the first to explicitly incorporate the role of acid catalysis in cellulose pyrolysis. Mamleev's scheme [18], indicated that there is an acid-catalysed (β-elimination) pathway with a higher activation energy ($E_a \approx 250$ kJ/mol) compared with the transglycosylation pathway ($E_a \approx 200$ kJ/mol) during cellulose pyrolysis. Based on kinetics work done by Banyasz et al. [104] and Capart et al. [111], it is shown in Figure 3.1 and Figure 3.2 that the acid-catalysed, (β-elimination) pathway is favoured as temperature increases.

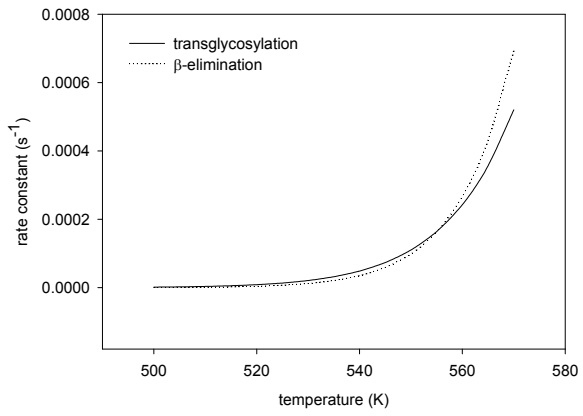

Figure 3.1: Comparison of reaction rates for β-elimination and transglycosylation

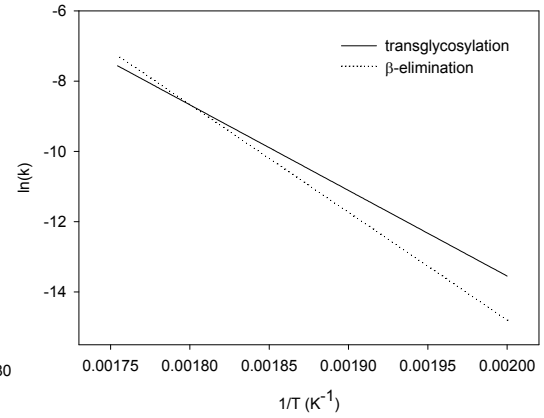

Figure 3.2: Comparison of ln(k) against reciprocal temperature.

The graphs in Figure 3.1 and Figure 3.2 also indicates that the "cross-over" temperature from transglycosylation dominated pyrolysis to ring-opening (β-elimination) dominated pyrolysis occurs at circa 555 K (282 °C).

The formation of levoglucosan is expected to occur solely via the transglycosylation mechanism. It is therefore expected that the yield of levoglucosan would decrease with increasing temperature and acidity. Although there have been some experimental evidence that supports this view, information in the literature has been rather mixed as shown in Section 2.2.2. This could indicate that the acids might have affected cellulose thermal conversion in other ways not directly related to the two pathways (transglycosylation and β-elimination).

We know that impurities within biomass such as alkali metal cations can prevent the formation of anhydrosaccharides (e.g. levoglucosan) and increase the relative yields of lower molecular weight compounds (e.g. aldehydes, ketones) as shown by Muller-

Hagedorn et al. [72] and Patwardhan et al. [73]. In addition, Kuzhiyil et al. [135] showed that mineral acids (H_2SO_4 and H_3PO_4) infused into cellulosic biomass were able to passivate alkaline earth metals resulting in increased levoglucosan yields.

In the work conducted by Dobele et al. [24-26], H_3PO_4 was shown to increase levoglucosenone yields by a combination of pre-treatment hydrolysis and decreasing cellulose crystallinity/degree of polymerisation. Therefore, the available literature has shown that acids could enhance anhydrosaccharide yields by altering the physical characteristics of cellulose such as ash (inorganic impurity) content, crystallinity and degree of polymerisation.

In contrast, from the mechanism proposed by Mamleev et al. [18] and the available literature, it follows that if acids were present within the cellulose particles, during pyrolysis, the acids should promote the ring-opening reactions (via β-elimination) at the expense of the transglycosylation pathway. This would in turn cause the amount of levoglucosan to be lowered. Conversely, if alkalis were infused into the cellulose particles, they should neutralise the organic acids formed as part of the pyrolysis process. The lowered $[H^+]$ levels would therefore suppress the β-elimination reaction and lead to increased levoglucosan yields.

Therefore, to study the influence of acids and alkalis described above, experiments showing the effects of selected acids (H_2SO_4, H_3PO_4 , H_3BO_3) and alkalis ($Ca(OH)_2$, NH_4OH) on the yields of anhydrosaccharides (levoglucosan, levoglucosenone, 1,4:3,6-dianhydro-α-d-glucopyranose, 1,6-anhydro-β-D-glucofuranose) is described and discussed in this chapter. Acid and alkali-infused cellulose were pyrolysed in a fixed-

bed reactor system. The condensable pyrolysis products were collected and analysed using a GC-MS to quantify the amount of anhydrosaccharides produced. These anhydrosaccharide yields reflect the relative dominance between the two conversion pathways under the different acid and alkali treatments.

3.1 Method and Materials

The experiments conducted consisted of two main stages namely pyrolysis of cellulose infused with suitable amounts of acids and alkalis and quantification of the anhydrosaccharides produced from this thermal conversion process.

3.1.1 Experimental Design

The factors that could affect the reproducibility of experiments for the thermal conversion of cellulose can be broadly classified into three main factors namely feedstock, reactor design and operating conditions [136, 137]. A discussion on these factors and the steps taken to control variations that could affect experimental reproducibility is given below.

3.1.1.1 Feedstock

Feedstock refers to the material undergoing thermal conversion. Characteristics of the feedstock that could affect experimental outcomes are particle size, ash and moisture content, crystallinity, porosity, density and sample amount. In the experiments conducted we have sought to limit variations in the feedstock characteristics by using a specific cellulose grade (Avicel) from a single reputable supplier (Sigma-Aldrich). All the experiments were conducted using cellulose from a single batch. Variations in sample amounts used were controlled by carefully weighing samples on a calibrated laboratory balance with a resolution of 0.1 mg.

3.1.1.2 Reactor design

Reactor design impacts the residence time, heat and mass transfer rates. These factors depend on the type of reactor (e.g. fixed-bed, fluidised-bed), materials of construction, reactor geometry and the heat source used.

Two reactor types were considered for these thermal conversion studies. A fluidised-bed reactor was designed and constructed to process up to 5 g/min of cellulose. However, experimental runs with this fluidised bed were severely affected by the solid feed rate variations from the screw feeder [138, 139] which resulted in poor experimental reproducibility. It was found that the minute-to-minute variation for the solid feed rate was more than 50 %. Alternatively, a fixed-bed reactor was designed and constructed and the geometry of the fixed-bed reactor is shown in Appendix C. By

eliminating an additional experimental variability (i.e. solid feed rate), the simpler mechanical design of the fixed-bed reactor resulted in better experimental control and results reproducibility.

Residence time variability was controlled by both the geometry (reactor volume) and the flow rate of the nitrogen sweep gas. The flow of nitrogen was controlled by a mass flow meter (Sierra Instruments-SmartTrak100) that has an accuracy of ±1 %. The gas flow rate was calibrated with a mass flow calibrator (CalTrak SL-500). In addition, due to the possibility of pressure drop changes (e.g. choking) within the experimental set-up, the CalTrak SL-500 was also placed at the outlet of the system to monitor the flow rate.

The heat source for the thermal conversion was provided by a horizontal tube furnace (Carbolite). The furnace temperature as measured by a thermocouple near the heating surface was recorded and monitored for stability during all experimental runs to ensure reproducibility of the heat flux supplied to the reactor.

3.1.1.3 Operating conditions:

The operating conditions of concern during thermal conversion are temperature, pressure and oxygen level. Two separate temperature measurements (furnace and reactor) were taken during the experiments. The reactor temperature was measured using a K-type thermocouple with its tip in contact with the pyrolysing sample.

The fixed-bed reactor was operated at ambient pressures due to the set-up being an open system. However, due to the pressure drops inherent in the system from the fixed bed and flow resistances within the system, the flow into and out of the reactor was measured during experimental runs to monitor the pressure drop changes (if any). Experimental runs were concluded before any significant change in pressure drop was detected.

The nitrogen sweep gas fulfils two functions. Earlier, the gas flow was used to ensure a steady residence time within the fixed-bed reactor and sweep out the products of the thermal conversion. Secondly, it ensures that the atmosphere within the reactor is inert. The reactor system was purged for about 1 hour before each experimental run to ensure oxygen is driven out of the system.

3.1.1.4 Experimental variables

The experiments conducted were based on a three-factor factorial design. There were a total of five types of additives (H_2SO_4, H_3PO_4, H_3BO_3, NH_4OH, $Ca(OH)_2$), three infusion levels (low, medium and high) and three temperature levels (550 °C, 600 °C, 650 °C) being studied. The main focus of the experiments was to find out the influence/response of these acid/alkali additives on anhydrosaccharide yield. There were therefore a total of 45 different combinations with 6 replicates done for each experimental combination. The three-factor analyses of variance for these experiments are discussed in Section 3.2.3.

3.1.2 Pyrolysis Reactor Setup

The experimental setup used to study anhydrosaccharide yield is shown in Figure 3.3 and a detailed cross-sectional view of the fixed-bed reactor is presented in Appendix C. It consists of a 1.5 inch diameter stainless steel outer vessel which holds within it a tubular fixed-bed reactor with a capacity of 15±1 cm^3 placed inside a horizontal furnace (Carbolite). The furnace is capable of heating the reactor up to 1200 °C and at a rate of 20 to 30 °C/min. The stainless steel outer vessel functions as part of the reactor set-up to position the fixed-bed reactor in the correct position within the furnace, ensure an inert atmosphere for the pyrolysis to take place, sweep the volatilised products out of the reaction zone of the fixed-bed and channel it to subsequent sections of the experimental set-up.

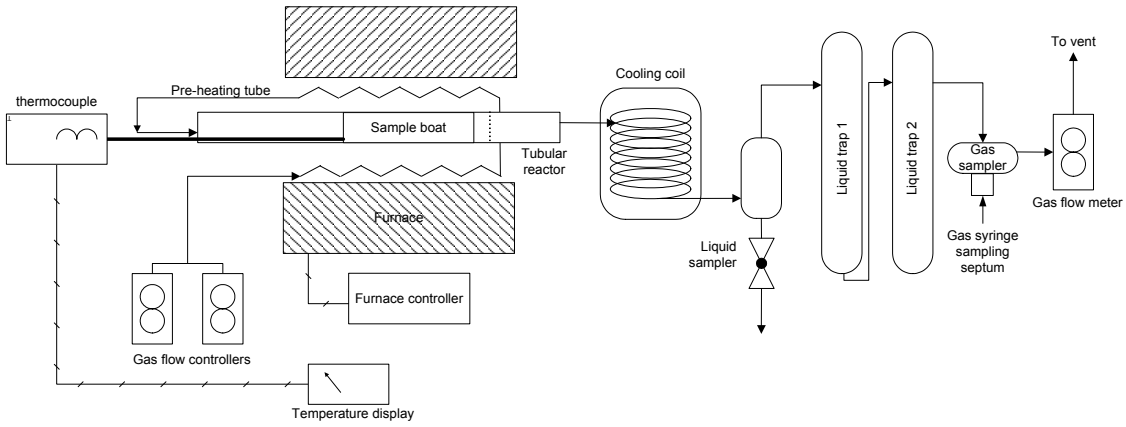

Figure 3.3: Fixed-bed pyrolysis experimental set-up

The longitudinal temperature profile is expected to be relatively linear across the fixed bed reactor of length 12 cm. This linear profile (up to 15 cm) was shown in the biomass thermal degradation experiments conducted by Gronli [99]. Making the assumption that the wall temperature remains constant along the 12 cm long reactor,

the estimated reactor outlet temperatures were obtained from Lerou and Froment [140] and is shown in Table 3.1 below:

Table 3.1: Estimates for the longitudinal variation of fixed-bed reactor temperature at three different furnace temperatures.

Furnace (°C)	550	600	650
Reactor Inlet (°C)	470	530	585
Reactor Outlet (°C)	490	550	605

The 20 °C difference is acceptable as there is no overlap at each temperature level making each level distinct. In terms of the relative rates between transglycosylation and β-elimination due to temperature difference across the bed, all the reactor temperature ranges were well within the region where β-elimination is dominant. Therefore, the cross-over effect between the transglycosylation and β-elimination pathways (at 282 °C) will not have an impact on the results.

The sweep gas was provided via the two gas flow controllers which enabled variations in gas compositions and reactor residence times. For the current work, a nitrogen flow rate of 650±10 ml/min was used and this translated to a residence time of 1.4±0.1 seconds within the fixed-bed reactor. A thermocouple was also placed inside the fixed-bed reactor in contact with the pyrolysing cellulose to ensure consistent reaction temperatures.

The incoming gas was preheated prior to contact with the pyrolysing sample. The volatile tars and gases then leave the reaction zone and were allowed to cool immediately via the cooling coil (ca. 0 - 4 °C). The condensed volatiles were then collected within the liquid sampler and subsequently analysed via GC-MS for

anhydrosaccharide content. Any entrained volatile tars were then trapped in Liquid traps 1 and 2 and the mass collected within them was carefully measured for mass balance calculations. The removal of entrained volatile tars was also important to prevent the tars from clogging and damaging the gas flow meter located at the end of the set-up. The volatile tars were also removed to minimise releases out of the set-up and into the vent.

The cleaned gas stream then passed through the gas sampler where sealed, evacuated vials collect ca. 5 ml of gas for GC analysis. Finally, the total gas flowrate was measured to check for the overall mass balance.

3.1.3 Acid/Alkali Infusion of Cellulose

Cellulose samples were prepared at different acid and alkali loadings by stirring microcrystalline cellulose (Avicel from Sigma-Aldrich) with the required acid (H_2SO_4, H_3PO_4, H_3BO_3) or alkali (NH_4OH and $Ca(OH)_2$) solution (0.5 to 5 wt%) at room temperature (ca. 25 °C) for 30 minutes. Low concentrations of acids/alkalis and the relatively low temperatures for this treatment were meant to ensure that the pyrolysis results obtained were due to action of the acid/alkali loaded and not due to hydrolysis which could break or weaken the cellulose bonds. The cellulose slurry was then filtered and dried overnight in an oven at 40 °C. After drying, the remaining moisture content was then measured using a Moisture Analyser based on Loss-on-Drying (Sartorius: MA150). The loadings of the various acids and alkalis in the cellulose powder were obtained using an Elemental Analyser (EuroEA3000) for carbon

(cellulose) and nitrogen (NH_4OH) content whilst X-ray Fluorescence (Bruker AXS-S4) was used to measure the sulphur (H_2SO_4), phosphorus (H_3PO_4) and calcium content ($Ca(OH)_2$),. However, the level of infusion of cellulose by H_3BO_3 was not measured since neither instrument was able to detect boron.

3.1.4 GC-MS Analysis of Anhydrosaccharide Content

The bio-oil produced from pyrolysis was extracted with methanol, filtered and the solvent was then removed using a rotary evaporator. The remaining bio-oil was carefully weighed and re-dissolved/diluted with an appropriate amount of methanol for subsequent GC-MS analysis. The settings for the GC-MS (Agilent: 7890A GC) are as listed in Table 3.2.

Table 3.2: GC-MS settings for anhydrosaccharide analysis

GC column:	DB-1701, 60 m x 0.25 mm ID, 0.25 μm
Inlet system:	1 μl, 50:1 split injector, 200 kPa He at 250 °C
Oven:	45 °C for 5 min followed by ramp at 3 °C/min to 250 °C and 5 min hold
Mass spectrometer:	EI mode (electron energy 70 eV); mass range 20-200 m/z; 6 min solvent delay. Ion source at 230 °C and transfer line at 275 °C

The various components of interest namely levoglucosan (LG) and its derivatives (levoglucosenone (LS), 1,4:3,6-dianhydro-α-D-glucopyranose (DGP), 1,6-anhydro-β-D-glucofuranose (AGF) were identified via their mass spectrum (NIST library) and their retention times. In the case of levoglucosan and levoglucosenone their retention

times were compared to pure compounds purchased from Sigma-Aldrich. However, there were no commercially available samples for DGP and AGF. The relevant data for the anhydrosaccharides are listed in Table 3.3.

Table 3.3: **Identification parameters for the main pyrolysis products**

Component	**LG**			**LS**			**DGP**			**AGF**		
Retention time (min)	22.9			17.5			18.8			24.6		
Main mass fragments (m/z)	60	57	73	98	96	39	69	29	57	73	69	44

For the quantification of the anhydrosaccharides, pure samples of levoglucosan and levoglucosenone were prepared with naphthalene used as an internal standard for comparison. Naphthalene was chosen as the internal standard because it elutes close to the compounds of interest without overlapping with those compounds and it gives a strong, sharp response on the GC-MS detector at low amounts. The levoglucosan and levoglucosenone samples were injected into the GC-MS at amounts varying from 0.1 μg to 1.0 μg together with 0.05 μg of naphthalene. The results obtained from the GC-MS enabled a five-point calibration line to be generated. A sample gas chromatogram is shown in Figure 3.4.

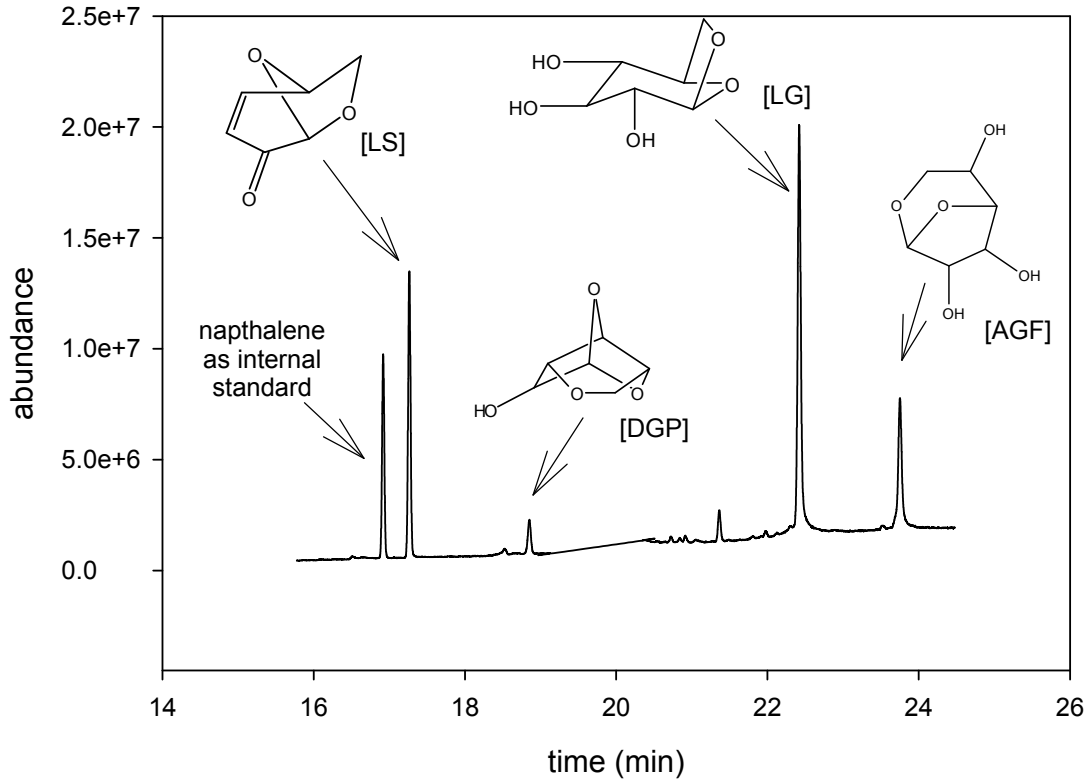

Figure 3.4: Chromatogram (GC-MS) from the pyrolysis of cellulose indicating the main components of interest

3.1.5 Conversion of Levoglucosan in Sulfolane

A 50 ml three-necked round bottom flask was used in this experimental setup. The flask was fitted with a condenser to minimise product and solvent loss and a thermocouple to monitor and control internal temperature. The reaction vessel was heated in a silicon oil bath and controlled via a mantle.

300 mg of levoglucosan was dissolved in 30 ml of sulfolane for each experimental run. The required amount of H_2SO_4 and H_3PO_4 was added at the start of the experiment,

once a stable temperature of 200 °C was reached. A glass sampling syringe was used to draw samples at regular time intervals. The drawn sample was then immediately quenched in an ice-bath and neutralised with barium hydroxide to precipitate out the sulphates and phosphates which could adversely affect the GC column. The precipitated barium salts were then separated via centrifugation followed by filtration with a 0.45 μm syringe filter. The remaining filtrate was then diluted with methanol and subsequently injected into the GC-MS for analysis of anhydrosaccharide content as described in Section 3.1.4.

3.2 Results and Discussion

From the gas chromatograms, the yields of levoglucosan and its anhydrosaccharide derivatives obtained from pyrolysing cellulose with varying acid/alkali loadings were calculated and compared as shown in Figure 3.5 to Figure 3.14. The plotted graphs compared how the acids and alkalis affected anhydrosaccharide yields relative to untreated cellulose. A comparison of the relative amounts of the four different anhydrosaccharides was also studied. Statistical analysis of the results obtained was also carried out to see the significance of the additive type (acid/alkali), infusion and temperature levels on anhydrosaccharide yields.

3.2.1 Effect of Acids on the Yield of Anhydrosaccharides

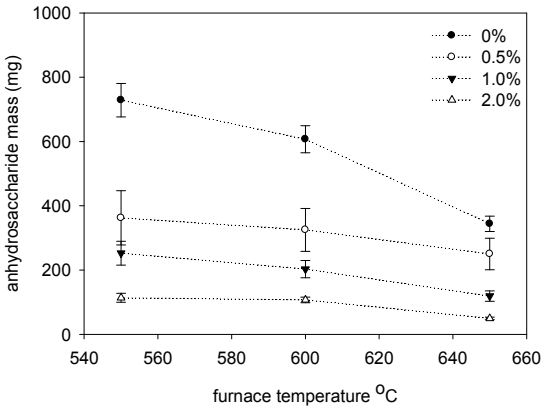

Figure 3.5: Yields of anhydrosaccharide from cellulose pyrolysis pre-treated with varying concentrations of H_2SO_4 (0.5 wt%, 1 wt% and 2 wt%)

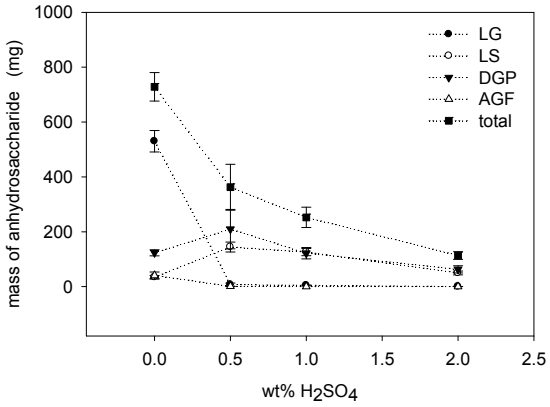

Figure 3.6: Anhydrosaccharide composition from cellulose pyrolysis at 550 °C pre-treated with varying concentrations of H_2SO_4 (0.5 wt%, 1 wt% and 2 wt%)

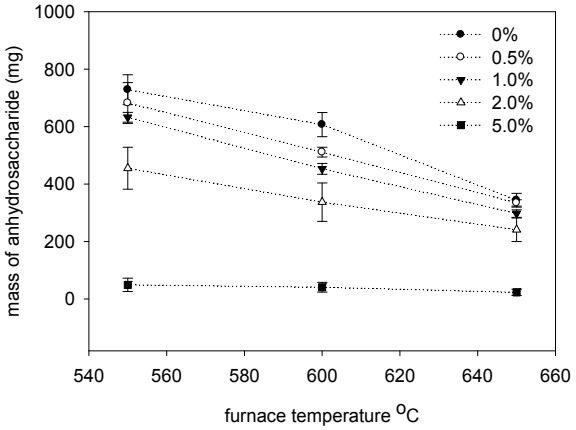

Figure 3.7: Yields of anhydrosaccharide from cellulose pyrolysis pre-treated with varying concentrations of H_3PO_4 (0.5 wt%, 1 wt%, 2 wt% and 5 wt%)

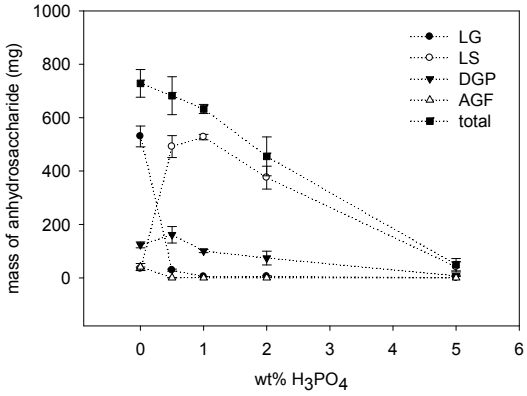

Figure 3.8: Anhydrosaccharide composition from cellulose pyrolysis at 550 °C pre-treated with varying concentrations of H_3PO_4 (0.5 wt%, 1 wt%, 2 wt% and 5 wt%)

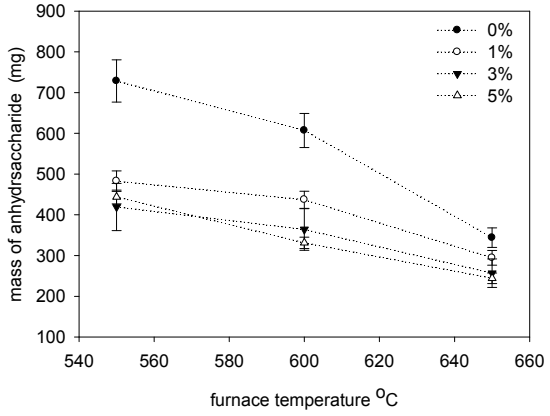

Figure 3.9: Yields of anhydrosaccharide from cellulose pyrolysis pre-treated with varying concentrations of H_3BO_3 (1 wt%, 3 wt% and 5 wt%)

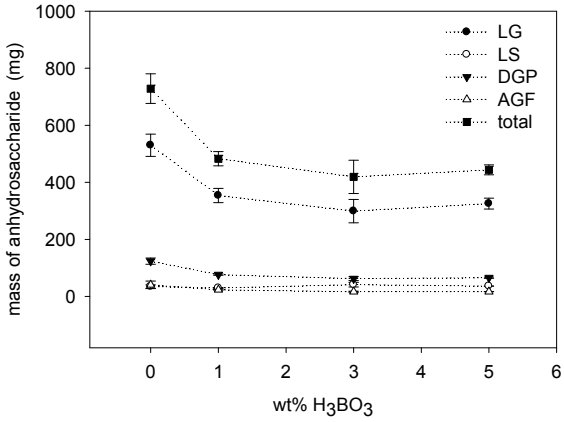

Figure 3.10: Anhydrosaccharide composition from cellulose pyrolysis at 550 °C pre-treated with varying concentrations of H_3BO_3 (1 wt%, 3 wt% and 5 wt%)

Looking at the results obtained for the acid-infused cellulose in Figure 3.5, Figure 3.7 and Figure 3.9, we can see that there is a general trend of decreasing anhydrosaccharide (levoglucosan, levoglucosenone, 1,4:3,6-dianhydro-α-D-glucopyranose, 1,6-anhydro-β-D-glucofuranose) yields with increasing temperatures. This was observed for the untreated (neat) cellulose as well as the cellulose infused with H_2SO_4, H_3PO_4 and H_3BO_3. This was expected based on the relative reaction rates of the β-elimination and transglycosylation pathways where β-elimination is favoured at higher temperatures as illustrated in Figure 3.1. Furthermore, the experimental temperatures were chosen to be significantly above the cross-over temperature of ca. 555 K (≈282 °C). At the lower furnace temperature of 550 °C, the internal reactor temperature measured at the pyrolysing cellulose samples was on average between 470 °C and 450 °C. This ensures that the experiments were conducted well within the region dominated by the β-elimination pathway.

The amount of acids infused into the cellulose powder generally follows the trend of higher infusion levels when higher concentrations (wt%) of acids were used during pre-treatment as shown in Table 3.4.

Table 3.4: Elemental ratio indicating level of infusion of acids within the cellulose powders and their corresponding anhydrosaccharide yield changes (pyrolysis at 550°C).

Acid	**H_2SO_4**			**H_3PO_4**			
wt%	0.5	1	2	0.5	1	2	5
X[1]/C	0.02	0.03	0.04	0.02	0.05	0.09	0.13
Anhydrosacharide yield change %	-50	-65	-84	-6	-13	-38	-93

Using the untreated (neat) cellulose as the basis for comparison, we observe that the acids infused cellulose had lower anhydrosaccharide yields. Increasing the concentration (wt%) of the acids used in the cellulose pre-treatment led to a progressive decrease in anhydrosaccharide levels from 50 % to 84 % for H_2SO_4 and 6 % to 93 % for H_3PO_4 at the furnace temperature of 550 °C . Although the H_3BO_3 infused cellulose also showed a significant reduction, the differentiation between the anhydrosaccharide yields at differing acid pre-treatment concentrations is not as distinct as the results obtained for H_2SO_4 and H_3PO_4. One possible explanation for this lack of a clear decreasing trend could be that the acidity of H_3BO_3 was weak as reflected in its pKa value of 9.2. Interestingly, H_3BO_3 does not dissociate in aqueous solution to give a Brønsted acid, instead it has been shown via Raman spectroscopy to behave as a Lewis acid [141, 142]. There are differences between the mechanism of Brønsted, and Lewis acid catalysis. Brønsted acid catalysis by H_2SO_4 and H_3PO_4 is

[1] X indicates S (sulphur) and P (phosphorus) for H_2SO_4 and H_3PO_4 respectively

less selective and is able to attack more sites and initiate bond scission. However, a Lewis acid like H_3BO_3 is more selective in that it seeks to coordinate with the electron-rich sites (e.g. alcohols). The rate limiting step for Lewis acid catalysis is different and could therefore become the limiting factor for thermal conversion via β-elimination. Consequently, higher levels of H_3BO_3 did not translate into significant additional shift away from transglycosylation.

At the higher furnace temperature (650 °C), we can see from Figure 3.5, Figure 3.7 and Figure 3.9 that the difference in anhydrosaccharide yields between neat cellulose and acid pre-treated cellulose was smaller than at the lower furnace temperature (550 °C). It is likely that at higher temperatures, as pyrolysis progresses, more organic acids are produced as part of cellulose degradation. This explanation is supported by the experiments carried out in Chapter 5 as shown by the results presented in Figure 5.15. If we analyse the difference between the anhydrosaccharide yield for neat sulfolane and acidified sulfolane (H_3PO_4), we can see that the difference in anhydrosaccharide yields narrows as temperature increases. Hence the additional effect of the mineral acid (H_2SO_4, H_3PO_4 and H_3BO_3) infused within the cellulose matrix is less significant.

From Table 3.4, we can see that at most infusion levels (as indicated via elemental ratios X/C), the suppression effect of H_2SO_4 on anhydrosaccharide yields was greater than that observed for H_3PO_4. We know that acid strength is reflected in the acid dissociation constant (pKa) values of an acid. The commonly quoted pKa values for the H_2SO_4 and H_3PO_4 indicate that the strength of the acids is in the order: H_2SO_4 [pKa = -3] > H_3PO_4 [pKa = 2.1].

We can therefore say that both the quantity and the type (or strength) of the acid affects the anhydrosaccharide yields. This seems to indicate the presence (or concentration) of hydrogen ions [H^+] within the cellulose matrix during pyrolysis influences the dominant pathway under which cellulose depolymerises. In this case, the hydrogen ions catalysed the β-elimination pathway.

3.2.2 Effect of Alkalis on the Yield of Anhydrosaccharides

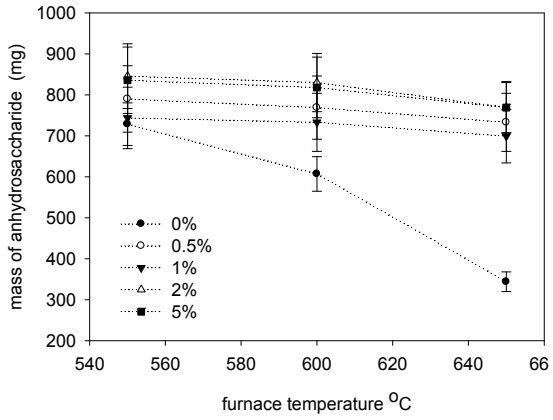

Figure 3.11: Yields of anhydrosaccharide from cellulose pyrolysis pre-treated with varying concentrations of NH_4OH (0.5 wt%, 1 wt%, 2 wt% and 5 wt%)

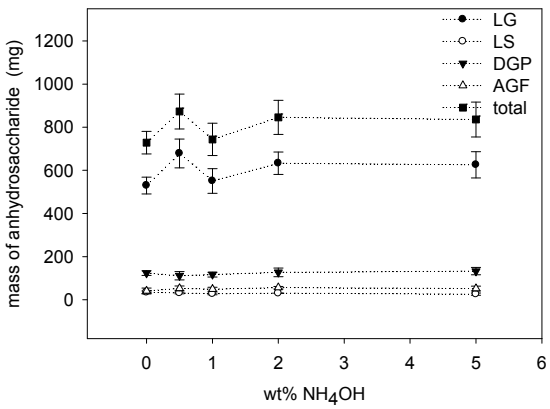

Figure 3.12: Anhydrosaccharide composition from cellulose pyrolysis at 550 °C pre-treated with varying concentrations of NH_4OH (0.5 wt%, 1 wt%, 2 wt% and 5 wt%)

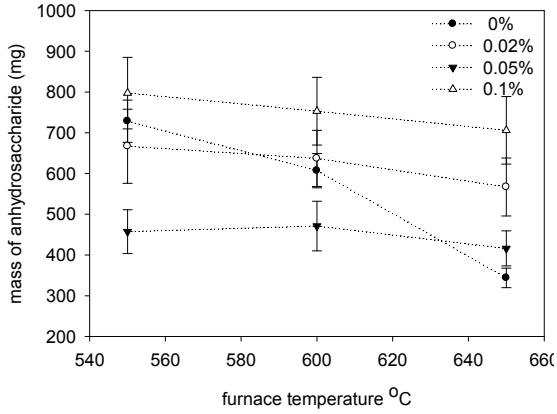

Figure 3.13: Yields of anhydrosaccharide from cellulose pyrolysis pre-treated with varying concentrations of $Ca(OH)_2$ (0.02 wt%, 0.05 wt%, and 0.1 wt%)

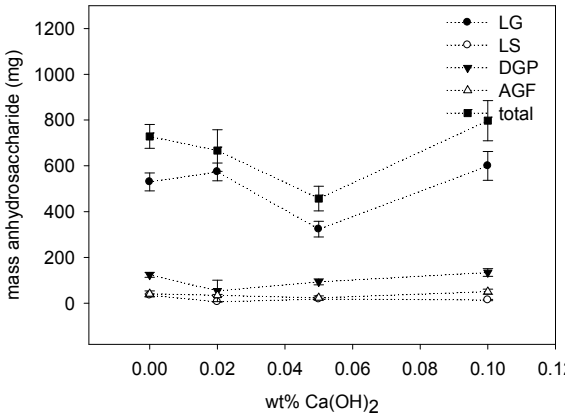

Figure 3.14: Anhydrosaccharide composition from cellulose pyrolysis at 550 °C pre-treated with varying concentrations of $Ca(OH)_2$ (0.02 wt%, 0.05 wt%, and 0.1 wt%)

If we then look at the results obtained for cellulose pyrolysis with alkalis, we observe slightly mixed results. In the case of NH_4OH, the trend (as shown in Figure 3.11) was clear that the alkali pre-treatment led to increased levels of anhydrosaccharide being produced. Although there was significant overlap for cellulose pre-treated with varying alkali concentrations (0.5 to 5 wt%), there was still a general trend at the extremes of the range. From Table 3.5, the cellulose pre-treated with 5 wt% NH_4OH yielded a 15 % increase in anhydrosaccharide yield compared with an 8 % anhydrosaccharide yield increase when 0.5 wt% NH_4OH was used.

Table 3.5: Elemental ratio indicating level of infusion of alkalis within the cellulose powders and their corresponding anhydrosaccharide yield changes (pyrolysis at 550 °C).

Acid	$Ca(OH)_2$			NH_4OH			
wt%	0.02	0.05	0.1	0.5	1	2	5
X^2/C	0.004	0.009	0.014	0.02	0.03	0.05	0.07
Anhydrosaccharide yield change %	-8	-37	+9	+8	+2	+16	+15

[2] X indicates Ca (calcium) and N (nitrogen) for $Ca(OH)_2$ and NH_4OH respectively

In addition, from Figure 3.11, we also see that the effect of NH_4OH infusion was also more significant at higher furnace temperatures (i.e. 650 °C). The NH_4OH-free cellulose had a sharper drop in anhydrosaccharide yield compared to the samples that were pre-treated with NH_4OH. Taking these two main observations together, we can suggest that the hydroxyl ions [OH^-] present within the cellulose matrix during pyrolysis were able to neutralise the hydrogen ions formed during pyrolysis. This in turn suppressed the β-elimination pathway whilst allowing cellulose depolymerisation to proceed via transglycosylation.

For cellulose pre-treated with $Ca(OH)_2$, the results (as shown in Figure 3.13) were slightly mixed. At the lower furnace temperature (550 °C), 0.02 wt% and 0.05 wt% $Ca(OH)_2$ pre-treated cellulose had lower anhydrosaccharide yields compared with alkali-free cellulose. From Table 3.5, we can see that only when the cellulose was pre-treated with 0.1 wt% $Ca(OH)_2$, was the anhydrosaccharide yield higher than that for alkali-free cellulose. Figure 3.11 also indicates that at the higher furnace temperature (650°C), all the $Ca(OH)_2$-infused cellulose samples had higher anhydrosaccharide yields compared to the alkali-free cellulose.

It has been reported that sodium, potassium and calcium ions generally prevents the formation of anhydrosaccharide-type compounds (e.g. levoglucosan) and increases the relative yields of lower molecular weight compounds (e.g. aldehydes, ketones). As shown by Muller-Hagedorn et al. [72], and Patwardhan et al. [73], the inhibiting influence of the cations are in the order of $K^+ > Na^+ > Ca^{2+}$. In addition, as described earlier in Section 2.2.2 of the Literature Review, metal ions such as Ca^{2+} have a tendency to reduce anhydrosaccharide yields via complex formation [143, 144] and

subsequent ring opening reactions. However, calcium-sugar complexes have been shown by Saladini et al. [145] to deprotonate when pH rises. The resulting deprotonated complex is significantly less stable resulting in the disassociation of the metal ion and the sugar ligand.

This supports our observation where at lower $Ca(OH)_2$ loadings (i.e. X/C = 0.004 and 0.009), there should be less deprotonation and greater complex stability which leads to greater sugar cracking and thus lower anhydrosaccharide yields. On the other hand, at the higher $Ca(OH)_2$ loading (X/C = 0.014), the situation is reversed with reduced calcium-sugar complex stability. In addition, the neutralising effect of the hydroxyl ion (OH^-) on the volatile organic acids at higher $Ca(OH)_2$ loadings becomes more significant resulting in higher yields of anhydrosaccharides.

3.2.3 Statistical Analysis of Results

Two types of statistical analysis were carried out on the results obtained from the thermal conversion of the acid and alkali-infused cellulose namely (i) Two-sample t-test and (ii) Analysis of variance.

Overall, the statistical analysis showed that anhydrosaccharide yields are significantly influenced by the three main factors of additives (H_2SO_4, H_3PO_4, H_3BO_3, NH_4OH and $Ca(OH)_2$), infusion level of the additives and the temperature of thermal conversion. When compared with untreated cellulose, the acids (H_2SO_4, H_3PO_4 and H_3BO_3)

suppresses anhydrosaccharide yields whilst the alkalis (NH_4OH and $Ca(OH)_2$) enhances anhydrosaccharide yields.

However, out of the three acids, H_3PO_4 seems to suppress anhydrosaccharide the least. This could have been partly the reason why the state-of-the-art had repeatedly made reference to the use of H_3PO_4 for the production of levoglucosenone. Another deviation in the overall trend is the lower anhydrosaccharide yield for $Ca(OH)_2$ at medium infusion levels compared with NH_4OH. The behaviour shown by $Ca(OH)_2$ is likely the result of the interplay between the effects of Ca^{2+} complex formation and the neutralising effect of OH^- during thermal conversion.

3.2.3.1 Two-sample t-test

A two-sample t-test was conducted on the acid-infused samples comparing them to the neat cellulose samples using Equation (3.1) and (3.2).

$$t_0 = \frac{\bar{y}_1 - \bar{y}_2}{S_p\sqrt{\frac{1}{n_1} + \frac{1}{n_2}}} \tag{3.1}$$

$$S_p{}^2 = \frac{(n_1 - 1){S_1}^2 + (n_2 - 1){S_2}^2}{n_1 + n_2 - 2} \tag{3.2}$$

Where $\bar{y}_1$ and $\bar{y}_2$ are the sample means, n_1 and n_2 are the sample sizes and $S_p{}^2$ is an estimate of the common variance.

The null hypothesis (H_0) was defined such that the means for acid-infused and neat cellulose were equal whilst the alternative hypothesis (H_a) was such that the mean for neat cellulose was greater than the mean for acid-infused cellulose. At a significance level of 0.05, we found that the mean anhydrosaccharide yield for neat cellulose was greater than the means for all the acid-infused cellulose except for the lowest H_3PO_4 infusion level (0.5 wt%).

A similar analysis was carried out for the alkali-infused cellulose samples. The two-sample t-test at the 0.05 significance level showed that the mean anhydrosaccharide yield for neat cellulose was less than the means for all the alkali-infused samples except for cellulose treated with 0.02 wt% and 0.05 wt% $Ca(OH)_2$.

3.2.3.2 Analysis of variance

The experiments conducted were based on a three-factor factorial design with five additive types (H_2SO_4, H_3PO_4, H_3BO_3, NH_4OH, $Ca(OH)_2$), three infusion levels (low, medium and high) and three temperature levels (550 °C, 600 °C, 650 °C). The response variable of interest was anhydrosaccharide yield. Six replicates were done for each of the 45 experimental combinations. The ANOVA tables generated by this analysis are shown in Appendix G.

Two separate analyses of variance were conducted, one each for the acids and alkalis. A comparison of the F statistics (F_0) for the acids' (H_2SO_4, H_3PO_4 and H_3BO_3) experiments with the corresponding F distribution ($F_{0.05,f,135}$) will show the statistical

significance (95 % confidence level) of each of the effects under consideration. The F_0 values for the acids, infusion levels and temperature effect were higher than the corresponding F distribution values. This implies that all three factors had a statistically significant influence on the anhydrosaccharide yield. There were also no significant temperature-infusion level and acid-temperature-infusion level interactions. However the F_0 values for acid-infusion effects shows that there is significant interaction between these factors. An examination of the interaction plots for acid-infusion levels shows that the three acids each have a different level of influence on anhydrosaccharide yields. There is no significant difference in anhydrosaccharide yields for H_3BO_3 at the medium and high infusion level. This behaviour of H_3BO_3 could be due to its action as a Lewis rather than a Brønsted acid as explained earlier in Section 3.2.1. Another possible reason for this observation is the levoglucosan suppressing anion ($B(OH)_4^-$) effect described by Mueller-Hagedorn et al. [72] working in tandem with the effects of $[H^+]$ on β-elimination. We also find that H_3PO_4 suppresses anhydrosaccharides the least among the three acids which explains why it is commonly used in state-of-the-art methods for levoglucosenone production.

The F_0 values for acid-temperature effects shows that there is significant interaction between these factors. An examination of the interaction plots for acid-temperature effects shows a clear trend among the three acids at the different temperature levels with anhydrosaccharide suppression being in the order of: **H_2SO_4 > H_3BO_3 > H_3PO_4**.

This seems to contradict the order of acid strength as represented by pKa values and its influence on anhydrosaccharide yields as observed earlier. Although we see that generally, the selected acids suppress anhydrosaccharide formation through increased

$[H^+]$ levels, the degree of suppression depends not only on the strength of the acid, other possible factors that contribute to variations within this general trend would include complex formation, acid catalysis mechanism and anion effect.

The analysis of variance for the alkalis (NH_4OH and $Ca(OH)_2$) show that The F_0 values for the alkalis, infusion levels and temperature effect were higher than the corresponding F distribution values. This implies that all three factors had a statistically significant (95 % confidence level) influence on the anhydrosaccharide yield. There were also no significant temperature-infusion level, alkali-temperature and alkali-temperature-infusion level interactions.

The remaining interaction of alkali-infusion level has an F_0 value that shows significant interaction between these factors. An examination of the interaction plots for alkali-infusion levels shows that generally, $Ca(OH)_2$ resulted in lower anhydrosaccharide yields when compared to NH_4OH. There is however a significant deviation in this trend in that at medium infusion level, $Ca(OH)_2$ had significantly lower anhydrosaccharide yields than at other infusion levels. The reason for this is the interplay between the effects of β-elimination suppression, Ca-complex stability and relative amounts of the Ca-complex. The nett result on anhydrosaccharide yields due to these countervailing effects is illustrated in Figure 3.15.

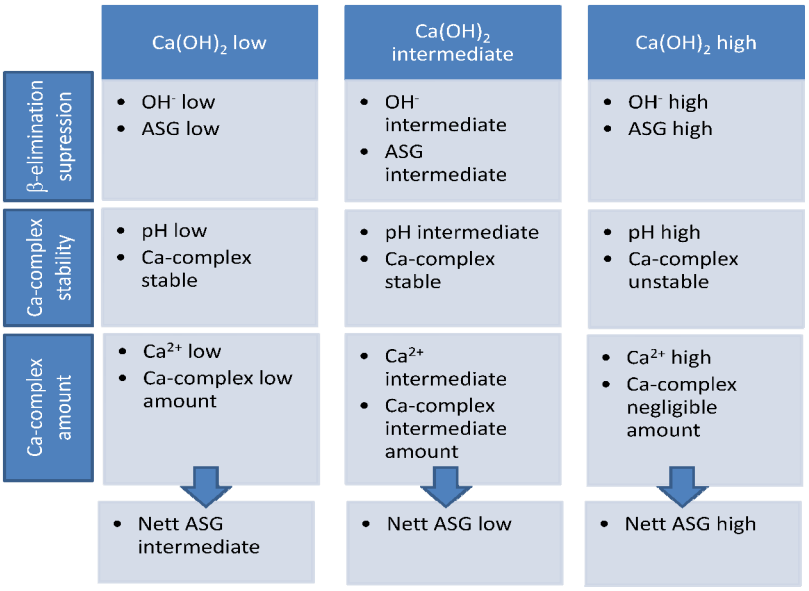

Figure 3.15: Effect on anhydrosaccharide yields due to complex formation by Ca^{2+}.

3.2.4 Effect of Acids and Alkalis on Anhydrosaccharide Composition

Apart from the observable trends relating to total anhydrosaccharide yields, we can also see significant patterns involving the anhydrosaccharide components (levoglucosan, levoglucosenone, 1,4:3,6-dianhydro-α-D-glucopyranose, 1,6-anhydro-β-D-glucofuranose). Although the total anhydrosaccharide yield may either show increasing or decreasing trends at varying acid and alkali loadings, qualitatively, Figure 3.6, Figure 3.8, Figure 3.10, Figure 3.12 and Figure 3.14 suggests that the relative yields or composition of the four main anhydrosaccharides might form distinctive profiles. Therefore, the average relative product composition for each additive was evaluated at the three experimental temperatures (550 °C, 600 °C and 650 °C) and a specific profile emerged for each additive. Figure 3.16 represents this profile across all five acid/alkaline additives and pure cellulose.

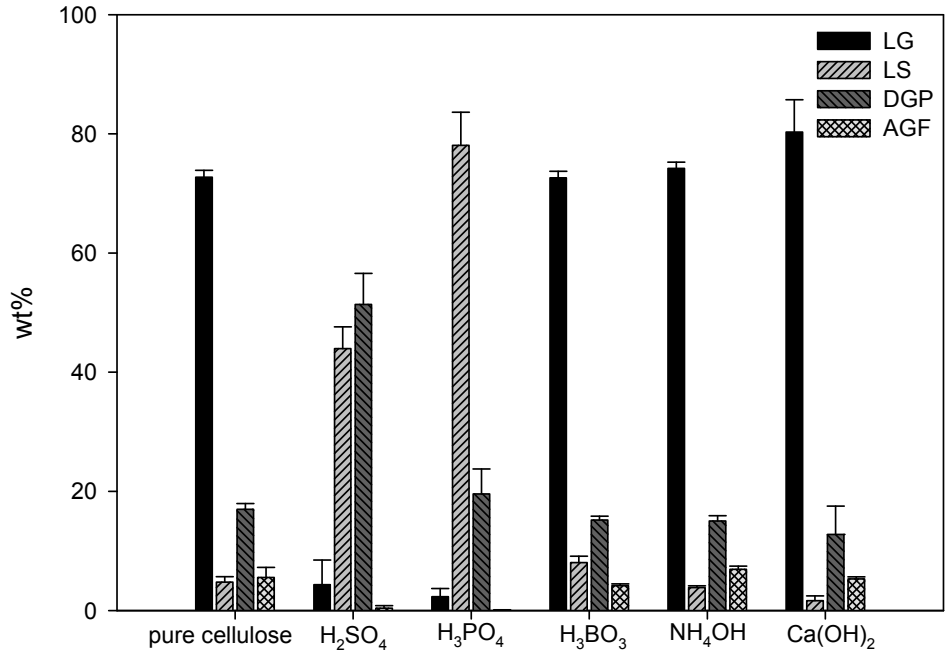

Figure 3.16: Comparison of the relative yields of the anhydrosaccharides (LG, LS, DGP and AGF) obtained for the various acid and alkali-treatments.

Figure 3.16 shows that for H_2SO_4 and H_3PO_4, the proportion of levoglucosenone is higher than levoglucosan (ca. 40 and 75 percentage points difference respectively). In addition, the levels of 1,4:3,6-dianhydro-α-D-glucopyranose are also higher than pure (untreated) cellulose and alkali-treated cellulose. The general profiles for pure cellulose, alkali-treated cellulose and H_3BO_3 treated cellulose are similar with levoglucosan being the major component.

Based on our results thus far, we can ask the question whether a lower anhydrosaccharide yield obtained in the presence of acids was due to the further breakdown (and elimination) of the anhydrosaccharides or was it due to promotion of the acid-catalysed β-elimination pathway. If we take a closer look at the boric acid treated cellulose runs, the relative amount of levoglucosan was higher than the amount

of levoglucosenone. We know from Kawamoto et al. [146, 147] that boric acid forms a stable complex with levoglucosan that prevents further transformation/breakdown. Hence in spite of this, we were still able to observe a decrease in total anhydrosaccharide yield for boric acid-infused cellulose. This therefore means that the cellulose depolymerised via the alternative β-elimination pathway.

We have also seen that at higher temperatures, the alkali-infused cellulose was able to maintain its anhydrosaccharide yields better than untreated cellulose. This stabilising effect of the alkalis is probably due to neutralisation of H^+ ions that are needed to catalyse the β-elimination pathway. This, in turn, allowed the transglycosylation pathway to be favoured during the pyrolysis.

3.2.5 Effect of Acids on the Conversion of Levoglucosan into Other Anhydrosaccharides

Another interesting aspect of the results is the seemingly large difference between the proportion of levoglucosenone obtained from H_2SO_4 and H_3PO_4 infused cellulose compared with the other samples. In fact, the levoglucosenone yield for H_3PO_4 was higher than H_2SO_4 by 35 percentage points. In order to understand these differences, we need to study the conversion of levoglucosan into the other anhydrosaccharides.

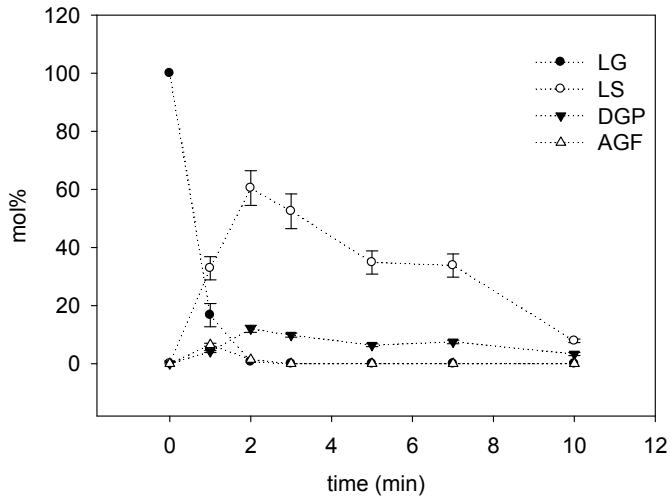

Figure 3.17: Thermochemical conversion of levoglucosan (at 200 °C) in sulfolane in the presence of 0.1 wt% H_2SO_4 into other anhydrosaccharides

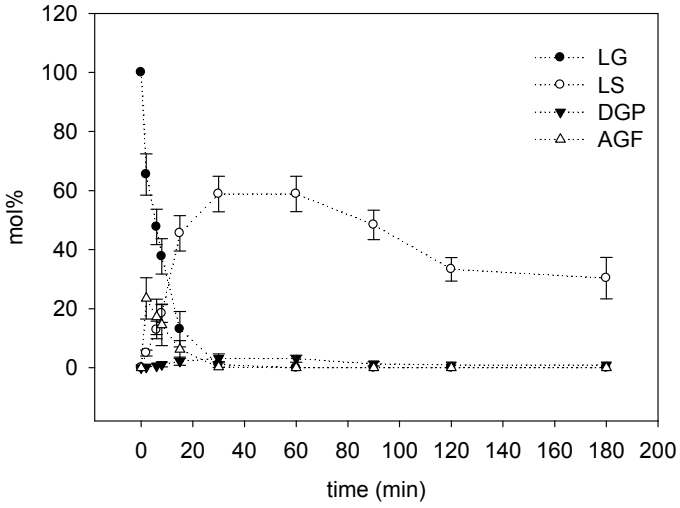

Figure 3.18: Thermochemical conversion of levoglucosan (at 200 °C) in sulfolane in the presence of 1 wt% H_3PO_4 into other anhydrosaccharides.

Figure 3.17 and Figure 3.18 show the conversion of levoglucosan into the other anhydrosaccharides (levoglucosenone (LS), 1,4:3,6-dianhydro-α-D-glucopyranose (DGP), 1,6-anhydro-β-D-glucofuranose (AGF) over a period of time. The results indicated that both H_2SO_4 and H_3PO_4 converted levoglucosan into mainly levoglucosenone. Both acids managed to achieve a maximum conversion of about 60 mol% of levoglucosenone. The main difference between them was in the rates of

conversion with the weaker acid (H_3PO_4) having a slower rate compared to the stronger acid (H_2SO_4). For H_2SO_4, most of the levoglucosan (>99 %) was converted to anhydrosaccharides and other degradation products (e.g. 5-hydroxymethyl furfural (HMF) and furfural (FF)) within 2 minutes. In comparison, levoglucosan in the presence of 1 wt% H_3PO_4 required ca. 30 minutes for 99 % conversion.

These observations explain why H_3PO_4 seems to produce more levoglucosenone compared to H_2SO_4. Due to the extremely fast conversion rates of levoglucosan in the presence of sulphuric acid, a large amount of levoglucosenone and most of the other anhydrosaccharides were degraded further to smaller compounds (e.g. hydroxymethyl furfural and furfural). On the other hand, phosphoric acid's slower conversion rate allowed more levoglucosenone to be isolated (and detected) because it degraded at a slower rate.

3.3 Summary of Acid/Alkali Effects

Based on these experimental results, it can be seen that the presence of an acid or an alkali have a significant effect on the yield of anhydrosaccharides during thermal conversion. We have observed that acids (H_2SO_4, H_3PO_4, and H_3BO_3) decreased the total amount of anhydrosaccharides. This is due to the acids catalysing the heterolytic reactions (ring-opening) that results in cellulose depolymerisation into furans as illustrated in Figure 1.2. For H_2SO_4 and H_3PO_4 infused cellulose, we also saw lower levels of levoglucosan. Here, the acids are promoting secondary dehydration reactions

which converts levoglucosan into other anhydrosaccharides like levoglucosenone, 1,4:3,6-dianhydro-α-d-glucopyranose and 1,6-anhydro-β-D-glucofuranose.

Although we see that generally, the selected acids suppress anhydrosaccharide formation through increased [H^+] levels, the degree of suppression depends not only on the strength of the acid. The three acids (H_2SO_4, H_3PO_4, and H_3BO_3) used in this study exhibited distinctive behaviours relative to each other. Hence, apart from acid strength, other possible factors that could contribute to variations within this general trend would include complex formation, acid catalysis mechanism and anion effect.

Higher temperatures were also seen to suppress anhydrosaccharide formation. This was likely due to the β-elimination pathway having a higher activation energy compared to transglycosylation. Reactions with higher activation energies tend to be favoured at higher temperatures as illustrated by Figure 3.1.

However, when cellulose was infused with alkalis (NH_4OH and $Ca(OH)_2$), the overall yield of anhydrosaccharides and levoglucosan increased accordingly. The reason for this is the neutralising effect of hydroxyl ions [OH^-] on the organic acids that are generated during pyrolysis. This in turn limits cellulose degradation via the β-elimination pathway and allows transglycosylation to proceed.

In line with available literature, we have observed the inhibiting influence of Ca^{2+} on anhydrosaccharide yields due to the likely formation of metal-sugar complexes. This effect is especially prominent at intermediate $Ca(OH)_2$ loadings. The interplay between

the countervailing effects of β-elimination suppression, Ca-complex stability and relative amounts of the Ca-complex influenced the nett anhydrosaccharide yields.

3.4 Conclusion

These observations indicate that although the β-elimination pyrolysis pathway is catalysed by the presence of acidic species at the expense of the transglycosylation pathway; it is possible to suppress the heterolytic reactions via the reduction of hydrogen ions [H^+]. As was shown in this work, the presence of hydroxyl ions [OH^-] could suppress the β-elimination pathway. However, the choice of acid or alkali is important due to the specific behaviours of the individual acid/alkali such as complex formation, acid catalysis mechanism and anion effects.

This then opens up the possibility of actively controlling and enhancing the yields of anhydrosaccharides that are potentially valuable (e.g. levoglucosenone) as pharmaceutical intermediates. Subsequently, in Chapter 4 and Chapter 5, we will focus on the kinetics of cellulose conversion and enhancing the yields of important anhydrosaccharides such as levoglucosan and levoglucosenone.

4. Influence of Acids and Alkalis on Cellulose Pyrolysis Kinetics

As seen earlier in Chapter 3, the presence of acidic and alkaline additives had affected/shifted the preference between the β-elimination and transglycosylation pyrolysis pathways. In doing so, the presence of such additives would necessarily affect the overall kinetics of cellulose pyrolysis. This would therefore manifest itself in terms of the apparent activation energy of cellulose degradation.

Practically all of the kinetics available in literature is based the degradation of pure cellulose during inert atmosphere pyrolysis. Hence, obtaining the kinetic parameters of the thermal conversion would be useful in gaining further insights into the effects of acidic and alkaline additives. We would then be able to obtain further evidence with regards to the preference of either the β-elimination or transglycosylation pathways in the presence of acid and alkaline species.

Thermogravimetric experiments were therefore conducted to study how cellulose infused with acids (H_3PO_4, H_3BO_3, H_2SO_4) and alkalis ($Ba(OH)_2$, $Ca(OH)_2$, NH_4OH) affect the apparent activation energy of cellulose thermal conversion/degradation. The apparent activation energy was found using the model-free isoconversional method. Subsequently a model-fitting method based on first-order decomposition kinetics was used to obtain the extent of cellulose conversion via the transglycosylation and β-elimination pathways. The apparent activation energy and the fraction of cellulose conversion via the pathways indicate the relative dominance of transglycosylation and β-elimination in the presence of acid and alkaline additives.

4.1 Kinetics of Cellulose Decomposition

The kinetics of cellulose thermal degradation or pyrolysis based on a single reaction, can be expressed in terms of mass conversion α by:

$$\frac{d\alpha}{dt} = k(T)f(\alpha) \tag{4.1}$$

Where $f(\alpha)$ is the reaction model and α is the conversion. The most common reaction model used is $f(\alpha)=1-\alpha$ (order one) although more recent literature have reported good fits using nuclei-growth models (e.g. Avrami-Erofeev, Prout-Tompkins) [111, 148]. The rate constant, k, obeys the Arrhenius law: $k=A\exp(-E_a/RT)$. For the activation energy E_a, a large variety of values were reported in literature which ranged from (100 to 250 kJ/mol) [111, 148-153] with the higher values being more reliable according Varhegyi et al. [154].

However, we have seen in Chapter 3, the thermal degradation of cellulose probably occurs via two-pathways namely transglycosylation and β-elimination with activation energies of ca. 200 kJ/mol and 250 kJ/mol respectively. We have also seen in Chapter 3 that the presence of acidic species (H_2SO_4, H_3PO_4, and H_3BO_3) tended to promote β-elimination whilst alkaline species (NH_4OH and $Ca(OH)_2$) promoted transglycosylation by suppressing β-elimination. Therefore, it follows that during thermal degradation, the apparent activation energy of acid-infused cellulose should be closer to 250 kJ/mol (i.e. β-elimination) whilst the apparent activation energy of alkali-infused cellulose should be closer to 200 kJ/mol (i.e. transglycosylation). Based on

these observations we can say that the use of a single activation energy to describe the thermal degradation of cellulose is not very appropriate since it actually represents the overall/average activation energy of the transglycosylation and β-elimination pathways. Apart from variations in experimental conditions, techniques and calculation methods, the large range of activation energy reported in the literature could also be attributed to the presence of these two pathways.

We will therefore show in this Chapter that the apparent thermal degradation activation energy of cellulose can be directly influenced to either increase or decrease by the presence of acids or alkalis within cellulose. In other words the magnitude of activation energies should be:

$$\mathbf{E_{a,acid\text{-}cellulose} > E_{a,pure\text{-}cellulose} > E_{a,alkali\text{-}cellulose}}$$

In addition, we will also show that the selection of the dominant pathway (transglycosylation or β-elimination) will result in a greater fraction of cellulose being degraded via that route

4.1.1 Determination of Kinetic Parameters

The available literature has shown that kinetic parameters can be found using model-fitting or model-free methods as seen in Section 2.4. In order to study the effects of acids and alkalis on cellulose thermal degradation, we will use both methods in two stages as follows:

i. Stage 1: model-free, isoconversional method to evaluate activation energy.

ii. Stage 2: model-fitting method to evaluate cellulose fraction thermally degraded by dominant pathway (transglycosylation or β-elimination).

4.1.1.1 Model-free isoconversional method (Friedman)

In the first stage, the model-free, isoconversional method was selected because the activation energy evaluated would otherwise be affected by variations being force-fitted or hidden within the reaction model parameters. Out of the several isoconversional methods available, the Friedman method was selected for use due to its utility and recommendations in recent publications as discussed in Section 2.4.4. The basic thermal degradation expression as stated in Equation (**4**.**1**) can be expressed as:

$$\ln\left(\frac{\mathrm{d}\alpha}{\mathrm{d}t}\right)_{\mathrm{i}} = \ln A + \ln[f(\alpha)] - \frac{E_\alpha}{RT_{\alpha,i}} \tag{4.2}$$

The activation energy E_a can therefore be evaluated by performing a series of thermogravimetric experiments at different heating rates. For a specific conversion α, the corresponding ($d\alpha/dt$) and temperature T can be obtained at the respective heating rates. A plot of $\ln\left(\frac{\mathrm{d}\alpha}{\mathrm{d}t}\right)$ against the reciprocal temperature should yield a straight line whose slope $\left(\frac{E_a}{R}\right)$ will provide the activation energy at that value of α. Repeating this procedure for values of α ranging from 0.05 to 0.9 will generate a profile of the variation of activation energy as the reaction progresses.

4.1.1.2 Model-fitting method

The kinetics work found in the literature is mainly focussed on obtaining the yields of the three main pyrolysis products namely char, tar and gas. In those studies, to get the kinetic parameters, the char, tar and gas yields needed to be measured instantaneously or at the end of each experimental run. Non-linear regression methods were then used on the experimental data to get the best-fitted kinetic parameters. In this study, the intermediates from β-elimination and transglycosylation are extremely difficult to isolate and measure temporally thus making the typical kinetic method unsuitable.

However, the kinetic method carried out by Capart et al. [111] is highly relevant in this study. Capart et al. have shown that cellulose thermal degradation proceeds via two pathways similar to the β-elimination and transglycosylation reaction pathways. The reaction pathways were modelled after the Prout-Tompkins nuclei-growth model and can be generally expressed as follows:

$$\frac{dx_i}{dt} = -k_i x_i^{n_i}(1 - qx_i)^{m_i} \tag{4.3}$$

Where the unreacted fraction $x = (1 - \alpha)$, α = mass conversion, initiation parameter q = 0.99 for nucleation models, n = 0.5 or 1 for Prout-Tompkins model, m = acceleration parameter and $k = Aexp\left(\frac{-E}{RT}\right)$. Subsequently, Equation (4.3) can be specifically re-written as shown in Equation (4.4) and Equation (4.5) for the two cellulose thermal degradation pathways.

(Reaction 1, Transglycosylation) with n_1 =1, Prout-Tompkins:

$$\frac{dx_1}{dt} = -k_1 x_1 (1 - 0.99x_1)^{m_1} \tag{4.4}$$

(Reaction 2, β-elimination) with m_2 =1 to ensure an induction time for generating volatiles from this pathway, which is generally thought to be the cracking route. This is because as $m_2 \rightarrow 1$, the rate of Reaction 2 (β-elimination) becomes slower. This allows transglycosylation to be faster or dominant at the initial stage whilst β-elimination lags. This is compatible with the view that acids are formed initially via further degradation of anhydrosaccharides that then promotes β-elimination:

$$\frac{dx_2}{dt} = -k_2 x_2^{n_2} (1 - 0.99x_2) \tag{4.5}$$

Where: x_1 and x_2 are the cellulose fractions involved in Reactions 1 and 2 respectively

$x_1 = f_1 \times x$ and $x_2 = f_2 \times x$, where f_1 and f_2 are the fractions of the raw cellulose involved in Reactions 1 and 2 respectively.

The 8 unknown parameters namely A_1, E_1, m_1, f_1, A_2, E_2, n_2 and f_2 were evaluated by solving the ordinary differential equations (ODEs) in MATLAB. The ODEs were solved using MATLAB's ODE45 solver which employs Runge-Katta (4,5). The equations were not stiff in this case with the ratio of eigen values being in the order of 1. The objective function used for this optimisation is the square of difference between the calculated (α_T) and experimentally obtained conversion ($\alpha_{expt,T}$) at each temperature (T) as described by the expression $\sum(\alpha_T - \alpha_{expt,T})^2$. The optimiser used is

MATLAB's in-built genetic algorithm (GA) [155] as the global optimiser for fitting the model parameters to the thermogravimetric experiment results.

The genetic algorithm based optimizer in MATLAB uses the principles of natural selection (or biological evolution) to find an optimised solution. At each iteration in the optimization process, the algorithm modifies a population of individual points by randomly selecting an individual point (parent) and mutating it to produce new points (children) for the next generation. Due to this random selection and evolution, the genetic algorithm improves the likelihood of obtaining an optimum global solution to the model-fitting. This is in contrast to local optimisers than can get trapped at local minima thus providing only locally optimised solutions.

Alternatively, the Prout-Tompkins model as expressed in Equation **(**4.4) will reduce to a first-order model when the acceleration parameter $m_1 = 0$ as shown in Equation **(**4.6). This greatly reduces the number of parameters that need to be fitted to just four (i.e. A_1, E_1, A_2, E_2**)**

$$\frac{dx_1}{dt} = -k_1 x_1 \tag{4.6}$$

Similarly, Equation **(**4.5) can also be reduced to a first-order expression:

$$\frac{dx_2}{dt} = -k_2 x_2 \tag{4.7}$$

The model-fitting method used here is typical for extracting kinetic parameters from thermogravimetric experiments and is well accepted in the field since the seminal work done by Coats and Redfern [113]. Since then, numerous workers have used these reviewed methods [114, 116, 156] to obtain kinetic parameters for various types of biomass [157, 158].

4.2 Method and Materials

In order to evaluate the activation energies and study the relative dominance between the transglycosylation and β-elimination pathways, a series of thermogravimetric experiments at different heating rates were required.

4.2.1 Experimental Design

The thermogravimetric experiments were carried out according to established protocols available in literature for the determination of activation energy [114, 116] in particular the round-robin tests [116-118] initiated by the International Confederation for Thermal Analysis and Calorimetry (ICTAC). Factors that affect the accuracy and reproducibility of the results are broadly similar to the ones discussed in the experimental design for Chapter 3 and involve the feedstock, instrument and operating conditions.

4.2.1.1 Feedstock, instrument and operating conditions

For the feedstock, variations in terms of physical characteristics (e.g. particle size, ash and moisture content) are controlled via the use of a single source of cellulose (Avicel from Sigma-Aldrich).

The instrument (TA Instruments SDT 2960) in this case acts as the reactor set-up and the pyrolysing sample is placed in a crucible. The instrument has been designed for the measurement of sample weight loss during thermal exposure and has been optimsed and calibrated to ensure reproducible measurements of temperature and weight. A schematic of the furnace and microbalance components of the Thermogravimetric Analyser (TGA) is shown in Appendix G. However, it is known that variations in thermogravimetric results are possible when using different types of TGA [117, 120, 153]. We therefore conducted round-robin assessments of the three TGAs available (Seteram Setsys-Evolution TGA, TA Instruments Q500 TGA and TA Instruments SDT 2960 DSC-TGA) for this study and the TGA chosen (SDT 2960) provided consistently accurate and reproducible results based on pure cellulose thermal conversion.

The sample amount used was kept to a minimum to ensure that the sample layer within the crucible is as thin as possible. This is to ensure uniform sample temperature and reduce diffusion resistance of products leaving the sample. However, there is a trade-off between ensuring a thin layer of sample within the crucible and accuracy of weight loss measurement. Using very small sample amounts limits the range of weight loss measurement. After conducting trials with cellulose samples ranging from 3 to 10 mg,

the amount of cellulose used in this study was fixed at 6 mg as it provided the most consistent kinetic parameters for cellulose thermal conversion when compared with literature values.

In terms of operating conditions, the instrument was purged with nitrogen to ensure an inert atmosphere during thermal conversion. The temperature profile of each experimental run was kept the same with variations made only to the heating rates during the temperature ramping stage for dynamic analysis.

4.2.1.2 Experimental variables

The experiments conducted were based on a two-factor factorial design. There were a total of six types of additives (H_3PO_4, H_3BO_3, H_2SO_4, $Ba(OH)_2$, $Ca(OH)_2$ and NH_4OH) and three infusion levels (low, medium and high) being studied. The main focus of the experiments was to find out the influence/response of these additives on the apparent activation energy. There were therefore a total of 18 different combinations. Since these thermogravimetric experiments were for kinetics analysis, five different heating rates were conducted for each combination to obtain a single activation energy value. In addition, 6 replicates were done for each experimental combination. The two-factor analyses of variance for these experiments are discussed in Section 4.3.5.

4.2.2 Sample Preparation

Cellulose samples were prepared using the same method described in Chapter 3. Different mineral acids (H_3PO_4, H_3BO_3 and H_2SO_4) and alkalis ($Ba(OH)_2$, $Ca(OH)_2$ and NH_4OH) were infused by stirring microcrystalline cellulose (Avicel from Sigma-Aldrich) with the required acid/alkali solution (0.5 to 5 wt %) at ca. 25 °C for 30 minutes. The slurry was then filtered and dried overnight at 40 °C.

For each acid (H_3PO_4, H_3BO_3 and H_2SO_4) and alkali ($Ba(OH)_2$, $Ca(OH)_2$ and NH_4OH) used for cellulose infusion, three sets of samples were prepared at varying loadings as shown in Table 4.1.

Table 4.1: Preparation solution concentration of acids and alkalis for cellulose infusion

Acid	H_3PO_4			H_3BO_3			H_2SO_4		
Preparation solution wt%	2	3	5	2	3	5	0.5	1	2
Alkali	$Ba(OH)_2$			$Ca(OH)_2$			NH_4OH		
Preparation solution wt%	0.1	0.5	1	0.1	0.5	1	2	3	5

As in Chapter 3, varying the concentration of the preparation solution will cause the loadings of the various acids and alkalis to also vary. Although initial infusion levels attempted for H_2SO_4 and NH_4OH were the same with the other acids and alkalis respectively, adjustments were made due to specific behaviours of H_2SO_4 and NH_4OH. The concentration used for H_2SO_4 used was lower than that used for H_3PO_4 and H_3BO_3 due to the strength of sulphuric acid having the potential to cause hydrolysis prior to the actual thermal analysis. In addition, the lower alkali concentrations for $Ba(OH)_2$

and $Ca(OH)_2$ were due to solubility constraints whilst higher concentrations of NH_4OH were used to offset the volatility of ammonia during thermal analysis.

4.2.3 Thermogravimetric Analysis

Thermogravimetric analyses were carried out with a TA Instruments SDT 2960 Simultaneous DSC-TGA. The system consists of a bifilar-wound furnace and a furnace tube enclosing two beams with platinum sensors at their ends where the sample and reference pans sit. Alumina pans with a volume of 90 µl were used. For each test, the sample pan was loaded with 6 mg of pure/treated cellulose sample and the reference pan was left empty. Nitrogen (flowrate = 200 ml/min) was used to purge the furnace tube throughout the test.

The thermal degradation was studied under non-isothermal conditions. The furnace temperature profile was programmed as follows:

i. linear increase at 5 °C/min from ambient to 50 °C: initial temperature ramp for sample drying
ii. isothermal at 50 °C for 30 minutes: to ensure stability of sample prior to actual thermal analysis
iii. linear increase at various rates (2, 3, 4, 5 and 6 °C/min) from 50 °C to 650 °C: non-isothermal thermal analysis region
iv. isothermal at 650 °C for 10 minutes: end of thermal analysis

Weight and temperature measurements were recorded from the DSC-TGA's micro-balance (sensitivity of 0.1 μg) and thermocouple (ΔT sensitivity of 0.001 °C) connected to the beams and processed via TA Universal Analysis software. The SDT 2960 was calibrated using three reference materials namely Tin (mp = 231.9 °C), Lead (mp = 327.5 °C) and Zinc (mp = 419.5 °C).

4.2.4 Coupled TGA-FTIR Analysis

The presence of secondary reactions could affect thermogravimetric analysis of cellulose thermal conversion/degradation. To study the onset of these secondary reactions, experiments were conducted using a coupled TGA – FTIR system which was interconnected via a heated transfer line, a valve manifold and a transmission cell adapted to gases. The TGA used was the Setaram Setsys Evolution and the coupled FTIR was the Digilab Excalibur FTS3000. A modified set-up was designed to allow for sampling of condensable pyrolysis products via the use of a liquid trap in between the TGA and FTIR. The experimental set-up is shown in Figure 4.1.

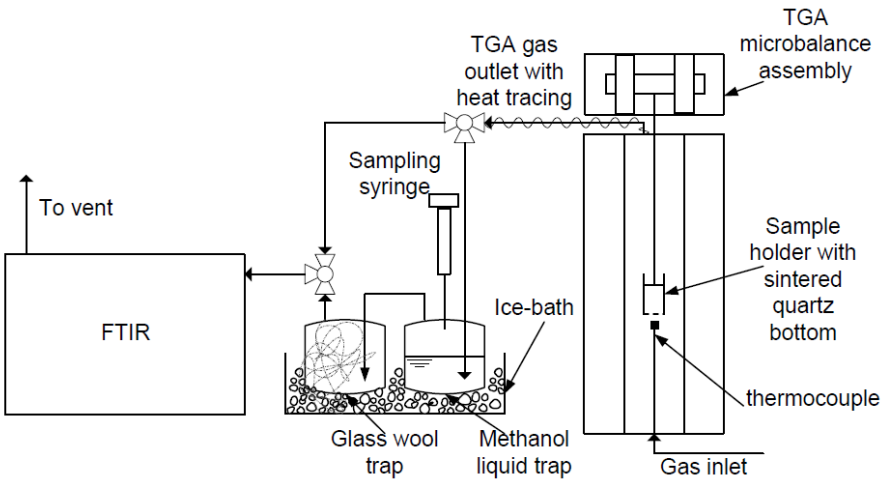

Figure 4.1: Schematic representation of the coupled TGA-FTIR analysis of cellulose thermal degradation

The TGA system comprises of a graphite furnace that contains a vertical tube in which the sample pan is hung on a beam balance with a resolution of 0.03 µg. The quartz sample pan is a cylindrical container with an approximate volume of 3 ml, an outer diameter of 12.7 mm and a height of 25.4 mm. The sample pan has a sintered bottom to allow for better heat and mass transfer.

The cellulose samples used were prepared according to the procedure stated in Section 4.2.2. For each run, 200 mg of sample was loaded into the pan and suspended in the furnace swept with nitrogen at a flow rate of 10 ml/min. The TGA-FTIR analyses were started simultaneously once mass readings began to stabilize. The heating profile performed on the samples was as follows:

(i) ramp at 10 °C/min from 25 °C to 50 °C

(ii) isothermal at 50 °C for 30 min

(iii) ramp at 5 °C/min from 50 °C to 650 °C

(iv) isothermal at 650 °C for 10 min

The pyrolysis vapour from the TGA was carried by the sweep gas to pass through a methanol liquid trap (0 – 4 °C) that condensed and captured furfurals from the pyrolysis vapours. Entrained aerosols were trapped in the neighbouring glass wool trap (0 – 4 °C) leaving predominantly non-condensable gases such as CO, CO_2 and CH_4 to pass through to the FTIR for real-time analysis. The FTIR spectrometer was set to collect spectra at 10 seconds interval during the evolved gas analysis and generate reconstructions of total IR response versus time. A scanning range of 600 to 4000 cm^{-1} and a resolution of 4 cm^{-1} were used for the experiments. The infrared spectrum of methane contains two strong absorption bands due to C-H stretching (3020 cm^{-1}) and bending (1300 cm^{-1}) modes. Methane was measured due to it being a product of secondary thermal conversion reactions.

In addition to the gas phase measurements for methane, another indicator of secondary reaction onset is the presence of furfurals. Furfurals are formed from scission and ring opening reactions that take place after the initial transglycosylation and β-elimination reactions. The furfurals were measured via sampling of the methanol trap at regular intervals. A volume of 1.5 ml was collected through a syringe, filtered through a 2 μm syringe filter and injected into the GC-MS for detection and quantification of furfurals. The settings for the GC-MS were as follows:

(i) GC column: DB-1701, 60 m x 0.25 mm, ID 0.25 μm

(ii) Inlet system: 1 μl, 50:1 split injector, 200 kPa He at 250 °C

(iii) Oven: 45 °C for 5 min followed by ramp at 15 °C/min to 250 °C and 5 min hold

(iv) Mass spectrometer: EI mode, scanning mass range 20-200 m/z, 6 min solvent delay. Ion source at 230 °C and transfer line at 280 °C

4.3 Results and Discussion

Thermal analysis using the DSC-TGA was first carried out on pure, untreated microcrystalline cellulose samples at the various heating rates. This was done to compare our results with literature values and verify the compatibility of our instrument and techniques. The activation energy for pure cellulose using Friedman's isoconversional method was then calculated and is shown in Table 4.2.

Table 4.2: Variation of activation energy of pure cellulose thermal degradation at various conversions.

α	**0.1**	**0.2**	**0.3**	**0.4**	**0.5**	**0.6**	**0.7**
E_a **(kJ/mol)**	175	193	199	200	208	213	230

The mean activation energy was found to be 203 ± 13 kJ/mol (at 95 % confidence limit) and this was very close to the values obtained by Capart et al. [111] which obtained activation energies of 203 kJ/mol (isothermal mode) and 200 kJ/mol (non-isothermal mode).

4.3.1 Conversion Rate Profiles of Cellulose Degradation

Following the results for pure cellulose, similar experiments and analysis were carried out for cellulose samples that were infused with the various acids (H_3PO_4, H_3BO_3 and H_2SO_4) and alkalis ($Ba(OH)_2$, $Ca(OH)_2$ and NH_4OH). An analysis of the cellulose degradation rates as expressed by ($d\alpha/dt$) against the progress of the reaction indicated by conversion α is useful in determining the presence of multiple reactions. It will also help us in determining the starting and ending points of the main thermal degradation reaction(s). The typical conversion profiles of the acid and alkali-infused cellulose are shown in Figure 4.2 to Figure 4.7 below. The rest of the profiles of the various acids and alkalis can be found in Appendix E1 and Appendix E2 respectively.

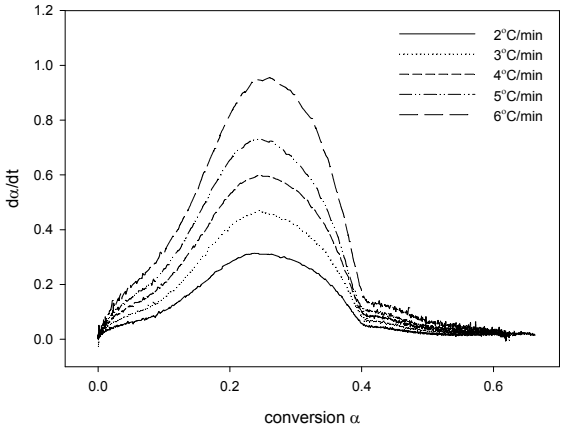

Figure 4.2: Variation of conversion rate ($d\alpha/dt$) for cellulose infused with 5 wt% H_3PO_4 at various TGA heating rates (2-6 °C/min).

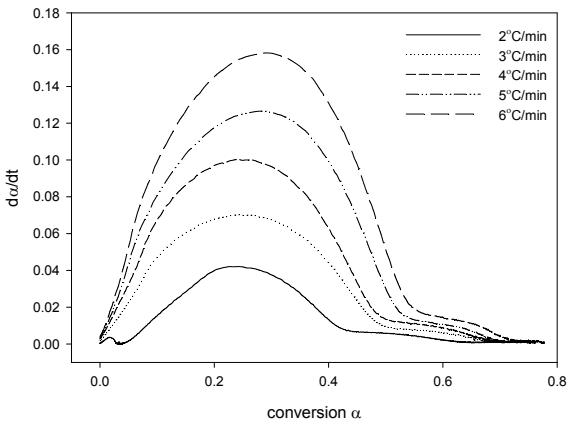

Figure 4.3: Variation of conversion rate ($d\alpha/dt$) for cellulose infused with 5 wt% H_3BO_3 at various TGA heating rates (2-6 °C/min).

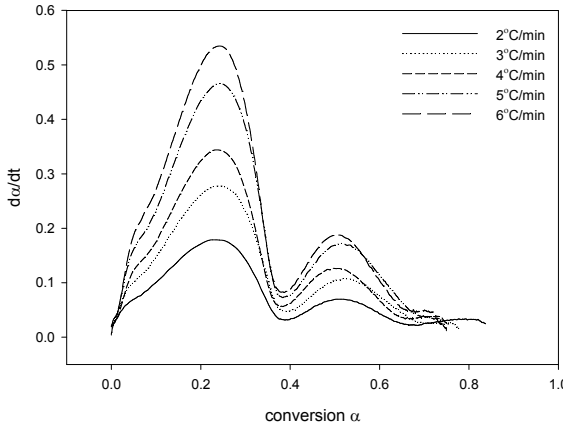

Figure 4.4: Variation of conversion rate (*dα/dt*) for cellulose infused with 2 wt% H_2SO_4 at various TGA heating rates (2-6 °C/min)

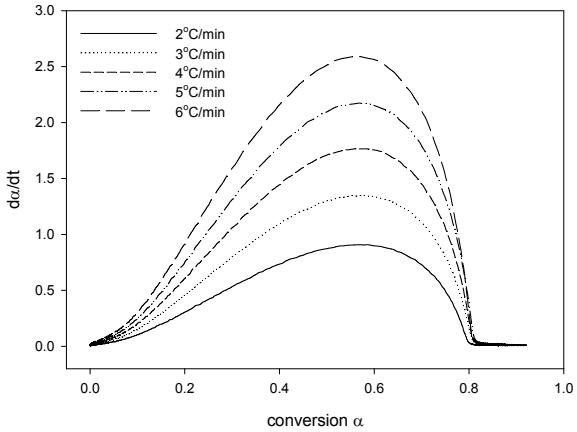

Figure 4.5: Variation of conversion rate (*dα/dt*) for cellulose infused with 1 wt% $Ba(OH)_2$ at various TGA heating rates (2-6 °C/min)

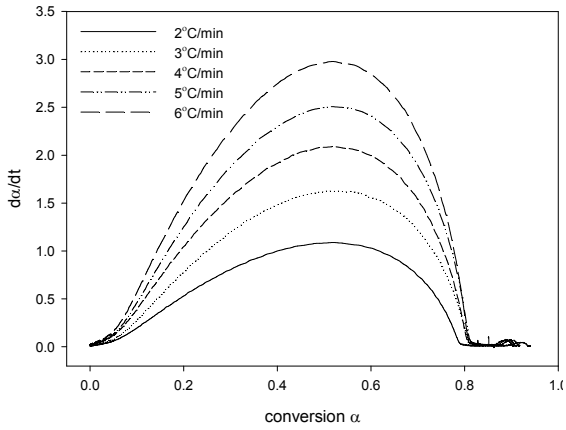

Figure 4.6: Variation of conversion rate (dα/dt) for cellulose infused with 1 wt% $Ca(OH)_2$ at various TGA heating rates (2-6 °C/min)

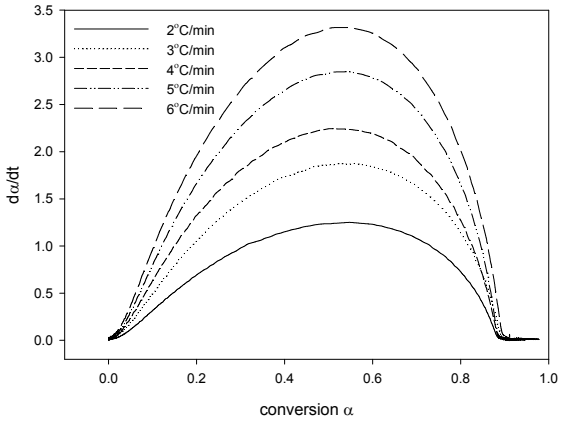

Figure 4.7: Variation of conversion rate (dα/dt) for cellulose infused with 5 wt% NH_4OH at various TGA heating rates (2-6 °C/min)

Based on these profiles, a few observations can be made. Firstly, for the three acids, it can be seen that the main thermal degradation reaction terminates when the conversion $\alpha = 0.4$. It is likely that a second reaction is occurring when $0.4 < \alpha < 0.8$ and this is prominently shown by the twin peaks in Figure 4.4 for cellulose infused with H_2SO_4. On the other hand, for the alkalis, the thermal degradation profiles were consistently

smooth indicating that there was a single primary reaction throughout conversion levels from $\alpha = 0$ to $\alpha = 0.7$. Hence, for the evaluation of activation energy, we will only consider the values of $0 < \alpha < 0.4$ for the acid-infused cellulose while for the alkalis, we will evaluate in the region $0 < \alpha < 0.7$.

4.3.2 Effect of Acids and Alkalis on Activation Energy

The thermogravimetric data that were presented in Section 4.3.1 were then analysed using the Friedman method to obtain the activation energy without the need to define a specific reaction model. This is to allow us to compare the activation energy of the dominant thermal degradation reaction without having potential variations caused by the acids and alkalis being subsumed into the kinetic pre-exponential factor of the reaction model parameters.

4.3.2.1 Activation energy for cellulose infused with acids

Figure 4.8, Figure 4.9 and Figure 4.10 show the activation energy isoconversion plots for H_3PO_4, H_3BO_3 and H_2SO_4-infused cellulose respectively.

We can see in Figure 4.8 that the activation energy for H_3PO_4 is clustered closely around the 250 kJ/mol level.

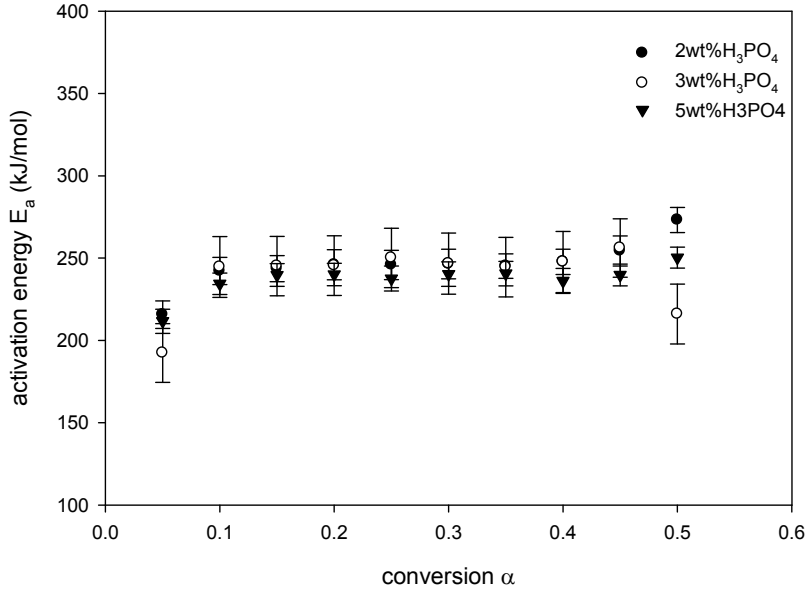

Figure 4.8: Variation of activation energy with conversion for cellulose degradation with various wt% H_3PO_4 added

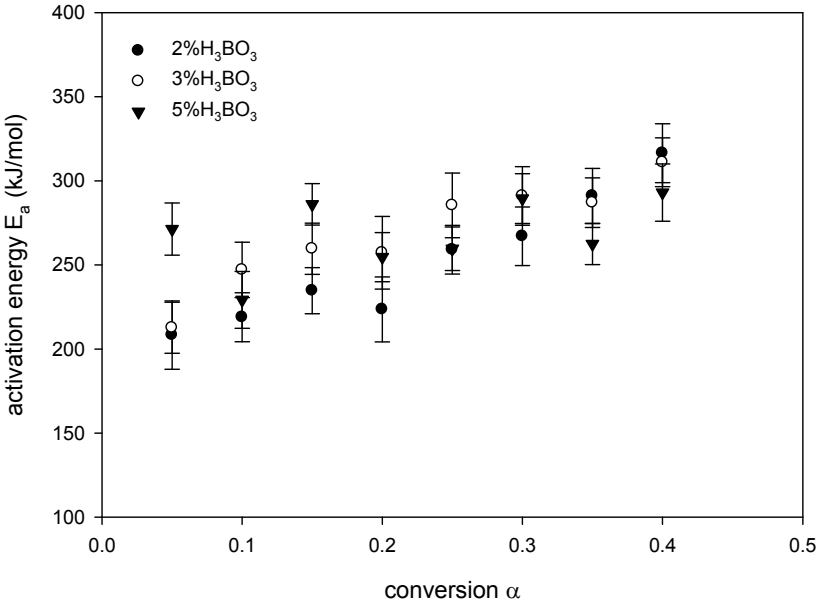

Figure 4.9: Variation of activation energy with conversion for cellulose degradation with various wt% H_3BO_3 added

In Figure 4.9, the activation energy scatter for H_3BO_3 infused cellulose seems to be more widely distributed although most seem to still cluster close to the 250 kJ/mol

level. The mean values are seen to range from ca. 310 kJ/mol to as low as ca. 220 kJ/mol.

For H_2SO_4 treated cellulose (see Figure 4.10), we can see that the results were again mostly clustered near the 250 kJ/mol value. The distinct variation here is that there is a trend when $\alpha > 0.3$ where the activation energy dips from the 250 kJ/mol level to as low as 100 kJ/mol. This low activation energy is symptomatic of char forming reactions occurring. This behaviour seen in the profile is corroborated by the larger amount of charred residue seen in the sample pans after the thermogravimetric experiments for H_2SO_4 treated cellulose.

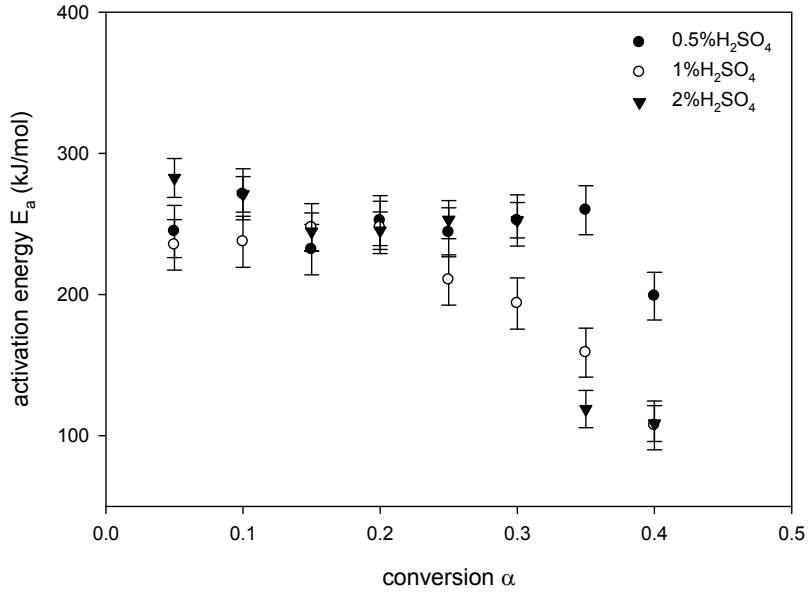

Figure 4.10: Variation of activation energy with conversion for cellulose degradation with various wt% H_2SO_4 added

The mean values of activation energies for all the acid treated samples were calculated and are presented in Table 4.3.

Table 4.3: Average activation energy of cellulose with the various acid additives

	2 wt% H_3PO_4	3 wt% H_3PO_4	5 wt% H_3PO_4
E_a(kJ/mol)	249 ± 9	247 ± 12	239 ± 6
	2 wt% H_3BO_3	3 wt% H_3BO_3	5 wt% H_3BO_3
E_a(kJ/mol)	252 ± 26	258 ± 26	268 ± 15
	0.5 wt% H_2SO_4	1 wt% H_2SO_4	2 wt% H_2SO_4
E_a(kJ/mol)	246 ± 15	235 ± 34	258 ± 47

4.3.2.2 Activation energy for cellulose infused with alkalis

Similar to the analysis done for the acid samples, the activation energies for alkalis ($Ba(OH)_2$, $Ca(OH)_2$ and NH_4OH) were calculated using Friedman's method and presented as isoconversion plots in Figure 4.11, Figure 4.12 and Figure 4.13 respectively.

In contrast to the acid treated cellulose plots which clustered mainly at the 250 kJ/mol level, the alkali-treated samples showed clustering at or just below the 200 kJ/mol level. The $Ba(OH)_2$ and $Ca(OH)_2$ plots were seen to be less scattered compared to the NH_4OH sample plots. The NH_4OH treated cellulose samples had activation energies ranging from ca. 180 to 210 kJ/mol. Overall the plots are seen to more consistent than the acid treated cellulose plots which is to be expected due to the smoother conversion rates plots shown in Section 4.3.1.

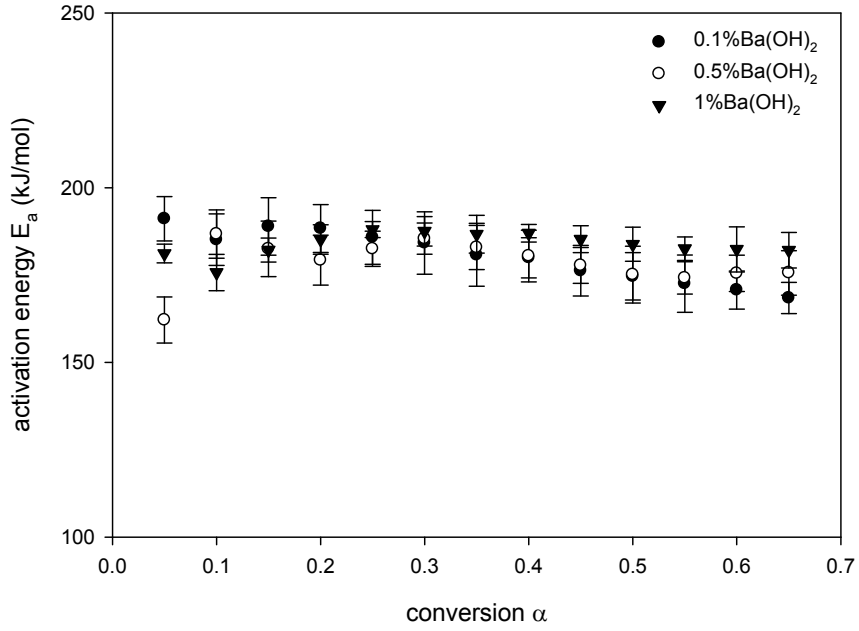

Figure 4.11: Variation of activation energy with conversion for cellulose degradation with various wt% $Ba(OH)_2$ added

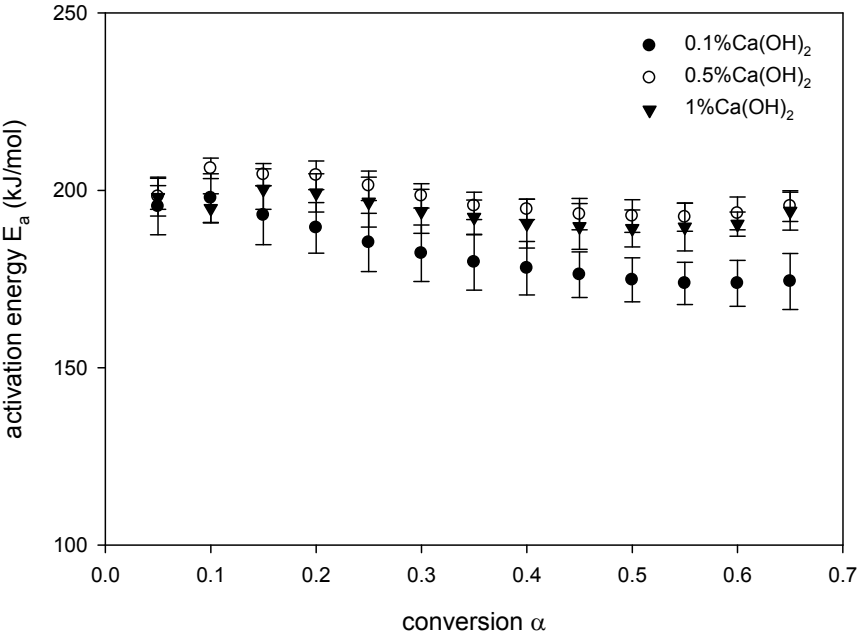

Figure 4.12: Variation of activation energy with conversion for cellulose degradation with various wt% $Ca(OH)_2$ added

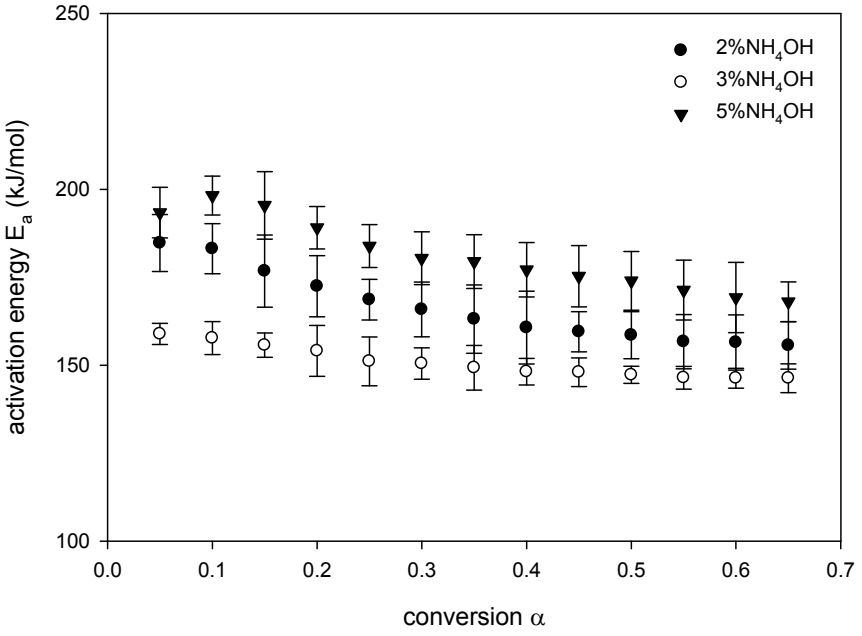

Figure 4.13: Variation of activation energy with conversion for cellulose degradation with various wt% NH_4OH added.

When the respective mean activation energies were calculated (see Table 4.4), it can be seen that the values are significantly less than the values obtained for the acid treated cellulose samples. In fact, they seem to be consistently below the 200 kJ/mol level as was initially expected for transglycosylation reaction. This is confirmed by the statistics obtained for the t-test.

Table 4.4: Average activation energy of cellulose with the various alkaline additives.

	0.1 wt% $Ba(OH)_2$	0.5 wt% $Ba(OH)_2$	1 wt% $Ba(OH)_2$
E_a(kJ/mol)	181 ± 5	178 ± 3	184 ± 2
	0.1wt% $Ca(OH)_2$	0.5wt% $Ca(OH)_2$	1 wt% $Ca(OH)_2$
E_a(kJ/mol)	183 ± 5	198 ± 2	194 ± 6
	2 wt% NH_4OH	3 wt% NH_4OH	5 wt% NH_4OH
E_a(kJ/mol)	166 ± 4	151 ± 3	181 ± 2

This shift of the activation energy to ca. 180 kJ/mol is lower than the expected activation energy of 200 kJ/mol for the transglycosylation pathway. This could be partially due to potential secondary effects of the cations of the alkalis. It does however provides some evidence that the β-elimination pathway was suppressed.

4.3.3 Effect of Acid and Alkali on Dominant Pathway

The results in Stage 1 as presented in Section 4.3.2 have shown that acids and alkalis can have a significant effect on the apparent activation energy of cellulose thermal degradation/pyrolysis. It would seem that the presence of acids would cause β-elimination to be the dominant thermal degradation pathway while alkalis would result in transglycosylation being the dominant pathway. However, the degree of dominance cannot be readily inferred from the activation energies alone. To get greater insight into the effect of acids and alkalis on the pathways, we needed to move from a model-free method towards a model-fitting method.

In Stage 2, we have attempted to use the nuclei-growth model as demonstrated by Capart et al. [111] along with the simple first-order model that have been used by numerous earlier workers. We conducted a comparison of these two models to ascertain their suitability based on our thermogravimetric data. We then proceeded to apply the selected model on the data we have obtained for the thermal degradation of acid (H_3PO_4 and H_3BO_3) and alkali ($Ba(OH)_2$ and $Ca(OH)_2$) infused cellulose samples. The parameters obtained from the model-fitting were then used to study the relative fractions of cellulose that thermally degrades via the transglycosylation and β-

elimination pathways. The thermogravimetric data for H_2SO_4 and NH_4OH were not used for this pathway analysis to focus the analysis on cellulose samples that were infused at similar levels of acids and alkalis.

4.3.3.1 Model-fitting for pure cellulose degradation

Model-fitting of the thermogravimetric data was carried out as described in Section 4.1.1.2. The model parameters used were as stipulated in Capart et al. [111] and shown in Table 4.5.

Table 4.5: Parameters used for Capart et al. [111] model.

Transglycosylation	n_1	m_1	f_1	A_1 **(1/s)**	E_1 **(kJ/mol)**
	1	0.481	0.75	1.94×10^{15}	202.65
β-elimination	n_2	m_2	f_2	A_2 **(1/s)**	E_2 **(kJ/mol)**
	22	1	0.163	1.63×10^{20}	255

The results of the simulated cellulose thermal degradation using Capart's model are shown in Figure 4.14. As can be seen in the plots, the Capart model does not seem to fit the experimental cellulose thermal degradation data that we have obtained. However, qualitatively, the overall shape of Capart's model curves are consistent with the experiment data.

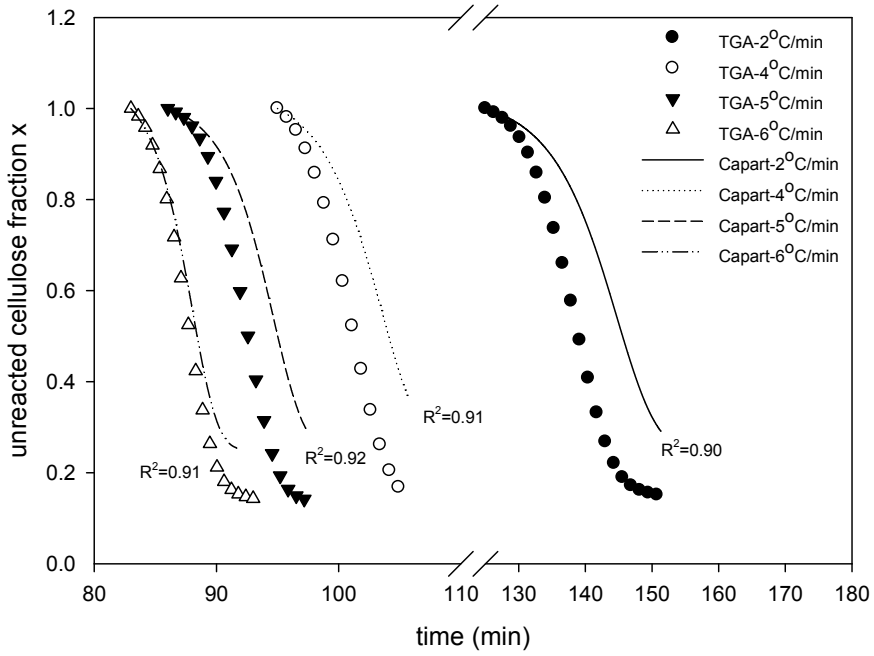

Figure 4.14: Comparison of Capart's model fit with pure cellulose degradation at varying heat rates (2 - 6 °C/min).

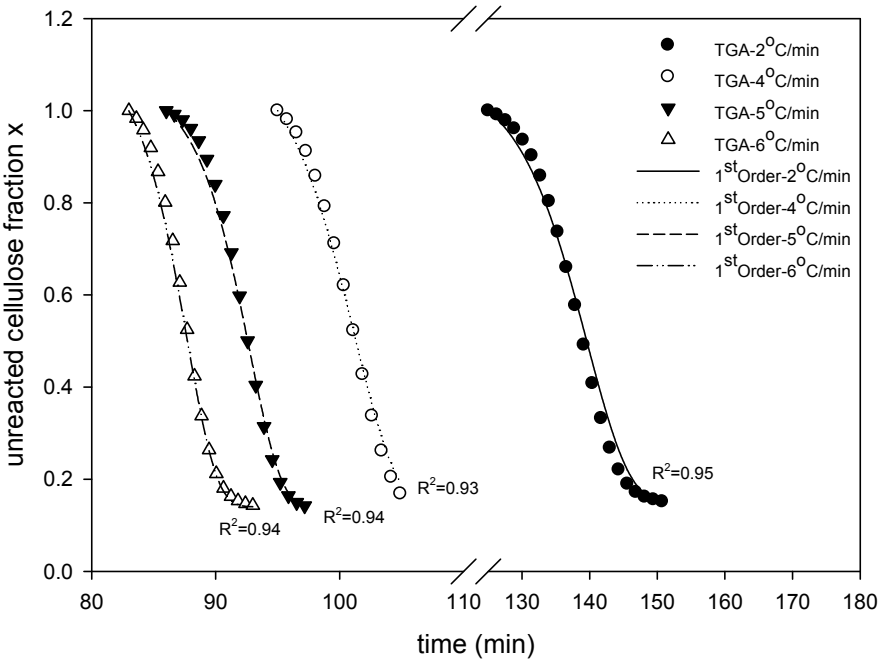

Figure 4.15: Comparison of first-order model fit for pure cellulose degradation at varying heating rates (2 - 6 °C/min).

We then freed the constraints on Capart's model parameters and allowed the MATLAB algorithm to optimise the parameters using the in-built genetic algorithm. The fitted model parameters obtained from this optimisation process are n_1=1.0, m_1=6.6x10^{-5}, n_2=1.0, m_2=0.02. These values practically collapse the nuclei-growth model into a first-order reaction model as described by Equation (4.6) and Equation (4.7).

We then proceeded with fitting the experimental data with this first-order model and obtained reasonably good fits as shown in Figure 4.15 for the different heating rates.

$$R^2 = 1 - \frac{\sum_{i=1}^{n}(y_i - f_i)^2}{\sum_{i=1}^{n}(y_i - \bar{y})^2} \tag{4.8}$$

Where y_i is the observed/experimental data value, f_i is the predicted value from the fit and $\bar{y}$ is the mean of the observed data.

Based on this first-order model, the amount of intermediates generated from transglycosylation and β-elimination was found. The final level of these intermediates gives an indication of the fraction of cellulose that degraded along each of the pathway. The results for pure cellulose thermal degradation are shown in Table 4.6.

Table 4.6: Fitted model parameters obtained for first-order thermal degradation model – pure cellulose.

Heating rate (°C/min)	f_1	f_2	A_1 (1/s)	E_1 (kJ/mol)	A_2 (1/s)	E_2 (kJ/mol)
6	0.75	0.11	1.46×10^{15}	203	2.00×10^{19}	260
5	0.62	0.24	1.46×10^{15}	203	2.00×10^{19}	255
4	0.55	0.26	1.46×10^{15}	203	2.00×10^{19}	254
2	0.50	0.35	4.55×10^{15}	208	1.43×10^{20}	261

The activation energy obtained from the MATLAB simulation showed that transglycosylation has a mean activation energy E_1 = 204 kJ/mol whilst β-elimination has a mean activation energy E_2 = 257 kJ/mol. These values are generally consistent with the expected values for the two pathways. We are also able to observe that the fraction of cellulose thermally degraded via transglycosylation was greater than that via β-elimination as evidenced by f_1 and f_2 values respectively. The fraction of cellulose that underwent thermal degradation via transglycosylation pathway varied from 0.5 to 0.75 with the fraction increasing with increasing heating rates. The ratio f_1:f_2 ranged from 1.4:1 to 6.8:1. This provides an indication that transglycosylation is the dominant pathway for pure cellulose thermal degradation/pyrolysis.

Cellulose thermal degradation (pyrolysis) has been widely modelled using the 1st order model. Capart et al. [111] proposed model was based on a Prout-Tompkins nucleation model. In this study, we have seen that the first-order model provides a better fit when compared to Capart's model [111]. This variation could be due to two factors that were inherent in the experimental method carried out by Capart et al. [111].

i. **Effect of different instrument:** Capart et al. [111] had used a Setaram TGA 92 to obtain their thermogravimetric data. It is known that the experimental

conditions, including instrument type, can have a significant effect on the results obtained [117, 120, 153]. In addition, we have also conducted a set of round-robin tests involving three different types of instruments namely, Seteram Setsys-Evolution TGA, TA Instruments Q500 TGA, and TA Instruments SDT 2960 DSC-TGA. The main source of difference between the three instruments lies in how the temperature of the heated sample is being measured. In the first two TGAs, the thermocouple is not in direct contact with the heated sample although it is placed very close to the sample surface. This is different for the SDT 2960 where the thermocouple is in direct contact with the sample crucible. Based on our round-robin tests, the SDT 2960 gave the most reliable and consistent results and this was the reason why the instrument was subsequently used in this study. This effect of thermocouple placement was also noted by Capart et al. [111] who had to incorporate a correction factor in his results to account for this effect.

ii. **Effect of heating rates:** Capart et al. [111] had used higher heating rates of up to 11 °C/min in his experiments to obtain the parameters for his model. This could be the reason why the fits for Capart's model [111] seem to be better at 6 °C/min rather than at the lower heating rates. We had used lower heating rates in order to discriminate between the different pathways that are likely to be present.

Therefore, the first-order model that was successfully used for pure cellulose was then applied to the acid (H_3PO_4 and H_3BO_3) and alkali ($Ba(OH)_2$ and $Ca(OH)_2$) -infused cellulose samples in the subsequent Section 4.3.3.2 to Section 4.3.3.5.

4.3.3.2 Modelling for H_3PO_4 infused cellulose degradation

The comparison plots of the first-order simulation results and experimental TGA data for H_3PO_4-infused cellulose degradation are shown in Figure 4.16 to Figure 4.18.

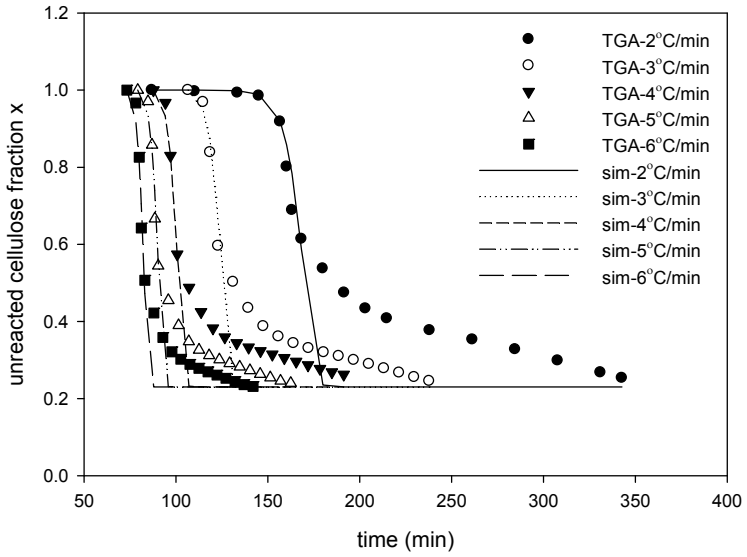

Figure 4.16: 1st order reaction model fit of cellulose (with 2 wt% H_3PO_4) degradation at various TGA heating rates (2-6 °C/min).

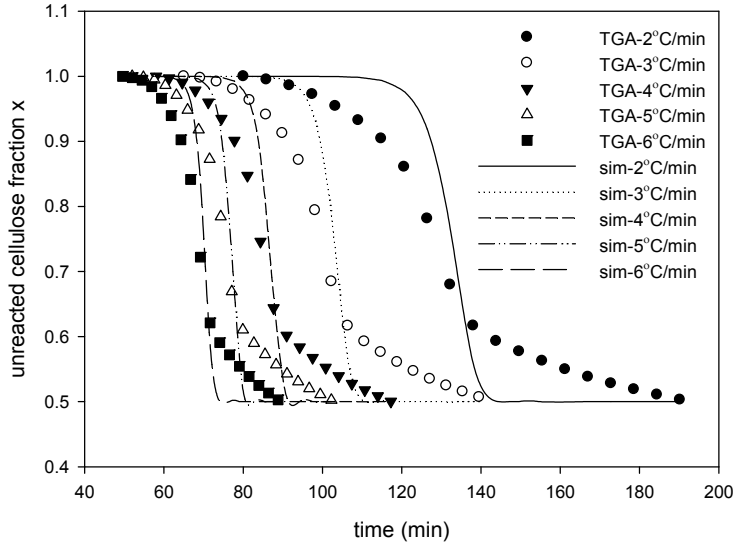

Figure 4.17: 1st order reaction model fit of cellulose (with 3 wt% H_3PO_4) degradation at various TGA heating rates (2-6 °C/min).

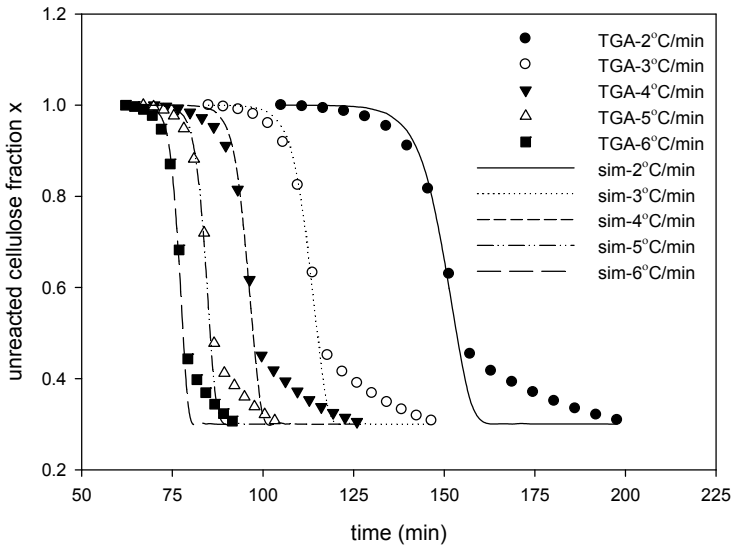

Figure 4.18: 1st order reaction model fit of cellulose (with 5 wt% H_3PO_4) degradation at various TGA heating rates (2-6 °C/min).

From a qualitative point of view, the first-order model seems to be able to provide an adequate fit for the experimental results. The fit is better in the initial stages compared to the latter stages of thermal degradation as seen from the deviation when the fraction of unreacted cellulose x is less than 0.4 (i.e. conversion $\alpha > 0.6$). The experimental data points indicated a decrease in degradation rate towards the end. This is probably due to the presence of secondary reactions (e.g. charring) that were discussed in Section 4.3.1 and Section 4.3.2. The overall goodness of fit as expressed by R^2 was greater than 0.92 (see Table E3.1) and can be generally thought to be reasonable with the understanding that the kinetic parameters obtained to be representative only of the initial stage of the thermal degradation process. Fittings of the Capart equations (Equations (4.4) and (4.5)) were also attempted on the acid-infused (H_3PO_4 and H_3BO_3) cellulose samples. The resulting fits of the first-order model for acid-infused cellulose were better than for Capart's model (R^2<0.8).

The fitted kinetic values obtained for the various levels of H_3PO_4 loadings are listed in Table E4.1. The results show that the activation energy for transglycosylation path, E_1 had a mean of 199 kJ/mol whilst β-elimination had a mean activation energy of 255 kJ/mol. These values are similar to the activation energy results for pure cellulose (literature and current work). More significantly, we note that the fraction of cellulose involved in β-elimination (f_2) was higher than the fraction for transglycosylation (f_1). The ratio of f_1:f_2 ranged from 1:2.5 to 1:5. This is a reversal from the results that we obtained for pure cellulose. It is also indicative of the β-elimination pathway being dominant during the thermal degradation of H_3PO_4 infused cellulose.

4.3.3.3 Modelling for H_3BO_3 infused cellulose degradation

Thermal degradation/pyrolysis data of H_3BO_3 infused cellulose was subjected to the same analysis and the model-fitting plots are presented in Figure 4.19, Figure 4.20 and Figure 4.21.

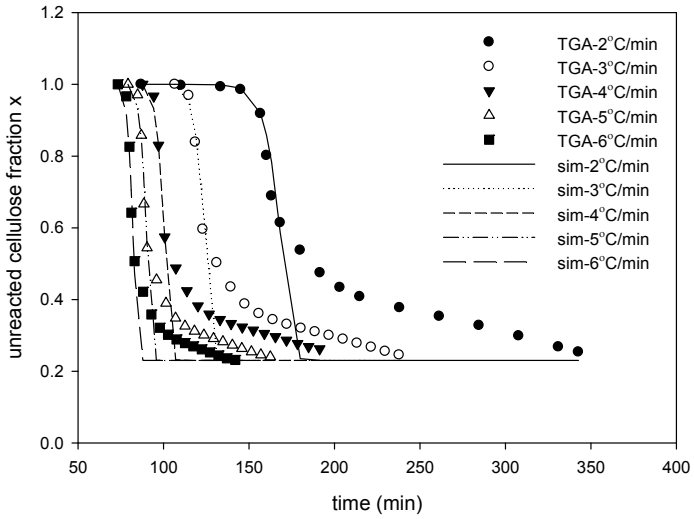

Figure 4.19: 1st order reaction model fit of cellulose (with 2 wt% H_3BO_3) degradation at various TGA heating rates (2-6 °C/min).

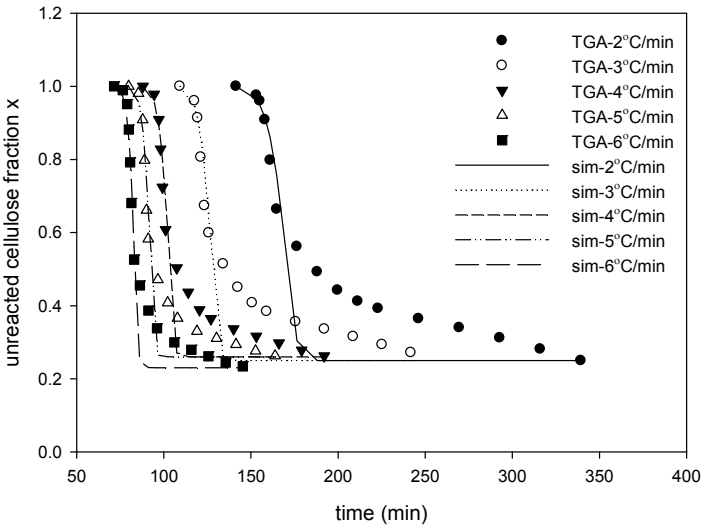

Figure 4.20: 1st order reaction model fit of cellulose (with 3 wt% H_3BO_3) degradation at various TGA heating rates (2-6 °C/min).

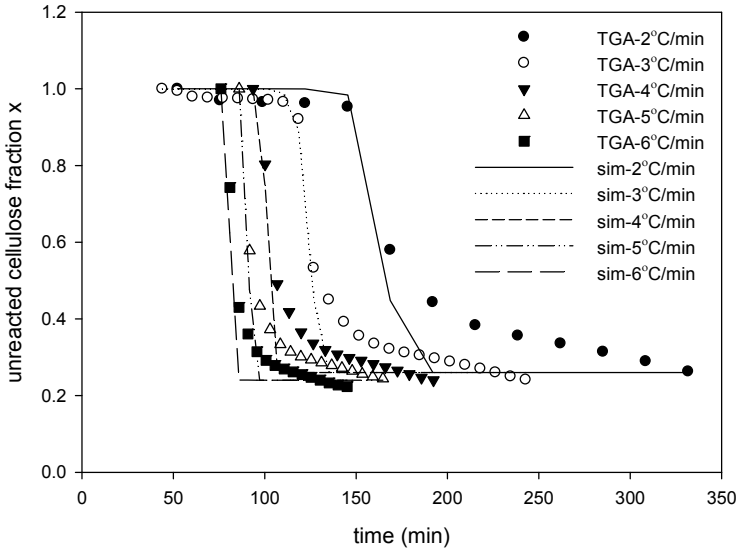

Figure 4.21: 1st order reaction model fit of cellulose (with 5 wt% H_3BO_3) degradation at various TGA heating rates (2-6 °C/min).

In comparison with the earlier fittings for H_3PO_4 infused cellulose, the results for H_3BO_3 were relatively poor. Except for the initial stage of thermal degradation (x < 0.5), the deviation of the model from the experimental data was rather obvious. In spite of this, the overall fit as characterised by the R^2 values (see Table E3.2) were still acceptable (i.e. $R^2 > 0.9$).

The fitting of the first-order model to the experimental results obtained for the various levels of H_3BO_3 loadings yielded the kinetic parameters as listed in Table E4.2. For the transglycosylation pathway, the activation energy, E_1 had a mean of 204 kJ/mol whilst the β-elimination pathway had a mean activation energy of 260 kJ/mol. These values are also similar to the activation energy results for pure cellulose. The fraction of cellulose involved in β-elimination (f_2) was found to be either slightly lower or slightly higher than the fraction for transglycosylation (f_1). This is reflected in the ratio of f_1:f_2 which ranged from 1:0.8 to 1:1.7. These values seemed to be in between the results

obtained for pure cellulose and H_3PO_4 infused cellulose. Although there is a shift in dominance from transglycosylation to β-elimination, this shift was not as large as the one we observed for the H_3PO_4 loadings. However, we can still see that this is still indicative of the β-elimination pathway becoming more dominant during the thermal degradation of H_3BO_3 infused cellulose.

4.3.3.4 Modelling for $Ba(OH)_2$ infused cellulose degradation

To compare and contrast the results we obtained for the acid-infused cellulose, similar model-fitting and analysis were carried out for the thermal degradation of $Ba(OH)_2$ infused cellulose. The model-fitting plots are shown in Figure 4.22, Figure 4.23 and Figure 4.24 for the different alkali loadings.

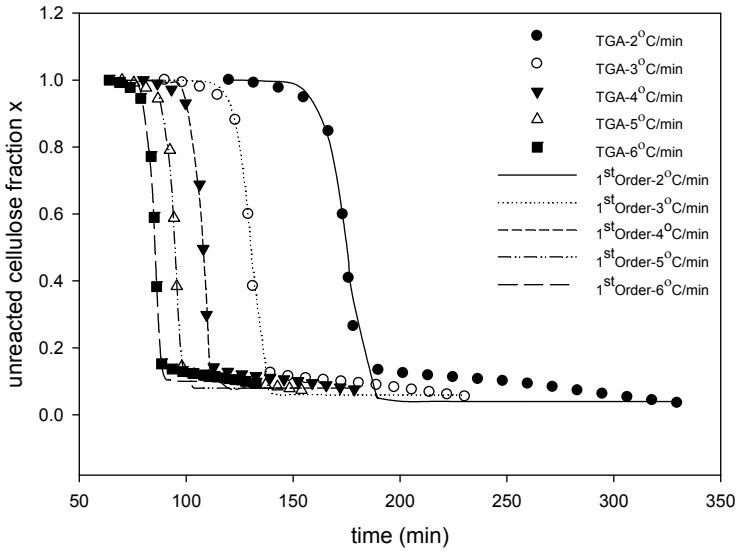

Figure 4.22: 1st order reaction model fit of cellulose (with 0.1 wt% $Ba(OH)_2$) degradation at various TGA heating rates (2-6 °C/min).

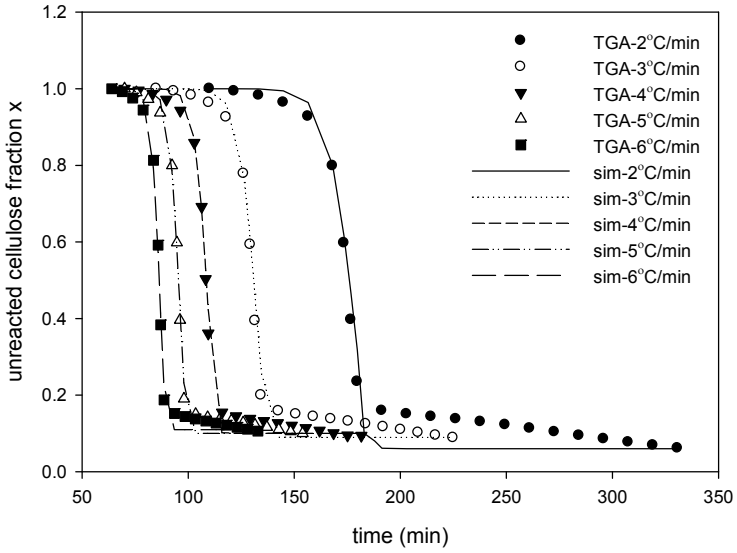

Figure 4.23: 1st order reaction model fit of cellulose (with 0.5 wt% $Ba(OH)_2$) degradation at various TGA heating rates (2-6 °C/min).

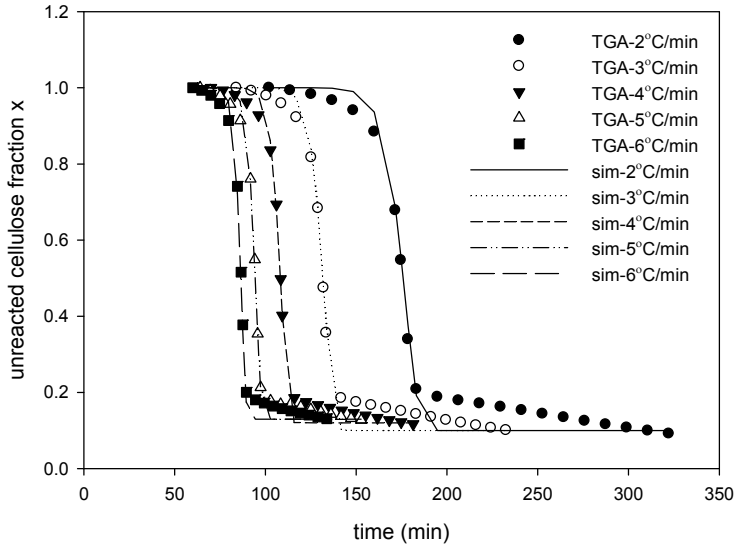

Figure 4.24: 1st order reaction model fit of cellulose (with 1 wt% $Ba(OH)_2$) degradation at various TGA heating rates (2-6 °C/min).

Generally, the first-order model fitted the $Ba(OH)_2$ experimental value rather well. As with the acid loadings, there still seemed to be a deviation towards the later stages of thermal degradation. However, this deviation occurred later when the fraction of

unreacted cellulose $x < 0.2$ compared to $x < 0.4$ for the acid-infused cellulose. The overall measure of fit as characterised by R^2 (see Table E3.3) were slightly better (i.e. $R^2 > 0.94$) than for pure cellulose. Again, an attempt was also made to fit the Capart equations (Equations (4.4) and (4.5)) on the alkali-infused ($Ba(OH)_2$ and $Ca(OH)_2$) cellulose samples. The resulting fits of the first-order model for alkali-infused cellulose were better than for Capart's model (R^2<0.93).

The model-fitting for the various $Ba(OH)_2$ loadings yielded the kinetic parameters for the two main thermal degradation pathways and the relative fractions of cellulose degraded along each of those pathways. These results are presented in Table E4.3. Here, the transglycosylation pathway was found to have a mean activation energy E_1=203 kJ/mol whilst β-elimination has a mean activation energy E_2=260 kJ/mol. These values are close to the literature values and to the ones obtained for pure cellulose. The fraction of cellulose involved in transglycosylation (f_1) was much higher than those obtained for the acid loadings. The ratio f_1:f_2 for $Ba(OH)_2$ loadings ranged from 3:1 to 5.4:1. Although these values indicate that transglycosylation is the likely dominant pathway, the values are within the f_1:f_2 range for pure cellulose. For pure cellulose, the spread of values is much greater with the ratio at the 2 °C/min heating rate being 1.4:1 whilst the ratio at 6 °C/min was 6.8:1. This would suggest that the alkalis do not directly promote the transglycosylation reaction. Instead, they seem to have a moderating effect by suppressing the β-elimination pathway.

4.3.3.5 Modelling for $Ca(OH)_2$ infused cellulose degradation

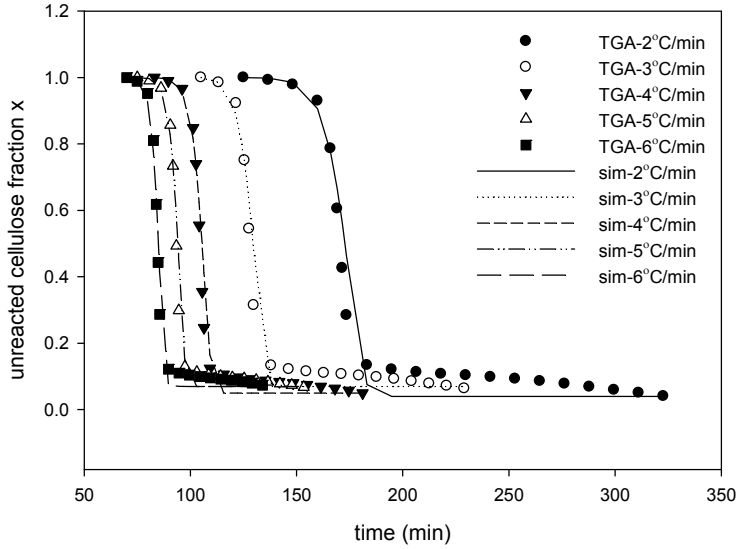

Figure 4.25: 1st order reaction model fit of cellulose (with 0.1 wt% $Ca(OH)_2$) degradation at various TGA heating rates (2-6 °C/min).

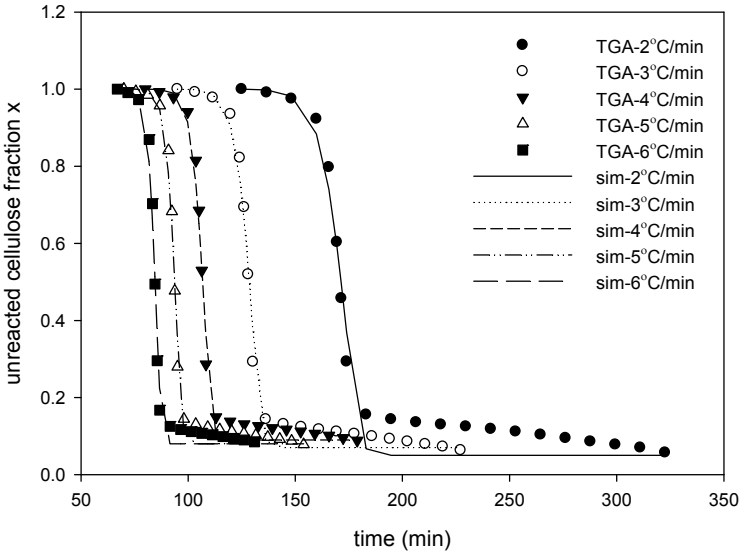

Figure 4.26: 1st order reaction model fit of cellulose (with 0.5 wt% $Ca(OH)_2$) degradation at various TGA heating rates (2-6 °C/min).

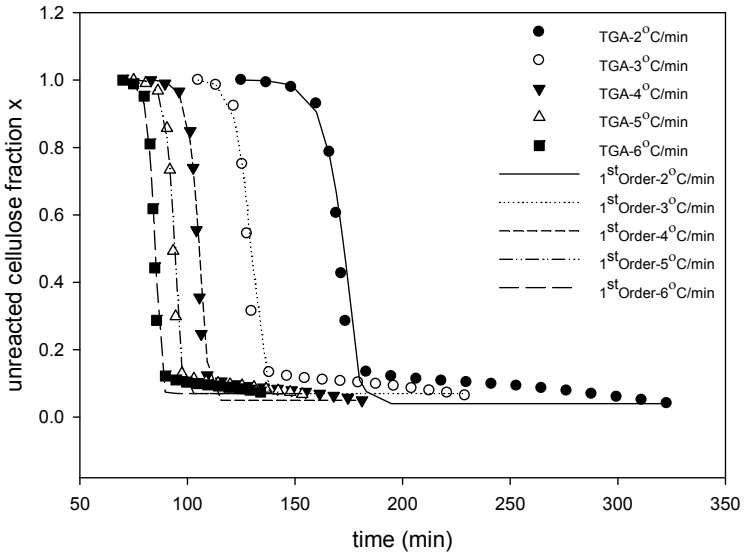

Figure 4.27: 1st order reaction model fit of cellulose (with 1 wt% $Ca(OH)_2$) degradation at various TGA heating rates (2-6 °C/min).

The model-fittings for $Ca(OH)_2$ as shown in Figure 4.25, Figure 4.26 and Figure 4.27, are generally acceptable and comparable with those obtained earlier for pure cellulose and $Ba(OH)_2$. The characteristic goodness fit measure is shown in Table E3.4 with $R^2 > 0.93$.

Consequently, the relevant kinetic parameters were found from the model-fittings and are tabulated in Table E4.4. The mean activation energy for transglycosylation E_1=200 kJ/mol whilst the mean activation energy for β-elimination E_2=257 kJ/mol. These values are comparable to the ones that have been obtained for pure cellulose, acid loaded cellulose and $Ba(OH)_2$. In terms of pathway degradation fraction, for transglycosylation, f_1 ranged from 0.6 to 0.78 whilst for β-elimination, f_2 ranged from 0.17 to 0.27. This showed that transglycosylation was the dominant pathway with the pathway degradation ratio (f_1:f_2) lying between 2.3:1 and 4.7:1.

4.3.3.6 Qualitative differences observed for acid and alkali-infused cellulose

For both acids (H_3PO_4 and H_3BO_3), the first-order model provide a qualitatively adequate fit for the experimental results. In terms of uncertainties in the model parameters, we have found that the fitted values for the Arrhenius constants (*A* and *E*) were rather stable for the different experimental combinations. The fraction of cellulose converted along the two pathways had deviations of less than 14 % across all the experiments.

The fit is better in the initial stages compared to the later stages of thermal degradation due to a decrease in degradation rate towards the end when the fraction of unreacted cellulose *x* is less than 0.6 (i.e. conversion $\alpha > 0.4$). This could be explained by the $d\alpha/dt$ plots shown in Figure 4.2 and Figure 4.3 which showed that the primary degradation rate curves ended around those points. What we can therefore say is that the transglycosylation and β-elimination pathways were the dominant reactions in the early part of cellulose degradation which is then followed by other secondary reactions (e.g. cracking to other lighter organics). This was shown by Mamleev et al. [149] in that it was observed that the relationship between activation energy and conversion α had two pronounced plateaus that corresponded with an initial primary degradation pathway that is then followed by secondary reactions that became dominant. These observations also find support in the recent work by Vinu and Broadbelt [159], where their quantum chemistry calculations and modelling were able to give reasonable predictions of levoglucosan but significant deviations from experimental results were observed when predicting the yields of light organics such as formic acid and

glycoaldehyde. They have attributed this to secondary reactions not considered by their model.

In addition, there is also a significant difference between the onset of the secondary reactions for pure and acid-infused cellulose. The acid-infused cellulose seems to exhibit an earlier and more prominent onset of the secondary reactions. Acids have been known to be active in dehydration reactions during the later stages of pyrolysis. It is also likely that the added mineral acids could have initiated or catalysed other secondary reactions that are not normally associated with the organic acids produced during pyrolysis. Therefore, apart from affecting the β-elimination pathway during the initial cellulose pyrolysis, the added acids (H_3PO_4 and H_3BO_3) are likely to have an effect on the secondary reactions themselves.

When we look at the results for the alkali-infused ($Ba(OH)_2$ and $Ca(OH)_2$) cellulose, deviations indicating the onset of the secondary reactions were occurring at a later stage ($x < 0.2$) when compared to the acid-infused cellulose. However, the secondary reactions caused by the added alkalis are more prominent than those for pure cellulose. This would indicate that the alkalis might also be initiating/catalysing secondary reactions that are not normally found during pure cellulose pyrolysis.

The inclusion of additional secondary reactions as a lumped parameter into the model may result in a better fit at the tails. However, the lack of specificity of the lumped parameters could result in the force-fitting of the thermogravimetric results into the lumped parameters at the expense of the kinetic parameters for transglycosylation and β-elimination as warned by Vyazovkin and Wight [114]. Since, the main aim was to

study the pathway dominance/shift between transglycosylation and β-elimination the secondary reactions were not included so that the fit will be representative of the initial stage of thermal conversion.

4.3.4 TGA-FTIR Results

A total of seven cellulose samples were subjected to TGA-FTIR analysis. The seven samples comprised of three acid-infused samples (H_3PO_4, H_3BO_3 and H_2SO_4,), three alkali-infused samples ($Ba(OH)_2$, $Ca(OH)_2$ and NH_4OH) and one pure cellulose sample. Five replicates of each sample type were tested. For each cellulose sample type, the TGA weight-loss curve, methane FTIR response and furfural yields were each plotted in a single graph. The graphs for all seven sample types are shown in Figure 4.28 to Figure 4.34.

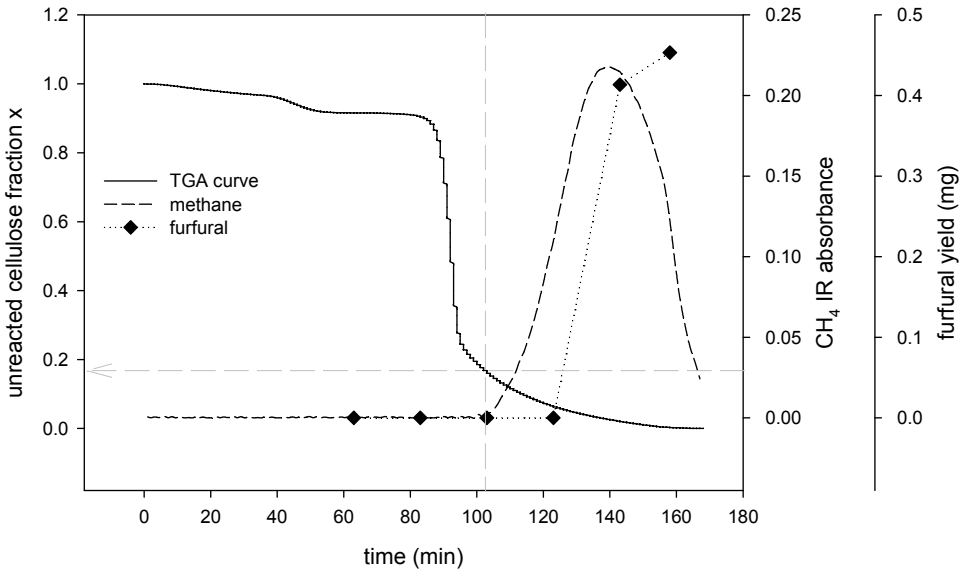

Figure 4.28: TGA-FTIR and furfural yield curves from the thermal degradation of pure cellulose

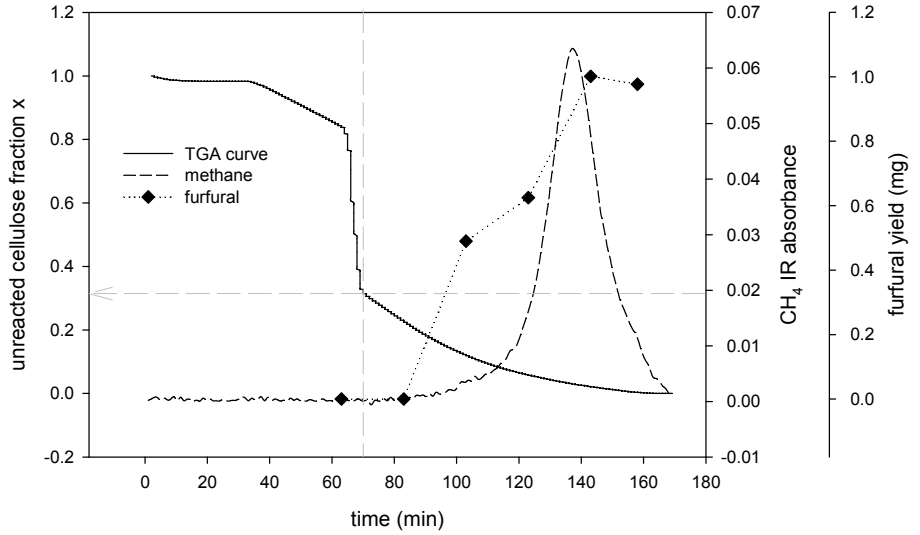

Figure 4.29: TGA-FTIR and furfural yield curves from the thermal degradation of cellulose infused with 5 wt% H_3PO_4

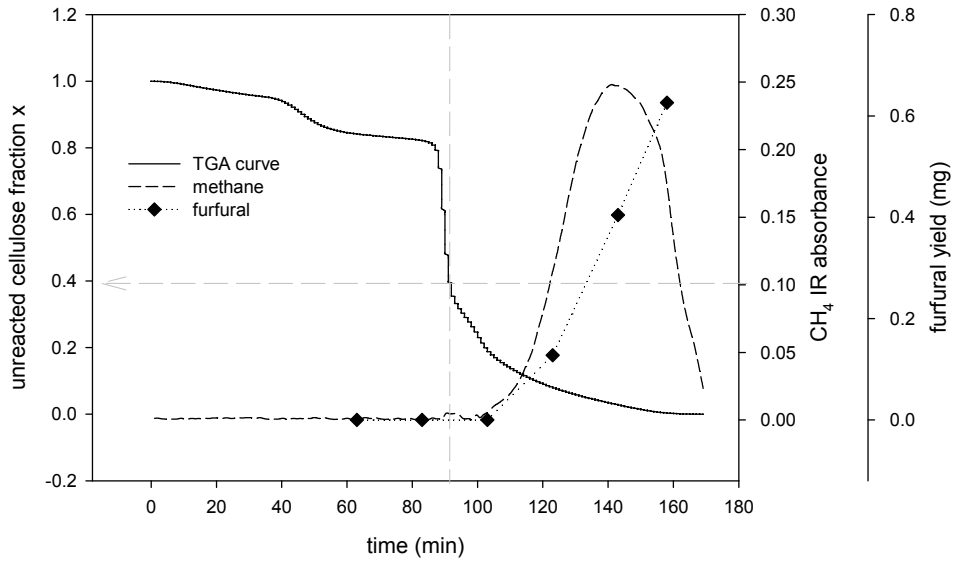

Figure 4.30: TGA-FTIR and furfural yield curves from the thermal degradation of cellulose infused with 5 wt% H_3BO_3

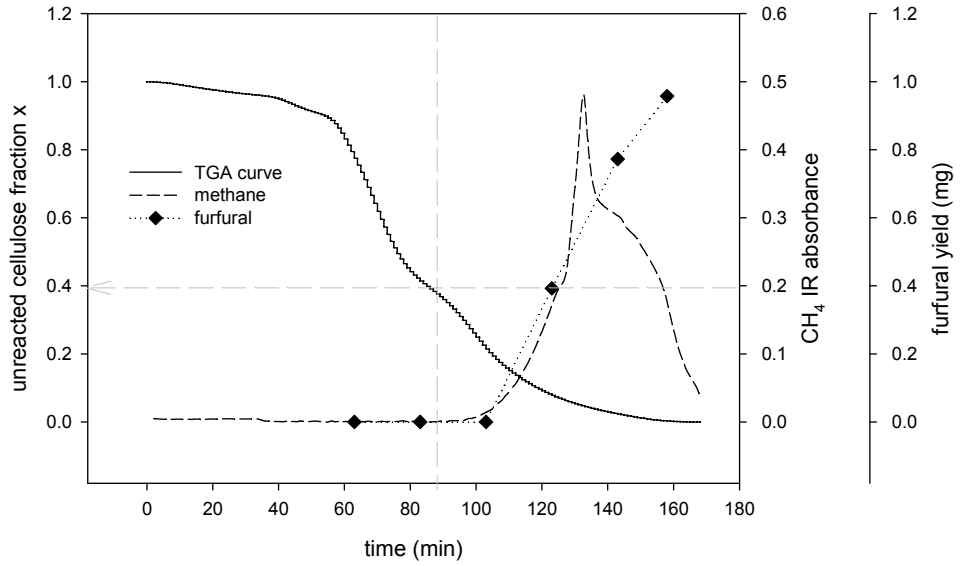

Figure 4.31: TGA-FTIR and furfural yield curves from the thermal degradation of cellulose infused with 2 wt% H_2SO_4

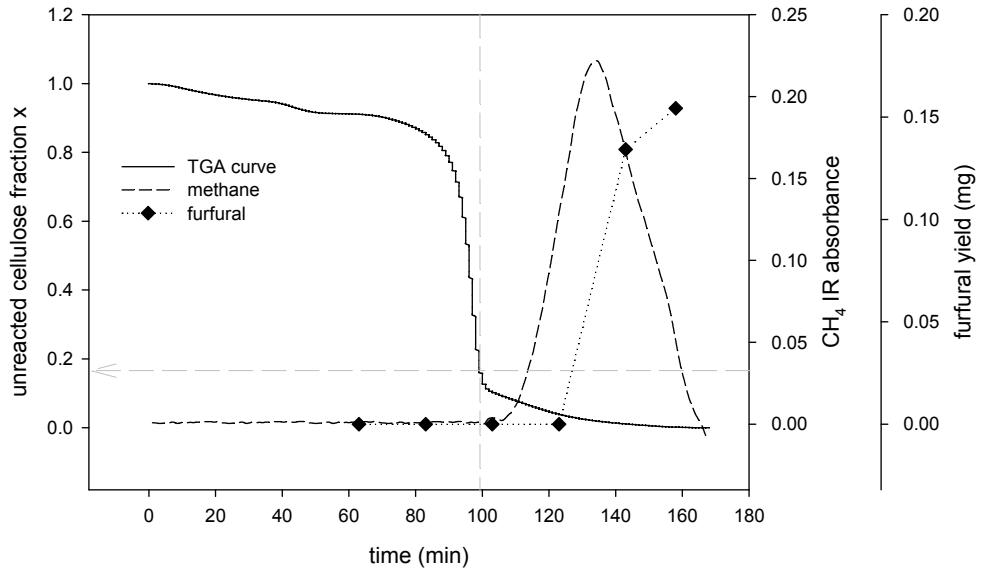

Figure 4.32: TGA-FTIR and furfural yield curves from the thermal degradation of cellulose infused with 1 wt% $Ba(OH)_2$

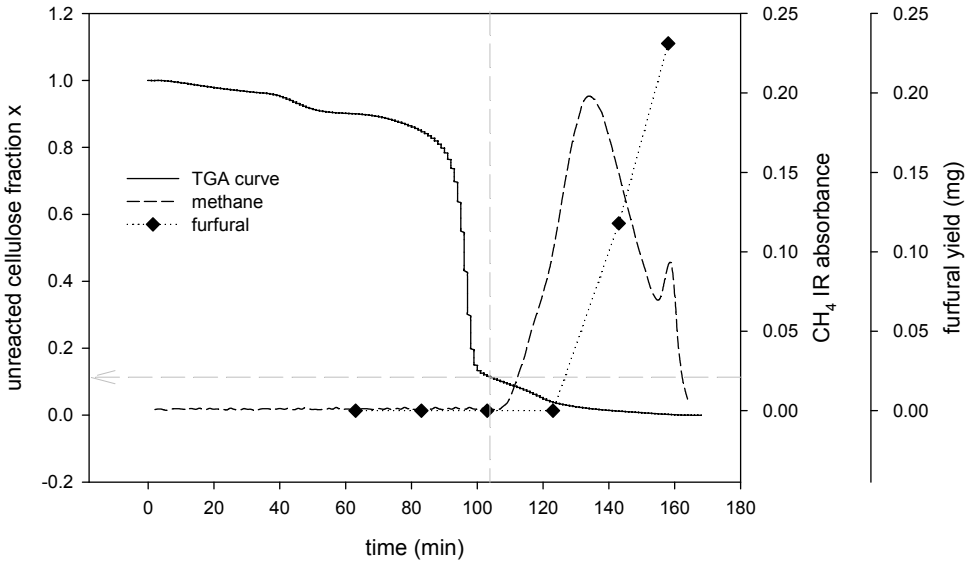

Figure 4.33: TGA-FTIR and furfural yield curves from the thermal degradation of cellulose infused with 1 wt% $Ca(OH)_2$

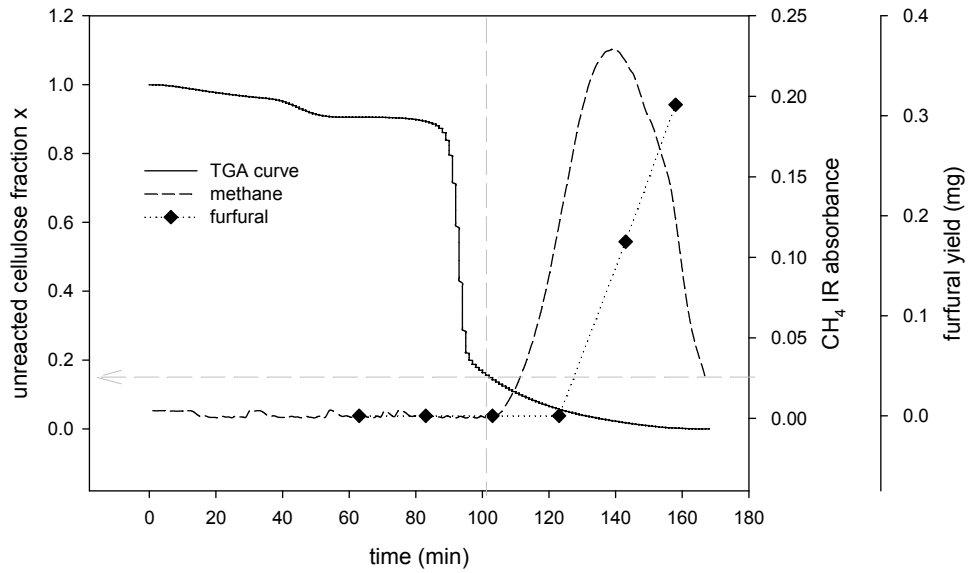

Figure 4.34: TGA-FTIR and furfural yield curves from the thermal degradation of cellulose infused with 5 wt% NH_4OH

Visually, the difference in the onset of secondary reactions for acid-infused cellulose is occurring much earlier during thermal conversion compared with the alkali-infused and pure cellulose samples. Furfural was also detected for all the sample types towards the later stages of thermal conversion. The presence of furfural and methane are indicative of the onset of secondary reactions. To quantify this observation, the onset point for secondary reactions was found from the graphs and the average values for the seven sample types are shown in Table 4.7.

Table 4.7: Average values of the onset of secondary reactions with respect to the fraction of unreacted cellulose (x).

Additive	H_3PO_4	H_3BO_3	H_2SO_4	Pure cellulose
Onset at x	0.41±0.01	0.38±0.02	0.32±0.02	0.17±0.01
Additive	$Ba(OH)_2$	$Ca(OH)_2$	NH_4OH	
Onset at x	0.15±0.03	0.12±0.02	0.16±0.02	

It can be seen that the acid-infused samples experience the onset of secondary reactions rather early when the fraction of unreacted cellulose was still in the range of x = 0.4 to 0.3. This onset range coincides with the region where the first-order model curves for the acid-infused cellulose deviated from the experimental data as shown in Section 4.3.3. Along with the evidence shown by the work done by Mamleev et al. [149] and Vinu and Broadbelt [159], who have also shown the presence of secondary reactions during thermal conversion, it is therefore important to note that the kinetic parameters obtained in this chapter refers to the initial phase of thermal conversion. This is indeed apt because the two pathways (transglycosylation and β-elimination) being studied are the initial routes for cellulose thermal conversion.

Additional statistical analyses of the TGA-FTIR results regarding the onset of secondary reactions are described in the following Section 4.3.5.

4.3.5 Statistical Analysis of Results

Two types of statistical analysis were carried out on the activation energy results obtained from the thermal conversion of the acid and alkali-infused cellulose namely (i) one-sample t-test and (ii) analysis of variance. Meanwhile, the results from the TGA-FTIR experiments were subjected to a two-sample t-test.

4.3.5.1 One-sample t-test

The activation energy values were tested using a one-sample t-test using Equation (4.9)

$$t_0 = \frac{\bar{y} - \mu_0}{S/\sqrt{n}} \tag{4.9}$$

Where $\bar{y}$ is the sample mean, μ_0 is test mean, S^2 in the sample variance and n is the sample size.

For acid-infused cellulose, the null hypothesis (H_0) was set as the mean activation energy E_a = 250 kJ/mol whilst the alternative hypothesis (H_a) was set as the activation energy $E_a \neq 250$ kJ/mol. At a significance level of 0.05, eight out of the nine samples analysed had means that were not significantly different from an activation energy

level E_a = 250 kJ/mol. Meanwhile, the remaining sample had a mean E_a = 240 kJ/mol (at 0.05 significance level). A complementary t-test was also conducted which showed that all the samples means were significantly higher than the activation energy E_a = 200 kJ/mol (at 0.05 significance level).

This shift of the activation energy to ca. 250 kJ/mol is close to the expected activation energy of 250 kJ/mol for the β-elimination pathway.

The one-sample t-test was also applied on the activation energies of the alkali-infused cellulose samples. However, in this case it was found that the activation energies E_a = 150, 170, 180, 190 and 195 (at 0.05 significance level). However, it can be clearly seen that all the activation energies for alkali-infused cellulose were significantly lower than those for acids.

This shift of the activation energy to ca. 180 kJ/mol is lower than the expected activation energy of 200 kJ/mol for the transglycosylation pathway. This could be partially due to potential secondary effects of the cations of the alkalis. It does however provides some evidence that the β-elimination pathway was suppressed.

4.3.5.2 Two-sample t-test

The onset of secondary reactions as presented in Table 4.7, were subjected to a series of two sample t-tests. The acid and alkali-infused samples were each compared with the onset point for pure cellulose. The null hypothesis (H_0) was defined such that the

secondary onset points for the acid and alkali-infused samples were equal to the onset points for pure cellulose. The alternative hypothesis (H_a) was then defined as the onset points for that acid and alkali samples being either greater or less than the onset for pure cellulose. At a significance level of 0.05, the t-tests showed that the onset points for NH_4OH and $Ba(OH)_2$-infused cellulose were not significantly different from that of pure cellulose. $Ca(OH)_2$ and the three acid-infused cellulose had secondary reaction onset points that were significantly different from that of pure cellulose.

4.3.5.3 Analysis of variance

The experiments conducted were based on a two-factor factorial design. The two factors considered were additives (i.e. acids and alkalis) and infusion levels. There were a total of six types of acid/alkali additives (H_2SO_4, H_3PO_4, H_3BO_3, NH_4OH, $Ca(OH)_2$ and $Ba(OH)_2$) and three infusion levels (low, medium, high) studied. The response variable of interest was the apparent activation energy. Separate analyses, one each for acid and alkali effects in comparison with infusion levels were done. The ANOVA tables generated are shown in Appendix G2. A comparison of the F statistics (F_0) for the experimental data with the corresponding F distribution ($F_{0.05,f,45}$) will show the significance of each of the effects under consideration.

Firstly, as shown in Table G 2.1, The F_0 values for the acids had a significant influence on the apparent energy. The infusion level effect was not significant but the acids-infusion levels interaction effect was significant. The different acids behaved differently from one another. This could be due to the activation of other secondary

reactions to varying degrees by the different acids. Therefore, the promotion of the β-elimination pathway by acids is also dependent on the acid type. The infusion levels did not affect the apparent activation energy probably due to all infusion levels being above the threshold of β-elimination pathway activation.

For the alkali-infused cellulose, all three effects of alkalis, infusion level and interaction effects were significant. The way in which the alkalis act is very different from the acids in that they do not directly promote the alternative transglycosylation pathway. Instead, they act by providing hydroxyl ions [OH^-] to neutralise the hydrogen ions [H^+] that are generated during thermal conversion. This explains why the effect of alkali infusion levels was significant. The use of different alkalis also had a significant effect probably due to the alkali earth metal cations influencing the thermal conversion.

4.4 Summary of Kinetic Analysis

Using the model-free isoconversional method, we were able to determine the apparent activation energy of pure cellulose and cellulose that have been loaded with acids (H_3PO_4, H_3BO_3 and H_2SO_4) and alkalis ($Ba(OH)_2$, $Ca(OH)_2$ and NH_4OH). The thermal degradation of pure cellulose has a mean activation energy of 203±13 kJ/mol and is consistent with recent literature values.

For the three acids, there is a main thermal degradation reaction which terminates when the conversion α = 0.4 and followed by secondary reactions. It is likely that at

least one secondary reaction is occurring when the conversion is between 0.4 and 0.8 and this is prominently shown by the twin peaks seen for cellulose infused with H_2SO_4.Via hypothesis testing using the one sample t-test, acid-infused cellulose activation energies are not significantly different from an activation energy level of E_a = 250 kJ/mol (0.05 significance level). In addition, all the samples means are significantly higher than the activation energy E_a = 200 kJ/mol (at 0.05 significance level). This apparent activation energy level of ca. 250 kJ/mol seems to indicate that β-elimination is the dominant pathway by which cellulose in the presence of acids thermally degrades.

For alkalis, the activation energy obtained from Friedman's isoconversional method ranged from 150 to 195 kJ/mol (0.05 significance level) and all of these activation energies are significantly lower than those for acids. This shift of the activation energy to ca. 180 kJ/mol is lower than the expected activation energy of 200 kJ/mol for the transglycosylation pathway. This could be partially due to potential secondary effects of the cations of the alkalis. It does however provide some evidence that the β-elimination pathway is suppressed.

We have therefore seen that acids are able to raise the apparent activation energy of cellulose thermal degradation whilst alkalis were able to decrease the apparent activation energy. The results show that:

$$\mathbf{E_{a,acid\text{-}cellulose} > E_{a,pure\text{-}cellulose} > E_{a,alkali\text{-}cellulose}}$$

An alternative method for evaluating kinetic parameters is via model-fitting. A reasonably good-fit was obtained for the experimental TGA data using a first-order model for pure cellulose (R^2 > 0.93), acid-infused cellulose (R^2 > 0.90) and alkali-infused cellulose (R^2 > 0.93). The activation energy results obtained from the first-order model-fitting are summarised in Table 4.8.

Table 4.8: Summary of model-fitting parameters obtained from first-order model.

	Transglycosylation E_1 (kJ/mol)	β-elimination E_2 (kJ/mol)	PDR (f_1:f_2) min	max
Pure cellulose	204	257	1.4:1.0	6.8:1.0
Cellulose + H_3PO_4	199	255	1.0:2.5	1.0:5.0
Cellulose + H_3BO_3	204	260	1.0:0.8	1.0:1.7
Cellulose + $Ba(OH)_2$	203	260	3.0:1.0	5.4:1.0
Cellulose + $Ca(OH)_2$	200	257	2.3:1.0	4.7:1.0

The fraction of pure cellulose thermally degraded via transglycosylation (f_1) was greater than that via β-elimination (f_2) as evidenced by the pathway degradation ratio (PDR) which is defined as f_1:f_2. This indicates that transglycosylation is probably the dominant pathway for pure cellulose thermal degradation/pyrolysis.

However, for H_3PO_4 loaded cellulose, the PDR ranged from 1:2.5 to 1:5. This is a reversal from the results that we obtained for pure cellulose. It is also indicative of the β-elimination pathway being dominant during the thermal degradation of H_3PO_4 infused cellulose. Meanwhile, for H_3BO_3 infused cellulose, the PDR was in the ratio of ca. 1:1 showing almost equal distribution of thermal degradation via transglycosylation and β-elimination. In spite of this we can still see that H_3BO_3 has resulted in β-elimination being more prominent (compared to pure cellulose) during the thermal degradation process.

When we turn to the alkalis, we see that for $Ba(OH)_2$ loadings, the PDR ranged from 3:1 to 5.4:1. Similar values are also found for $Ca(OH)_2$ infused cellulose. Although these values indicate that transglycosylation is the likely dominant pathway, the values are within the PDR range for pure cellulose. This means that alkalis do not directly promote the transglycosylation reaction. Instead, they have a moderating effect by suppressing the β-elimination pathway.

It was also observed that the activation energy was different at the later stages of thermal conversion. A similar trend which showed a deviation of the two-pathway first-order model from experimental data was also evident. Both these deviations were especially prominent for the acid-infused cellulose. This deviation is probably due to the onset of secondary reactions at the later stages and this was shown (from TGA-FTIR) by the increase in methane and furfural levels.

4.5 Conclusion

The findings in this Chapter have provided more support to the observations made in Chapter 3. Overall we can see that the presence of acids and alkalis have a significant effect of the kinetics of cellulose thermal degradation or pyrolysis. Acids influence the thermal degradation by promoting the β-elimination pathway which leads to more cellulose degrading via that route at the expense of transglycosylation. This then manifests itself as an increase in the overall apparent activation energy. On the other hand, alkalis have a suppressing effect on the acid-catalysed β-elimination pathway

which then allows more cellulose to degrade via transglycosylation. This is subsequently seen as a lowering of the overall apparent activation energy.

The findings thus far naturally lead to the idea that we might be able to selectively increase the yields of anhydrosaccharides. This could be achieved by controlling or manipulating the acidity/alkalinity of the environment in which cellulose thermally degrades or pyrolyses. We will explore the utility of this idea further in the following Chapter 5.

5. Selective Anhydrosaccharide Production from Cellulose Conversion

As we have seen in Section 2.2.3 of the Literature Review, several methods have been attempted to boost the yields of levoglucosan (LG) and levoglucosenone (LS). These chiral molecules are of interest due to their potential use as intermediates in the production of speciality chemicals and pharmaceuticals.

The state-of-the-art for LG and LS production has generally included the addition of acidic species (e.g. phosphoric acid) to boost yields. It is likely that the acids enhanced anhydrosaccharide yields by inducing changes to the physical condition of cellulose in terms of its ash content, crystallinity and degree of polymerisation. However, we can see from our experimental results in Chapter 3 and Chapter 4, the presence of acidic species actually promotes the β-elimination pathway which ultimately results in lowered LG and LS yields. This means that the state-of-the art methods are likely sub-optimal in that the acids used to enhance yields would ultimately suppress anhydrosaccharide formation.

In contrast, we have seen that the reduction of the available acidic species (i.e. H^+ ions) via the introduction of alkalis led to the suppression of the β-elimination pathway thus allowing transglycosylation to be the dominant thermal degradation route. Since anhydrosaccharides like LG and LS can only be formed via transglycosylation, it would mean that to increase yields of anhydrosaccharides, we need to manipulate the route through which cellulose decomposition occurs. Based on our earlier experimental results, this could be achieved via the control of the concentration of acidic species present or the concentration of hydrogen ions [H^+] during pyrolysis.

Hence, in our effort to enhance anhydrosaccharide yields we will need to demonstrate the utility of [H^+] control in relation to anhydrosaccharide yields. To do so, we are going to:

i. Measure temporal variations of anhydrosaccharides and furans during the thermal conversion process.
ii. Measure [H^+] changes during cellulose conversion.
iii. Model anhydrosaccharide and furan yields with a suitable model.

5.1 Method and Materials

The experimental work involved here relies on the thermal conversion of cellulose within a liquid reaction medium. This enables us to directly control and measure the amounts of acid and alkalis introduced into the system. Such a system will also allow us to make time-based measurements of anhydrosaccharides, furans and hydrogen ion concentrations.

5.1.1 Experimental Design

The experimental requirements in this chapter is different from the two preceding chapters in that dry pyrolysis of cellulose would not be able to give us the ability to measure changes in the [H^+] levels during the thermal conversion. With this in mind, a

liquid-based reaction media was chosen to allow us to make measurements of pH in addition to the compounds of interest (anhydrosaccharides and furans).

In spite of the change from dry to wet pyrolysis, the factors that could affect the reproducibility of results remains unchanged with the feedstock and transport (heat and mass) phenomena being of primary importance.

5.1.1.1 Feedstock and reactor type

With regards to the cellulose particle itself, issues relating to variability in particle size, crystallinity, density and ash (inorganic) content were addressed via the use of cellulose from a single source as described in the experimental designs of Chapter 3 and Chapter 4.

In terms of heat and mass transfer, the type of reactor used has the greatest impact. The choice in reactor type will need to take into consideration sampling (analysis) of product composition, isothermality, residence time measurement, time-averaging disguise, construction difficulty and cost [160]. Our reaction system will essentially comprise of a two-phase (solid-liquid) reaction mixture. Based on this, the suitable reactor type as recommended by Weekman [160] would be the stirred batch reactor which was given good ratings for sampling, isothermality (good mixing), residence time measurement and ease of construction. Although the stirred-batch reactor is rated as poor due to time-averaging of products, this can be overcome by regular sampling and fast quenching during the thermal conversion experiments.

5.1.1.2 Experimental variables

The experiments conducted were based on a two-factor factorial design. There were a total of three types of sulfolane [H^+] conditions (neat, H_3PO_4 and $Ba(OH)_2$) and three temperature levels (190 °C, 200 °C, 210 °C) being studied. The main focus of the experiments was to find out the influence/response of these additives on the yield of anhydrosaccharides and furans. There were therefore a total of 9 different combinations. with 6 replicates were done for each experimental combination. The two-factor analyses of variance for these experiments are discussed in Section 5.2.3.

5.1.2 Cellulose Pyrolysis in Sulfolane

Based on the experimental design considerations discussed earlier, we found that the best option would be to conduct wet pyrolysis using sulfolane as the reaction media within which cellulose can thermally degrade. Sulfolane (2,3,4,5-tetrahydrothiophene-1,1-dioxide) is a colourless liquid commonly used in the chemical industry as an extractive distillation solvent or reaction solvent. It was chosen due to its properties:

i. High boiling point (285 °C) and stability: allows thermochemical conversion temperatures to be reached (ca. 200 °C) without using high pressures.
ii. Polar (fully soluble in water): able to dissolve the anhydrosaccharides and furans produced.
iii. Aprotic: does not introduce additional hydrogen ions [H^+] into the reacting system which could otherwise mask the [H^+] changes that we are interested in.

The experiments involving cellulose conversion in sulfolane were carried out with neat, acidified (0.13 M H_3PO_4) and alkaline (0.01 M $Ba(OH)_2$) sulfolane at varying temperatures. The experimental setup consisted of a 50 ml jacketed glass reactor, an overhead glass condenser and a sampling system as shown in Figure 5.1. Nitrogen gas was used for inerting purposes.

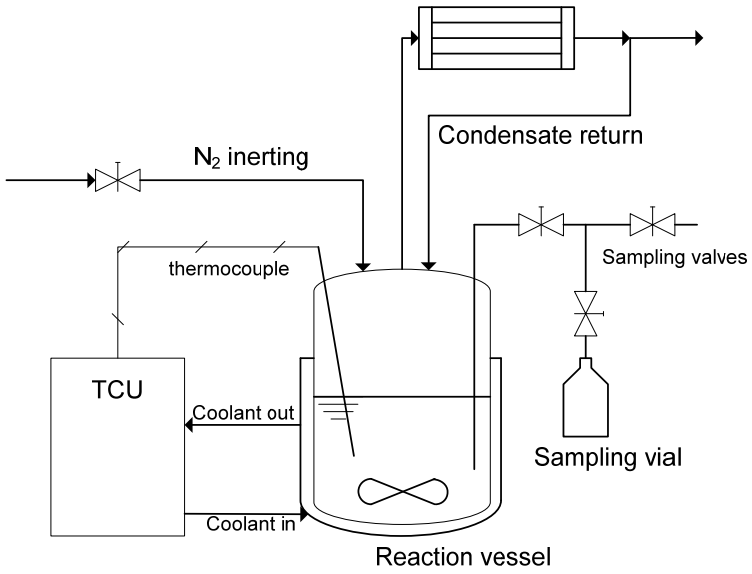

Figure 5.1: Experimental reactor setup for cellulose conversion in sulfolane.

For a stirred batch reactor, maintaining consistent stirring and heat flux to the reactor are factors that can impact heat and mass transfer during the reaction. Therefore, the computer controlled stirring from Mettler-Toledo's Multimax system was incorporated into the batch reactor set-up to ensure consistently high mixing. At the same time, heat was supplied to the jacketed reactor by a Julabo HT30-M1 High Temperature Circulator with DW-Therm HT as the heat transfer fluid.

The system was first purged with nitrogen at the start and subsequently a very small bleed of nitrogen was introduced by adjusting the needle valve. Sulfolane (30 ml) was

then poured into the reactor and heated up to the required process temperature. In order to find the Arrhenius kinetic parameters, the reactor was operated isothermally at various temperatures (180 °C, 190 °C, 200 °C, 210 °C and 220 °C). Microcrystalline cellulose (750 mg - Avicel) was then charged into the reactor to form a suspension of 25 mg-cellulose/ml-sulfolane. When required, the relevant acid (0.13 M H_3PO_4) or alkali (0.01 M $Ba(OH)_2$) was subsequently added. Samples collected from the reaction mixture at regular intervals were immediately cooled in an ice bath for one minute to quench the reaction. A known volume of each sample collected was then neutralized with either H_2SO_4 or $Ba(OH)_2$ solution and filtered through a 0.45 μm syringe filter to remove the precipitated salts. A fraction of this processed sample was diluted with an appropriate amount of distilled water for pH measurement and HPLC analysis while the remaining fraction was dried using a rotary evaporator and re-dissolved in an appropriate amount of methanol for GCMS analysis.

5.1.3 Anhydrosaccharides and Furans Quantification

The anhydrosaccharides were identified and quantified using a GC-MS (Agilent 7890A/5975C GC-MSD) using the same procedure described earlier in Section 3.1.4. The only difference was that in this case, the mass spectrometer was switched off between the 19 and 20 minute mark due to the elution of sulfolane from the column within this period. This did not impact the anhydrosaccharides because they were eluted either before (LS, DGP) or after (LG, AGF) this interval.

The preparation of samples for the GCMS analysis leads to some loss of furans. Therefore a separate method was required to quantify the furans produced in the thermal conversion. This was achieved by HPLC analysis (Shimadzu LC-20A) operated under the conditions listed in Table 5.1.

Table 5.1: HPLC settings for furan analysis

Column:	Hi Plex H, 300 mm x 7.7 mm, ID 8 μm
Column temperature:	60 °C
Eluent:	2 mM H_2SO_4 aqueous solution
Flow rate:	0.5 ml/min
Run time:	65 min
Injection volume:	20 μl
Detector:	RID and UV

5.1.4 Kinetic Mechanism Modelling

Apart from the experimental set-up, a suitable reaction scheme was developed to support the complimentary modelling work. This would allow us to study the possible use of models to describe and predict yields as well as uncover limitations in their use. Due to our earlier experimental observations, the required model should have the following features:

i. Two initial pathways (i.e. transglycosylation and β-elimination)

ii. Predicts the yields of anhydrosaccharides and furans

iii. Feedback mechanism for acid catalysis of the β-elimination pathway

The reaction mechanism that we settled on was based on the diagram shown in Figure 1.2 and is expressed as a reaction scheme in Figure 5.2.

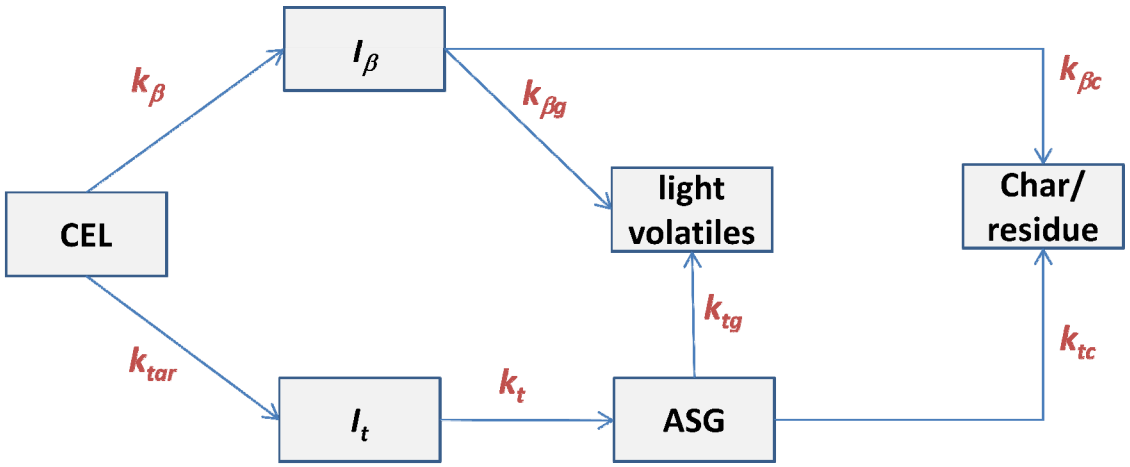

Figure 5.2: Proposed reaction scheme for thermal conversion of cellulose.

Where CEL is cellulose, I_t is the transglycosylation intermediate, I_β is the intermediate from β-elimination, ASG represents the anhydrosaccharides, light volatiles consists of furans (FRN), organic acids (H^+) and other light organic compounds whilst Char represents solid residue. The various k's represent the Arrhenius kinetic rate constants.

The thermal conversion of cellulose via transglycosylation (k_{tar}) and β-elimination (k_β) was described by Mamleev et al. [18] to form disrupted polymer chains with levoglucosan (LG), reducing (R) and non-reducing (NR) ends. In our proposed scheme, the cellulose polymer chains with LG-ends are represented by I_t whilst chains with R- and NR-ends are represented by I_β. The polymer chains with LG-ends (I_t) then undergo glycosydic bond cleavage (k_t) to produce levoglucosan and other anhydrosaccharides. The anhydrosaccharides produced can subsequently undergo secondary dehydration/cracking reactions (k_{tg}) as described by Lin et al. [21] and Shen and Gu [22], to give light volatiles. Meanwhile, I_β can also undergo similar secondary

reactions ($k_{\beta g}$) to produce the light volatiles [18, 30]. In addition, both intermediates can further react (k_{tc} and $k_{\beta c}$) to form char [133, 161].

This model should be seen as a first approximation of the complex reaction network that actually takes place during cellulose thermal conversion. Apart from the initial step of transglycosylation and the alternative β-elimination pathway, subsequent pathways involving the secondary reactions that we observed in Chapter 4 have not been fully considered.

The major underlying assumption in this scheme is therefore the treatment of secondary reactions and its light organic products collectively. Strictly speaking, this is not true because products formed during pyrolysis number more than 300 [42] and many secondary reaction pathways [22, 30, 64, 162] have been proposed in the literature. In spite of this, our proposed scheme that partially uses the common lumped methodology will at least allow us to see how the model performs in terms of anhydrosaccharide formation without going into the specifics of the secondary reactions.

It has been opined in recent literature [31, 163] that future work in cellulose pyrolysis should focus on the measurement of these numerous intermediates and their respective secondary reaction pathways so that meaningful production of targeted intermediates can be realised. Our aim for this modelling effort therefore, is to see to what extent the two initial transglycosylation and β-elimination pathways can contribute towards an overall model that maps the entire cellulose thermal conversion reaction network.

Other variations of this model were considered (see Appendix F1) but were not subsequently used because they were found to either give a poorer fit or did not offer additional improvements whilst requiring a larger set of model parameters to be fitted.

This model can be expressed using a set of ordinary differential equations (mass balance) as follows:

$$\frac{dC_{EL}}{dt} = -k_{tar}(f_{tar}C_{EL}) - k_{\beta}\left(f_{\beta}C_{EL}\right)H^{+} \tag{5.1}$$

$$\frac{dI_t}{dt} = k_{tar}(f_{tar}C_{EL}) - k_t I_t \tag{5.2}$$

$$\frac{dI_{\beta}}{dt} = k_{\beta}\left(f_{\beta}C_{EL}\right)H^{+} - k_{\beta g}I_{\beta} - k_{\beta c}I_{\beta} \tag{5.3}$$

$$\frac{dA_{SG}}{dt} = k_t I_t - k_{tg}A_{SG} - k_{tc}A_{SG} \tag{5.4}$$

$$\frac{dF_{RN}}{dt} = \left(k_{tg}A_{SG} + k_{\beta g}I_{\beta}\right)f_{FRN} \tag{5.5}$$

$$\frac{dH^{+}}{dt} = \left(k_{tg}A_{SG} + k_{\beta g}I_{\beta}\right)f_{H^{+}} \tag{5.6}$$

$$\frac{dR}{dt} = k_{tc}A_{SG} + k_{\beta c}I_{\beta} \tag{5.7}$$

Where C_{EL}=cellulose, I_t=transglycosylation intermediate, I_{β}=β-elimination intermediate, A_{SG}=anhydrosaccharides, F_{RN}=furans, H^{+}=organic acids and R=solid residue/char. Meanwhile f_{tar}=fraction of cellulose conversion via transglycosylation, f_{β}= fraction of cellulose conversion via β-elimination, f_{FRN}=fraction of furans within the light volatiles and $f_{H^{+}}$=fraction of organic acids within the light volatiles.

The model-fitting was carried out using MATLAB by solving the ODEs (Equations (5.1) to (5.7)) with the model parameters optimised using the in-built genetic algorithm (GA). It is usually accepted that Sequential Quadratic Programming (e.g. Fmincon) should be used in the first instance for local optimisation. This was tried but the consistency of the output parameters obtained were poor with different initial conditions giving very different results due to it being trapped in a local minimum. The genetic algorithm was subsequently used and it provided better consistency.

The numerical method used was similar to the one used in Section 4.1.1.2 with adjustments made to accommodate the larger number of parameters and ODEs. Once a set of *k*-values were obtained for the various temperatures, the relationship between ln(*k*) against the reciprocal temperature was checked for linearity. If the resulting relationships were not linear, the *k*-values were evaluated again in the next iteration. This was continued until a satisfactory level of linearity ($R^2 > 0.9$) was achieved. Hence, the 11 parameters were fitted to the experimental results using 7 ODEs and 7 linearity constraints (*k*-values). Once the fitted *k*-values (Arrhenius kinetic constants) were finalised, the corresponding activation energies and pre-exponential factors were obtained from the plots of ln(*k*) against the reciprocal temperature.

This two-step method for obtaining the kinetic parameters was used because:

i. Reducing parameters to be fitted in the first instance (*k*-values) helps with speed of running simulations.
ii. Convergence was affected due to high correlation between the Arrhenius parameters *A* and *E*. It is better to find more independent parameters (various *k* values) first and then obtain the specific Arrhenius parameters separately.

5.2 Results and Discussion

Three different sets of results were obtained that show:

i. Influence of $[H^+]$ on the yield of anhydrosaccharides and furans

ii. Change in $[H^+]$ as the thermal conversion progressed.

iii. The reaction scheme utility/limits in expressing the anhydrosaccharide and furan yields

5.2.1 Anhydrosaccharide and Furan Profiles

The thermal conversion of cellulose in sulfolane was found to produce 6 main products LG, LS, DGP, AGF, HMF and FF. Their temporal profiles are shown in Figure 5.3 to Figure 5.14.

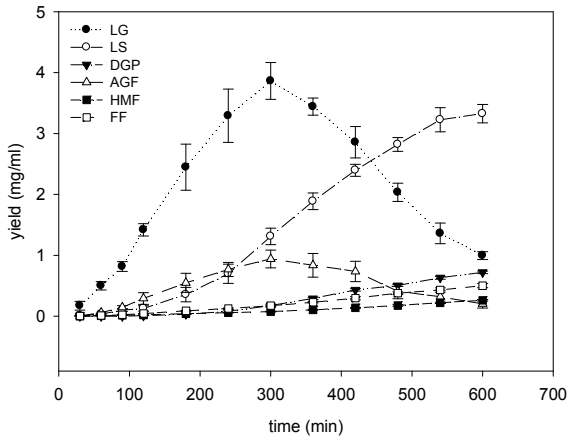

Figure 5.3: Product profile for cellulose conversion in sulfolane at 180 °C

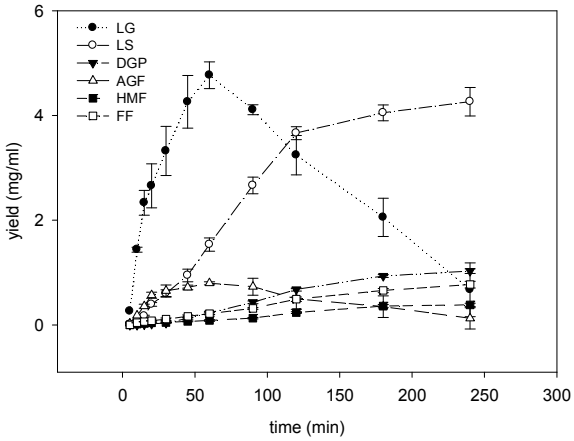

Figure 5.4: Product profile for cellulose conversion in sulfolane at 200 °C

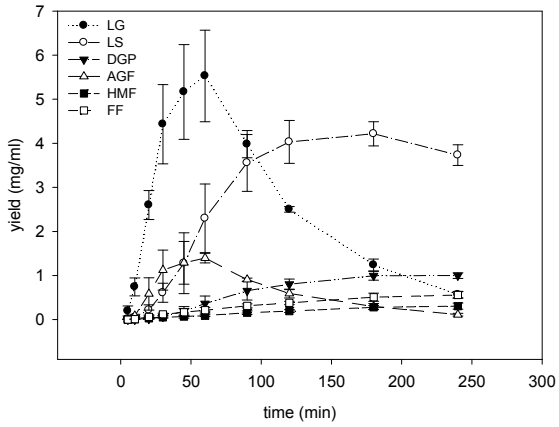

Figure 5.5: Product profile for cellulose conversion in sulfolane at 210 °C

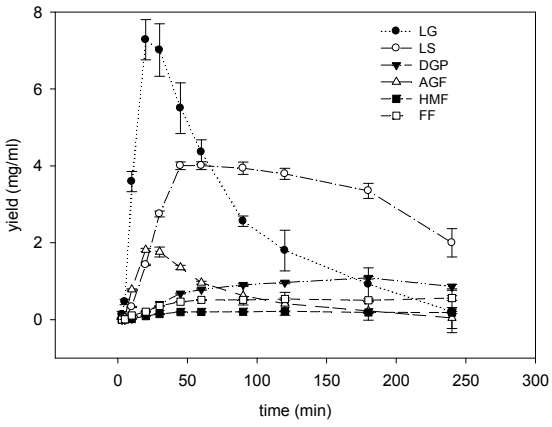

Figure 5.6: Product profile for cellulose conversion in sulfolane at 220 °C

The profile for the thermal conversion of pure cellulose in sulfolane showed that levoglucosan (LG) was the primary anhydrosaccharide formed. At all reaction temperatures, LG also had the highest yield amongst all anhydrosaccharides with the order being LG > LS > AGF > DGP. In addition, LS was always produced after LG as the conversion progressed which signals that LS is the product of LG dehydration. The profile for LG and AGF can also be seen to be very similar in that they increase and decrease concurrently. This provides evidence that the conversion between LG and AGF is a reversible reaction.

Meanwhile, the overall yields of furans (HMF and FF) were generally much lower than the anhydrosaccharides. This is probably due to transglycosylation being the primary pathway for cellulose conversion which corroborates our findings in Chapter 3 and Chapter 4. The yields of FF were greater than HMF which reflects their relative stability within the reaction mixture.

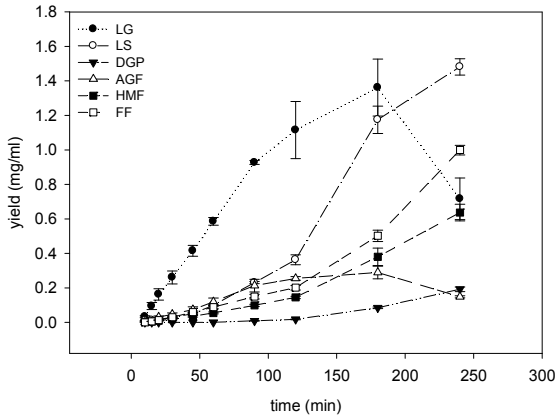

Figure 5.7: Product profile for cellulose conversion in sulfolane (with 0.13 M H_3PO_4) at 180 °C

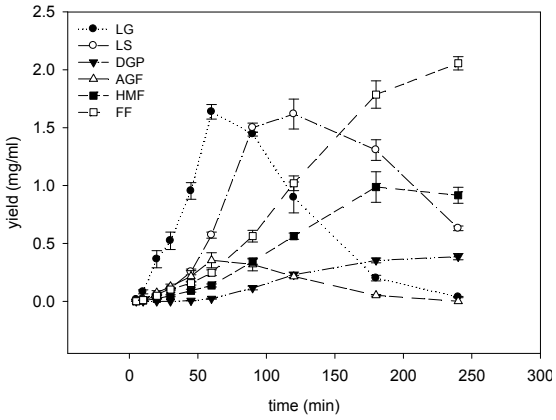

Figure 5.8: Product profile for cellulose conversion in sulfolane (with 0.13 M H_3PO_4) at 190 °C

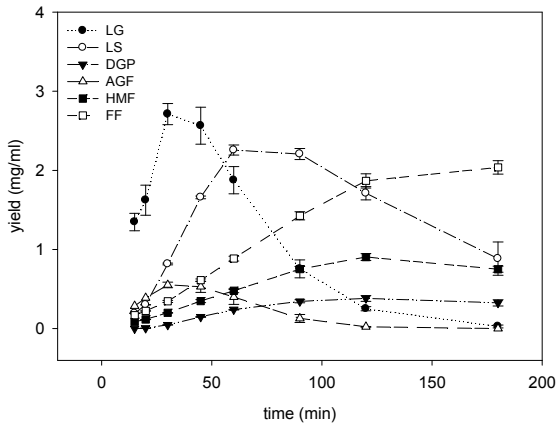

Figure 5.9: Product profile for cellulose conversion in sulfolane (with 0.13 M H_3PO_4) at 200 °C

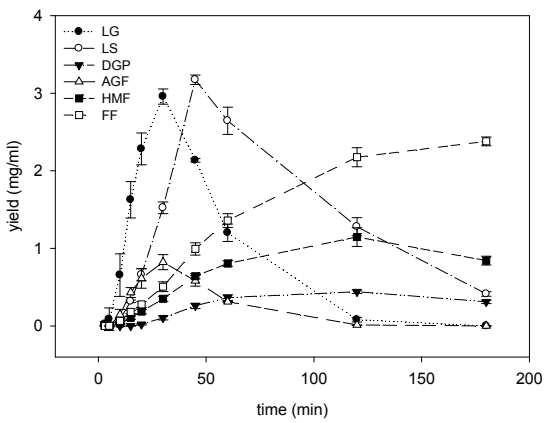

Figure 5.10: Product profile for cellulose conversion in sulfolane (with 0.13M H_3PO_4) at 210 °C

For cellulose conversion in acidified (0.13 M H_3PO_4) sulfolane, we see that there are significant differences in the profile when compared to that of neat sulfolane. Here, the yields of LG are either about equal or LS > LG. The acid accelerated the conversion of LG into LS. This observation provides an explanation as to why the literature had advocated the use of acids (especially H_3PO_4) in the production of LS. However, we should also note that while LS yields were higher than LG, the overall levels were lower than the results obtained with neat sulfolane.

We also see that the amount of furans produced were much higher than the levels seen with neat sulfolane. In fact the amount of FF and HMF produced was roughly similar to the amounts of LG and LS (i.e. between 2-3 mg/ml). This shows that the β-elimination pathway was playing a more dominant role in the cellulose conversion process. Hence, the method of adding acids (e.g. H_3PO_4) to boost LS yields is non-optimal as it probably leads to only a local maximum in the LS yields.

Another key feature of the profiles is that even with acidified sulfolane, the formation of furans increased only towards the later stages of the reaction with the anhydrosaccharides appearing first. Firstly, this shows that the initial conversion process is probably transglycosylation producing the anhydrosaccharides that subsequently degrades further to form smaller organic compounds including acids that then autocatalyses the β-elimination pathway. Secondly, the reactions producing furans are probably a number of reaction steps further down the degradation mechanism with several other unknown/undetected intermediates between them.

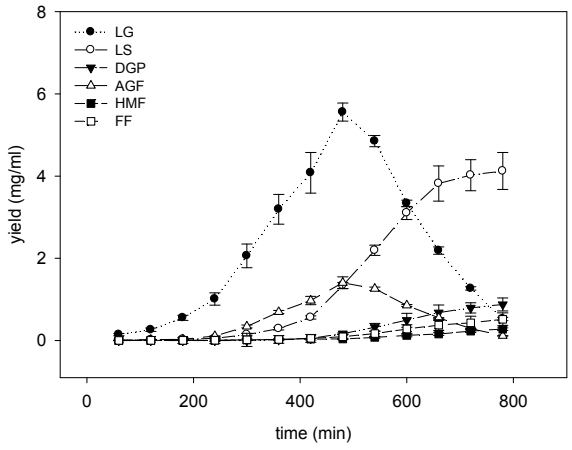

Figure 5.11: Product profile for cellulose conversion in sulfolane (with 0.01M $Ba(OH)_2$) at 190 °C

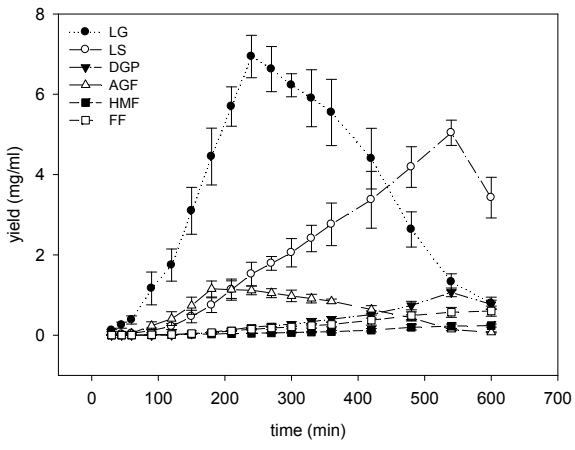

Figure 5.12: Product profile for cellulose conversion in sulfolane (with 0.01 M $Ba(OH)_2$) at 200 °C

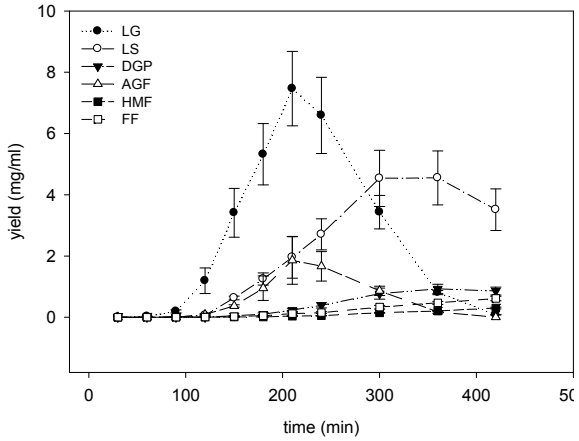

Figure 5.13: Product profile for cellulose conversion in sulfolane (with 0.01 M $Ba(OH)_2$) at 210 °C

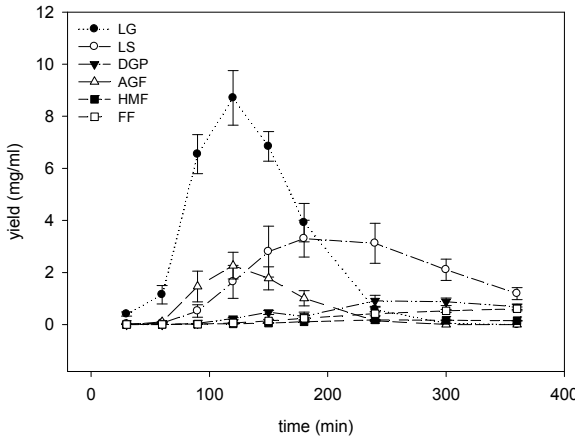

Figure 5.14: Product profile for cellulose conversion in sulfolane (with 0.01 M $Ba(OH)_2$) at 220 °C

In many aspects, the profiles for alkaline (0.01 M $Ba(OH)_2$) sulfolane are similar to the ones obtained for neat sulfolane. The yields of LG are greater than that of LS and the slopes of LG and AGF are also concurrent. The most striking difference is that the whole conversion process was slowed down considerably. Previously, for neat sulfolane, the peak yields of LG occurred at between 30 to 300 minutes. However, for alkaline sulfolane, peak levels of LG are seen between 120 to 500 minutes. Although slower, the thermal conversion of cellulose now produced higher levels of LG and LS and lower levels of furans (HMF and FF). This indicates the likelihood that the transglycosylation pathway is again the dominant route.

A consolidated view of the results obtained from the thermal conversion of cellulose in neat, acidified and alkaline sulfolane are presented by the bar charts in Figure 5.15 and Figure 5.16.

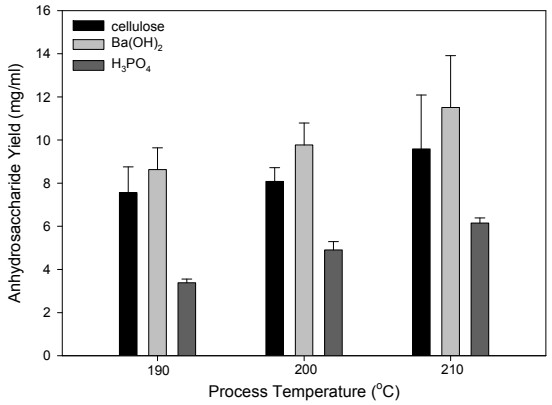

Figure 5.15: Comparison of maximum anhydrosaccharide yields in acidic and alkaline sulfolane at various temperatures

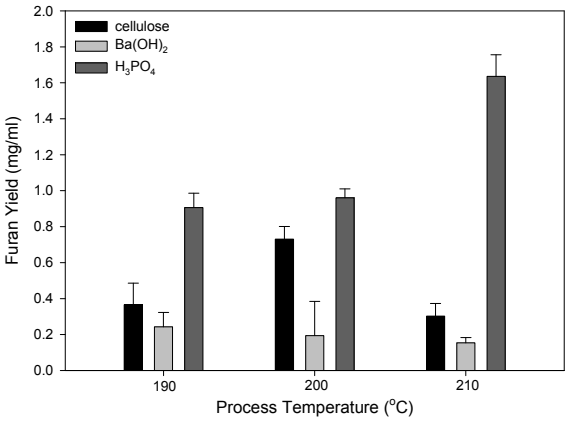

Figure 5.16: Comparison of corresponding furan yields in acidic and alkaline sulfolane at various temperatures

The results in Figure 5.15 show that cellulose conversion in alkaline sulfolane consistently produces the highest anhydrosaccharide yields whilst acidic sulfolane results in significantly lower yields. The use of 0.01 M $Ba(OH)_2$ in sulfolane increases the mean anhydrosaccharide yield by up to 20% when compared with cellulose conversion in neat sulfolane. On the other hand, the addition of 0.13 M H_3PO_4 decreases the yield of anhydrosaccharide by up to 55%.

In contrast, we see from Figure 5.16 that the use of 0.01 M $Ba(OH)_2$ in sulfolane also suppresses the production of furans (HMF and FF) when compared with acidified and neat sulfolane. This gives the added advantage of a purer anhydrosaccharide (LG and LS) product.

The results in Figure 5.15 also supports the observation in Section 3.2.1 where it was noted that more acids were generated at higher temperatures during pyrolysis thus rendering the influence of added mineral acids to be less significant. A comparison between cellulose pyrolysed in neat sulfolane compared with acidified sulfolane

(H_3PO_4) showed that the difference in the yield of anhydrosaccharide decreases from 4 mg/ml to 3 mg/ml as the temperature increases from 190 °C to 210 °C.

5.2.2 Variation of Anhydrosaccharide Yield with $[H^+]$ Changes

Due to the high reaction temperatures, we were not able to track the $[H^+]$ levels in situ as the conversion progressed. Bio-oil pH measurements have been commonly cited in literature [42, 164-166]. Therefore as an alternative, we measured the pH of cooled samples that were taken at various time intervals. These pH measurements were then converted to $[H^+]$ values using Equation (5.8).

$$pH = -log[H^+] \tag{5.8}$$

The variation of anhydrosaccharide and furan yields along with the $[H^+]$ changes is presented in Figure 5.17 to Figure 5.21 .

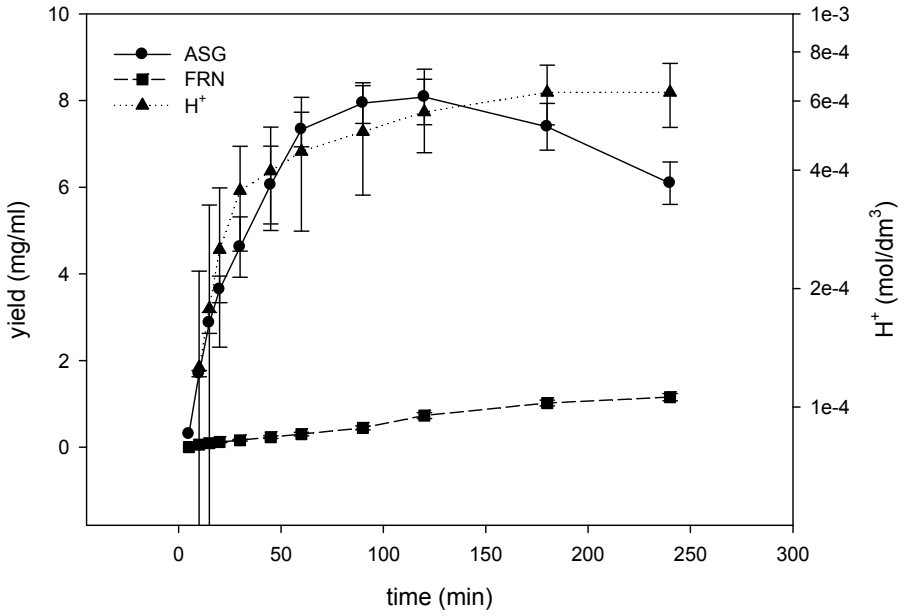

Figure 5.17: Profile of anhydrosaccharide (ASG) and furan (FRN) yields with the corresponding $[H^+]$ variations for cellulose conversion in neat sulfolane at 200 °C

Overall, the conversion of cellulose in neat sulfolane (Figure 5.17) occurred within the acidic range (pH < 4.2). The corresponding level of $[H^+]$ ranged from $6.3x10^{-5}$ mol/dm^3 to $6.3x10^{-4}$ mol/dm^3 due to the organic acids produced from the conversion process itself. The yield of anhydrosaccharides appeared to dip once $[H^+]$ exceeded $5x10^{-4}$ mol/dm^3. The increase in $[H^+]$ is also seen to coincide with an increase in furan levels. It is noted that the error bars for $[H^+]$ appears to be large due to its logarithmic relationship with pH. A small change in pH reading would result in a large change in $[H^+]$ values.

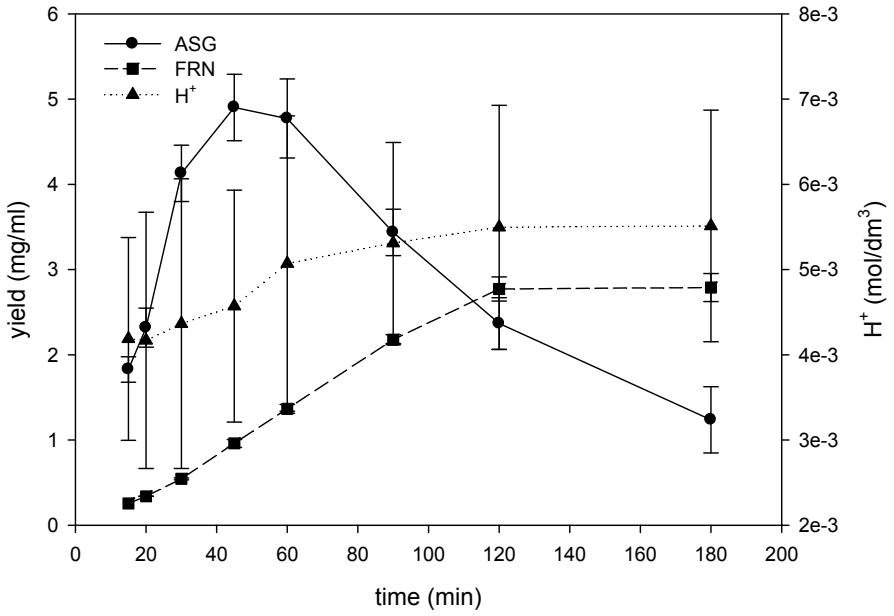

Figure 5.18: Profile of anhydrosaccharide (ASG) and furan (FRN) yields with the corresponding [H^+] variations for cellulose conversion in acidic (0.13 M H_3PO_4) sulfolane at 200 °C

Similarly, acidic sulfolane (Figure 5.18) had pH that was indicative of high [H^+] levels (pH< 3). The addition of 0.13 M H_3PO_4, resulted in a very significant increase in the initial [H^+] levels to $4.2x10^{-3}$ mol/dm^3. These levels were much higher than those experienced during cellulose conversion in neat sulfolane. As the thermal conversion progressed, the [H^+] levels increased to $5.5x10^{-3}$ mol/dm^3. This increase in [H^+] levels by $1.3x10^{-3}$ mol/dm^3 had a big influence on anhydrosaccharide and furan yields as seen from the 38 % decrease in anhydrosaccharides and 300 % increase in furans (peak yields). This emphasised the catalytic nature of [H^+] within the reaction system. Interestingly, the profile of the [H^+] curve was similar to the furans curve. This shows that the increase in [H^+] levels were due to the organic acids produced by the secondary reactions that had also formed the furans.

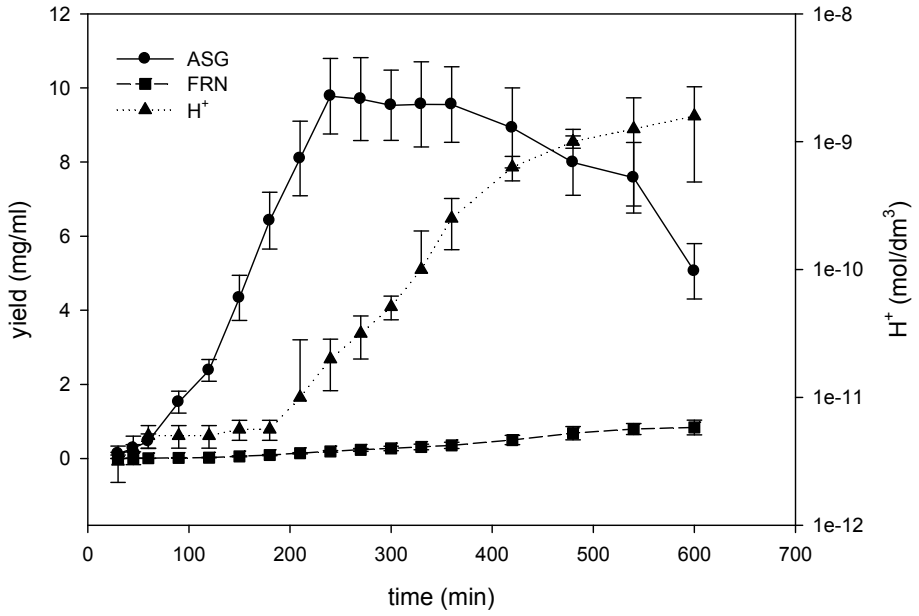

Figure 5.19: Profile of anhydrosaccharide (ASG) and furan (FRN) yields with the corresponding [H^+] variations for cellulose conversion in alkaline (0.01 M $Ba(OH)_2$) sulfolane at 200 °C

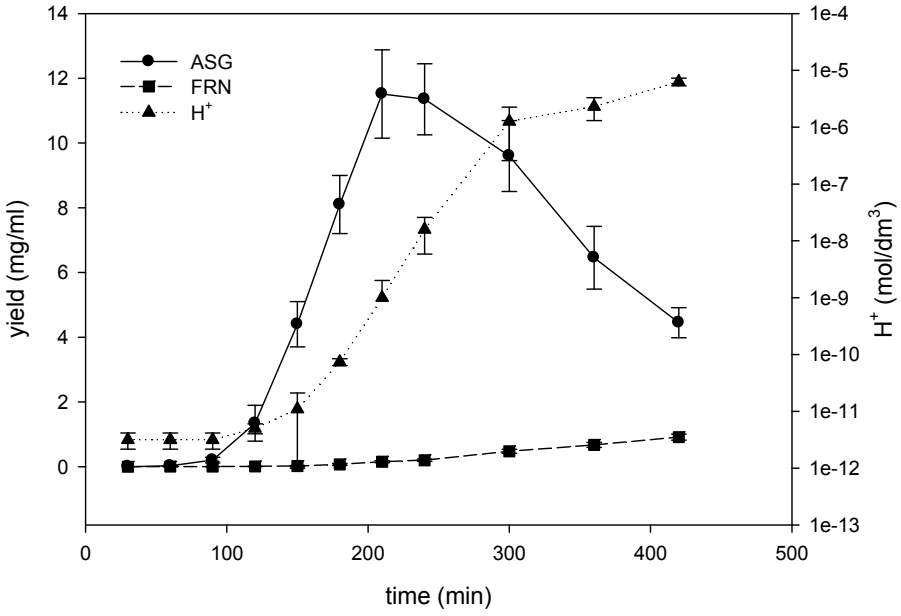

Figure 5.20: Profile of anhydrosaccharide (ASG) and furan (FRN) yields with the corresponding [H^+] variations for cellulose conversion in alkaline (0.01 M $Ba(OH)_2$) sulfolane at 210 °C

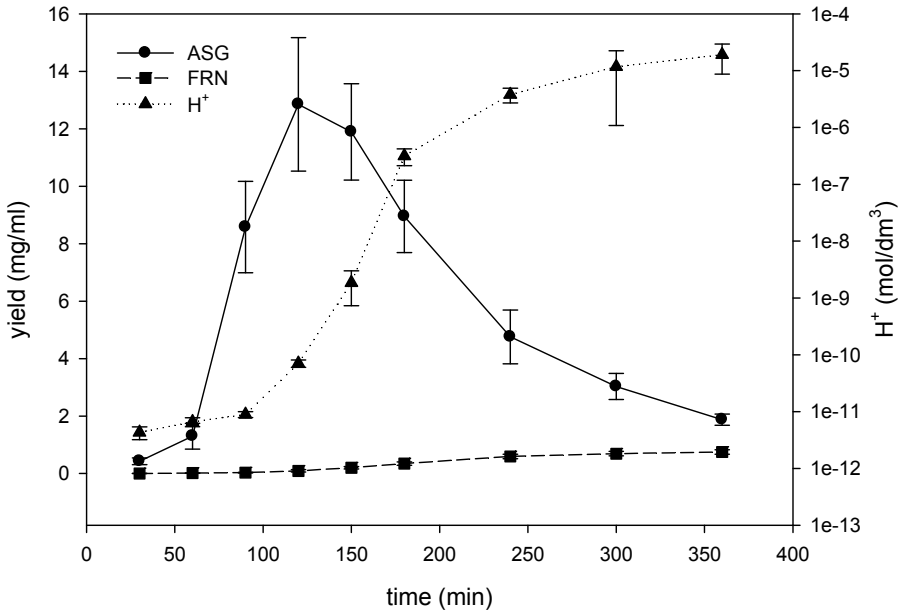

Figure 5.21: Profile of anhydrosaccharide (ASG) and furan (FRN) yields with the corresponding $[H^+]$ variations for cellulose conversion in alkaline (0.01 M $Ba(OH)_2$) sulfolane at 220 °C

For alkaline sulfolane (Figure 5.19 to Figure 5.21), a very different picture emerges. The pH measured showed a very large change from an initial level of pH≈11 to pH≈5 towards the end. At the start of all the experiments, the $[H^+]$ levels were about $3.0x10^{-12}$ mol/dm^3. The final $[H^+]$ levels were $1.6x10^{-9}$ mol/dm^3, $6.3x10^{-6}$ mol/dm^3 and $1.9x10^{-5}$ mol/dm^3 for the thermal conversion temperatures of 200 °C, 210 °C and 220 °C respectively. This shows that at higher temperatures more organic acids were produced which meant that the secondary reactions became more prominent with increasing temperatures.

We also saw that $[H^+]$ levels were initially slow to increase until it increased significantly around the midway point of the experiments. This point when $[H^+]$ levels increased also marked the downturn in anhydrosaccharide yields. Prior to this, anhydrosaccharide levels were at their maximum when $[H^+]$ levels were between

$1.0x10^{-10}$ mol/dm^3 and $1.0x10^{-9}$ mol/dm^3. This provides additional evidence that controlling the $[H^+]$ levels can lead to enhanced anhydrosaccharide yields.

5.2.3 Statistical Analysis of Results

Analysis of variance was carried out on the results obtained from the thermal conversion of the cellulose in sulfolane (neat, H_3PO_4 and $Ba(OH)_2$).

The experiments conducted were based on a two-factor factorial design. The two factors being studied were sulfolane $[H^+]$ conditions (neat, H_3PO_4 and $Ba(OH)_2$) and temperature (190 °C, 200 °C and 210 °C) . The response variable of interest was anhydrosaccharide and furan yields. The ANOVA tables generated by this analysis are shown in Appendix G3.

A comparison of the F statistics (F_0) for the experimental data with the corresponding F distribution ($F_{0.05,f,45}$) will show the significance of each of the effects under consideration. The F_0 values for the sulfolane $[H^+]$ conditions and temperature effect were higher than the corresponding F distribution values. This implies that sulfolane acidity/alkalinity and temperature had a statistically significant influence on the anhydrosaccharide and furan yields. On the other hand, the F_0 value for interaction was lower than its corresponding F distribution value for anhydrosaccharide yield but higher for furan yield. This meant that while the interaction between sulfolane $[H^+]$ conditions and temperatures were not significant for anhydrosaccharide yield, these two factors had an interaction effect for furan yield. This would be expected because

acid dissociation is dependent on temperature and higher concentration of H^+ will promote secondary reactions (e.g. dehydration) that produce furans.

5.2.4 Modelling of Cellulose Thermal Conversion in Sulfolane

The model-fitting was done for the data sets obtained from the experimental cellulose conversions in neat, acidic and alkaline sulfolane at varying process temperatures. Comparison plots of the modelling results (sims) and experimental data at the process temperature of 190 °C are shown in Figure 5.22 to Figure 5.24. The remaining comparison plots can be found in Appendix F2. In addition, all the fitted model parameters can be found in Appendix F3.

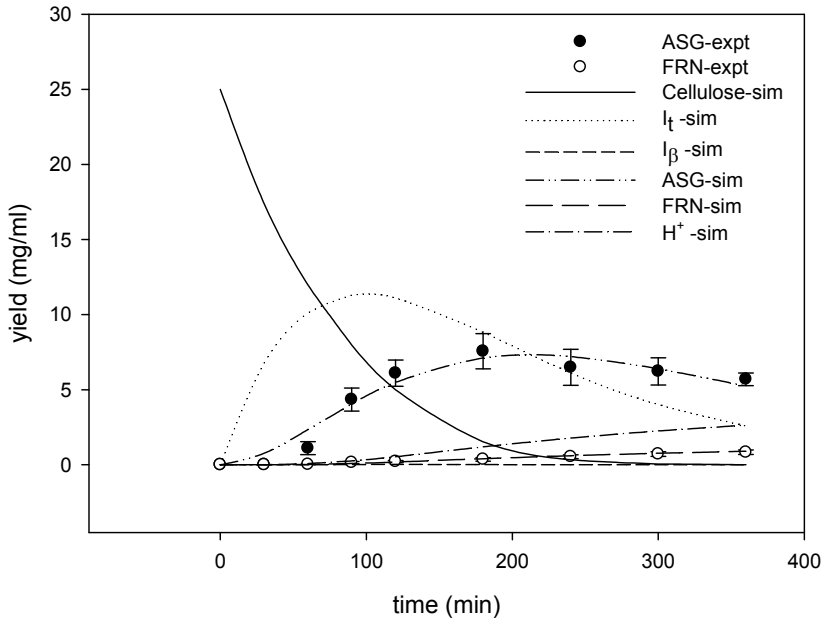

Figure 5.22: Model-fitting of anhydrosaccharides (ASG) and furans (FRN) for cellulose conversion in neat sulfolane at 190 °C

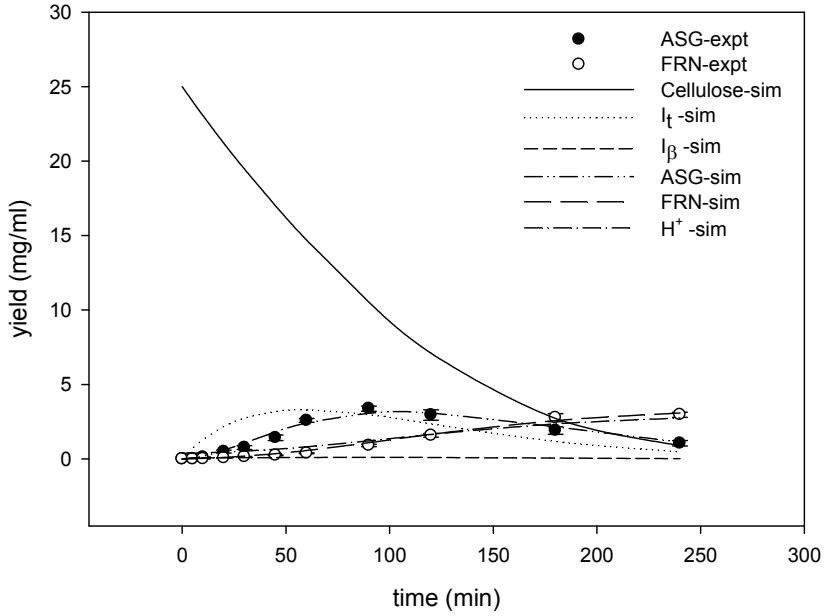

Figure 5.23: Model-fitting of anhydrosaccharides (ASG) and furans (FRN) for cellulose conversion in acidic (0.13 M H_3PO_4) sulfolane at 190 °C

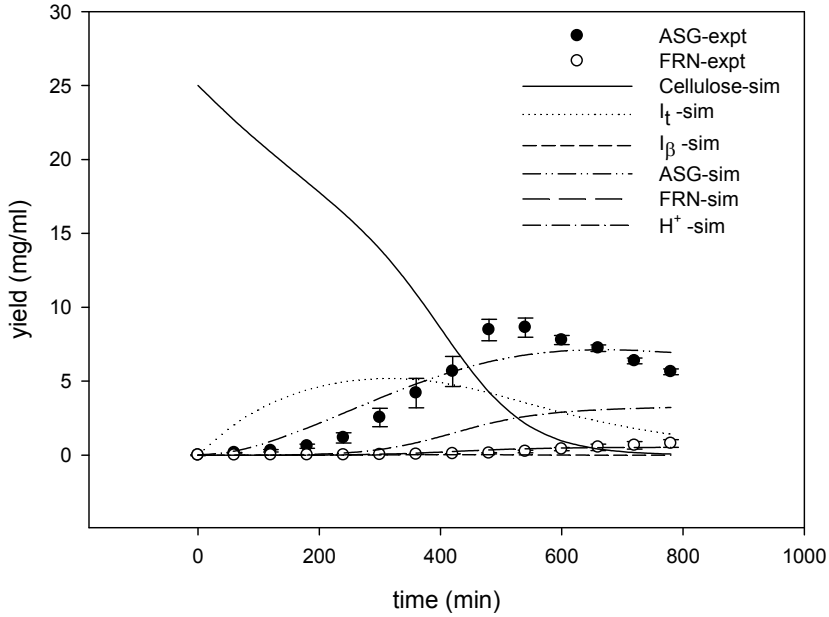

Figure 5.24: Model-fitting of anhydrosaccharides (ASG) and furans FRN) for cellulose conversion in alkaline (0.01 M $Ba(OH)_2$) sulfolane at 190 °C

Table 5.2: Goodness-of-fit for modelling cellulose conversion in sulfolane.

R^2-value	180 °C	190 °C	200 °C	210 °C	220 °C
neat	0.985	0.953	0.987	0.966	0.906
H_3PO_4	0.981	0.978	0.988	0.914	-
$Ba(OH)_2$	-	0.876	0.950	0.723	0.793

The model-fitting obtained for cellulose conversion in neat and acidic sulfolane was found to be reasonable with the goodness-of-fit measure $R^2 > 0.9$. However, as observed in the plots (Figure 5.24) and the R^2-values in Table 5.2, the model fit of cellulose conversion in alkaline sulfolane was significantly poorer ($0.72 < R^2 < 0.95$). Because of this, only the activation energies for cellulose conversion in neat and acidic sulfolane were evaluated as shown in Table 5.3.

Table 5.3: Activation energies (E) for the cellulose conversion in neat and H_3PO_4-sulfolane

	k_{tar}	k_β	k_t	k_{tg}	k_{tc}	$k_{\beta g}$	$k_{\beta c}$
				Neat-sulfolane			
***E* (kJ/mol)**	201.6	257.4	79.6	46.6	20.3	66.5	86.0
				H_3PO_4 - sulfolane			
***E* (kJ/mol)**	161.8	242.7	84.2	39.0	65.3	167.5	115.6

The modelled profiles obtained for cellulose conversion in neat and acidic sulfolane showed that the two-pathway model could adequately describe the anhydrosaccharide and furan yields. We also found that in terms of dominant pathways, for cellulose conversion in neat sulfolane, transglycosylation was the main route with the pathway degradation ratio (PDR – f_{tar}:f_β) being 1.6:1. On the other hand, for conversion in

acidic sulfolane, the PDR = 1:3.7 which indicated that β-elimination was the dominant pathway. These trends for pathway dominance is similar to those obtained in Chapter 4 that were obtained from thermogravimetry.

The evaluated activation energies for transglycosylation and β-elimination were found to be consistent with the values obtained from the thermogravimetric studies conducted in Chapter 4. This provides evidence that cellulose conversion in sulfolane proceeded via the same mechanism as the thermal degradation of dry cellulose. However, the activation energies obtained for the other rate constants should be treated carefully because of the lumped method used in the reaction scheme for dealing with the secondary reaction pathways. The clear difference in the secondary reactions' activation energies for neat and acidified sulfolane showed the possibility that different secondary reactions were initiated in the presence of the mineral acid (H_3PO_4) when compared to the organic acids that are usually generated during cellulose pyrolysis.

One of the most significant observations is the significant deviation in the model when handling cellulose conversion in alkaline sulfolane. The available literature has shown that apart from the initial transglycosylation and β-elimination pathways, there is a large number of products and secondary reaction pathways. Instead, we had to make the major assumption of lumping all the secondary reactions and their respective products together. These results highlight the limits in the use of the lumped parameter description of secondary reactions and light organics in the proposed reaction scheme.

This limitation in the-state-of-the-art to identify and track temporally all the intermediates (ca. 300 compounds) formed within the reaction system has been

described as “non-trivial” by Mettler et al. [31] in their recent publication. The current analytical method (GC-MS and HPLC) managed to detect only the 6 main components thus preventing us from identifying all the potential H^+ contributors within the system that could affect the overall conversion process. This was important because the interactions of the organic acids and $Ba(OH)_2$ in the reaction mixture have a direct impact on both the initial (transglycosylation and β-elimination) and secondary reactions.

5.3 Summary of Selective Cellulose Conversion

We have studied how the manipulation of $[H^+]$ levels via the use of H_3PO_4 and $Ba(OH)_2$ can directly affect the yields of anhydrosaccharides and furans from the thermal conversion of cellulose in a polar, aprotic solvent (sulfolane).

Experiments carried out using neat sulfolane showed that levoglucosan (LG) was the primary anhydrosaccharide formed with LG > LS > AGF > DGP whilst the furans had much lower yields compared to the anhydrosaccharides. This conversion occurred within the acidic range (pH < 4) and the corresponding level of $[H^+]$ was between $6.3x10^{-5}$ mol/dm^3 to $6.3x10^{-4}$ mol/dm^3. With the increase in $[H^+]$ due to the organic acids produced from the conversion process itself. In spite of this, transglycosylation is the likely primary pathway for cellulose conversion. This was corroborated by our modelling results which indicated that the fraction of cellulose converted via transglycosylation was 1.6 times that of β-elimination (i.e. PDR=1.6:1)

When sulfolane was acidified with 0.13 M H_3PO_4, it resulted in the $[H^+]$ levels during thermal conversion to vary from $4.2x10^{-3}$ mol/dm^3 to $5.5x10^{-3}$ mol/dm^3. This increase of $1.3x10^{-3}$ mol/dm^3 in $[H^+]$ resulted in a decrease of anhydrosaccharide yield of up to 55% and a 300% increase in furans (peak yields). This illustrates the catalytic nature of $[H^+]$ within the reaction system. In addition, the yields of LG were either about equal or LS > LG and the acid seems to have accelerated the conversion of LG into LS. This could probably be the reason why the state-of-the-art has indicated the use of acids in the production of LS. However, the use of H_3PO_4 had also boosted the yields of furans (HMF and FF). The furans were also seen to be produced during the later stages of thermal conversion showing that they are the likely products of secondary reactions. Here, it is likely that the β-elimination pathway is more dominant and this was also reflected in our modelling results which indicated a PDR value of 1:3.7. Hence, by adding acids (e.g. H_3PO_4), we might get more LS but this yield is non-optimal as it is likely to be only a local maximum for LS.

Subsequent experiments carried out with sulfolane with added alkali (0.01 M $Ba(OH)_2$), resulted in increased anhydrosaccharide yields of up to 20 % when compared with cellulose conversion in neat sulfolane and up to 155 % when compared with acidified (H_3PO_4) sulfolane. However, the conversion process was slowed down considerably with the transglycosylation pathway the likely dominant route. This slowdown could potentially be due to acids playing an initiation role in the physical transformation of crystalline cellulose to its amorphous forms. These amorphous regions within the cellulose particles are the likely locations where the ends of the cellulose chains unzip (depolymerise) and kick-off the entire conversion process.

The $[H^+]$ level during the reaction varied widely during the progress of the thermal conversion with the pH values ranging from 11.5 to 4.7. However we can see that the peak yields of anhydrosaccharides were obtained at $[H^+]$ levels of between $1x10^{-10}$ mol/dm^3 to $1x10^{-9}$ mol/dm^3. This means that an optimum $[H^+]$ level could exist where we obtain the benefit of more anhydrosaccharides and less furans.

In our attempt to devise a model for this conversion process, we obtained good model fits for cellulose thermal conversion in neat and acidic (H_3PO_4) sulfolane. The corresponding activation energies for transglycosylation and β-elimination were found to be consistent with the values obtained from the thermogravimetric studies conducted in Chapter 4. This provides evidence that cellulose conversion in sulfolane proceeded via the same mechanism as the thermal degradation of dry cellulose.

In terms of modelling the conversion of cellulose in alkaline ($Ba(OH)_2$) sulfolane, we were unable to get a good fit from the experimental results. This was mainly due to the underlying assumptions in the model that treated secondary reactions and their light organic products as a lumped parameter. This assumption was enforced on the model due to the unknown identities and quantities of all the intermediates and the secondary reaction pathways that generate them. This limitation in the state-of-the-art has also been acknowledged in recent literature and is a non-trivial challenge that needs to be overcome in future.

5.4 Conclusion

Overall, we can see that the state-of-the-art method for enhancing anhydrosaccharide yields using acids (e.g. H_3PO_4) to produce anhydrosaccharides (e.g. levoglucosan and levoglucosenone) is non-optimal. Instead, by using a suitable alkali (e.g. $Ba(OH)_2$) to manipulate or reduce the $[H^+]$ levels within the reaction mixture, we can switch cellulose conversion towards the transglycosylation pathway to achieve enhanced anhydrosaccharide yields. There seem to also be optimum $[H^+]$ level of around $1x10^{-10}$ mol/dm^3 to $1x10^{-9}$ $mol/dm^3$for anhydrosaccharide production.

However, it is noted that the use of acids can enhance anhydrosaccharide production by changing the physical characteristics (ash content, crystallinity, degree of polymerisation) of cellulose. Therefore, an acid-free pre-treatment stage to reduce ash content, cellulose crystallinity and degree of polymerisation followed by a thermal conversion process with controlled $[H^+]$ levels can result in even greater yields. By combining the state-of-the art and the results we have obtained here, a new and novel method to enhance anhydrosaccharide production can be developed. This new process would enable the selective production of such valuable chiral intermediates in the first instance and even towards specific compounds further down the cellulose thermal degradation pathway.

6. Overall Insights and Conclusions

It is known that the thermal conversion of cellulose occurs primarily via two competing pathways, namely transglycosylation and β-elimination. The presence of acids and alkalis can greatly influence the thermal conversion of cellulose via their impact on the main conversion pathways. However, the direct influence of acids and alkalis on transglycosylation and β-elimination has not been demonstrated in literature. The available literature has instead shown rather mixed results with regards to the effects of acids and alkalis on cellulose conversion and the yields of anhydrosaccharides like levoglucosan (LG) and levoglucosenone (LS). These studies showed that increased anhydrosaccharide yields from acid treatments were due to the removal of inorganic impurities, alteration of crystallinity and degree of polymerisation of cellulose. In fact, a number of patents have made use of acids (e.g. H_3PO_4) to boost the yields of levoglucosenone.

Consequently, we hypothesised that we can suppress the β-elimination route by manipulating the amount of hydrogen ions [H^+] present in the system. Hence, by lowering the level of [H^+], we can boost cellulose conversion via transglycosylation and subsequently increase the yields of anhydrosaccharides.

In experiments carried out using a fixed-bed reactor, we have observed that acids (H_2SO_4, H_3PO_4, and H_3BO_3) decreased the total amount of anhydrosaccharides. The extent of conversion via the β-elimination pathway depends on the type of acid, amount of acid present and strength of the acid (indicated by pKa values). Generally, cellulose degradation via β-elimination is promoted by higher amounts and stronger

acids but deviation from this occurs due to other factors such as anion effects and acid catalysis mechanisms.

Conversely, when cellulose was infused with alkalis (NH_4OH and $Ca(OH)_2$), the overall yield of anhydrosaccharides and levoglucosan increased accordingly. The reason for this is the neutralising effect of hydroxyl ions [OH^-] on the organic acids that are generated during pyrolysis. This in turns limits cellulose degradation via the β-elimination pathway and allows transglycosylation to proceed.

However, our results have also shown a deviation in that at lower infusion levels, cellulose infused with $Ca(OH)_2$ show some degree of reduced anhydrosaccharide yields. We know that metal ions such as Ca^{2+} have a tendency to reduce anhydrosaccharide yields via complex formation [143, 144] and subsequent ring opening reactions which would therefore dominate at the lower infusion levels. These calcium-sugar complexes have also been shown by Saladini et al. [145] to deprotonate and destabilise when pH rises. Hence, at higher $Ca(OH)_2$ infusion levels (i.e. higher pH) the complex formation effect is minimised and the neutralising effect of [OH^-] become more pronounced leading to enhance anhydrosaccharide yields. This result highlights the confounding effect of the use of alkali and alkali earth metal hydroxides in manipulating [H^+] levels.

From these results, we can see that the β-elimination pyrolysis pathway is catalysed by the presence of acidic species. However, it is possible to suppress these heterolytic reactions via the reduction or control of the hydrogen ion [H^+] concentration.

To bolster the results we obtained earlier, we proceeded to study the effects of selected acids (H_3PO_4, H_3BO_3 and H_2SO_4) and alkalis ($Ba(OH)_2$, $Ca(OH)_2$ and NH_4OH) on the kinetics associated with transglycosylation and β-elimination. Using the model-free, Friedman's isoconversional method, we saw that acids influence thermal degradation by promoting the β-elimination pathway which led to more cellulose degrading via that route at the expense of transglycosylation. For the three acids (H_3PO_4, H_3BO_3 and H_2SO_4), this manifested itself as an increase in the apparent activation energy level of ca. 250 kJ/mol. On the other hand, alkalis ($Ba(OH)_2$, $Ca(OH)_2$ and NH_4OH) had a suppressing effect on the acid-catalysed β-elimination pathway which then allows more cellulose to degrade via transglycosylation. This was seen as a lowering of the apparent activation energy to ca. 180 kJ/mol.

We have thus seen that acids were able to raise the apparent activation energy of cellulose thermal degradation whilst alkalis were able to decrease the apparent activation energy. The results show that:

$$\mathbf{E_{a,acid\text{-}cellulose} > E_{a,pure\text{-}cellulose} > E_{a,alkali\text{-}cellulose}.}$$

In addition, via model-fitting, we were also able to get a quantitative comparison between the propensity that cellulose would degrade via each of the two pathways. Based on the pathway degradation ratios (PDR) we were able to see clearly that the fraction of cellulose that degraded via β-elimination was higher when acids were present. On the other hand, when alkalis were introduced, the PDR showed a clear shift towards transglycosylation. However, the alkalis do not directly promote the

transglycosylation reaction. Instead, they have a moderating effect by suppressing the β-elimination pathway.

From the thermogravimetric data in this study, we observed that secondary reactions became more prominent towards the later stages of thermal conversion. This manifested itself as a deviation at the tail-ends during model-fitting. The presence of these secondary reactions was confirmed from the results we obtained from the TGA-FTIR experiments conducted. Evidence was also found in the work done by Mamleev et al. [149] and Vinu and Broadbelt [159], who have also shown the presence of secondary reactions during thermal conversion. Our thermogravimetric analysis is therefore focussed on the initial phase of thermal conversion where transglycosylation and β-elimination are our primary targets for the enhancement of anhydrosaccharide yields.

Consequently, it is therefore possible that the manipulation of $[H^+]$ levels can directly affect the yields of anhydrosaccharides and furans from the thermal conversion of cellulose in a polar, aprotic solvent (sulfolane). We saw that the current use of acidic additives to produce levoglucosenone (LS) is probably non-optimal. Instead, by using a suitable agent (e.g. hydroxyl ions $[OH^-]$) to manipulate or reduce the $[H^+]$ levels within the reaction mixture, we can switch cellulose conversion towards the transglycosylation pathway to achieve enhanced anhydrosaccharide (LG and LS) yields.

One drawback that emerged with the use of alkaline sulfolane was that the conversion process was slowed down considerably. This slowdown could be due to acids playing

an initiation role in the physical transformation of crystalline cellulose to its amorphous forms. These amorphous regions within the cellulose particles are the likely locations where the entire conversion process kicks-off when the ends of the cellulose chains unzip and depolymerises. This highlights the potentially conflicting effect of the use of acids in thermal conversion of cellulose. On one hand it is helpful in disrupting the crystalline structure of cellulose which aids conversion but on the other hand, it is detrimental to the yields of anhydrosaccharides. Therefore, a likely solution might be to introduce a staged process whereby cellulose is first amorphised (by non-acid means) before it is thermally converted to anhydrosaccharides.

In the course of this study, we have seen that there exists an optimal hydrogen ion [H^+] level of around $1x10^{-10}$ mol/dm^3 to $1x10^{-9}$ mol/dm^3 that would maximise the yields of valuable chiral compounds in the form of anhydrosaccharides. One way to achieve this is by using alkalis whose hydroxyl ions [OH^-] will interact/neutralise the hydrogen ions [H^+] present in the reaction system thus suppressing the β-elimination pathway and allowing conversion to proceed via transglycosylation. Although cheap and easy to implement, the use of alkalis such as $Ba(OH)_2$ to manipulate H^+ has its limitation due to cation related complex formation and cracking reactions.

Overall, we can see that the state-of-the-art method for enhancing anhydrosaccharide yields using acids (e.g. H_3PO_4) to produce anhydrosaccharides (e.g. levoglucosan and levoglucosenone) is non-optimal. Acids enhance anhydrosaccharide production by changing the physical characteristics (ash content, crystallinity, degree of polymerisation) of cellulose but they will subsequently suppress the production of anhydrosaccharides. Instead, by using a suitable alkali (e.g. $Ba(OH)_2$) to manipulate or

reduce the [H^+] levels within the reaction mixture, we can switch cellulose conversion towards the transglycosylation pathway to achieve enhanced anhydrosaccharide yields.

Therefore, an acid-free pre-treatment stage to reduce ash content, cellulose crystallinity and degree of polymerisation followed by a thermal conversion process with controlled [H^+] levels can result in even greater yields. By combining the state-of-the art and the results we have obtained here, a new and novel process with enhanced anhydrosaccharide yields can be developed. An economic costing was carried out and it showed that the estimated cost of producing levoglucosan and levoglucosenone via this proposed method should be about 0.30 S$/g compared with the current market price of more than 150 S$/g. We believe that if this price is brought down to around 10 S$/g it will be more viable for use as pharmaceutical intermediates.

This new process would enable the selective production of such valuable chiral intermediates in the first instance and even towards specific compounds further down the cellulose thermal degradation pathway.

The key scientific contributions of this thesis are:

i. We have shown conclusively that the presence of acids during the thermal conversion of cellulose result in a decrease in anhydrosaccharide produced whilst alkali presence boosted the anhydrosaccharide yields.

ii. The β-elimination pathway can be suppressed by the neutralising presence of hydroxyl ions [OH^-] thereby increasing cellulose conversion via transglycosylation.

iii. The apparent activation energy for cellulose thermal degradation can be increased or decreased by the presence of acids and alkalis respectively.

iv. The control/manipulation of hydrogen ion [H^+] levels at an optimum level (between $1x10^{-10}$ mol/dm^3 to $1x10^{-9}$ mol/dm^3) can pave the way towards the selective and enhanced production of high value anhydrosaccharides.

7. Proposed Future Work

Our current work has opened two main areas that can be tackled in future. This first involves the downstream research of seeking different methods in manipulating or controlling the [H^+] levels within the cellulose conversion process whilst the other involves the upstream research of studying the conversion intermediates and pathways in greater detail.

Firstly, the manipulation or control of hydrogen ion [H^+] levels can be achieved via the use of one or a combination of the following methods:

i. Use of acidic and alkaline species
ii. Use of solid media that can absorb acidic species generated by cellulose thermo-chemical conversion: suitably treated/prepared solid supports that can preferentially absorb and/or adsorb [H^+] generated by the thermal conversion process.
iii. Use of buffered reaction media (e.g. buffered sulfolane): buffered solutions that are able to maintain the reaction mixture at an optimum [H^+] level will allow conversion to take place mainly via transglycosylation.
iv. Use of membranes for preferential sorption, transport/removal of H^+: membrane reactors fitted with ion-exchange membranes that can function at high temperatures could remove [H^+] from within the reaction mixture thus suppressing the β-elimination pathway.
v. Use of multi-phase reaction media that will preferentially separate the acidic species generated by the reaction from the anhydrosaccharide products.

In the current work, we have attempted only the first method from this list. We noted that in situ measurements of [H^+] levels will also enable the direct control of pH levels during thermal conversion. However, typical pH probes available in the market do not operate at temperatures far above 100 °C. This is due to the fact that most probes deviate from the Nernst equation (equation (7.1)) at higher temperatures.

$$\epsilon = \epsilon^0 + \frac{RT}{F}\ln(a_{H+}) \tag{7.1}$$

Where ε is a measured potential, ε^0 is the standard electrode potential, R is the gas constant, T is the temperature in Kelvin, F is the Faraday constant and a_{H+} is the hydrogen ion activity.

A porous zirconia probe (by Corr Instruments, USA) was found to be able to respond according to the Nernst equation and measure [H^+] levels at temperatures of up to 300 °C. The drawback to this probe is that it is designed to function in an aqueous environment and it has been found to be unsuitable for use in sulfolane. It should be noted here that thermal conversion of cellulose in an aqueous media is governed by a different set of chemistry that does not lead to the formation of anhydrosaccharides. Development work on the use of this probe is continuing as it will ultimately allow us to directly maintain or control the conversion process at an optimum [H^+] level.

The other research opportunity is to identify and quantify all the intermediates and pathways within the reaction mechanism. It has been opined in the literature [30, 31, 163] that in seeking to produce targeted molecules from thermal conversion, the

traditional lumped parameter method is no longer useful. Instead, a more detailed understanding of the entire, complex reaction network would be needed.

One potential method that might be useful in the non-trivial mapping of this complex reaction network is the use of in situ Raman and/or FTIR coupled with the use of a signal processing/deconvolution algorithm like band-target entropy minimization (BTEM) [167, 168]. This method has been successfully applied in various forms to tackle problems related to identifying intermediates in catalysis that are difficult to isolate [169, 170]. BTEM has also proven to be robust in identifying compounds with overlapping spectra without a priori information of the identities of the components in the mixture. In addition, this method has also been applied to the study of chemical reactions in situ to identify intermediates and obtain kinetics of reactions [171-174]. BTEM analysis produces the best results when a large set of inherently varying spectra is processed and would therefore be suitable for this problem. Together with developments in high speed spectral data acquisition, BTEM is therefore a good candidate for the extremely challenging task of defining a detailed picture of cellulose thermal conversion.

REFERENCES

1. **C. N. Hamelinck, R. A. A. Suurs, and A. P. C. Faaij**, International bioenergy transport costs and energy balance, *Biomass and Bioenergy*, 29(2), pp.114-134 (2005).

2. **L. Lardon, A. Hélias, B. Sialve, J.-P. Steyer, and O. Bernard**, Life-Cycle Assessment of Biodiesel Production from Microalgae, *Environmental Science & Technology*, 43(17), pp.6475-6481 (2009).

3. **H. H. Khoo, P. N. Sharratt, P. Das, R. K. Balasubramanian, P. K. Naraharisetti, and S. Shaik**, Life cycle energy and CO2 analysis of microalgae-to-biodiesel: Preliminary results and comparisons, *Bioresource Technology*, 102(10), pp.5800-5807 (2011).

4. **H. H. Khoo, C. Y. Koh, M. S. Shaik, and P. N. Sharratt**, Bioenergy co-products derived from microalgae biomass via thermochemical conversion – Life cycle energy balances and CO_2 emissions, *Bioresource Technology*, 143, pp.298-307 (2013).

5. **A. J. Ragauskas, C. K. Williams, B. H. Davison, G. Britovsek, J. Cairney, C. A. Eckert, W. J. Frederick, J. P. Hallett, D. J. Leak, C. L. Liotta, J. R. Mielenz, R. Murphy, R. Templer, and T. Tschaplinski**, The Path Forward for Biofuels and Biomaterials, *Science*, 311(5760), pp.484-489 (2006).

6. **C. Briens, J. Piskorz, and F. Berruti**, Biomass valorization for fuel and chemicals production - A review *International Journal of Chemical Reactor Engineering*, 6, pp.1-49 (2008).

7. **A. Corma, S. Iborra, and A. Velty**, Chemical routes for the transformation of biomass into chemicals, *Chemical Reviews*, 107, pp.2411-2502 (2007).

8. **F. W. Lichtenthaler and S. Peters**, Carbohydrates as green raw materials for the chemical industry, *Comptes Rendus Chimie*, 7(2), pp.65-90 (2004).

9. **W. S. Trahanovsky, J. M. Ochaoda, C. Wang, K. D. Revell, K. B. Arvidson, Y. Wang, H. Zhao, S. Chung, and S. Chang**, in *Carbohydrate Synthons in Natural Products Chemistry* pp. 21-31, American Chemical Society (2002).

10. **H. M. R. Hoffmann and J. Rabe**, Synthesis and Biological Activity of α-Methylene-γ-butyrolactones, *Angewandte Chemie International Edition in English*, 24(2), pp.94-110 (1985).

11. **P. Herdewijn, J. Balzarini, E. De Clercq, R. Pauwels, M. Baba, S. Broder, and H. Vanderhaeghe**, 3'-Substituted 2',3'-dideoxynucleoside analogs as

potential anti-HIV (HTLV-III/LAV) agents, *Journal of Medicinal Chemistry*, 30(8), pp.1270-1278 (1987).

12. **P. McKendry**, Energy production from biomass (part 2): conversion technologies, *Bioresource Technology*, 83(1), pp.47-54 (2002).

13. **A. Demirbas**, Biomass resource facilities and biomass conversion processing for fuels and chemicals, *Energy Conversion and Management*, 42(11), pp.1357-1378 (2001).

14. **R. C. Saxena, D. K. Adhikari, and H. B. Goyal**, Biomass-based energy fuel through biochemical routes: A review, *Renewable and Sustainable Energy Reviews*, 13(1), pp.167-178 (2009).

15. **L. R. Lynd, W. H. v. Zyl, J. E. McBride, and M. Laser**, Consolidated bioprocessing of cellulosic biomass: an update, *Current Opinion in Biotechnology*, 16(5), pp.577-583 (2005).

16. **C. E. Wyman, B. E. Dale, R. T. Elander, M. Holtzapple, M. R. Ladisch, and Y. Y. Lee**, Coordinated development of leading biomass pretreatment technologies, *Bioresource Technology*, 96(18), pp.1959-1966 (2005).

17. **F. X. Johnson and C. Linke-Heep**, Industrial Biotechnology and Biomass Utilisation, United Nations Industrial Development Organization, (2007).

18. **V. Mamleev, S. Bourbigot, M. L. Bras, and J. Yvon**, The facts and hypotheses relating to the phenomenological model of cellulose pyrolysis. Interdependence of the steps, *Journal of Analytical and Applied Pyrolysis*, 84, pp.1-17 (2009).

19. **R. G. Graham, B. A. Bergougnou, and R. P. Overend**, Fast pyrolysis of biomass, *Journal of Analytical and Applied Pyrolysis*, 6, pp.95-135 (1984).

20. **F. Shafizadeh**, Introduction to pyrolysis of biomass, *Journal of Analytical and Applied Pyrolysis*, 3, pp.283-305 (1982).

21. **Y. C. Lin, J. Cho, G. A. Tompsett, P. R. Westmoreland, and G. W. Huber**, Kinetics and mechanism of cellulose pyrolysis, *Journal of Physical Chemistry C*, 113(46), pp.20097–20107 (2009).

22. **D. K. Shen and S. Gu**, The mechanism for thermal decomposition of cellulose and its main products, *Bioresource Technology*, 100, pp.6496-6504 (2009).

23. **F. Shafizadeh, R. H. Furneaux, T. G. Cochran, J. P. Scholl, and Y. Sakai**, Production of levoglucosan and glucose from pyrolysis of cellulosic materials, *Journal of Applied Polymer Science*, 23(12), pp.3525-3539 (1979).

24. **G. Dobele, G. Rossinskaja, G. Telysheva, D. Meier, and O. Faix**, Cellulose dehydration and depolymerization reactions during pyrolysis in the presence of phosphoric acid, *Journal of Analytical and Applied Pyrolysis*, 49(1–2)**,** pp.307-317 (1999).

25. **G. Dobele, D. Meier, O. Faix, S. Radtke, G. Rossinskaja, and G. Telysheva**, Volatile products of catalytic flash pyrolysis of celluloses, *Journal of Analytical and Applied Pyrolysis*, 58–59**,** pp.453-463 (2001).

26. **G. Dobele, T. Dizhbite, G.Rossinskaja, G.Telysheva, D.Meier, S.Radtke, and O. Faix**, Pre-treatment of biomass with phosphoric acid prior to fast pyrolysis: A promising method for obtaining 1,6-anhydrosaccharides in high yields, *Journal of Analytical and Applied Pyrolysis*, 68–69**,** pp.197-211 (2003).

27. **D. S. Scott and J. Piskorz**, *Process for the production of fermentable sugars from biomass*, CA1330991, 1994.

28. **L. Moens**, *Isolation of levoglucosan from lignocellulosic pyrolysis oil derived from wood or waste newsprint*, US5432276, 1995.

29. **D. S. Scott**, *Process for the production of anhydrosugars and fermentable sugars from fast pyrolysis liquids*, CA2091373, 1997.

30. **V. Agarwal, P. J. Dauenhauer, G. W. Huber, and S. M. Auerbach**, Ab Initio Dynamics of Cellulose Pyrolysis: Nascent Decomposition Pathways at 327 and 600 °C, *Journal of the American Chemical Society*, 134(36)**,** pp.14958-14972 (2012).

31. **M. S. Mettler, S. H. Mushrif, A. D. Paulsen, A. D. Javadekar, D. G. Vlachos, and P. J. Dauenhauer**, Revealing pyrolysis chemistry for biofuels production: Conversion of cellulose to furans and small oxygenates, *Energy & Environmental Science*, 5(1)**,** pp.5414-5424 (2012).

32. **M. S. Miftakhov, F. A. Valeev, and I. N. Gaisina**, Levoglucosenone: the properties, reactions, and use in fine organic synthesis, *Russian Chemical Reviews*, 63(10)**,** pp.869-882 (1994).

33. **T. K. Ng, R. M. Busche, C. C. McDonald, and R. W. F. Hardy**, Production of Feedstock Chemicals, *Science*, 219(4585)**,** pp.733-740 (1983).

34. **D. Lau**, White Paper on Biorenewable Chemicals, Agency for Science, Technology and Research, (2011).

35. **R. Massey, M. Jacobs, L. A. Gallagher, A. Dlugolecki, K. Geiser, and S. Edwards**, Global Chemicals Outlook, United Nations Environment Programme, (2012).

36. **D. Pimentel, A. F. Warneke, W. S. Teel, K. A. Schwab, N. J. Simcox, D. M. Ebert, K. D. Baenisch, and M. R. Aaron**, Food versus biomass fuel: Socioeconomic and environmental impacts in the United States, Brazil, India, and Kenya, *Advances in Food Research*, 32**,** pp.185-230 (1988).

37. **K. G. Cassman and A. J. Liska**, Food and fuel for all: realistic or foolish?, *Biofuels, Bioproducts and Biorefining*, 1(1)**,** pp.18-23 (2007).

38. **G. W. Huber, S. Iborra, and A. Corma**, Synthesis of transportation fuels from biomass: Chemistry, catalysts and engineering, *Chemical Reviews*, 106**,** pp.4044-4098 (2006).

39. **P. McKendry**, Energy production from biomass (part 1): Overview of biomass, *Bioresource Technology*, 83**,** pp.37-46 (2002).

40. **A. V. Bridgwater**, Renewable fuels and chemicals by thermal processing of biomass, *Chemical Engineering Journal*, 91**,** pp.87-102 (2003).

41. **S. Link, S. Arvelakis, H. Spliethoff, P. D. Waard, and A. Samoson**, Investigation of biomasses and chars obtained from pyrolysis of different biomasses with solid state ^{13}C and ^{23}Na Nuclear Magnetic Resonance Spectroscopy, *Energy & Fuels*, 22**,** pp.3523 - 3530 (2008).

42. **D. Mohan, C. U. PittmanJr, and P. H. Steele**, Pyrolysis of wood/biomass for bio-oil: A critical review, *Energy & Fuels*, 20(3)**,** pp.848 - 889 (2006).

43. **A. G. Collot, Y. Zhuo, D. R. Dugwell, and R. Kandiyoti**, Co-pyrolysis and co-gasification of coal and biomass in bench-scale fixed-bed and fluidised bed reactors, *Fuel*, 78(6)**,** pp.667-679 (1999).

44. **F. N. Islam, R. Zailani, and F. N. Ani**, Pyrolytic oil from fluidised bed pyrolysis of oil palm shell and itscharacterisation, *Renewable Energy*, 17(1)**,** pp.73-84 (1999).

45. **J. Lede**, Comparison of contact and radiant ablative pyrolysis of biomass, *Journal of Analytical and Applied Pyrolysis*, 70(2)**,** pp.601-618 (2003).

46. **W.-K. Tu, J.-L. Shie, C.-Y. Chang, C.-F. Chang, C.-F. Lin, S.-Y. Yang, J.-T. Kuo, D.-G. Shaw, and D.-J. Lee**, Pyrolysis of Rice Straw Using Radio-Frequency Plasmaâ€ *Energy & Fuels*, 22(1)**,** pp.24-30 (2007).

47. **Y. F. Huang, W. H. Kuan, S. L. Lo, and C. F. Lin**, Total recovery of resources and energy from rice straw using microwave-induced pyrolysis, *Bioresource Technology*, 99(17)**,** pp.8252-8258 (2008).

48. **C. Xu and J. Lancaster**, Conversion of secondary pulp/paper sludge powder to liquid oil products for energy recovery by direct liquefaction in hot-compressed water, *Water Research*, 42(6-7)**,** pp.1571-1582 (2008).

49. **Wahyudiono, M. Sasaki, and M. Goto**, Recovery of phenolic compounds through the decomposition of lignin in near and supercritical water, *Chemical Engineering and Processing: Process Intensification*, 47(9-10)**,** pp.1609-1619 (2008).

50. **D. C. Elliott, D. Beckman, A. V. Bridgwater, J. P. Diebold, S. B. Gevert, and Y. Solantausta**, Developments in direct thermochemical liquefaction of biomass: 1983-1990, *Energy & Fuels*, 5(3)**,** pp.399-410 (1991).

51. **N. P. Vasilakos and D. M. Austgen**, Hydrogen-donor solvents in biomass liquefaction, *Industrial & Engineering Chemistry Process Design and Development*, 24(2)**,** pp.304-311 (1985).

52. **M. Kleinert and T. Barth**, Phenols from Lignin, *Chemical Engineering & Technology*, 31(5)**,** pp.736-745 (2008).

53. **M. Kleinert and T. Barth**, Towards a Lignincellulosic Biorefinery: Direct One-Step Conversion of Lignin to Hydrogen-Enriched Biofuel, *Energy & Fuels*, 22(2)**,** pp.1371-1379 (2008).

54. **F. Shafizadeh**, The Chemistry of Pyrolysis and Combustion, *The Chemistry of Solid Wood*, 207(207)**,** pp.489-529 (1984).

55. **A. L. Brown, D. C. Dayton, and J. W. Daily**, A Study of Cellulose Pyrolysis Chemistry and Global Kinetics at High Heating Rates, *Energy & Fuels*, 15(5)**,** pp.1286-1294 (2001).

56. **J.-P. Lange**, Lignocellulose conversion: an introduction to chemistry, process and economics, *Biofuels, Bioproducts and Biorefining*, 1(1)**,** pp.39-48 (2007).

57. **M. Antal, Jr.**, in *Advances in Solar Energy*, K. Böer and J. Duffie, Eds. pp. 175-255, Springer US (1985).

58. **Y. Lin, J. Cho, J. M. Davis, and G. W. Huber**, Reaction-transport model for the pyrolysis of shrinking cellulose particles, *Chemical Engineering Science*, 74**,** pp.160-171 (2012).

59. **P. M. Molton and T. F. Demmitt**, Reaction mechanisms in cellulose pyrolysis: a literature review, Battelle Pacific Northwest Labs, (1977).

60. **V. Kothari and M. J. Antal**, Numerical studies of the flash pyrolysis of cellulose, *Fuel*, 64**,** pp.1487-1494 (1985).

61. **O. Boutin, M. Ferrer, and J. Lédé**, Flash pyrolysis of cellulose pellets submitted to a concentrated radiation: experiments and modeling, *Chemical Engineering Science*, 57**,** pp.15-25 (2002).

62. **J. Lede**, Cellulose pyrolysis kinetics: An historical review on the existence and role of intermediate active cellulose, *Journal of Analytical and Applied Pyrolysis*, 94**,** pp.17-32 (2012).

63. **G.-J. Kwon, D.-Y. Kim, S. Kimura, and S. Kuga**, Rapid-cooling, continuous-feed pyrolyzer for biomass processing: Preparation of levoglucosan from cellulose and starch, , *Journal of Analytical and Applied Pyrolysis*, 80**,** pp.1-5 (2007).

64. **G. A. Byrne, D. Gardiner, and F. H. Holmes**, The pyrolysis of cellulose and the action of flame-retardants, *Journal of Applied Chemistry*, 16(3)**,** pp.81-88 (1966).

65. **S. L. Madorsky, V. E. Hart, and S. Straus**, Pyrolysis of Cellulose in a Vacuum, *Journal of Research of the National Bureau of Standards*, 56**,** pp.343 (1956).

66. **X. Zhang, W. Yang, and W. Blasiak**, Kinetics of levoglucosan and formaldehyde formation during cellulose pyrolysis process, *Fuel*, 96**,** pp.383-391 (2012).

67. **F. Behrendt, Y. Neubauer, M. Oevermann, B. Wilmes, and N. Zobel**, Direct liquefaction of biomass, *Chemical Engineering & Technology,* , 31(5)**,** pp.667-677 (2008).

68. **A. Demirbas**, Mechanisms of liquefaction and pyrolysis reactions of biomass, *Energy Conversion & Management*, 41**,** pp.633-646 (2000).

69. **M. Kleinert and T. Barth**, Phenols from Lignin, *Chemical Engineering & Technology*, 31**,** pp.736-745 (2008).

70. **V. L. Budarin, J. H. Clark, B. A. Lanigan, P. Shuttleworth, S. W. Breeden, A. J. Wilson, D. J. Macquarrie, K. Milkowski, J. Jones, T. Bridgeman, and A. Ross**, The preparation of high grade bio-oils through the controlled, low temperature microwave activation of wheat straw, *Bioresource Technology*, 100**,** pp.6064-6068 (2009).

71. **E. M. Hassan and P. H. Steele**, Characterization of fast pyrolysis bio-oils produced from pretreated pine wood, *Applied Biochemistry and Biotechnology*, 154**,** pp.182-192 (2009).

72. **M. Muller-Hagedorn, H. Bockhorn, L. Krebs, and U. Muller**, A comparative kinetic study on the pyrolysis of three different wood species, *Journal of Analytical and Applied Pyrolysis*, 68**,** pp.231-249 (2003).

73. **P. R. Patwardhan, J. A. Satrio, R. C. Brown, and B. H. Shanks**, Influence of inorganic salts on the primary pyrolysis products of cellulose, *Bioresource Technology*, 101(12)**,** pp.4646-4655 (2010).

74. **A. Saddawi, J. M. Jones, and A. Williams**, Influence of alkali metals on the kinetics of the thermal decomposition of biomass, *Fuel Processing Technology*, Article in Press**,** (2012).

75. **H. Kawamoto, S. Saito, W. Hatanaka, and S. Saka**, Catalytic pyrolysis of cellulose in sulfolane with some acidic catalysts, *Journal of Wood Science*, 53(2)**,** pp.127-133 (2007).

76. **J. A. Knight and C. W. Gorton**, *Oil production by entrained pyrolysis of biomass and processing of oil and char*, US Patent 4,891,459, 1990.

77. **A. V. Bridgwater**, Principles and practice of biomass fast pyrolysis processes for liquids, *Journal of Analytical and Applied Pyrolysis*, 51(1–2)**,** pp.3-22 (1999).

78. **F. Shafizadeh and Y. L. Fu**, Pyrolysis of cellulose, *Carbohydrate Research*, 29(1)**,** pp.113-122 (1973).

79. **M. Sagehashi, N. Miyasaka, H. Shishido, and A. Sakoda**, Superheated steam pyrolysis of biomass elemental components and Sugi (Japanese cedar) for fuels and chemicals, *Bioresource Technology*, 97(11)**,** pp.1272-1283 (2006).

80. **D.S. Scott and J. Piskorz**, *Process for the production of fermentable sugars from biomass*, US Patent 4,880,473, 1989.

81. **L. Moens**, *Isolation of levoglucosan from lignocellulosic pyrolysis oil derived from wood or waste newsprint*, US Patent 5,432,276, 1995.

82. **D. S. Scott, J. Piskorz, D. Radlein, and P. Majerski**, *Process for the production of anhydrosugars and fermentable sugars from fast pyrolysis liquids*, CA Patent 2,091,373, 1997.

83. **G. Dobele, G. Rossinskaja, T. Dizhbite, G. Telysheva, D. Meier, and O. Faix**, Application of catalysts for obtaining 1,6-anhydrosaccharides from cellulose and wood by fast pyrolysis, *Journal of Analytical and Applied Pyrolysis*, 74(1–2)**,** pp.401-405 (2005).

84. **D. Fabbri, C. Torri, and V. Baravelli**, Effect of zeolites and nanopowder metal oxides on the distribution of chiral anhydrosugars evolved from pyrolysis

of cellulose: An analytical study, *Journal of Analytical and Applied Pyrolysis*, 80(1), pp.24-29 (2007).

85. **Z. Wang, Q. Lu, X.-F. Zhu, and Y. Zhang**, Catalytic Fast Pyrolysis of Cellulose to Prepare Levoglucosenone Using Sulfated Zirconia, *ChemSusChem*, 4(1), pp.79-84 (2011).

86. **H. Kawamoto, W. Hatanaka, and S. Saka**, Thermochemical conversion of cellulose in polar solvent (sulfolane) into levoglucosan and other low molecular-weight substances, *Journal of Analytical and Applied Pyrolysis*, 70(2), pp.303-313 (2003).

87. **H. Kawamoto, M. Murayama, and S. Saka**, Pyrolysis behavior of levoglucosan as an intermediate in cellulose pyrolysis: polymerization into polysaccharide as a key reaction to carbonized product formation, *Journal of Wood Science*, 49(5), pp.469-473 (2003).

88. **H. Kawamoto and S. Saka**, Heterogeneity in cellulose pyrolysis indicated from the pyrolysis in sulfolane, *Journal of Analytical and Applied Pyrolysis*, 76(1-2), pp.280-284 (2006).

89. **A. Takagaki and K. Ebitani**, Glucose to Value-added Chemicals: Anhydroglucose Formation by Selective Dehydration over Solid Acid Catalysts, *Chemistry Letters*, 38(7), pp.650-651 (2009).

90. **M. Ohara, A. Takagaki, S. Nishimura, and K. Ebitani**, Syntheses of 5-hydroxymethylfurfural and levoglucosan by selective dehydration of glucose using solid acid and base catalysts, *Applied Catalysis A: General*, 383(1–2), pp.149-155 (2010).

91. **G. Dobele, G. Rossinskaja, T. Dizhbite, G. Telysheva, D. Meier, and O.Faix**, Application of catalysts for obtaining 1,6-anhydrosaccharides from cellulose and wood by fast pyrolysis, *Journal of Analytical and Applied Pyrolysis*, 74(1–2), pp.401-405 (2005).

92. **B. V. Babu**, Biomass pyrolysis: a state-of-the-art review, *Biofuels, Bioproducts and Biorefining*, 2, pp.393-414 (2008).

93. **W. C. R. Chan, M. Kelbon, and B. B. Kreiger**, Modelling and experimental verification of physical and chemical processes during pyrolysis of a large biomass particle, *Fuel*, 64, pp.1505-1513 (1985).

94. **C. DiBlasi**, Modelling chemical and physical processes of wood and biomass pyrolysis, *Progress in Energy and Combustion Science*, 34, pp.47-90 (2008).

95. **C. DiBlasi**, Modeling and simulation of combustion processes of charring and non-charring solid fuels, *Progress in Energy and Combustion Science*, 19**,** pp.71-104 (1993).

96. **C. DiBlasi**, Modelling the fast pyrolysis of cellulosic particles in fluid-bed reactors, *Chemical Engineering Science*, 55**,** pp.5999-6013 (2000).

97. **B. Moghtaderi**, The state-of-the-art in pyrolysis modeling of lignocellulosic solid fuels, *Fire and Materials*, 30**,** pp.1-34 (2003).

98. **N. Prakash and T. Karunanithi**, Kinetic modeling in biomass pyrolysis, *Journal of Applied Sciences Research*, 4(12)**,** pp.1627-1636 (2008).

99. **M. G. Gronli**, A theoretical and experimental study of the thermal degradation of biomass. PhD Thesis, *NTNU*, Trondheim, Norway. (1996).

100. **F. Shafizadeh and P. S. Chin**, Thermal deterioration of wood, wood technology: chemical aspects, *ACS Symposium Series*, 43**,** pp.57-81 (1977).

101. **A. Broido and M. A. Nelson**, Char yield on pyrolysis of cellulose, *Combustion and Flame*, 24**,** pp.263-268 (1975).

102. **A. G. W. Bradbury, Y. Sakai, and F. Shafizadeh**, A kinetic model for pyrolysis of cellulose, *Journal of Applied Polymer Science*, 23**,** pp.3271-3280 (1979).

103. **A. G. Liden, F. Berruti, and D. S. Scott**, A kinetic model for the production of liquids from the flash pyrolysis of biomass, *Chemical Engineering Communications*, 65**,** pp.207-221 (1988).

104. **J. L. Banyasz, S. Li, J. Lyons-Hart, and K. H. Shafer**, Gas evolution and the mechanism of cellulose pyrolysis, *Fuel*, 80**,** pp.1757-1763 (2001).

105. **M. G. Gronli and M. C. Melaaen**, Mathematical Model for Wood PyrolysisComparison of Experimental Measurements with Model Predictions, *Energy & Fuels*, 14(4)**,** pp.791-800 (2000).

106. **M. R. Hajaligol, J. B. Howard, J. P. Longwell, and W. A. Peters**, Product compositions and kinetics for rapid pyrolysis of cellulose, *Industrial & Engineering Chemistry Process Design and Development*, 21(3)**,** pp.457-465 (1982).

107. **C. Sheng and J. L. T. Azevedo**, Modeling biomass devolatilization using the chemical percolation devolatilization model for the main components, *Proceedings of the Combustion Institute*, 29(1)**,** pp.407-414 (2002).

108. **T. R. Nunn, J. B. Howard, J. P. Longwell, and W. A. Peters**, Product compositions and kinetics in the rapid pyrolysis of milled wood lignin, *Industrial & Engineering Chemistry Process Design and Development*, 24(3), pp.844-852 (1985).

109. **D. S. Scott, J. Piskorz, and D. Radlein**, Liquid products from the continuous flash pyrolysis of biomass, *Industrial & Engineering Chemistry Process Design and Development*, 24(3), pp.581-588 (1985).

110. **P. Murugan, N. Mahinpey, K. E. Johnson, and M. Wilson**, Kinetics of the Pyrolysis of Lignin Using Thermogravimetric and Differential Scanning Calorimetry Methods, *Energy & Fuels*, 22(4), pp.2720-2724 (2008).

111. **R. Capart, L. Khezami, and A. K. Burnham**, Assessment of various kinetic models for the pyrolysis of a microgranular cellulose, *Thermochimica Acta*, 417, pp.79-89 (2004).

112. **J. J. M. Órfão**, Review and evaluation of the approximations to the temperature integral, *AIChE Journal*, 53(11), pp.2905-2915 (2007).

113. **A. W. Coats and J. P. Redfern**, Kinetic Parameters from Thermogravimetric Data, *Nature*, 201(4914), pp.68-69 (1964).

114. **S. Vyazovkin and C. A. Wight**, Model-free and model-fitting approaches to kinetic analysis of isothermal and nonisothermal data, *Thermochimica Acta*, 340–341, pp.53-68 (1999).

115. **S. Vyazovkin**, A unified approach to kinetic processing of nonisothermal data, *International Journal of Chemical Kinetics*, 28(2), pp.95-101 (1996).

116. **M. E. Brown, M. Maciejewski, S. Vyazovkin, R. Nomen, J. Sempere, A. Burnham, J. Opfermann, R. Strey, H. L. Anderson, A. Kemmler, R. Keuleers, J. Janssens, H. O. Desseyn, C.-R. Li, T. B. Tang, B. Roduit, J. Malek, and T. Mitsuhashi**, Computational aspects of kinetic analysis: Part A: The ICTAC Kinetics Project-data, methods and results, *Thermochimica Acta*, 355(1–2), pp.125-143 (2000).

117. **M. Maciejewski**, Computational aspects of kinetic analysis: Part B: The ICTAC Kinetics Project-the decomposition kinetics of calcium carbonate revisited, or some tips on survival in the kinetic minefield, *Thermochimica Acta*, 355(1-2), pp.145-154 (2000).

118. **S. Vyazovkin**, Computational aspects of kinetic analysis: Part C: The ICTAC Kinetics Project-the light at the end of the tunnel?, *Thermochimica Acta*, 355(1-2), pp.155-163 (2000).

119. **A. K. Burnham**, Computational aspects of kinetic analysis: Part D: The ICTAC Kinetics Project-multi-thermal-history model-fitting methods and their relation to isoconversional methods, *Thermochimica Acta*, 355(1-2)**,** pp.165-170 (2000).

120. **B. Roduit**, Computational aspects of kinetic analysis: Part E: The ICTAC Kinetics Project-numerical techniques and kinetics of solid state processes, *Thermochimica Acta*, 355(1-2)**,** pp.171-180 (2000).

121. **J. H. Flynn and L. A. Wall**, General treatment of the thermogravimetry of polymers, *Journal of Research of the National Bureau of Standards —A. Physics and Chemistry*, 70A(6)**,** pp.487-523 (1966).

122. **T. Ozawa**, Kinetic analysis of derivative curves in thermal analysis, *Journal of Thermal Analysis and Calorimetry*, 2(3)**,** pp.301-324 (1970).

123. **H. L. Friedman**, Kinetics of thermal degradation of char-forming plastics from thermogravimetry. Application to a phenolic plastic, *Journal of Polymer Science Part C: Polymer Symposia*, 6(1)**,** pp.183-195 (1964).

124. **H. L. Friedman**, in *Journal of Macromolecular Science: Part A - Chemistry* pp. 57-79, Taylor & Francis (1967).

125. **S. V. Vyazovkin and A. I. Lesnikovich**, An approach to the solution of the inverse kinetic problem in the case of complex processes: Part 1. Methods employing a series of thermoanalytical curves, *Thermochimica Acta*, 165(2)**,** pp.273-280 (1990).

126. **S. V. Vyazovkin, V. I. Goryachko, and A. I. Lesnikovich**, An approach to the solution of the inverse kinetic problem in the case of complex processes. Part III. Parallel independent reactions, *Thermochimica Acta*, 197(1)**,** pp.41-51 (1992).

127. **S. Vyazovkin**, Conversion dependence of activation energy for model DSC curves of consecutive reactions, *Thermochimica Acta*, 236**,** pp.1-13 (1994).

128. **S. Vyazovkin and W. Linert**, Kinetic analysis of reversible thermal decomposition of solids, *International Journal of Chemical Kinetics*, 27(1)**,** pp.73-84 (1995).

129. **S. Vyazovkin**, An approach to the solution of the inverse kinetic problem in the case of complex processes: Part 4. Chemical reaction complicated by diffusion, *Thermochimica Acta*, 223**,** pp.201-206 (1993).

130. **M.-J. Lazaro, R. Moliner, and I. Suelves**, Non-isothermal versus isothermal technique to evaluate kinetic parameters of coal pyrolysis, *Journal of Analytical and Applied Pyrolysis*, 47(2)**,** pp.111-125 (1998).

131. **T. Vlase, G. Vlase, N. Birta, and N. Doca**, Comparative results of kinetic data obtained with different methods for complex decomposition steps, *Journal of Thermal Analysis and Calorimetry*, 88(3), pp.631-635 (2007).

132. **P. E. Sanchez-Jimenez, L. A. Perez-Maqueda, A. Perejon, J. Pascual-Cosp, M. Benitez-Guerrero, and J. M. Criado**, An improved model for the kinetic description of the thermal degradation of cellulose, *Cellulose*, 18(6), pp.1487-1498 (2011).

133. **I. Milosavljevic, V. Oja, and E. M. Suuberg**, Thermal Effects in Cellulose Pyrolysis:Relationship to Char Formation Processes, *Industrial & Engineering Chemistry Research*, 35(3), pp.653-662 (1996).

134. **J. Jansen and L. Machado**, Using ordinary differential equations system to solve isoconversional problems in non-isothermal kinetic analysis, *Journal of Thermal Analysis and Calorimetry*, 87(3), pp.913-918 (2007).

135. **N. Kuzhiyil, D. Dalluge, X. Bai, K. H. Kim, and R. C. Brown**, Pyrolytic Sugars from Cellulosic Biomass, *ChemSusChem*, 5(11), pp.2228-2236 (2012).

136. **P. A. Brownsort**, Biomass pyrolysis processes: performance parameters and their influence on biochar system benefits. Thesis, University of Edinburgh, (2009).

137. **L. Devi, K. J. Ptasinski, and F. J. J. G. Janssen**, A review of the primary measures for tar elimination in biomass gasification processes, *Biomass and Bioenergy*, 24(2), pp.125-140 (2003).

138. **J. Dai and J. R. Grace**, Biomass screw feeding with tapered and extended sections, *Powder Technology*, 186(1), pp.56-64 (2008).

139. **M. Fang, L. Yang, G. Chen, Z. Shi, Z. Luo, and K. Cen**, Experimental study on rice husk combustion in a circulating fluidized bed, *Fuel Processing Technology*, 85(11), pp.1273-1282 (2004).

140. **J. J. Lerou and G. F. Froment**, Velocity, temperature and conversion profiles in fixed bed catalytic reactors, *Chemical Engineering Science*, 32(8), pp.853-861 (1977).

141. **J. O. Edwards, G. C. Morrison, V. F. Ross, and J. W. Schultz**, The Structure of the Aqueous Borate Ion, *Journal of the American Chemical Society*, 77(2), pp.266-268 (1955).

142. **M. J. S. Dewar and R. Jones**, New heteroaromatic compounds. XXV. Studies of salt formation in boron oxyacids by boron-11 nuclear magnetic resonance, *Journal of the American Chemical Society*, 89(10), pp.2408-2410 (1967).

143. **S. J. Angyal**, in *Advances in Carbohydrate Chemistry and Biochemistry*, R. S. Tipson and H. Derek, Eds. pp. 1-43, Academic Press (1989).

144. **B. Gyurcsik and L. Nagy**, Carbohydrates as ligands: coordination equilibria and structure of the metal complexes, *Coordination Chemistry Reviews*, 203(1)**,** pp.81-149 (2000).

145. **M. Saladini, L. Menabue, and E. Ferrari**, Sugar complexes with metal2+ ions: thermodynamic parameters of associations of Ca2+, Mg2+ and Zn2+ with galactaric acid, *Carbohydrate Research*, 336(1)**,** pp.55-61 (2001).

146. **H. Kawamoto, S. Saito, and S. Saka**, Inhibition of acid-catalyzed depolymerization of cellulose with boric acid in non-aqueous acidic media, *Carbohydrate Research*, 343(2)**,** pp.249-255 (2008).

147. **H. Kawamoto, S. Saito, and S. Saka**, Stable complex formation with boric acid in pyrolysis of levoglucosan in acidic media, *Journal of Analytical and Applied Pyrolysis*, 82(1)**,** pp.78-82 (2008).

148. **H. Barud, C. Ribeiro, J. Capela, M. Crespi, S. Ribeiro, and Y. Messadeq**, Kinetic parameters for thermal decomposition of microcrystalline, vegetal, and bacterial cellulose, *Journal of Thermal Analysis and Calorimetry*, 105(2)**,** pp.421-426 (2011).

149. **V. Mamleev, S. Bourbigot, and J. Yvon**, Kinetic analysis of the thermal decomposition of cellulose: The change of the rate limitation, *Journal of Analytical and Applied Pyrolysis*, 80**,** pp.141-150 (2007).

150. **V. Mamleev, S. Bourbigot, and J. Yvon**, Kinetic analysis of the thermal decomposition of cellulose: The main step of mass loss, *Journal of Analytical and Applied Pyrolysis*, 80**,** pp.151-165 (2007).

151. **M. Poletto, V. c. Pistor, M. Zeni, and A. J. Zattera**, Crystalline properties and decomposition kinetics of cellulose fibers in wood pulp obtained by two pulping processes, *Polymer Degradation and Stability*, 96(4)**,** pp.679-685

152. **I. Milosavljevic and E. M. Suuberg**, Cellulose Thermal Decomposition Kinetics: Global Mass Loss Kinetics, *Industrial & Engineering Chemistry Research*, 34(4)**,** pp.1081-1091 (1995).

153. **M. Gronli, M. J. Antal, and G. Varhegyi**, A Round-Robin Study of Cellulose Pyrolysis Kinetics by Thermogravimetry, *Industrial & Engineering Chemistry Research*, 38(6)**,** pp.2238-2244 (1999).

154. **G. Varhegyi, M. J. Antal, T. Szekely, and P. Szabo**, Kinetics of the thermal decomposition of cellulose, hemicellulose, and sugarcane bagasse, *Energy & Fuels*, 3(3)**,** pp.329-335 (1989).

155. **A. J. Chipperfield and P. J. Fleming**, The MATLAB Genetic Algorithm Toolbox, *IEE Seminar Digests*, 1995(14)**,** pp.10-10 (1995).

156. **J. E. White, W. J. Catallo, and B. L. Legendre**, Biomass pyrolysis kinetics: A comparative critical review with relevant agricultural residue case studies, *Journal of Analytical and Applied Pyrolysis*, 91(1)**,** pp.1-33 (2011).

157. **J. A. Caballero, R. Font, and A. Marcilla**, Comparative study of the pyrolysis of almond shells and their fractions, holocellulose and lignin. Product yields and kinetics, *Thermochimica Acta*, 276(0)**,** pp.57-77 (1996).

158. **F. Yao, Q. Wu, Y. Lei, W. Guo, and Y. Xu**, Thermal decomposition kinetics of natural fibers: Activation energy with dynamic thermogravimetric analysis, *Polymer Degradation and Stability*, 93(1)**,** pp.90-98 (2008).

159. **R. Vinu and L. J. Broadbelt**, A mechanistic model of fast pyrolysis of glucose-based carbohydrates to predict bio-oil composition, *Energy & Environmental Science*, 5(12)**,** pp.9808-9826 (2012).

160. **V. W. Weekman**, Laboratory reactors and their limitations, *AIChE Journal*, 20(5)**,** pp.833-840 (1974).

161. **I. Pastorova, R. E. Botto, P. W. Arisz, and J. J. Boon**, Cellulose char structure: a combined analytical Py-GC-MS, FTIR, and NMR study, *Carbohydrate Research*, 262(1)**,** pp.27-47 (1994).

162. **F. Shafizadeh, R. H. Furneaux, T. T. Stevenson, and T. G. Cochran**, Acid-catalyzed pyrolytic synthesis and decomposition of 1,4:3,6-dianhydro-α-d-glucopyranose, *Carbohydrate Research*, 61(1)**,** pp.519-528 (1978).

163. **H. B. Mayes and L. J. Broadbelt**, Unraveling the Reactions that Unravel Cellulose, *The Journal of Physical Chemistry A*, 116(26)**,** pp.7098-7106 (2012).

164. **M. Ikura, M. Stanciulescu, and E. Hogan**, Emulsification of pyrolysis derived bio-oil in diesel fuel, *Biomass and Bioenergy*, 24(3)**,** pp.221-232 (2003).

165. **X. Junming, J. Jianchun, S. Yunjuan, and L. Yanju**, Bio-oil upgrading by means of ethyl ester production in reactive distillation to remove water and to improve storage and fuel characteristics, *Biomass and Bioenergy*, 32(11)**,** pp.1056-1061 (2008).

166. **Q. Lu, X.-l. Yang, and X.-f. Zhu**, Analysis on chemical and physical properties of bio-oil pyrolyzed from rice husk, *Journal of Analytical and Applied Pyrolysis*, 82(2)**,** pp.191-198 (2008).

167. **E. Widjaja, C. Li, W. Chew, and M. Garland**, Band-Target Entropy Minimization. A Robust Algorithm for Pure Component Spectral Recovery. Application to Complex Randomized Mixtures of Six Components, *Analytical Chemistry*, 75(17)**,** pp.4499-4507 (2003).

168. **S. Y. Sin, E. Widjaja, L. E. Yu, and M. Garland**, Application of FT-Raman and FTIR measurements using a novel spectral reconstruction algorithm, *Journal of Raman Spectroscopy*, 34(10)**,** pp.795-805 (2003).

169. **W. Chew, E. Widjaja, and M. Garland**, Band-Target Entropy Minimization (BTEM):An Advanced Method for Recovering Unknown Pure Component Spectra. Application to the FTIR Spectra of Unstable Organometallic Mixtures, *Organometallics*, 21(9)**,** pp.1982-1990 (2002).

170. **A. D. Allian, Y. Wang, M. Saeys, G. M. Kuramshina, and M. Garland**, The combination of deconvolution and density functional theory for the mid-infrared vibrational spectra of stable and unstable rhodium carbonyl clusters, *Vibrational Spectroscopy*, 41(1)**,** pp.101-111 (2006).

171. **F. Gao, A. D. Allian, H. Zhang, S. Cheng, and M. Garland**, Chemical and kinetic study of acetophenone hydrogenation over Pt/Al2O3: Application of BTEM and other multivariate techniques to quantitative on-line FTIR measurements, *Journal of Catalysis*, 241(1)**,** pp.189-199 (2006).

172. **E. Widjaja, Y. Y. Tan, and M. Garland**, Application of Band-Target Entropy Minimization to On-Line Raman Monitoring of an Organic Synthesis. An Example of New Technology for Process Analytical Technology, *Organic Process Research & Development*, 11(1)**,** pp.98-103 (2006).

173. **M. Tjahjono, C. Huiheng, E. Widjaja, K. Sa-ei, and M. Garland**, Combined on-line transmission FTIR measurements and BTEM analysis for the kinetic study of a consecutive reaction in aqueousâ€“organic phase medium, *Talanta*, 79(3)**,** pp.856-862 (2009).

174. **M. Tjahjono, X. Li, F. Tang, K. Sa-ei, and M. Garland**, Kinetic study of a complex triangular reaction system in alkaline aqueous-ethanol medium using on-line transmission FTIR spectroscopy and BTEM analysis, *Talanta*, 85(5)**,** pp.2534-2541

APPENDIX

Appendix A **: Publications**

Technical Disclosure

1. S.M. Shaik, C.Y. Koh, Production of high-value intermediates via controlling cellulose decomposition pathways, 201207522-2, Oct 2012.

Journal Papers

1. S.M. Shaik, P.N. Sharratt, R.B.H. Tan, Influence of Selected Mineral Acids and Alkalis on Cellulose Pyrolysis Pathways and Anhydrosaccharide Formation, Journal of Analytical and Applied Pyrolysis, (accepted, in-press DOI: 10.1016/j.jaap.2013.07.010)

2. S.M. Shaik, C.Y. Koh, P.N. Sharratt, R.B.H. Tan, Influence of Acids and Alkalis on Transglycosylation and β-Elimination Pathway Kinetics during Cellulose Pyrolysis, Thermochimica Acta, 566, pp. 1-9 (2013).

Conferences

1. S.M. Shaik, C.Y. Koh, P.N. Sharratt, The Effects of Cationic and Anionic Species on Cellulosic Biomass Pyrolysis/Gasification, 10th European Gasification Conference, Amsterdam, Netherlands, October 2010. (poster presentation)

Appendix B **: Biomass Thermochemical Conversion**

Appendix B1 : Thermochemical techniques for biomass conversion

Table B1.1: Description of various thermochemical conversion technologies

Process	Conditions	Products
Carbonization	Temperature: 300 °C Pressure: 1 to 10 bars Heating rates: 5 °C/min Reduced O2 atmosphere	Primarily solid char (yield: 35%)
Torrefaction	Temperature: 200-300 °C Pressure: 1 bar Heating rates: <50 °C/min Inert atmosphere	Primarily solid (yield: 80% dry basis)
Pyrolysis (e.g. fast-, flash-, ultra-, vacuum-pyrolysis)	Temperature: 500-800 °C Pressure: 1< to 10 bars Heating rates: up to 10,000 °C/min Inert atmosphere	Primarily liquids (75%) [acids, alcohols, aldehydes, esters, ketones, sugars, phenols, guaiacols, syringols, furans]
Hydropyrolysis	Temperature: 400 °C Pressure: 5 to 100 bars Heating rates: up to 300 °C/min Reducing atmosphere (H2, CO)	Primarily liquids (60%) [similar to pyrolysis but with lower O content, less acidic, more hydrophobic]
Liquefaction	Temperature: 250-450 °C Pressure: 50 to 300 bars Heating rates: 20 °C/min Reducing atmosphere (H2, CO) and or catalyst/H-donor solvents	Primarily liquids (75%) [similar to pyrolysis but with lower O content, less acidic, more hydrophobic]
Gasification	Temperature: 700-1000 °C Pressure: 1< to 10 bars Heating rates: up to 10,000 °C/min Inert atmosphere	Primarily gases (85%) [CO, CO2, H2 and CH4]

Appendix B2 : Cellulose pyrolysis mechanisms

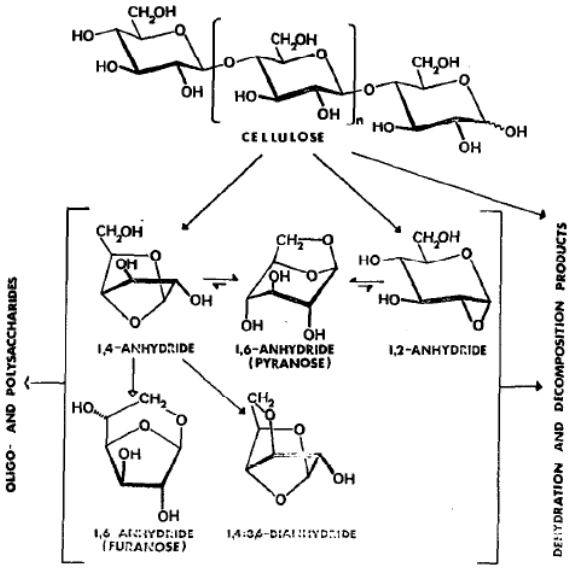

Figure B2.1:Shafizadeh's cellulose pyrolysis mechanism

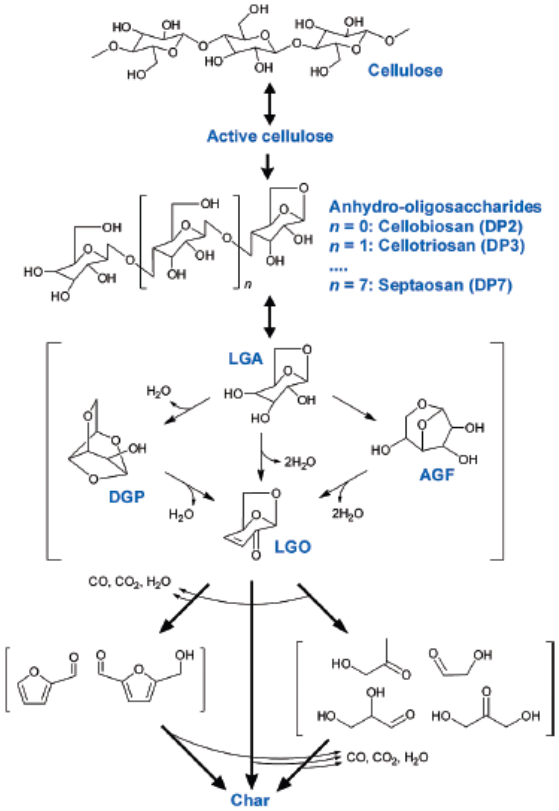

Figure B2.2: Li's cellulose pyrolysis mechanism

Appendix B3 : Commonly used reaction models

Table B3.1: Reaction models f(α) and their corresponding integral functions g(α).

Model	$f(\alpha)$	$g(\alpha)$
Reaction order (n)	$(1-\alpha)^n$	
0		α
1		$-\ln(1-\alpha)$
≥2		$[1/(n-1)](1-\alpha)1-n$
Phase boundary reaction		
Cylindrical symmetry	$2(1-\alpha)^{0.5}$	$1-(1-\alpha)0.5$
Spherical symmetry	$3(1-\alpha)^{2/3}$	$1-(1-\alpha)1/3$
Diffusional		
One-dimensional	$1/2\alpha$	α^2
Two-dimensional	$[-\ln(1-\alpha)]^{-1}$	$(1-\alpha)[\ln(1-\alpha)]+\alpha$
Three-dimensional spherical symmetry, Jander equation	$1.5(1-\alpha)^{2/3}[1-(1-\alpha)^{1/3}]^{-1}$	$[1-(1-\alpha)^{1/3}]^2$
Three-dimensional spherical symmetry, Ginstling–Brounshtein	$1.5[(1-\alpha)^{-1/3}-1]^{-1}$	$(1-2\alpha/3)-(1-\alpha)^{2/3}$
Nuclei-growth		
Avrami–Erofeev (n = 1.5, 2, 3, 4)	$n(1-\alpha)[-\ln(1-\alpha)]^{(n-1)/n}$	$[-\ln(1-\alpha)]^{1/n}$
Prout–Tompkins	$(1-\alpha)\alpha^m$	
m = 0.5		$\ln[(1+\alpha^{0.5})/(1-\alpha^{0.5})]$
m = 1		$\ln[\alpha/(1-\alpha)]$

Appendix C **: Mechanical design of fixed-bed reactor**

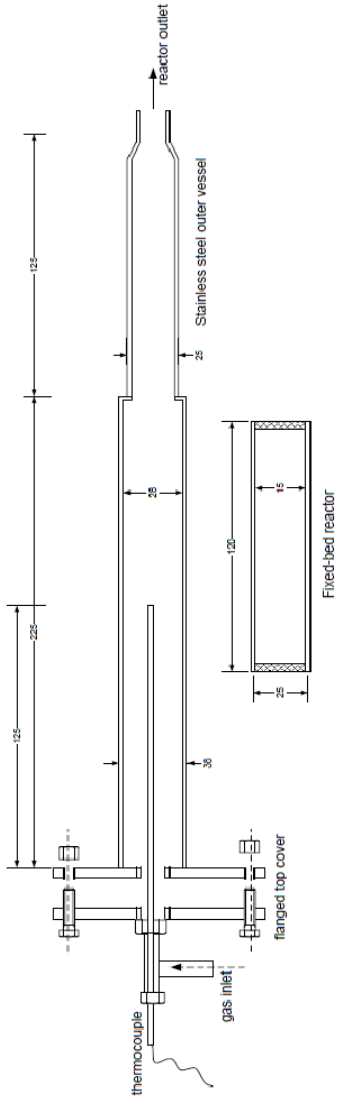

Figure C1.1: Cross-sectional view of fixed-bed reactor

Appendix D **: Schematic of Thermogravimetric Analyser**

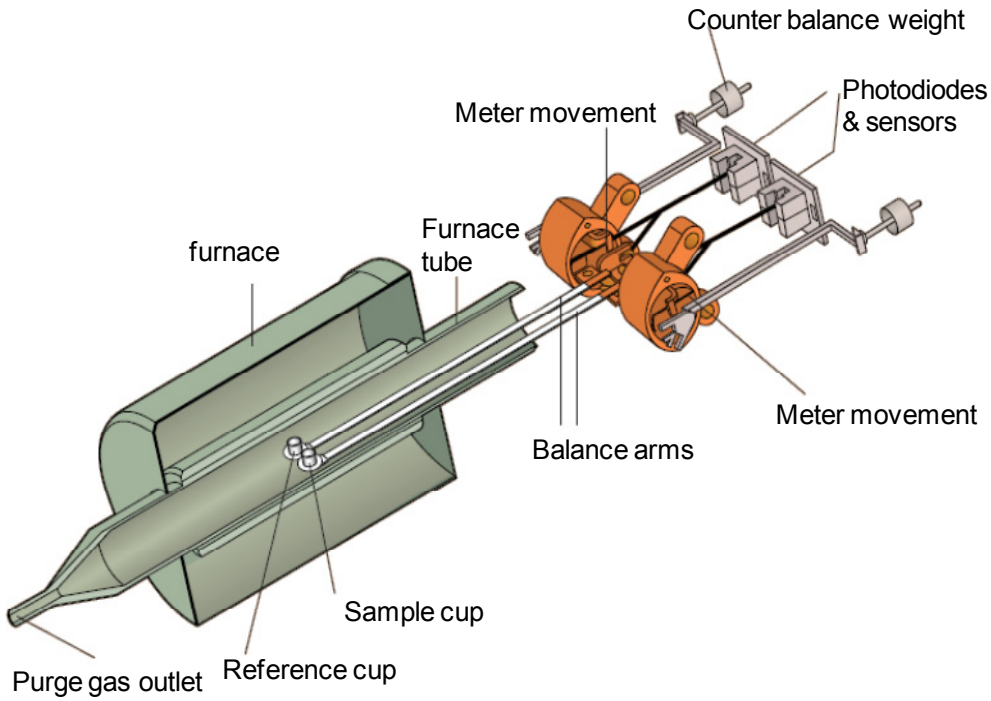

Figure D1.1: Schematic of the TA Instruments SDT 2960 Simultaneous DSC-TGA (adapted from http://www.tainstruments.com)

Appendix E **: TGA data for cellulose thermal degradation**

Appendix E1 : TGA profiles for acids

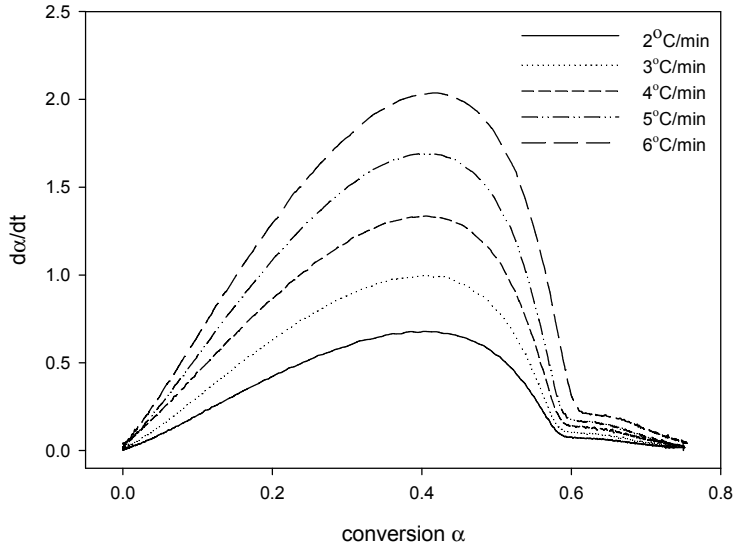

Figure E1.1: Variation of conversion rate (dα/dt) for cellulose infused with 2 wt% H_3PO_4 at various TGA heating rates (2-6 °C/min)

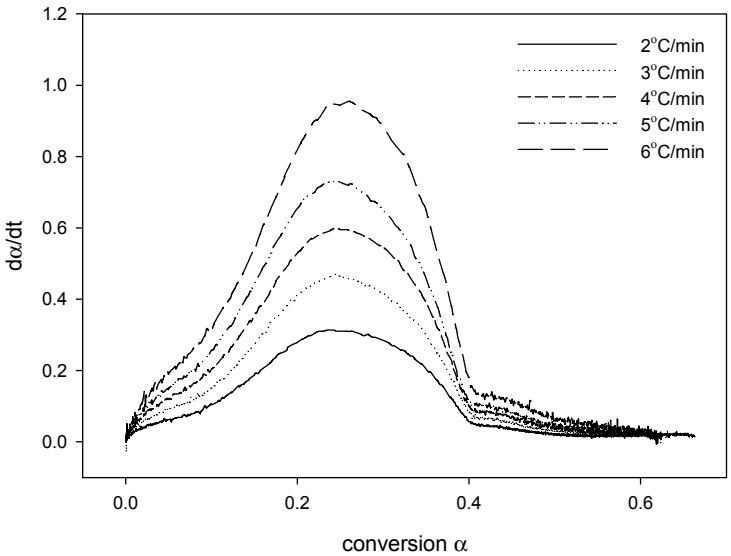

Figure E1.2: Variation of conversion rate (dα/dt) for cellulose infused with 3 wt% H_3PO_4 at various TGA heating rates (2-6 °C/min)

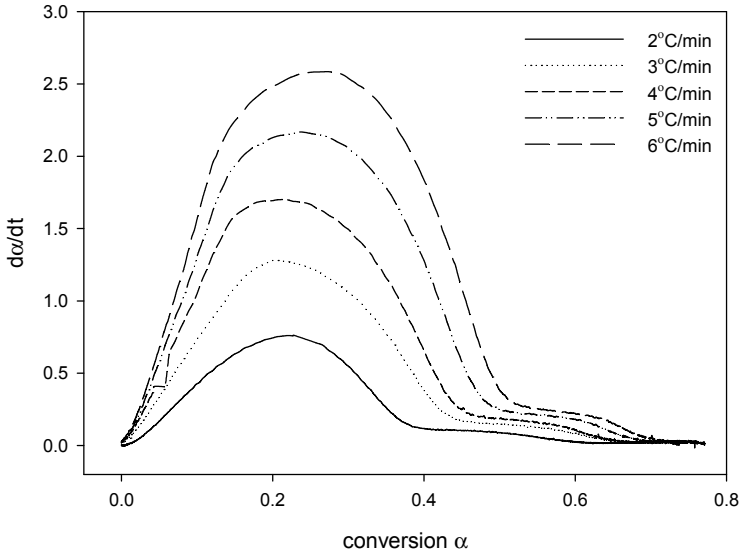

Figure E1.3: Variation of conversion rate (dα/dt) for cellulose infused with 2 wt% H_3BO_3 at various TGA heating rates (2-6 °C/min)

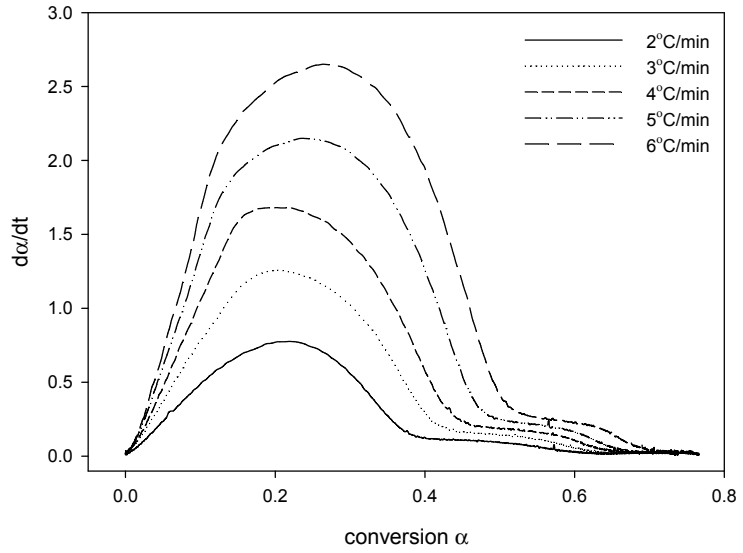

Figure E1.4: Variation of conversion rate (dα/dt) for cellulose infused with 3 wt% H_3BO_3 at various TGA heating rates (2-6 °C/min)

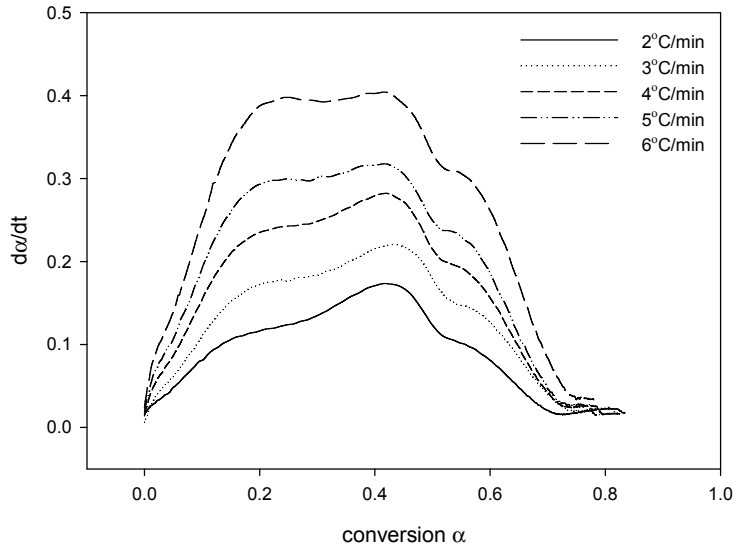

Figure E1.5: Variation of conversion rate (dα/dt) for cellulose infused with 0.5 wt% H_2SO_4 at various TGA heating rates (2-6 °C/min)

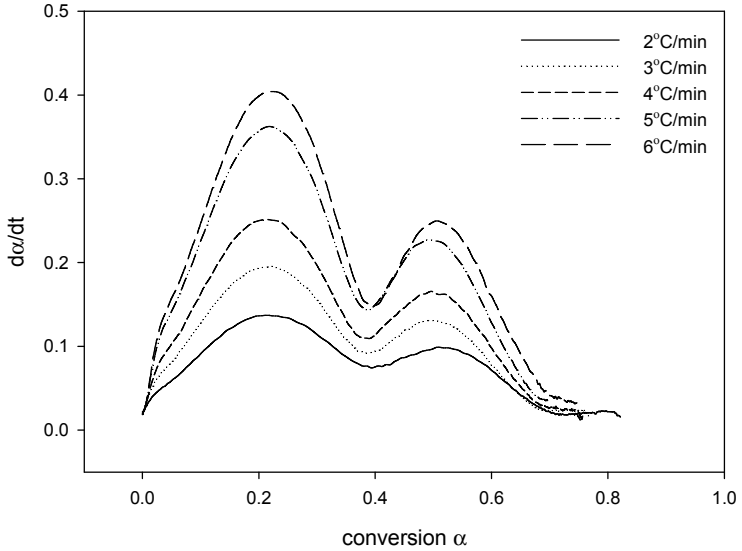

Figure E1.6: Variation of conversion rate (dα/dt) for cellulose infused with 1 wt% H_2SO_4 at various TGA heating rates (2-6 °C/min)

Appendix E2 : TGA profiles for alkalis

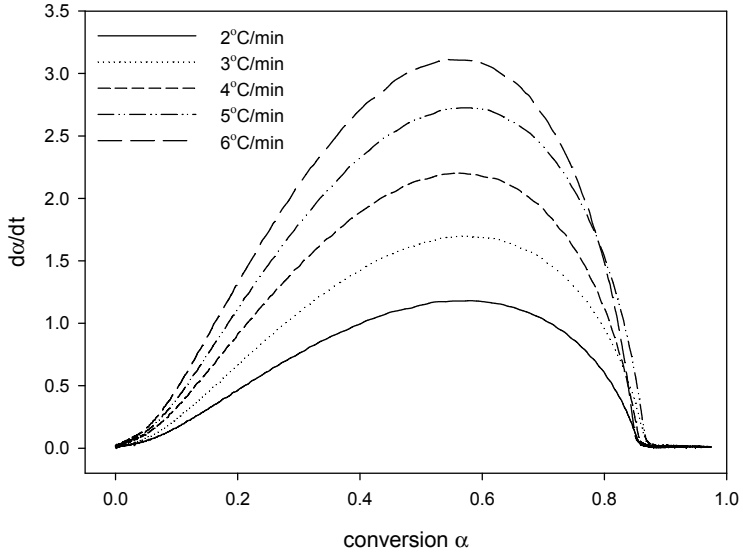

Figure E2.1: Variation of conversion rate (dα/dt) for cellulose infused with 0.1 wt% $Ba(OH)_2$ at various TGA heating rates (2-6 °C/min)

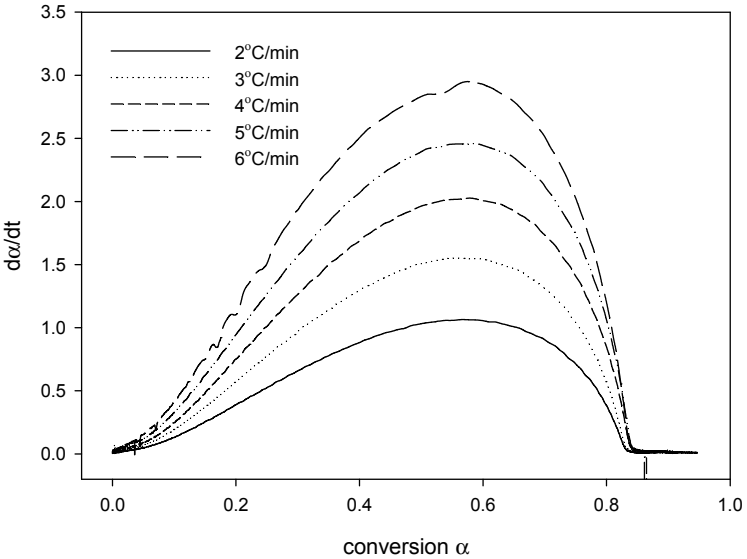

Figure E2.2: Variation of conversion rate (dα/dt) for cellulose infused with 0.5 wt% $Ba(OH)_2$ at various TGA heating rates (2-6 °C/min)

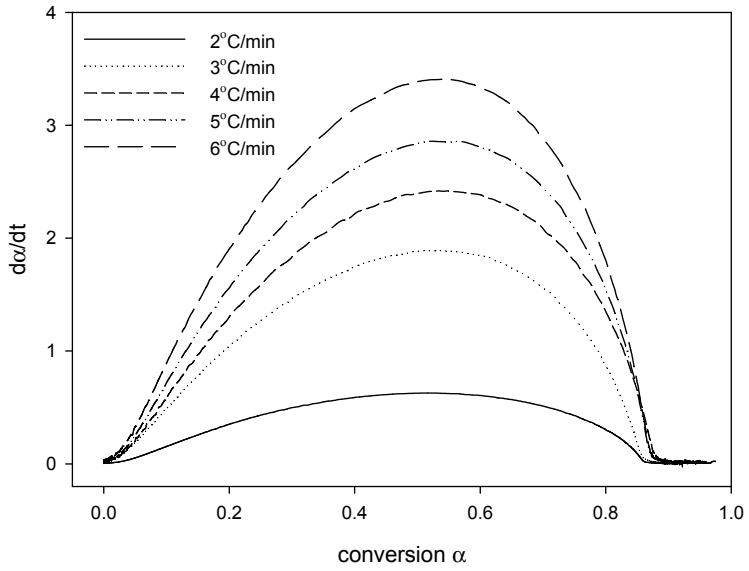

Figure E2.3: Variation of conversion rate (dα/dt) for cellulose infused with 0.1 wt% $Ca(OH)_2$ at various TGA heating rates (2-6 °C/min)

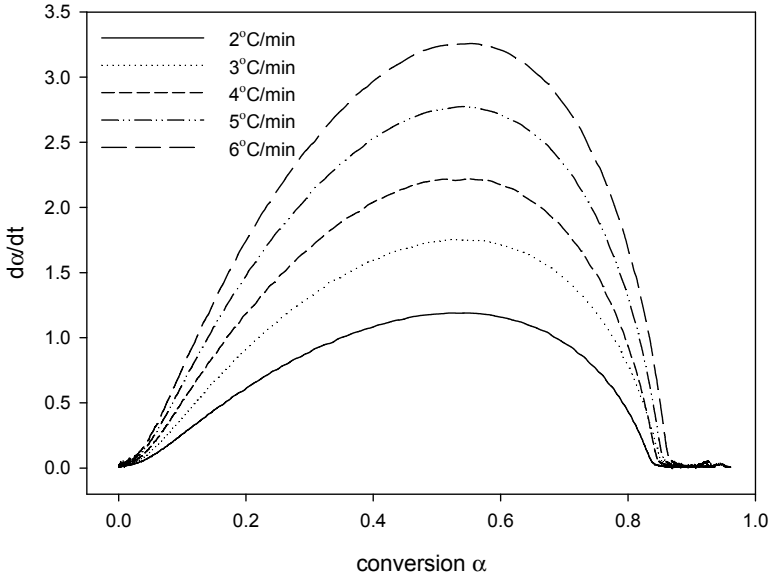

Figure E2.4: Variation of conversion rate (dα/dt) for cellulose infused with 0.5 wt% $Ca(OH)_2$ at various TGA heating rates (2-6 °C/min)

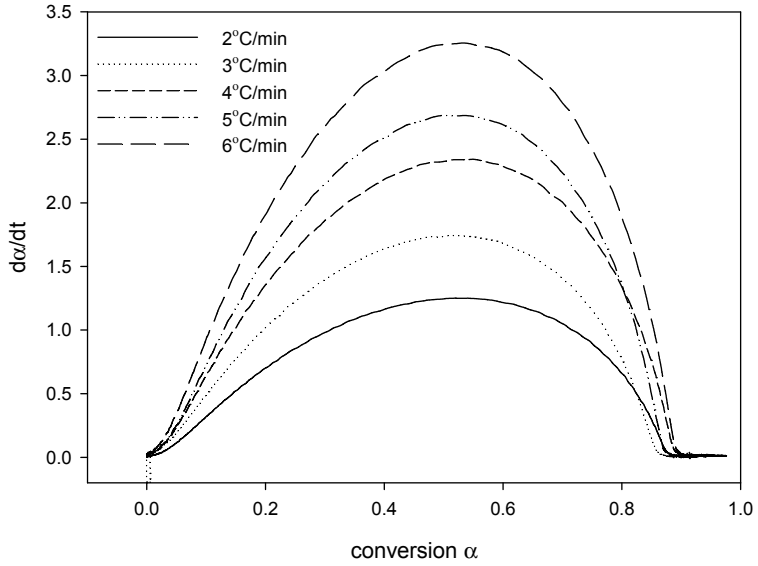

Figure E2.5: Variation of conversion rate (dα/dt) for cellulose infused with 2 wt% NH_4OH at various TGA heating rates (2-6 °C/min)

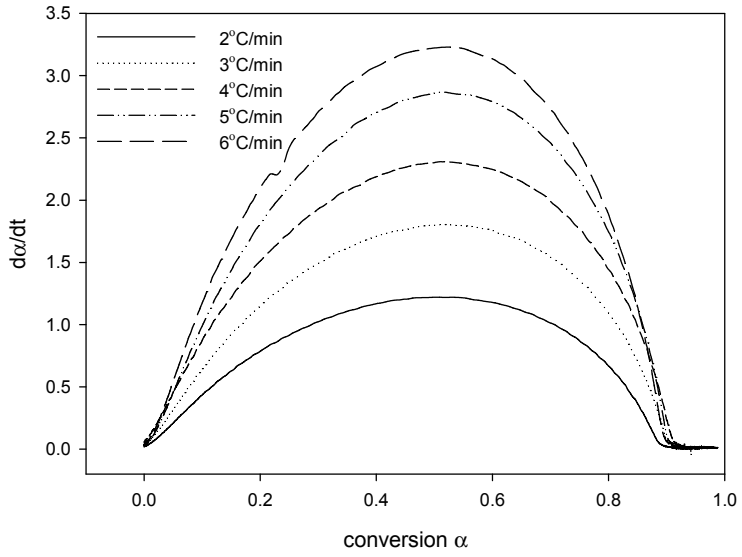

Figure E2.6: Variation of conversion rate (dα/dt) for cellulose infused with 2 wt% NH_4OH at various TGA heating rates (2-6 °C/min)

Appendix E3 : First-order model goodness of fit

Table E3.1: Goodness of fit of the 1st order model for the degradation of cellulose with H_3PO_4 at various TGA heating rates.

	2 °C/min	3 °C/min	4 °C/min	5 °C/min	6 °C/min
R^2 value (2 wt% H_3PO_3)	0.93	0.93	0.95	0.92	0.95
	2 °C/min	**3 °C/min**	**4 °C/min**	**5 °C/min**	**6 °C/min**
R^2 value (3 wt% H_3PO_3)	0.93	0.92	0.92	0.92	0.92
	2 °C/min	**3 °C/min**	**4 °C/min**	**5 °C/min**	**6 °C/min**
R^2 value (5 wt% H_3PO_3)	0.94	0.93	0.94	0.92	0.92

Table E3.2: Goodness of fit of the 1st order model for the degradation of cellulose with H_3BO_3 at various TGA heating rates.

	2 °C/min	3 °C/min	4 °C/min	5 °C/min	6 °C/min
R^2 value (2 wt% H_3BO_3)	0.91	0.91	0.92	0.92	0.92
	2 °C/min	**3 °C/min**	**4 °C/min**	**5 °C/min**	**6 °C/min**
R^2 value (3 wt% H_3BO_3)	0.90	0.90	0.90	0.90	0.91
	2 °C/min	**3 °C/min**	**4 °C/min**	**5 °C/min**	**6 °C/min**
R^2 value (5 wt% H_3BO_3)	0.91	0.95	0.90	0.90	0.90

Table E3.3: Goodness of fit of the 1st order model for the degradation of cellulose with $Ba(OH)_2$ at various TGA heating rates.

	2 °C/min	3 °C/min	4 °C/min	5 °C/min	6 °C/min
R^2 value (0.1 wt% $Ba(OH)_2$)	0.95	0.95	0.95	0.94	0.94
	2 °C/min	**3 °C/min**	**4 °C/min**	**5 °C/min**	**6 °C/min**
R^2 value (0.5 wt% $Ba(OH)_2$)	0.95	0.95	0.95	0.94	0.94
	2 °C/min	**3 °C/min**	**4 °C/min**	**5 °C/min**	**6 °C/min**
R^2 value (1 wt% $Ba(OH)_2$)	0.95	0.95	0.95	0.95	0.94

Table E3.4: Goodness of fit of the 1st order model for the degradation of cellulose with $Ca(OH)_2$ at various TGA heating rates.

	2 °C/min	3 °C/min	4 °C/min	5 °C/min	6 °C/min
R^2 value (0.1 wt% $Ca(OH)_2$)	0.94	0.94	0.94	0.94	0.93
	2 °C/min	**3 °C/min**	**4 °C/min**	**5 °C/min**	**6 °C/min**
R^2 value (0.5 wt% $Ca(OH)_2$)	0.95	0.95	0.94	0.94	0.94
	2 °C/min	**3 °C/min**	**4 °C/min**	**5 °C/min**	**6 °C/min**
R^2 value (1 wt% $Ca(OH)_2$)	0.95	0.95	0.94	0.94	0.94

Appendix E4 : Fitted kinetic parameters

Table E4.1: Fitted model parameters obtained for first-order thermal degradation model – H_3PO_4 infused cellulose

2 wt% H_3PO_4						
Heating rate (°C/min)	f_1	f_2	A_1 (1/s)	E_1 (kJ/mol)	A_2 (1/s)	E_2 (kJ/mol)
6	0.16	0.54	6.68×10^{15}	204	3.30×10^{21}	260
5	0.16	0.54	6.68×10^{15}	204	3.30×10^{21}	260
4	0.17	0.53	6.68×10^{15}	204	3.30×10^{21}	260
3	0.17	0.53	6.68×10^{15}	204	3.26×10^{21}	260
2	0.17	0.53	6.68×10^{15}	204	7.03×10^{21}	263
3 wt% H_3PO_4						
Heating rate (°C/min)	f_1	f_2	A_1 (1/s)	E_1 (kJ/mol)	A_2 (1/s)	E_2 (kJ/mol)
6	0.08	0.42	7.30×10^{15}	191	7.68×10^{21}	244
5	0.09	0.41	7.30×10^{15}	191	7.68×10^{21}	244
4	0.09	0.41	7.30×10^{15}	191	7.68×10^{21}	244
3	0.09	0.41	7.30×10^{15}	191	7.68×10^{21}	244
2	0.10	0.40	7.30×10^{15}	191	7.68×10^{21}	244
5 wt% H_3PO_4						
Heating rate (°C/min)	f_1	f_2	A_1 (1/s)	E_1 (kJ/mol)	A_2 (1/s)	E_2 (kJ/mol)
6	0.17	0.53	6.46×10^{15}	203	5.10×10^{21}	261
5	0.17	0.53	6.46×10^{15}	203	5.10×10^{21}	261
4	0.18	0.52	6.46×10^{15}	203	5.10×10^{21}	261
3	0.19	0.51	6.46×10^{15}	203	5.10×10^{21}	261
2	0.20	0.50	6.46×10^{15}	203	5.10×10^{21}	261

Table E4.2: Fitted model parameters obtained for first-order thermal degradation model – H_3BO_3 infused cellulose

2 wt% H_3BO_3						
Heating rate (°C/min)	f_1	f_2	A_1 **(1/s)**	E_1 **(kJ/mol)**	A_2 **(1/s)**	E_2 **(kJ/mol)**
6	0.39	0.38	1.46×10^{15}	204	1.10×10^{20}	260
5	0.40	0.37	1.46×10^{15}	204	1.10×10^{20}	260
4	0.41	0.36	1.46×10^{15}	204	1.10×10^{20}	260
3	0.42	0.35	1.46×10^{15}	204	1.10×10^{20}	260
2	0.44	0.33	1.46×10^{15}	204	1.10×10^{20}	260
3 wt% H_3BO_3						
Heating rate (°C/min)	f_1	f_2	A_1 **(1/s)**	E_1 **(kJ/mol)**	A_2 **(1/s)**	E_2 **(kJ/mol)**
6	0.36	0.41	1.46×10^{15}	204	1.10×10^{20}	260
5	0.35	0.39	1.46×10^{15}	204	1.10×10^{20}	260
4	0.36	0.38	1.46×10^{15}	204	1.10×10^{20}	260
3	0.37	0.37	1.46×10^{15}	204	1.10×10^{20}	260
2	0.40	0.35	1.46×10^{15}	204	1.10×10^{20}	260
5 wt% H_3BO_3						
Heating rate (°C/min)	f_1	f_2	A_1 **(1/s)**	E_1 **(kJ/mol)**	A_2 **(1/s)**	E_2 **(kJ/mol)**
6	0.29	0.47	1.46×10^{15}	203	2.70×10^{20}	260
5	0.29	0.47	1.46×10^{15}	203	2.70×10^{20}	260
4	0.30	0.44	1.46×10^{15}	203	2.70×10^{20}	260
3	0.31	0.43	1.46×10^{15}	203	2.70×10^{20}	260
2	0.33	0.41	1.46×10^{15}	203	2.70×10^{20}	260

Table E4.3: Fitted model parameters obtained for first-order thermal degradation model – $Ba(OH)_2$ infused cellulose

0.1 wt% $Ba(OH)_2$						
Heating rate (°C/min)	f_1	f_2	A_1 (1/s)	E_1 (kJ/mol)	A_2 (1/s)	E_2 (kJ/mol)
6	0.72	0.18	$1.46x10^{15}$	208	$1.02\ x10^{19}$	260
5	0.75	0.17	$1.46x10^{15}$	208	$1.02\ x10^{19}$	260
4	0.75	0.17	$1.46x10^{15}$	208	$1.02\ x10^{19}$	260
3	0.78	0.16	$1.46x10^{15}$	208	$1.02\ x10^{19}$	260
2	0.81	0.15	$1.46x10^{15}$	208	$1.02\ x10^{19}$	260
0.5 wt% $Ba(OH)_2$						
Heating rate (°C/min)	f_1	f_2	A_1 (1/s)	E_1 (kJ/mol)	A_2 (1/s)	E_2 (kJ/mol)
6	0.69	0.20	$3.30x10^{14}$	201	$1.01\ x10^{19}$	261
5	0.70	0.20	$3.30x10^{14}$	201	$1.01\ x10^{19}$	261
4	0.71	0.19	$3.30x10^{14}$	201	$1.01\ x10^{19}$	261
3	0.73	0.18	$3.30x10^{14}$	201	$1.01\ x10^{19}$	261
2	0.77	0.17	$3.30x10^{14}$	201	$1.01\ x10^{19}$	261
1 wt% $Ba(OH)_2$						
Heating rate (°C/min)	f_1	f_2	A_1 (1/s)	E_1 (kJ/mol)	A_2 (1/s)	E_2 (kJ/mol)
6	0.65	0.22	$3.30x10^{14}$	201	$1.01\ x10^{19}$	260
5	0.66	0.21	$3.30x10^{14}$	201	$1.01\ x10^{19}$	260
4	0.68	0.20	$3.30x10^{14}$	201	$1.01\ x10^{19}$	260
3	0.70	0.20	$3.30x10^{14}$	201	$1.01\ x10^{19}$	260
2	0.72	0.18	$3.30x10^{14}$	201	$1.01\ x10^{19}$	260

Table E4.4: Fitted model parameters obtained for first-order thermal degradation model – $Ca(OH)_2$ infused cellulose

0.1 wt% $Ca(OH)_2$						
Heating rate (°C/min)	f_1	f_2	A_1 (1/s)	E_1 (kJ/mol)	A_2 (1/s)	E_2 (kJ/mol)
6	0.68	0.25	$4.00x10^{14}$	200	$1.07 x10^{19}$	257
5	0.69	0.24	$4.00x10^{14}$	200	$1.07 x10^{19}$	257
4	0.72	0.23	$4.00x10^{14}$	200	$1.07 x10^{19}$	257
3	0.71	0.22	$4.00x10^{14}$	200	$1.07 x10^{19}$	257
2	0.75	0.21	$4.00x10^{14}$	200	$1.07 x10^{19}$	257
0.5 wt% $Ca(OH)_2$						
Heating rate (°C/min)	f_1	f_2	A_1 (1/s)	E_1 (kJ/mol)	A_2 (1/s)	E_2 (kJ/mol)
6	0.72	0.20	$4.93x10^{14}$	200	$1.07 x10^{19}$	257
5	0.73	0.19	$4.93x10^{14}$	200	$1.07 x10^{19}$	257
4	0.73	0.18	$4.93x10^{14}$	200	$1.07 x10^{19}$	257
3	0.75	0.18	$4.93x10^{14}$	200	$1.07 x10^{19}$	257
2	0.78	0.17	$4.93x10^{14}$	200	$1.07 x10^{19}$	257
1 wt% $Ca(OH)_2$						
Heating rate (°C/min)	f_1	f_2	A_1 (1/s)	E_1 (kJ/mol)	A_2 (1/s)	E_2 (kJ/mol)
6	0.60	0.27	$4.10x10^{14}$	201	$1.07 x10^{19}$	257
5	0.61	0.26	$4.10x10^{14}$	201	$1.07 x10^{19}$	257
4	0.63	0.25	$4.10x10^{14}$	201	$1.07 x10^{19}$	257
3	0.65	0.17	$4.10x10^{14}$	201	$1.07 x10^{19}$	257
2	0.69	0.23	$4.10x10^{14}$	201	$1.07 x10^{19}$	257

Appendix F : **Model-fitting of cellulose conversion in sulfolane**

Appendix F1 : Various kinetic mechanisms

Figure F1.1: Sequential model of cellulose conversion

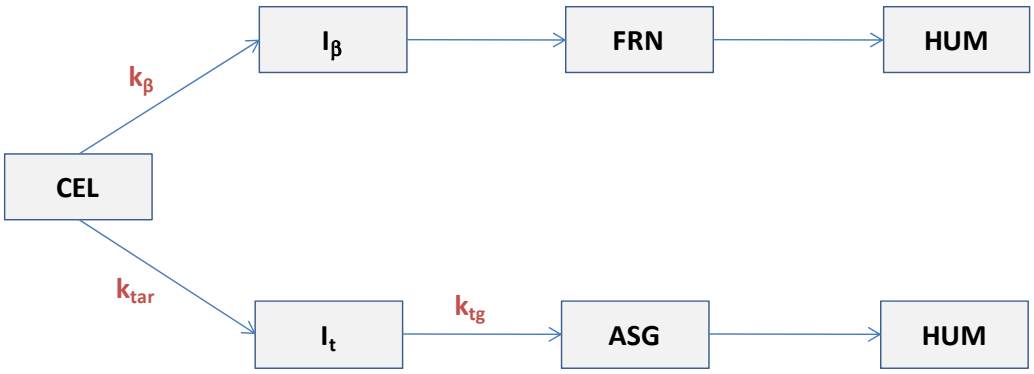

Figure F1.2: Two independent, competing pathways for cellulose conversion

*HUM: humic compounds including organic acids and other light volatiles

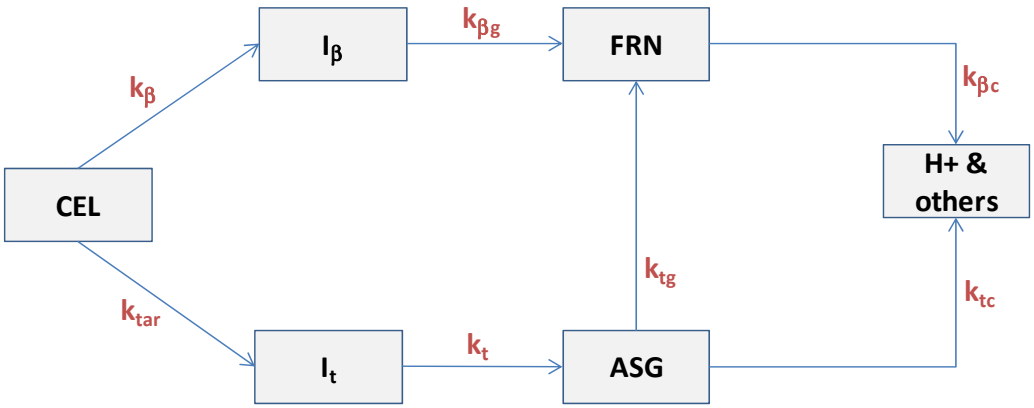

Figure F1.3: Two competing pathways (with interconnection) for cellulose conversion

Appendix F2 : Comparison of experimental and modelled conversion yields

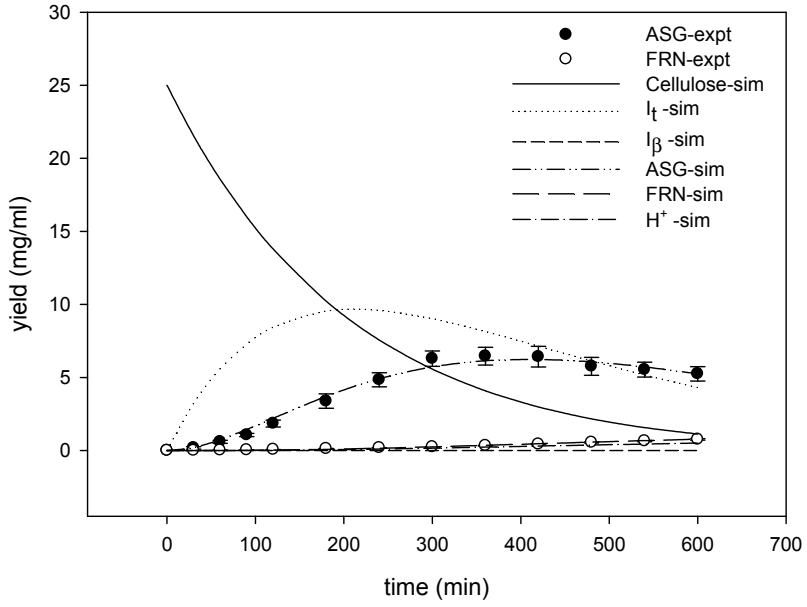

Figure F2.1: Model-fitting of anhydrosaccharides (ASG) and furans (FRN) for cellulose conversion in neat sulfolane at 180 °C

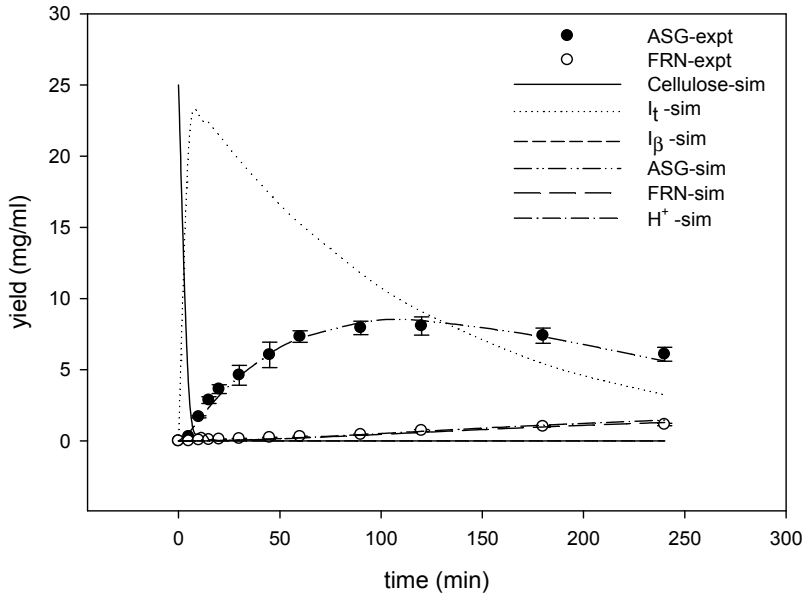

Figure F2.2: Model-fitting of anhydrosaccharides (ASG) and furans (FRN) for cellulose conversion in neat sulfolane at 200 °C

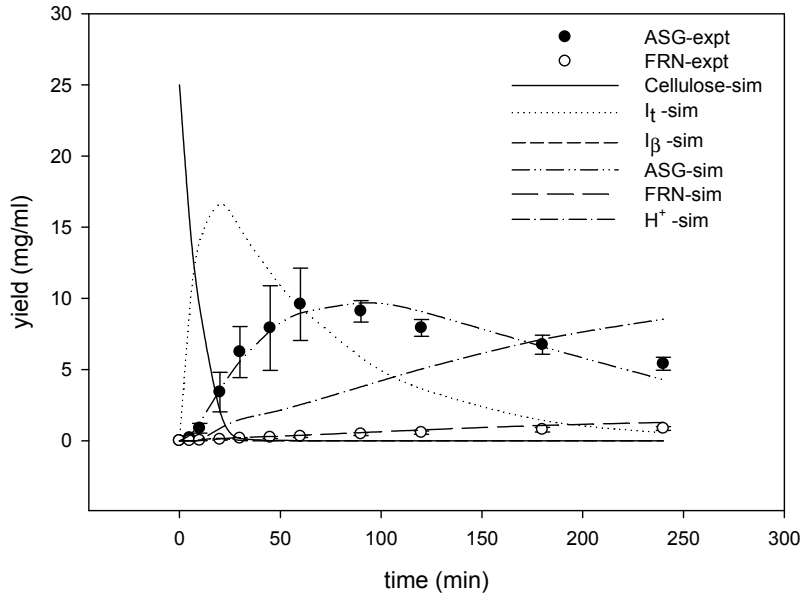

Figure F2.3: Model-fitting of anhydrosaccharides (ASG) and furans (FRN) for cellulose conversion in neat sulfolane at 210 °C

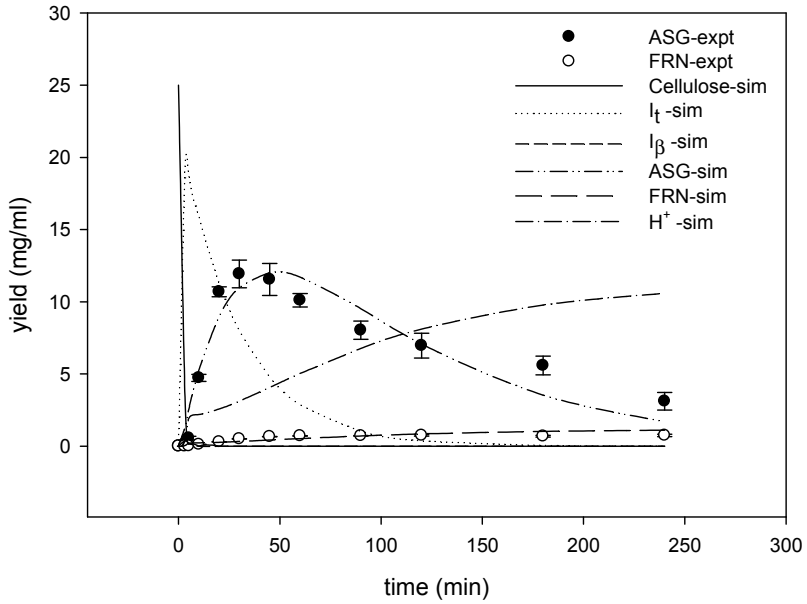

Figure F2.4: Model-fitting of anhydrosaccharides (ASG) and furans (FRN) for cellulose conversion in neat sulfolane at 220 °C

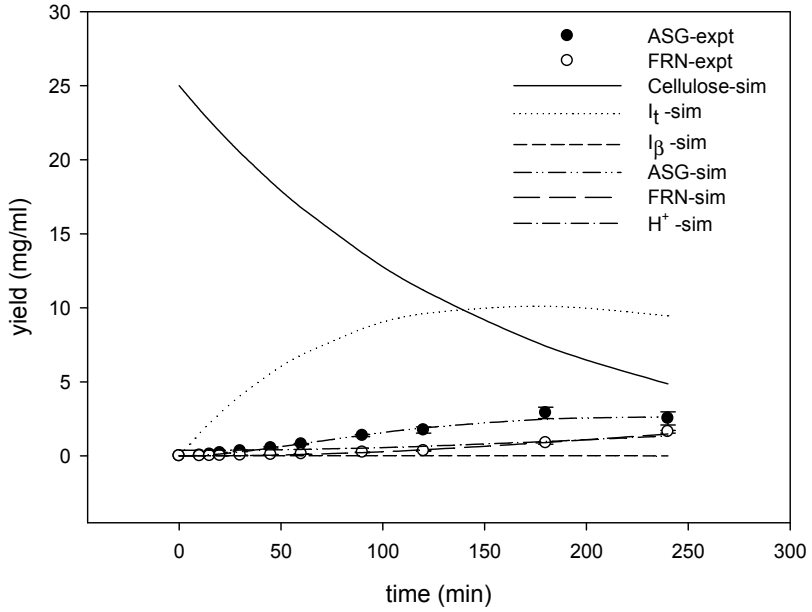

Figure F2.5: Model-fitting of anhydrosaccharides (ASG) and furans (FRN) for cellulose conversion in acidic (0.13 M H_3PO_4) sulfolane at 180 °C

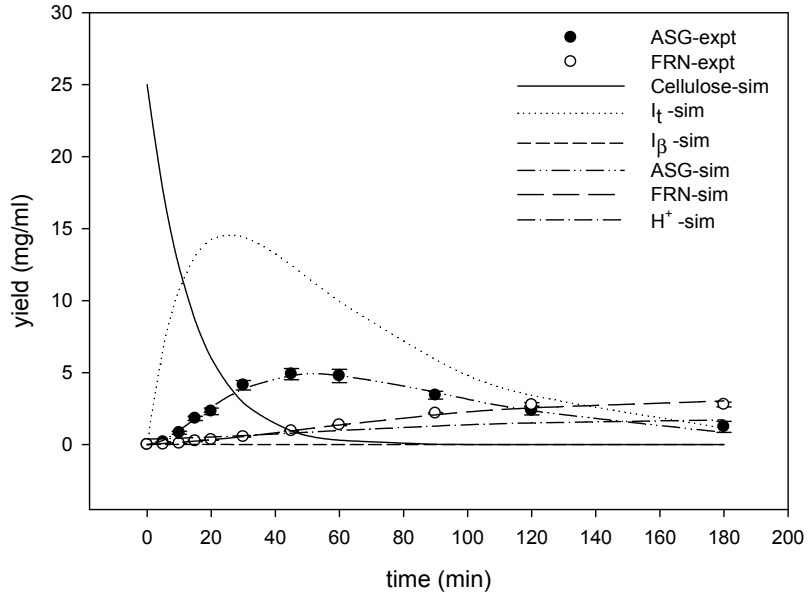

Figure F2.6: Model-fitting of anhydrosaccharides (ASG) and furans (FRN) for cellulose conversion in acidic (0.13 M H_3PO_4) sulfolane at 200 °C

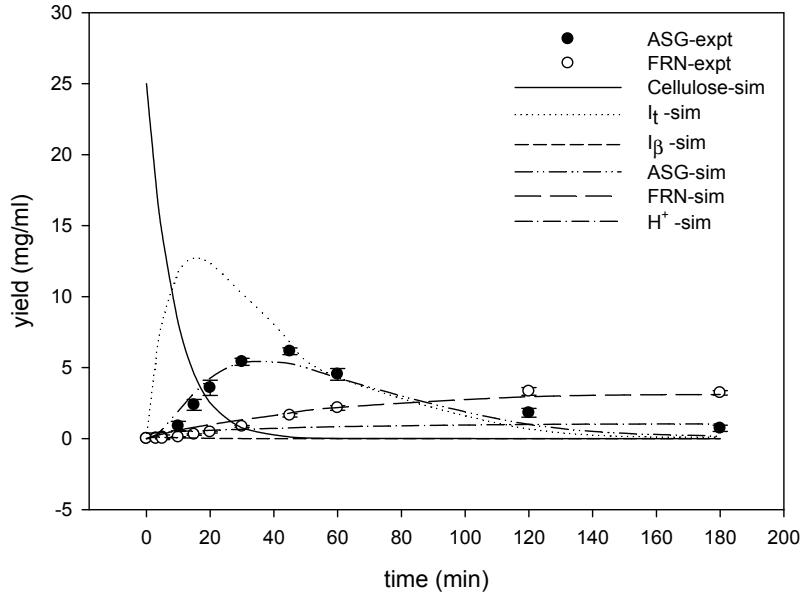

Figure F2.7: Model-fitting of anhydrosaccharides (ASG) and furans (FRN) for cellulose conversion in acidic (0.13 M H_3PO_4) sulfolane at 210 °C

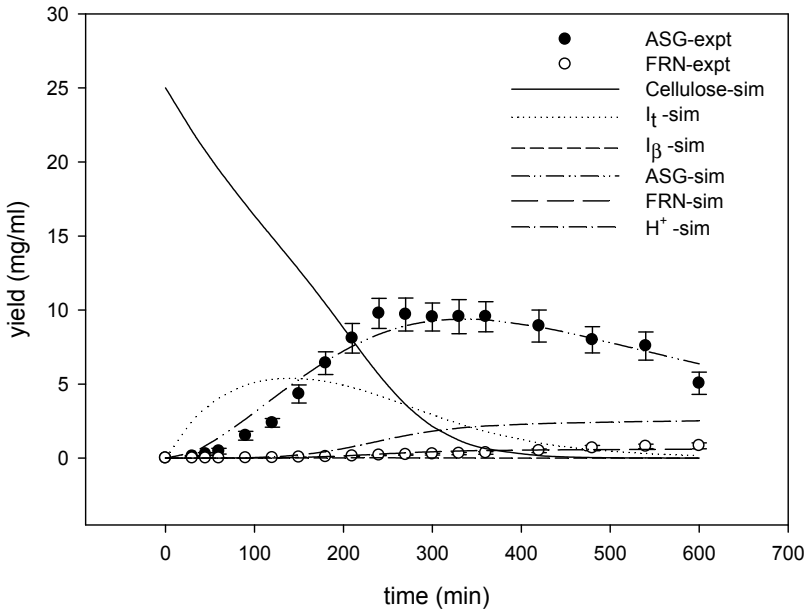

Figure F2.8: Model-fitting of anhydrosaccharides (ASG) and furans FRN) for cellulose conversion in alkaline (0.01 M $Ba(OH)_2$) sulfolane at 200 °C

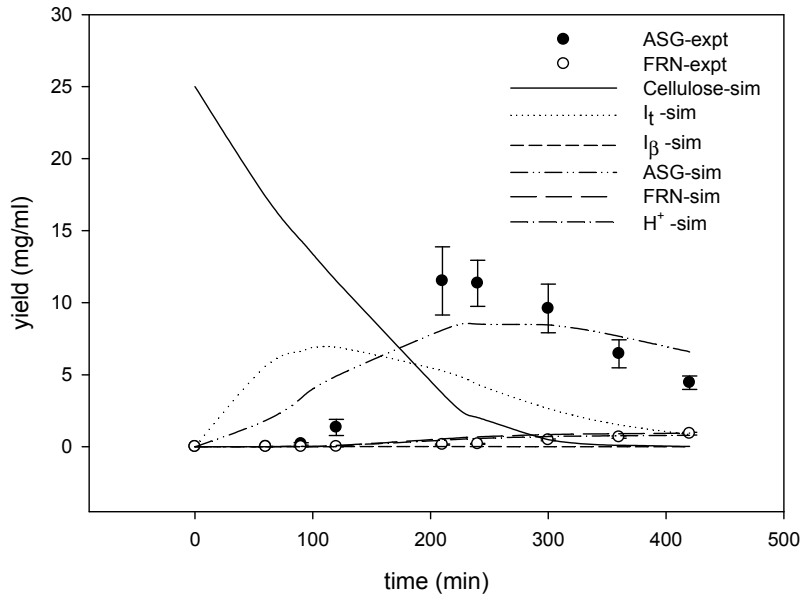

Figure F2.9: Model-fitting of anhydrosaccharides (ASG) and furans FRN) for cellulose conversion in alkaline (0.01 M $Ba(OH)_2$) sulfolane at 210 °C

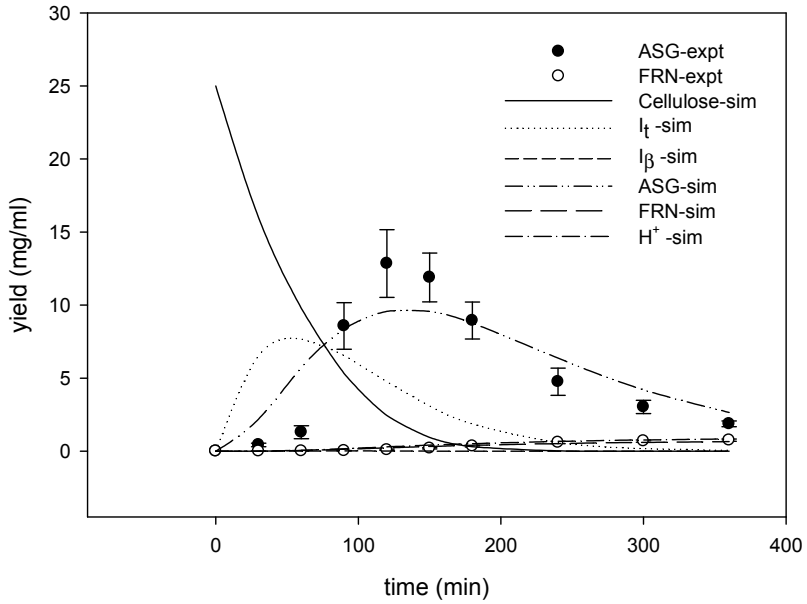

Figure F2.10: Model-fitting of anhydrosaccharides (ASG) and furans FRN) for cellulose conversion in alkaline (0.01 M $Ba(OH)_2$) sulfolane at 220 °C

Appendix F3 : Fitted model parameters

Table F3.1: Fitted model parameters for cellulose conversion in neat sulfolane

	180 °C	**190 °C**	**200 °C**	**210 °C**	**220 °C**
f_{tar}	0.6010	0.5248	0.7428	0.5663	0.3891
f_{β}	0.3990	0.4752	0.2572	0.4337	0.6109
f_{FRN}	0.1352	0.0906	0.4685	0.1028	0.0840
f_{H+}	0.0885	0.2655	0.5270	0.6798	0.8025
k_{tar}	0.0082	0.0230	0.5137	0.1700	1.3790
k_{β}	0.0027	0.0185	1.5041	0.2968	1.6910
k_{t}	0.0045	0.0074	0.0086	0.0157	0.0343
k_{tg}	0.0020	0.0041	0.0017	0.0065	0.0067
k_{tc}	0.0032	0.0033	0.0083	0.0034	0.0058
$k_{\beta g}$	0.3020	0.5498	0.8575	0.7043	1.9909
$k_{\beta c}$	0.0944	0.2493	0.9640	0.7560	0.7476

Table F3.2: Fitted model parameters for cellulose conversion in acidic (0.013 M H_3PO_4) sulfolane

	180 °C	**190 °C**	**200 °C**	**210 °C**
f_{tar}	0.225	0.1247	0.2940	0.2110
f_{β}	0.775	0.8753	0.7060	0.7890
f_{FRN}	0.588	0.5659	0.4873	0.4870
f_{H+}	0.385	0.4339	0.2148	0.1020
k_{tar}	0.029	0.0498	0.2265	0.4430
k_{β}	0.001	0.0055	0.0150	0.0550
k_t	0.005	0.0276	0.0183	0.0310
k_{tg}	0.006	0.0070	0.0111	0.0110
k_{tc}	0.013	0.0174	0.0313	0.0380
$k_{\beta g}$	0.093	0.1033	1.1284	1.1910
$k_{\beta c}$	0.281	0.4490	1.8661	1.7480

Table F3.3: Fitted model parameters for cellulose conversion in alkaline (0.01M $Ba(OH)_2$) sulfolane

	190 °C	**200 °C**	**210 °C**	**220 °C**
f_{tar}	0.8042	0.7817	0.8411	0.8060
f_{β}	0.1958	0.2183	0.1589	0.1940
f_{FRN}	0.0898	0.1263	0.2773	0.0900
f_{H+}	0.5444	0.5304	0.2331	0.0931
k_{tar}	0.0021	0.0053	0.0072	0.0074
k_{β}	0.0212	0.0359	0.1683	0.2084
k_{t}	0.0042	0.0103	0.0100	0.6716
k_{tg}	0.0002	0.0002	0.0002	0.0006
k_{tc}	0.0011	0.0022	0.0039	0.0047
$k_{\beta g}$	0.5801	0.7521	1.0793	1.2735
$k_{\beta c}$	0.7427	0.9364	1.5919	0.9486

Appendix G : **Analysis of Variance**

Appendix G1 : Analyses of variance for the influence of acid/alkali infused cellulose on anhydrosaccharide yields

Table G1.1: ANOVA table for the comparison of infusion levels, acids (H_2SO_4, H_3PO_4 and H_3BO_3) and temperature effects on anhydrosaccharide yield

source of variation	sum of squares	degree of freedom (f)	mean square	F_0	$F_{0.05,f,135}$
A-infusion level	614129	2	307065	79.46	3.06
B-acids	1626485	2	813242	210.44	3.06
C-temperature	1036670	2	518335	134.13	3.06
AB - interaction	137046	4	34262	8.87	2.44
AC - interaction	21228	4	5307	1.37	2.44
BC- interaction	178176	4	44544	11.53	2.44
ABC- interaction	30256	8	3782	0.98	2.44
Error	521705	135	3864		
Total	4165696	161			

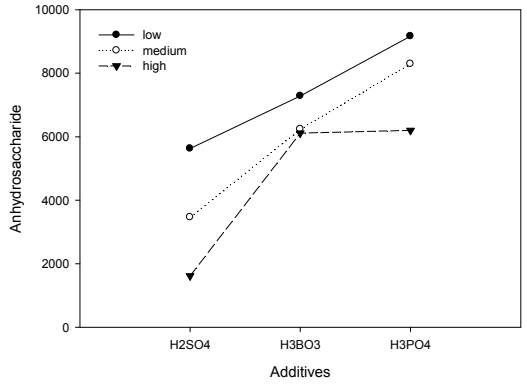

Figure G1.1: Plot for acid-infusion level interaction

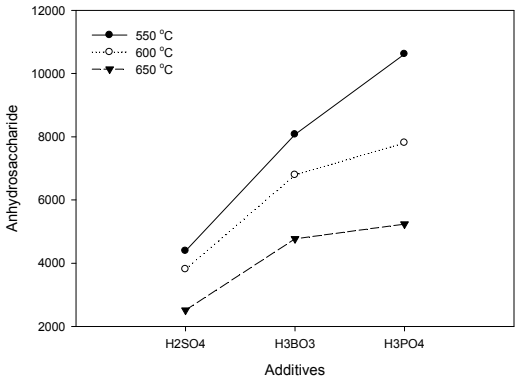

Figure G1.2: Plot for acid-temperature interaction

Table G1.2: ANOVA table for the comparison of infusion levels, alkalis (NH_4OH and $Ca(OH)_2$) and temperature effects on anhydrosaccharide yield

source of variation	sum of squares	degree of freedom (f)	mean square	F_0	$F_{0.05,f,90}$
A-infusion level	415892	2	207946	16.64	3.10
B-alkalis	826158	1	826158	66.11	3.95
C-temperature	95322	2	47661	3.81	3.10
AB - interaction	506988	2	253494	20.29	3.10
AC - interaction	3131	4	783	0.06	2.47
BC- interaction	1059	2	530	0.04	3.10
ABC- interaction	7295	4	1824	0.15	2.47
Error	1124662	90	12496		
Total	2980509	107			

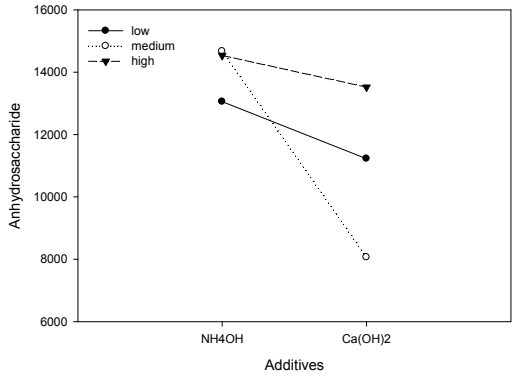

Figure G1.3: Plot for alkali-infusion level interaction

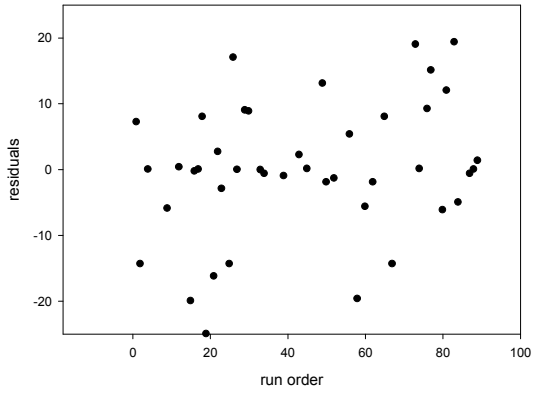

Figure G1.4: Plot of residuals versus run number

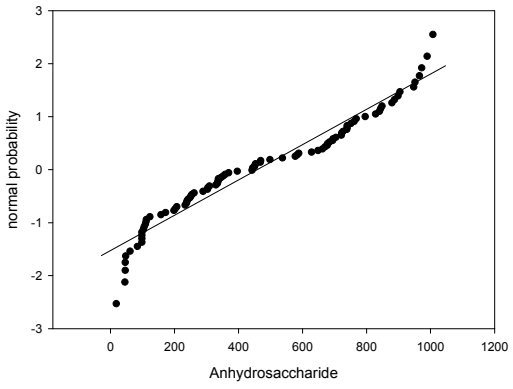

Figure G1.5: Normal probability plot of response variable

Appendix G2 : Analyses of variance for the influence of acid/alkali infused cellulose on apparent activation energy

Table G2.1: ANOVA table for the comparison of acids (H_2SO_4, H_3PO_4, H_3BO_3) and infusion levels effects on apparent activation energy

source of variation	sum of squares	degree of freedom (f)	mean square	F_0	$F_{0.05,f,45}$
Acids effect	2287	2	1144	2.95	3.21
Infusion level effect	1406	2	703	1.82	3.21
Interaction effect	4434	4	1109	2.86	2.59
Error	17424	45	387		
Total	25552	53			

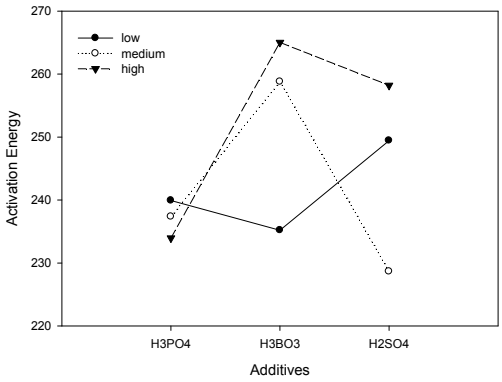

Figure G2.1: Plot for acid-infusion level interaction

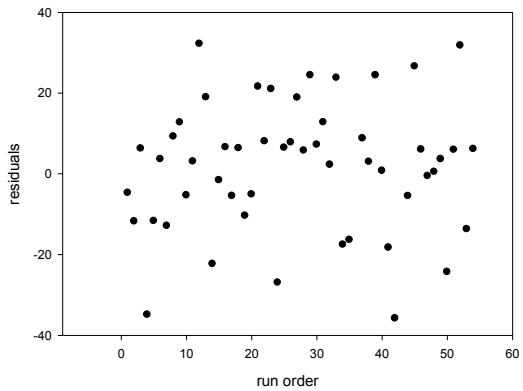

Figure G2.2: Plot of residuals versus run number

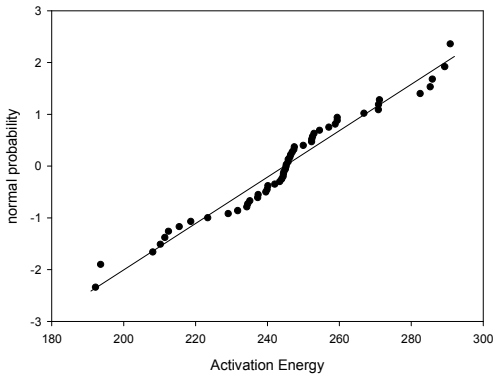

Figure G2.3: Normal probability plot of response variable

Table G2.2: Table: ANOVA table for the comparison of alkalis (NH_4OH, $Ca(OH)_2$, $Ba(OH)_2$) and infusion levels effects on apparent activation energy

source of variation	sum of squares	degree of freedom (f)	mean square	F_0	$F_{0.05,f,45}$
Alkalis effect	4907	2	2453	78.49	3.21
Infusion level effect	1158	2	579	18.52	3.21
Interaction effect	3211	4	803	25.69	2.59
Error	1407	45	31		
Total	10682	53			

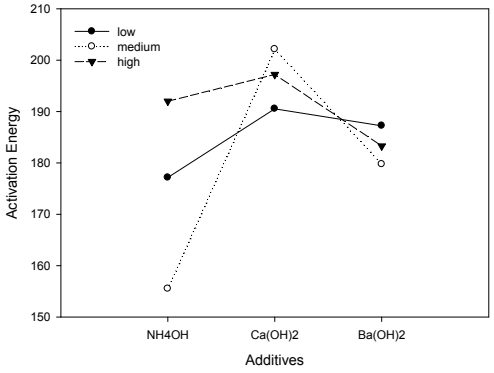

Figure G2.4: Plot for alkali-infusion level interaction

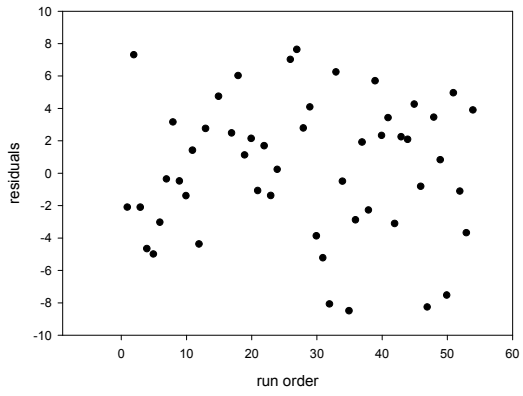

Figure G2.5: Plot of residuals versus run number

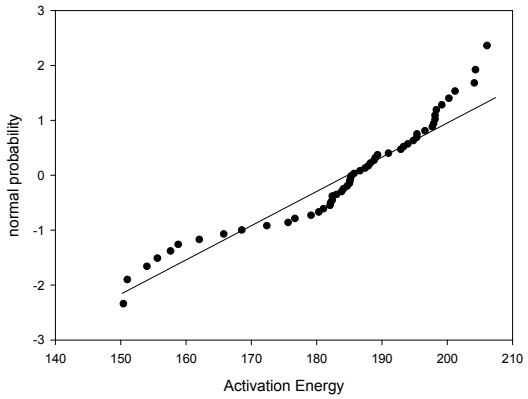

Figure G2.6: Normal probability plot of response variable

Appendix G3 : Analyses of variance for the influence of sulfolane [H+] condition on peak anhydrosaccharide and furan yields

Table G3.1: ANOVA table for the comparison of sulfolane [H+] condition (neat, H_3PO_4 and $Ba(OH)_2$) and temperature (190 °C, 200 °C, 210 °C) effects on peak anhydrosaccharide yields.

source of variation	sum of squares	degree of freedom (f)	mean square	F_0	$F_{0.05,f,45}$
Sulfolane [H^+] effect	254.92	2	127.46	772.77	3.21
Temperature effect	61.58	2	30.79	186.66	3.21
Interaction effect	1.55	4	0.39	2.35	2.59
Error	7.42	45	0.16		
Total	325.47	53			

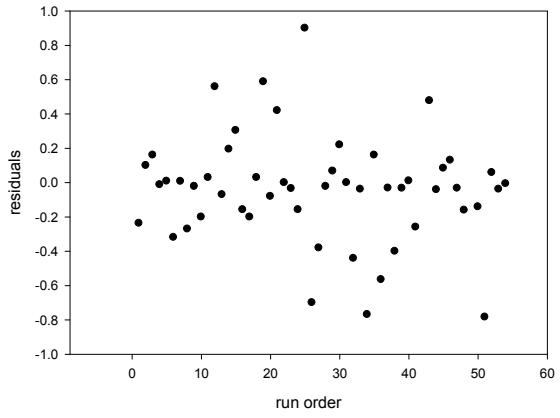

Figure G3.1: Plot of residuals versus run number

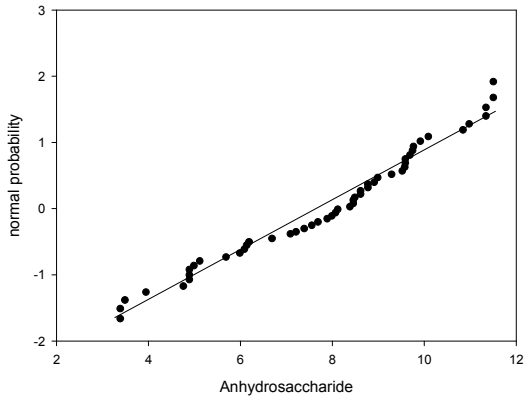

Figure G3.2: Normal probability plot of response variable

Table G3.2: ANOVA table for the comparison of sulfolane [H+] condition (neat, H_3PO_4 and $Ba(OH)_2$) and temperature (190 °C, 200 °C, 210 °C) effects on furan yields.

source of variation	sum of squares	degree of freedom (f)	mean square	F_0	$F_{0.05,f,45}$
Sulfolane [H^+] effect	8.45	2	4.23	559.87	3.21
Temperature effect	0.38	2	0.19	25.40	3.21
Interaction effect	2.30	4	0.58	76.25	2.59
Error	0.34	45	0.01		
Total	11.48	53			

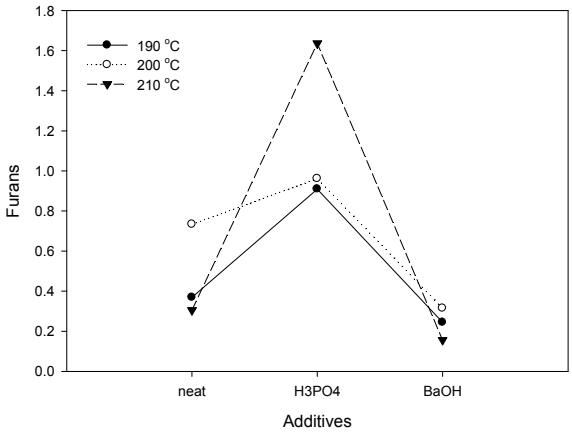

Figure G3.3: Plot for sulfolane [H^+]-infusion level interaction

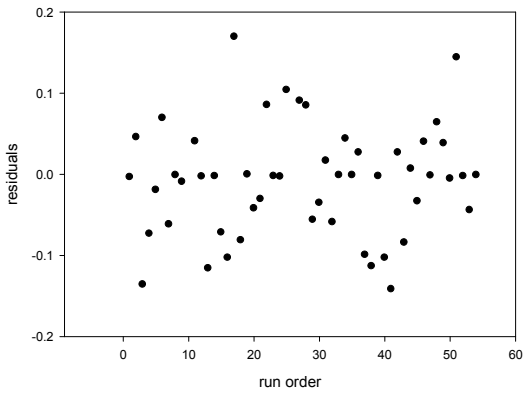

Figure G3.4: Plot of residuals versus run number

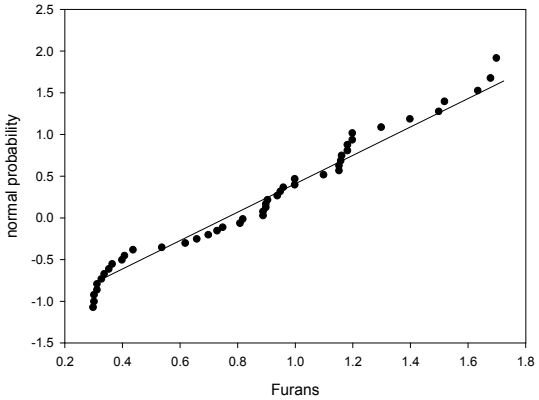

Figure G3.5: Normal probability plot of response variable

END